University of Southampton

Faculty of Engineering and Physical Science

MPhil Thesis

The Development of a Conceptual Design Algorithm of Multicopters and the Study of its Applications

Yangzi Guo

April 2020

This page is left intentionally blank.

Abstract

Multicopters is a large branch of unmanned aerial vehicles (UAVs). Due to the high agility and simple structure of multicopters, they are popularly used in many commercial and civilian applications. However, for a long time, there have existed few systematic algorithms to design multicopters. Most manufacturers and amateurs tend to design multicopters based on experience rather than engineering principles.

In this thesis, a conceptual design algorithm of multicopters is developed which has a better confidence of estimation than in previous works. The main part of this algorithm is a process which determines the minimum gross take-off mass ($GTOM$) of a certain combination of design parameters. This process calls the layer_2 function; it begins with a guessed $GTOM$, considers the given mission requirements, and then calculates the required power for different flight conditions. Next, the required performances of each component are calculated based on the power and are used for estimating the components' mass and price. At the end, the total mass is summed as the estimated $GTOM$. If the error between the initial $GTOM$ and the estimated $GTOM$ is close to zero, the initial $GTOM$ can be considered the minimum valid $GTOM$. Outside of this process, an external loop proceeds through all the design parameter combinations and develops a pool of valid designs (can converge to the minimum $GTOM$). Optimised designs can be filtered out with given targets (e.g. $MTOM$, total price, endurance and the maximum speed, among others).

Compared with the previous methods of multicopter conceptual design, this algorithm offers the following innovations:

- This algorithm considers the entire aircraft rather than focussing on a single separated system.
- The forest-tree-bagging technique is applied on the regression process of components, achieving better accuracy of component selection.
- The methods used in previous works are normally valid for only a narrow range of products, while this algorithm is valid for small (approximately 100 g) to relatively large (approximately 30 kg) multicopters.
- The algorithm can optimise not only the maximum take-off mass ($MTOM$) but also the price, endurance, total energy consumed and maximum speed.

This algorithm is validated for four aspects: the components estimation, total mass estimation, function output and optimisation process. Sensitivity analyses are then conducted for some selected parameters.

With the aforementioned advantages, this validated algorithm can be used as a tool for studying some specific flight mission problems. The algorithm can not only determine the most suitable

design for a specific mission but can also be used to evaluate the extent to which a design is matched to a mission, compare several designs for a mission or even help to improve the mission. This is one of the primary contributions of this thesis, since such a tool for multicopters has not yet been seen.

An example scenario is provided at the end of this thesis. For a long-range mission involving several multicopters, the signal should remain connected throughout the mission. One multicopter would serve as the leader to complete the mission, while the others will remain at each waypoint to function as repeaters. For such a mission, the multicopters can be organised into different configurations, similar to how a mother carries several children. Three configurations are proposed and compared based on several aspects.

Words Count: 54270

Table of Contents

This page is left intentionally blank.

List of Tables

List of Figures

xiii

xiv

Declaration of Authorship

I, Yangzi Guo

declare that this thesis and the work presented in it are my own and has been generated by me as the result of my own original research.

[title of thesis] The Development of a Conceptual Design Algorithm of Multicopters and the Study of its Applications

I confirm that:

1. This work was done wholly or mainly while in candidature for a research degree at this University;

2. Where any part of this thesis has previously been submitted for a degree or any other qualification at this University or any other institution, this has been clearly stated;

3. Where I have consulted the published work of others, this is always clearly attributed;

4. Where I have quoted from the work of others, the source is always given. With the exception of such quotations, this thesis is entirely my own work;

5. I have acknowledged all main sources of help;

6. Where the thesis is based on work done by myself jointly with others, I have made clear exactly what was done by others and what I have contributed myself;

7. Either none of this work has been published before submission, or parts of this work have been published as: [please list references below]:

Signed: ……………………………………………………

This page is left intentionally blank.

Acknowledgements

Thanks to my girlfriend Tiffany, who brought me light in my darkest time.

Thanks to my parents for their ever-lasting support.

Sincere gratitude to Dr David Toal, who helped me when I almost lost hope. He gave me a lot of valuable advices on this research.

Thanks to Prof Neil Bressloff who encouraged me on this research and also gave me good advices.

This research is funded by China Scholarship Council.

This page is left intentionally blank.

Glossary of Terms

AFDD	Aero-flight-dynamics Directorate
BEC	Battery Elimination Circuit
BEMT	Blade Element Modified Theory
BLDC	Brushless Direct Current (motor)
CAAC	Civil Aviation Administration of China
CAD	Computer-Aided Design
CATS	Civil Aviation Technical Standards
CFD	Computational Fluid Dynamics
COBYLA	Constrained Optimization BY Linear Approximation
COG	Centre of Gravity
COM	Communication
CPACS	Common Parametric Aircraft Configuration Schema
DARPA	Defence Advanced Research Programmes Agency
DC	Direct Current
DGPS	Differential GPS
DL	Disc Loading
DOC	Direct Operating Cost
DOF	Degree of Freedom
DS	Docking Station
EASA	European Aviation Safety Agency
EC	European Commission
EM	Electro-Magnetic
EMF	Electromotive Force
EMW	Electromagnetic Wave
EPM	Electronic Permanent Magnet
ESC	Electronic Speed Controller
EVLOS	Extended Visual Line of Sight
FAA	Federal Aviation Administration
FCE	Flight Control Electronics
FEA	Finite Element Analysis
FM	Figure of Merit
FPV	First-Person-View
GA	Genetic Algorithm
GCS	Ground Control Station
GPS	Global Positioning System
GTOM	Gross Take-off Mass
GTOW	Gross Take-off Weight
HOST	Helicopter Overall Simulation Tool
IMU	Inertial Measurement Unit
IPE	Individual Position Error
LED	Light-Emitting Diode
LiPo	Lithium-Polymer
LOS	Line of Sight
MAV	Micro Aerial Vehicle
MEP	Mission Equipment Package
MTOM	Maximum Take-off Mass
MTOW	Maximum Take-off Weight
NASA	National Aeronautics and Space Administration

NDARC	NASA Design and Analysis of Rotorcraft
NLOS	Non-Line of Sight
OFCOM	Office of Communications
OSD	On Screen Display
P3P	Perspective-Three-Point
PDF	Possibility Distribution Function
RC	Radio Control
RF	Radio Frequency
RGB	Red, Green and Blue
RLOS	Radio Line of Sight
RPA	Remotely Piloted Aircraft
RPAS	Remote Piloted Aerial System
RPE	Relative Position Error
RPM	Revolution per Minute
RTKGPS	Real-Time Kinematic GPS
RTL	Research and Technology Laboratories (RTL) of the U.S. Army Aviation R&D Command
RVLOS	Restricted Visual Line of Sight.
Rx	Receiver
SACAA	South African Civil Aviation Authority
SBC	Single Board Computer
SLAM	Simultaneous Localisation and Mapping
SMA	Shaped Memory Alloy
SRR	Self-Reconfigurable Robot
SUA	Small Unmanned Aircraft
SVM	Support Vector Machine
TLAR	Top Layer Aircraft Requirements
Tx	Transmitter
UAS	Unmanned Aerial System
UAV	Unmanned Aerial Vehicle
UGV	Unmanned Ground Vehicle
UHF	Ultra-High Frequency
UOC	UAS Operator's Certificate
USAAF	US Army Air Forces
VBA	Visual Basic Application
VFR	Visual Flight Rules
VLOS	Visual Line of Sight
VMC	Visual Meteorological Conditions
VRS	Vortex Ring State
VTOL	Vertical Take-off and Landing
WLAN	Wireless LAN

Nomenclature

Symbol	Description	SI unit
$\left(\frac{D}{q}\right)$	The drag area	m^2
h_{lg}	Landing Gear Height	m
A_1	The projected area on the top plane of a multicopter	m^2
A_2	The projected area on the front plane of a multicopter	m^2
A_∞	The area of flow of a rotor in the venaaacnootracta	m^2
A_{blades}	The area of the propeller blades	m^2
A_d	The drag area	m^2
C_T	The dynamic thrust coefficient of a propeller	
C_{T0}	The static thrust coefficient of a propeller	
C_d	The drag coefficient	
C_f	The fuselage downwash coefficient	
C_{ol}	The coefficient of overlap between the propellers and the body of the multicopter	
C_p	The dynamic power coefficient of a propeller	
$C_{p0,h}/C_{p0}$	The static power coefficient of the propeller.	
C_{tf}	The ratio between the top area and the front area of the multicopter	
E_h	Endurance for Hovering	s
$E_{b,useful}$	The useful energy of the battery	$W \cdot h = kg \cdot m^2/s^2$
$E_{bat,tot}/E_{b,full}$	The max energy the battery can provide	$W \cdot h = kg \cdot m^2/s^2$
E_c	Endurance for Cruising	s
E_{spec}	The energy density of the batter	$W \cdot h/kg$

E_{tot}	The ideally required max energy to complete the mission	J
I_{hov}	The required current of the motor in hovering mode	A
I_{arm}	The input current of one arm	A
$I_{b,output,max}$	The max output current of the battery	A
$I_{esc,max}/I_{esc,output}$	The max current that is safe to go through the ESC	A
$I_{max,mot}$	The max current the motor can safely work under	A
$I_{maxThru}$	The max required curernt of the motor in max thrust mode	A
L_a	The length of arms	m
$L_{d,max}$	The maximum allowed aircraft diagonal distance	m
$MTOM_{max}$	Maximum $MTOM$	kg
Mat_{body}	The material of the body	
M_{env}	The total moment produced by the environmental turbulence	$N \cdot m$
M_{total}	The total moment on a multirotor	$N \cdot m = kg \cdot m/s$
N_{arm}	The number of arms	
N_{bl}	Number of propeller blades	
N_{cell}/N_c	Number of Li-Po battery cells	
N_{layer}	The number of plate layers	
N_r	Number of rotors	
$P_{h,s}$	The required power of a single motor of the multicopter in hover	W
P_{PL_std}	Standard Payload Power	W
P_{arm}	The input power to an arm	W
P_{av}	Avionics Power	W
$P_{bat,tot}$	The max battery output power	W
$P_{esc,input}$	The input power of an ESC	W
$P_{esc,loss}$	The power loss of an ESC	W
$P_{esc}/P_{esc,output}$	The output power of an ESC	W

$P_{g,s}$	The required power of a single rotor in a general flight condition	W
P_i	The induced power of a rotor	W
$P_{in,mot,maxThru}$	The input power ot the motor in max thrust mode	W
P_{mot}/P_m	The output power of a motor	W
$P_{out,max}$	The output power of a single motor	W
P_{prop}/P_p	The output power of a propeller	W
$P_{req,h}$	The required power for hovering of an aircraft	$W = kg \cdot m^2/s^3$
$P_{req,f}$	The required power for forward flying of an aircraft	W
$P_{tot,i}$	The required power of each flight phase	W
P_{useful}	Useful power of a rotor which makes the aircraft move	W
R_{ESC}	The resistance of the ESC	Ω
R_{ESC}	The resistance of the ESC	Ω
R_b	The resistance of the battery	Ω
R_b	The resistance of the battery	Ω
R_{mot}	The resistance of the motor	Ω
R_{mot}	The resistance of the motor	Ω
$T_{h,s}$	The thrust of a single motor of the multicopter in hover	N
$T_{h,tot}$	The total thrust of the multicopter in hover	N
T_{actual}	Actual thrust of a rotor	N
$T_{g,s}$	The thrust of a single rotor in a general flight condition	N
T_{ideal}	Ideal thrust of a rotor	N
T_{motors}	The total torque produced by the motors	$N \cdot m$
TrW_{max}	The maximum thrust to weight ratio	
V_b/U	The output voltage of the battery	V

V_c	The volume of material of the central body	m^3
V_{cell}/U_c	Voltage of a single battery cell	V
$V_{maxThru}$	The required voltage in max thrust mode	V
V_{mot}	The total voltage on the motor	V
V_{mot}	The voltage of the motor	V
V_{out}	The output voltage of the battery	V
W_{arm}	The weight of a single arm	N
W_b	The weight of battery	N
W_{pl}	The weight of payload	N
d_c	The diameter of the central body round plate	m
d_{max}	Maximum Size	m
d_p	The propeller diameter	m
d_{pi}	The diameter of propeller in inch	$inch$
d_{pro}	The propeller size	m
e_{mot}	The useful voltage on the motor to work	V
f_{DOD}	The factor of depth of discharge of the battery	
f_w	Empty thrust weight ratio (defined as $(W_{empty} + W_{pl})/W_{empty}$)	
gr_p	The gap over propeller diameter ratio	
l_{bat}	The feature size of the battery	m
l_{esc}	The feature size of the ESC	m
l_{mot}	The feature size of the motor	m
m_A	The mass of the airframe	kg
m_{DC}	The mass of a brushed DC motor	kg
m_{ESC}	The mass of a ESC	kg
m_{PL_std}	Standard Payload Mass	kg

$m_{Pl,max}$	The maximum payload mass	kg
m_{Pl}/PL	The mass of the payload	kg
m_{arm}	The mass of the arm	kg
m_{av}	The mass of the avionics	kg
m_b	The mass of the battery	kg
m_c/m_{body}	The mass of the chassis/body	kg
m_{ec}	The mass of the general electronic components	kg
m_i	The mass of a tiny part on the object	kg
m_{lg}	The mass of the landing gear	kg
$m_{m,tot}$	The total mass of all the motors of a multicopter	kg
m_{mot}/m_m	The mass of motor	kg
m_{pl}	The mass of payload	kg
m_{pp}	The mass of the propulsion system	kg
m_{prop}	The mass of a propeller	kg
m_{tot}	The final estimated empty mass	kg
n_h	The rotation speed of a rotor in hover	rev/s
$n_{max,mot}$	The max rotation speed the motor can get to	rev/s
$n_{maxThru}$	The required motor rotation speed in max thrust mode	rev/s
pr_{ESC}	The price of the ESC	$
pr_{arm}	The price of the arm	$
pr_b	The price of the battery	$
pr_{body}	The price of the body/chassis	$
pr_m	The price of the motor	$
pr_{max}	Maximum Cost (Budget)	$
pr_p	The price of the propeller	$
pr_{tot}	The total price	$

r_∞	The radius of the area of flow of a rotor in the vena contracta	m
r_i	The distance from this tiny part to the rotation axis	m
r_p	The radius of the propeller	m
th_c	The thickness of the central body plate	m
t_{tot}/FT	Mission total flight time	s
v_∞	the flow velocity in the vena contracta	m/s
v_h	The rotor induced velocity in the plane of the rotor	m/s
v_{a_max}	Maximum Ascending Velocity	m/s
v_{cr_std}	Standard Cruising Speed	m/s
v_f	The forward flight speed	m/s
v_{f_max}	Maximum Forward Velocity	m/s
v_i	The induced velocity in the plane of the rotor	m/s
$v_{inf,p}$	The component of v_{inf} parallel to the rotor disk plane	m/s
$v_{inf,v}$	The component of v_{inf} vertical to the rotor disk plane	m/s
v_{inf}	The velocity of the coming air flow	m/s
$v_{through}$	The flow velocity perpendicular to the rotor disk plane	m/s
v_x/v_h	The horizontal velocity of a multicopter	m/s
v_y/v_c	The vertical/climb velocity of a multicopter	m/s
η_d	The discharge efficiency of the battery	
η_e	The electrical efficiency	
η_{esc}	The efficiency of an ESC	
η_m	The mechanical efficiency	
η_p	The propeller efficiency	

h	The distance from the lens to the image plane	m
σ	Propeller solidity	
A/A_{tot}	The total disk area	m^2
ATP	The percentage of time that the aircraft fly in max thrust mode (defined as t_{max}/t_{tot})	
As/A_{disk}	The area of the single propeller disk	m^2
B	The strength of magnetic field of a motor	T
C	The vector of constants	
$Cstr$	The vector of constraints	
D	The drag	$N = kg \cdot m/s^2$
DL	The disk loading	$N = kg \cdot m/s^2$
$DsPm$	The vector of design parameters	
FM	Figure of Merit	
FUN_{output}	The output vector of the layer_2 function	
G	Weight caused by gravity	N
$GTOM_0$	The initial guessed gross take-off mass	kg
$GTOW_0$	The initial guessed gross take-off weight	N
$GTOM$	The gross take-off mass	kg
$GTOW$	The gross take-off weight	N
I	The moment of inertia on the direction of the rotation	$kg \cdot m^2$
J	The advance ratio of the propeller (normally used by the front propeller of fixed wing aircraft)	
KV	The voltage constant of a motor	rpm/V
Km	The current constant of a motor	N/A
L	The stator length of a motor	m
MP	The table of material properties	

MPr	The table of material prices	
$MTOM$	The maximum take-off mass of an aircraft	kg
$MTOW$	The maximum take-off weight of an aircraft	N
N	The number of coils of a motor	
Q	Motor torque	$N.m$
R_{st}	The stator radius of a motor	m
R	The radius of the rotor disc's area	m
S	Total range	m
T	Motor thrust	N
TrW	The thrust to weight ratio	
c	The average chord of the propeller blade	m
e	The Oswald's efficiency factor	
err_{flag}	The error flags for constrtaints check	
$err_{percent}$	The error ratio of the mass	
f	The downwash of the fuselage	
gap	The gap between two adjacent propellers	m
n	The rotation speed of a rotor	rev/s
p/d_p	The propeller pitch diameter ratio	
q	The dynamic pressure	$kg \cdot m^{-1} \cdot s^{-2}$
r	The radius of the circles	m
t	The thickness of the circles	m
v	The relative velocity between the air and the object	m/s
Ω	The angular velocity of the forot	rad/s
α	The angle between the coming air flow direction and the rotor disk plane	rad
β_{rad}	The angular acceleration of the object	rad/s^2

β	The pitch angle of the multicopter	rad
γ	The climb path angle	rad
θ	The view angle of the lens	rad
κ	An empirical coefficient to fix the error between the measured C_T and actual C_T	
μ	The helicotper advance ratio	
ρ	The density of the air	kg/m^3
ω	The velocity in the vena contracta	m/s

This page is left intentionally blank.

Chapter 1 Introduction

1.1 Background and Motivations

Multicopters have developed quickly in recent years (Doyle and Donaldson, 2008; Chesebro, 2011; Unknown, 2014). Compared with large rotorcraft, small multicopters are low cost and less risky to the public. Compared with conventional fixed-wing remotely piloted aircraft (RPA), multicopters can hover and are capable of vertical take-off and landing (VTOL); furthermore, they have high agility and can fly through narrow passages and fly close to the surface (Morris, 2002). Due to these features, multicopters have become powerful competitors to large rotorcraft and fixed-wing RPA in both military and civilian applications.

The fixed-wing aircraft and large helicopters have mature designs and optimisation processes. However, for a long time, the design of multicopters was based on experience rather than engineering principles and procedures. Examples include those introduced by Verbeke *et al.* (2014), Gadda (2015) and Hystad and Lehn (2015). Due to the structural simplicity and low cost of multicopters, researchers tend to focus more on the development of the control system or discovery of new applications rather than the study of the design and optimisation procedure. In the civilian market, according to Yang (2016), the revolutionary technologies which can be considered core competences for a company were the 'autopilot' prior to 2010; the 'stabilised gimbal' from 2010–2013; the 'optical flow assisted navigation', '4k camera' and 'high definition video transmission' prior to 2016; and 'environmental awareness' and the development of 'AI' algorithms at present. Compared with these technologies, the improvement of aircraft design offers too little a benefit to a company.

In most cases, a multicopter is simply a platform for carrying all the high-tech sensors and payloads. The design target is 'enough' rather than 'the most suitable'. However, from a research point of view, a scientific design and optimisation procedure is still necessary to improve the performance of a multicopter, such as increasing the endurance or reducing the cost. The traditional design process for both fixed-wing aircraft and rotorcraft includes three phases: conceptual design, preliminary design and detailed design (Leishman, 2006; Raymer, 2012; Weiand *et al.*, 2020). For a mission, if multiple solutions are proposed, it is during the conceptual design phase that all the concepts are being analysed and compared to determine the 'most suitable solution' to the mission requirements. This phase costs the least amount of money and efforts and has an impact of 65% on the total aircraft life cycle costs.

The conceptual design phase can provide a basis and evidence for decision making in the early stages. This benefit is not only for single multicopter missions but would also be useful in multiple aircraft cooperation scenarios. Only until recently have more efforts been seen to introduce engineering design procedures and principles into multicopter design (Russell, Theodore and

Sekula, 2018; Theodore, 2018). However, there is still no usable and validated tool to automatically proceed with the conceptual design and optimisation task. A major obstacle is that the models of components and some empirical parameters are suitable for only large rotorcraft. When scaling down, the algorithm must be tuned.

In this thesis, the principles of multicopters are introduced, and based on an exhaustive database of components and multicopter platforms, a conceptual design algorithm is developed. Empirical equations are concluded in a statistical manner based on the database. Compared with large rotorcraft design algorithms, the uncertainty of the estimation results of these equations is improved due to the large number of members in the database. Moreover, this algorithm is validated by existing multicopters. Other than helping design multicopters, this algorithm can be used as an analysis tool to solve a specific scenario in which several multicopters cooperate to complete a long-range mission.

1.2   Research Targets

The research targets are to develop a trustworthy multicopter conceptual design algorithm and to use this algorithm to solve some practical design problems.

1.3   Research Questions

- What is the process of multicopter design optimisation?
- What are the necessary mission requirements?
- How can the performance of each component be calculated?
- How can the mass and price of each component be estimated?
- How can the algorithm be validated?
- What are the potential applications of the conceptual design tool?

1.4   Novelties

- A complete conceptual design process is proposed which combines the advantages from the literature and improves on some of the drawbacks. It considers up to five parameters as possible optimisation objectives. Although the optimisation process is still single objective, the result is a valid design configuration pool, which is possible for use in further multi-objective optimisation analysis. It also considers all the flight conditions when determining the maximum required power.
- An abundant database of multicopter platforms and multicopter components is formed using a spider tool. The regression results from previous literature are validated by the database. A problem in the regression of motor mass was seen, an observation which no previous literature has mentioned. This problem was solved by introducing the random forest technique for regression. The new technique improved the accuracy of estimation and expanded the applicable range of the component models.
- The proposed algorithm is validated, and a sensitivity study has been performed.

- The proposed algorithm is used to analyse a novel signal repeating scenario by evaluating four possible configurations. Three of the solutions take advantage of multiple aircraft cooperating work, while two of them involve the aerial docking between multicopters.

- Instead of using a finite element analysis (FEA) simulation, the basic material mechanics theory is introduced for the evaluation of the arm strength and optimisation of the arm geometries. The FEA method is time consuming and is more suitable for the preliminary design or detailed design phase, while the proposed theory is quicker and is suitable for the conceptual design phase. The material mechanics theory is not new, but it is novel to apply this theory to multicopter conceptual design.

1.5   Report Structure

This thesis is organised into six chapters.

Chapter 1 presents the introduction to the conceptual design of multicopters. Here, the background, motivations, aims and sub-tasks of this research topic are explained.

Chapter 2 provides an extensive literature review of four related aspects: the design process of fixed-wing aircraft and large rotorcraft; the efforts of introducing or adapting a design process that follows engineering principles to multicopters; the current methods of concluding empirical equations; and the optimisation methods related to aircraft or multicopter design. Other than the four topics, some basic knowledge is also introduced where they are mentioned in later chapters. These include the aerodynamic principles of rotorcraft; the principle of components such as direct-current (DC) motors, propellers and lithium-polymer (LiPo) batteries, among others; and the structural mechanics for the arm strength calculation.

The development of the conceptual design algorithm is discussed in Chapter 3. This includes a detailed introduction to the algorithm structure and workflow, the tools used, and the database, input, output, calculation process and constraints.

In Chapter 4, the algorithm is validated. The validation is based on three aspects: the components estimation, the mass estimation under the same given parameters and the full design with the same given mission. Then, some parameters used as constants are analysed, and finally, the sensitivity study is performed on selected parameters.

Chapter 5 is dedicated to introducing the application of the algorithm. One practical problem is presented in which multiple multicopters are used to complete a long-range mission, and several solutions are proposed. In each solution, the organisation of the multicopters occurs in different configurations. The proposed conceptual design algorithm is used to solve the problem of each candidate multicopter configuration. The results are analysed in depth to determine with the most suitable solutions for different targets.

Finally, the conclusion is provided in Chapter 6.

Chapter 2 Literature Review

2.1 The Design Process of Fixed-Wing Aircraft and Rotorcraft

For fixed-wing aircraft and large rotorcraft, there exists a mature design process, after which the most suitable solutions can be proposed and designed for given missions.

2.1.1 Fixed-Wing Aircraft Design Process

Raymer (2012) introduced the general design process for fixed-wing aircraft. In his opinion, the word 'design' primarily refers to the creation of the appearance and the arrangement of the components. However, a design is more than drawings, since a successful design should fulfill the requirements without requiring further major corrections to the centre of gravity, aerodynamics features and mechanical limitations, among others. To achieve a successful design, a process consisting of engineering analysis is necessary. The entire process includes three phases: the conceptual design phase, preliminary design phase and detailed design phase (see Figure 2.1).

The conceptual design phase aims to determine a single configuration for further phases. This phase begins from the requirements; then, multiple configurations are proposed and evaluated to answer the ultimate question: 'can a satisfactory aircraft be made with the given money?' A simple aerodynamic analysis and weight analysis are performed during this phase to support the designs. Optimisation may be applied during this phase to select the most suitable design.

Afterwards, in the preliminary design phase, more sophisticated analyses and experiments are performed in all the main aspects, such as the structure, aerodynamics features, propulsion system characteristics, system stability and control systems, among others. More detailed shape design and components arrangement are also performed in this phase. In the end, a proposal will be made for the company to decide whether to pay more money to complete the design.

If the proposal is accepted, the detailed design phase begins. In this phase, all the components and parts are designed in detail. The completed engineering drawings should be capable of being directly used by the manufacturer. The manufacture process design is also completed during this phase.

A similar process can be found in (Nicolai and Carichner, 2010).

REQUIREMENTS

↓

CONCEPTUAL
DESIGN

WILL IT WORK ?

WHAT DOES IT LOOK LIKE ?

WHAT REQUIREMENTS DRIVE THE DESIGN ?

WHAT TRADE-OFFS SHOULD BE CONSIDERED ?

WHAT SHOULD IT WEIGH AND COST ?

↓

PRELIMINARY
DESIGN

FREEZE THE CONFIGURATION

DEVELOP LOFTING

DEVELOP TEST AND ANALYTICAL BASE

DESIGN MAJOR ITEMS

DEVELOP ACTUAL COST ESTIMATE   (" YOU-BET-YOUR-COMPANY ")

↓

DETAIL
DESIGN

DESIGN THE ACTUAL PIECES TO BE BUILT

DESIGN THE TOOLING AND FABRICATION PROCESS

TEST MAJOR ITEMS - STRUCTURE, LANDING GEAR, ...

FINALIZE WEIGHT AND PERFORMANCE ESTIMATES

↓

FABRICATION

Figure 2.1 The three phases of aircraft design.(Raymer, 2012)

2.1.2 Rotorcraft Design Process

The traditional design process of helicopters is described by Johnson (1994), Jiang (2005) and Zhang (2007). The design process of helicopters is the same as that of fixed-wing aircraft and is divided into three phases.

A recent article (Weiand *et al.*, 2020) has reviewed the existing design tools and proposed a new integrated design process for rotorcraft. In this article, the design process is described as follows: "A virtual configuration is the outcome of the design process. It is the synonym for the not existing product during its development and the basis for the digital or virtual twin when the overall process proceeds to product lifecycle management. The goal of a design project for aerial vehicles is to increase the accuracy of the virtual configuration with every step in the sizing process."

Design tools are short programs which can solve problems in a certain area. Some well-known tools are the NDARC (NASA Design and Analysis of Rotorcraft) project (Johnson, 2010), the CPACS (Common Parametric Aircraft Configuration Schema) data model (Bachmann *et al.*, 2009; Liersch and Hepperle, 2011), the HOST (Helicopter Overall Simulation Tool) for flight mechanical simulation (Benoit *et al.*, 2000), the COBYLA (Constrained Optimization BY Linear Approximation) optimisation algorithm (Powell, 2007), the VSAERO software for aerodynamic simulation (Maskew, 1987) and the AFDD (U.S. Army Aeroflightdynamics Directorate) mass models (Johnson, 2010), among others.

The different design tools can be divided into four levels based on their computation time and the uncertainty in the results. Higher-ranked tools consume more computation time but provide more accurate results. The level0 and level1 tools are considered suitable for the conceptual design phase, as several concepts may be proposed during this phase, and they must be evaluated quickly. However, the preliminary design and detailed design phases are normally based on a single decided concept, so more sophisticated calculations (level2 and level3 tools) are possible.
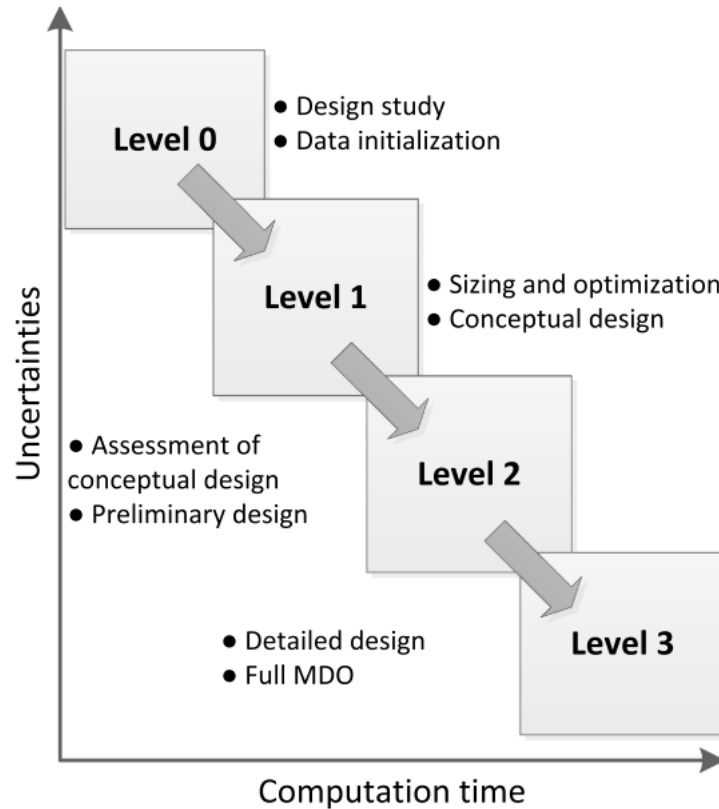
Figure 2.2 Uncertainties of the design tool as a function of the computation time.
(Weiand et al., 2020)

2.1.3 A Detailed Conceptual Design Process

In the later parts of the previous article (Weiand *et al.*, 2020), a detailed conceptual design algorithm is introduced. The conceptual design process begins with the TLARs (top-level aircraft requirements), from which the initial data set is determined. With the initial data set as the input, the primary loop of the level1 process consists of a design leg and an analysis leg (see Figure 2.3). This loop ends when the $MTOM$ converges. Then, the conceptual design is finished, and the main geometries, parameters and performances of the design are ready for further design phases.

Initial dataset (level 0)
& updates (level 2)

Sizing Loop
(level 1)

MTOM
convergence?

No — Yes →

Design

Rotor blade planform optimization

3D-surface generation

Fuselage aerodynamics

Twist optimization

Analysis

Estimation of operating empty mass

Flight-performance & estimation of fuel mass
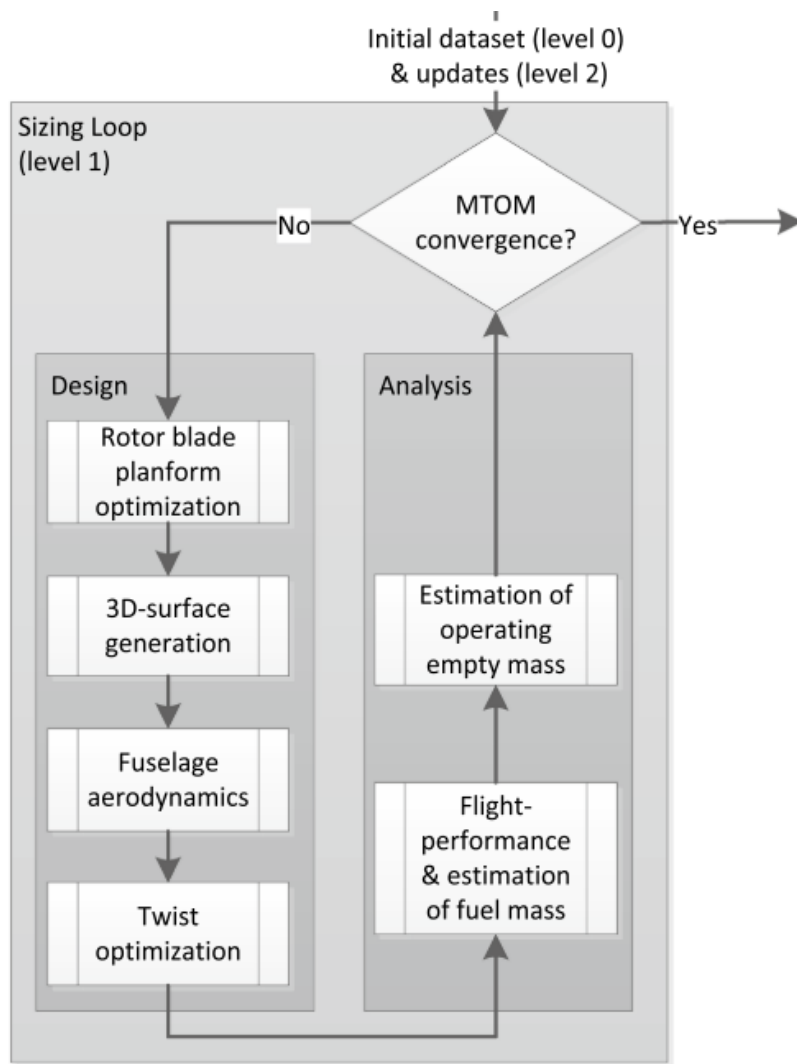
Figure 2.3 Flowchart of the sizing loop applying level 1 tools for the conceptual design.
(Weiand et al., 2020)

2.1.3.1 TLARs and the Level0 Process

The TLARs should include at least the parameters in Table 2.1. Among them, the payload mass, cruise speed and range comprise the performance triangle of an aircraft. In addition to these, there are sometimes other optional requirements, such as the volume of the cabin, the cargo hold payload fraction or the dimensions of the cabin, among others.

Table 2.1 The basic TLARs.

Name	Type of parameter	Symbol	Unit
Payload mass	Continuous	m_{Pl}	kg
Cruise speed	Continuous	v_{cr}	m/s
Range	Continuous	S	m
Number of main rotor blades	Discrete	N_{bl}	−
Main rotor configuration	Selection	−	−

The initial data set includes several basic aspects of a rotorcraft:

- Mass: The initial maximum take-off mass. This consists of the basic empty mass, operators' mass, payload mass and fuel mass.
- Dimensions: The dimensions of the different parts of a simplified fuselage model. The whole fuselage is divided into several basic geometries, such as the cylindric fuselage mid, cone fuselage front and spar fuselage tail, among others.
- Rotor size: The mass and moment of inertia of the rotor can be calculated based on the radius and solidity. They are in turn used for a flight mechanics simulation in the next level.
- Power estimation: The maximum required power should be higher than the induced power in hovering; hence, an empirical ratio is introduced for the estimation.

In the process of developing the initial database, many empirical parameters or relations are used and are all based on statistics regression. For example, the basic empty mass is estimated using a statistical database, which includes 159 existing helicopters designed for several main purposes. Then, by treating the initial $MTOM$ as the variable, the feature size (diameter of the fuselage mid) of the fuselage, the radius and the solidity of the rotor can be estimated using empirical equations. These equations are also concluded from the database of the helicopters. The Lock number of the rotor and the installed power ratio are empirical constants based on the purpose of the rotorcraft.

2.1.3.2 The Level1 Process

The level1 process proceeds a series of design optimisation and analysis based on the initial data set from level0 (see Figure 2.3).

1. Rotor Blade Planform Optimisation

The COBYLA algorithm is used here to optimise the radius, chord and angular velocity of the rotor, and a series of characteristic rotor parameters is calculated and used as optimisation constraints. These are the aspect ratio, solidity, blade loading, tip Mach number, advance ratio, tip velocity, energy ratio, and Lock number. The recommended ranges for these parameters are based on experience.

2. 3D Modelling and Aerodynamic Simulation of the Fuselage

With the dimensions determined in level0, a 3D model of the fuselage is built and used for the aerodynamic simulation. The aerodynamic properties are calculated using VSAERO, a commercial software with quicker calculation speed than a full computational fluid dynamics (CFD) simulation. Only the clean fuselage (not considering the rotor hub, empennage or landing gears, among others) is calculated in this step to further reduce the calculation time. At the end, the lift and drag due to the pressure distribution are calculated.

3. Twist Optimisation of the Blade

The purpose of twist optimisation is to minimise the required power for the given flight condition. A linear twist distribution is assumed here, and the process is performed with the help of HOST.

4. Fuel Mass Estimation

Trim calculations are performed by HOST. By changing the available fuel mass, the possible flight range can be estimated. The fuel mass can be reduced until the possible range is no longer than the required range.

5. Estimation of Operating Empty Mass

An estimation of the operating empty mass was performed in level0 with an empirical equation. It sets the initial guess of the $MTOM$, and in this step, the detailed mass of each component is calculated to estimate a new $MTOM$. Five estimation methods are compared here (Beltramo, 1980; Layton, 1992; Palasis, 1992; Prouty, 2002; Johnson, 2010), with error values ranging from 5% to 20%. It should be noticed that all five methods are suitable for the mass estimation of helicopter components. Regarding multicopters, new methods must be developed, or the old methods must be tuned properly for the new database.

The five steps are repeated until the $MTOM$ converges. Both the level0 and level1 processes comprise the conceptual design phase.

2.2 Multicopter Parametric Design

For a long time, the design of quadcopters has relied on separate empirical conclusions and does not often follow engineering procedures. In most papers that involve the content of multicopter design, the word 'design' refers to the design of the autopilot or control system, while the design of the other systems is greatly simplified or not covered at all (Hanafi *et al.*, 2013; Devaprakash and Raj, 2014; Gadda, 2015; Hystad and Lehn, 2015; Magnussen, Ottestad and Hovland, 2015; Quan, 2017; Mascarello, no date). This phenomenon is mainly caused by two reasons:

1. The entire design process is not necessary for most studies related to remote piloted aircraft (RPA). The most popular method for multicopter development is 'building and testing'. For a multicopter of less than $7\ kg$, the design process typically begins directly with a full-scale vehicle and uses a sketch, build, fly and iterate the process without the need for extensive use of design tools. This approach can get a vehicle flying quickly. (Theodore, 2018)
2. 'The availability of accurate and validated conceptual design tools for these novel types and sizes have not kept pace with the new markets and vehicles themselves.' (Theodore, 2018)

However, it is certain that a systematic way of performing technology and mission trade-studies can ensure that an aircraft concept work for a particular mission, and that its geometries be optimised. It is not until recently, does the parametric design process of multicopter gradually draw more attention.

Hassanalian and Abdelkefi (2017) have reviewed all types of drones, including multicopters. They confirm the three classic phases of aircraft design and identify that the most important step in the conceptual design phase is sizing. There are five steps of sizing: a) define the mission, b) propose the RPA type and make clear the flight conditions, c) select the wing shape and aspect ratio (for fixed-wing aircraft), or select the rotor parameters (for rotorcraft), d) perform a constraints analysis, involving the mechanics and dynamics and e) estimate the $MTOM$. This is the general process for all RPA design, while for multicopters, it is the number, position and geometries of the rotos that should be considered in step c).

NASA already uses NDARC as a powerful tool for rotorcraft design, and it has now proposed a new framework for the design of multicopters and other novel structures, known as the DELIVER project (Theodore, 2018). The new framework is adapted from NDARC given the similarity between multicopters and helicopters. In addition, the new framework aims to be valid for a large range of multicopter sizes, ranging from hand-sized micro RPA to air taxis that can carry two to four adults.

As part of the DELIVER project, Russell, Theodore and Sekula (2018) present an effort to extend NDARC into the design of multicopters. They insist that the design process of NDARC is suitable for multicopters; the analytical models simply require validated updates with the help of wind tunnel test results, individual component weights and performance. After calibration with the new database, the CAMRAD II algorithm involved in NDARC can yield relatively more accurate estimation to the hovering thrust, but it slightly overestimates the hovering power and the thrust and power in forward flight.

Other people have proposed their own design procedures.

In (Wang et al., 2014), a standardised design method is proposed for multicopters and is illustrated in Figure 2.4. The main goal is to develop a system that can hover with a certain payload while simultaneously meeting constraints on endurance, budget and size. This paper emphasises the advantages of a standardised design procedure (i.e. more industrialisation-friendly and easier use for scenario comparison). In addition, it addresses many significant ground rules for multicopter design.
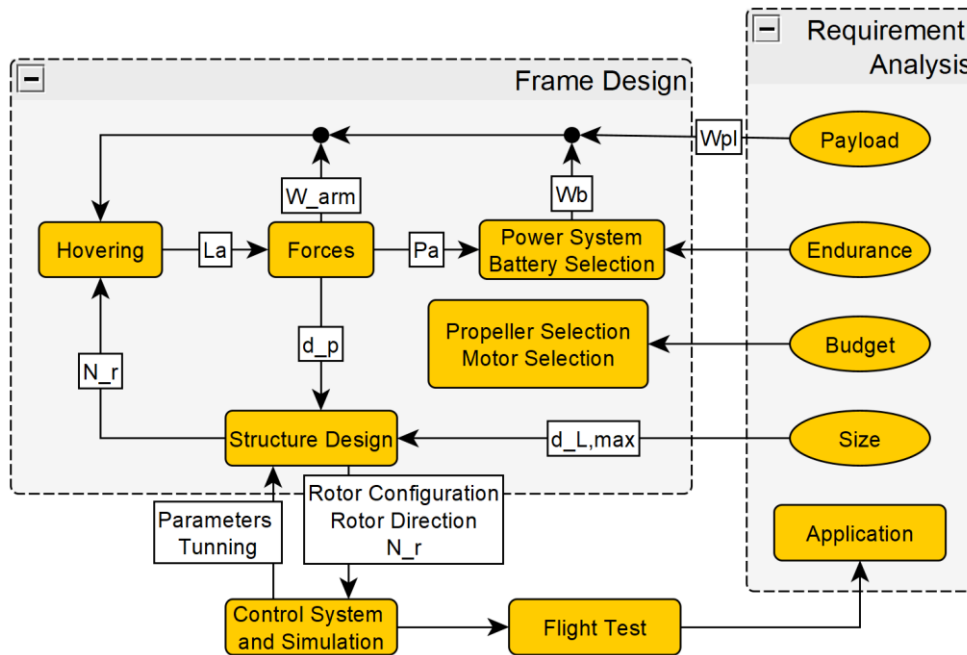
Figure 2.4 The standardised design process proposed by (Wang *et al.*, 2014)*.*

Ampatis and Papadopoulos (2014) provide a completed algorithm and corresponding codes for multicopter conceptual design. This clearly divides the initial data into 'design requirements' and 'design vector (parameters)'. Furthermore, it includes a section about the sensitivity study of parameters and utilises a different approach for system design optimisation. If Wang's algorithm considers the straightforward logic, then Ampatis's algorithm follows the reversed logic. Instead of starting with a guessed $MTOM$ in a common iteration-based procedure, this algorithm starts with attempted design parameters and relies on the optimisation process for everything else (see Figure 2.5). It does not include an $MTOM$ convergence process, and the components sizing logic also differs. For all the components, the characteristics and performance parameters are related to their featured size. In the calculation of a battery's total energy (one of the optimisation objectives), a full accurate circuit model of the entire system is developed considering the inner resistance of all the components (see Figure 2.6). By doing so, the power loss can be determined in an accurate manner. The proposed algorithm was verified by two case studies. Taking two products from the market, Ampatis and Papadopoulos attempted to optimise the total energy consumed for the first model and optimised the size for the second model. In the end, the target performance was optimised, while the other performances were kept nearly the same. With the proposed algorithm, the influences of payload and the number of rotors are studied.
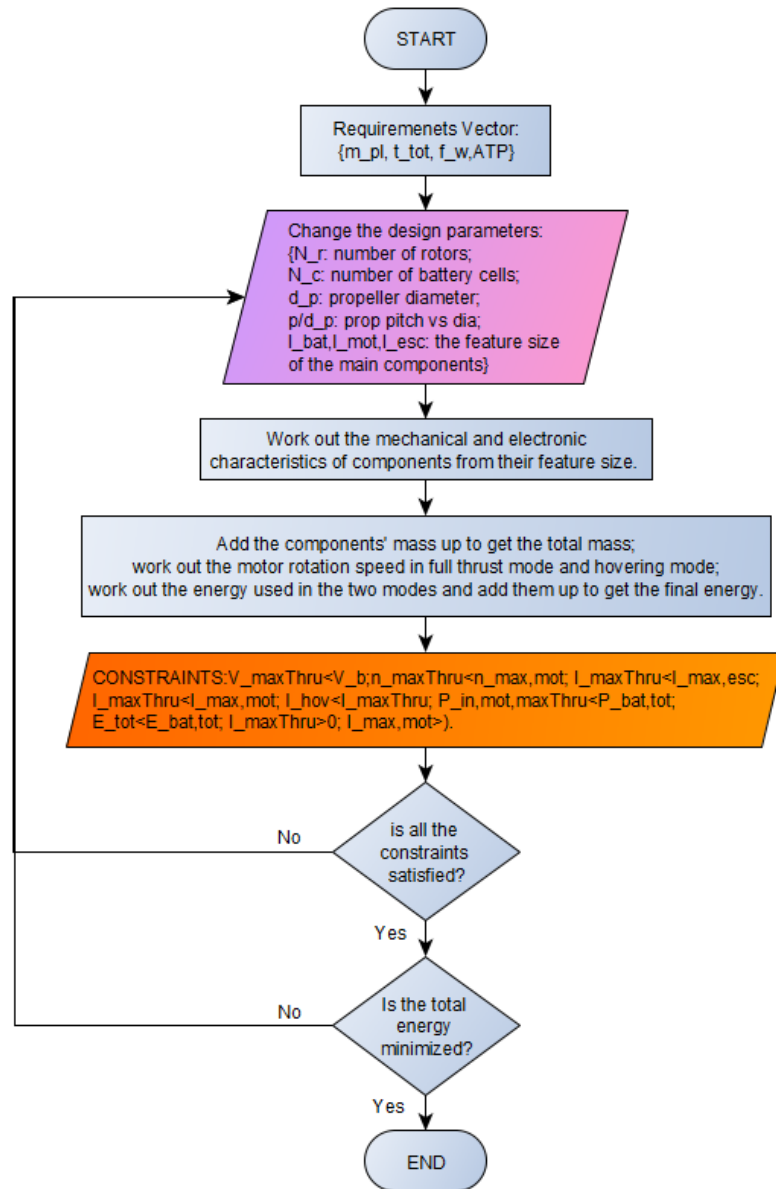
Figure 2.5 The propulsion system optimisation process.
(Ampatis and Papadopoulos, 2014)
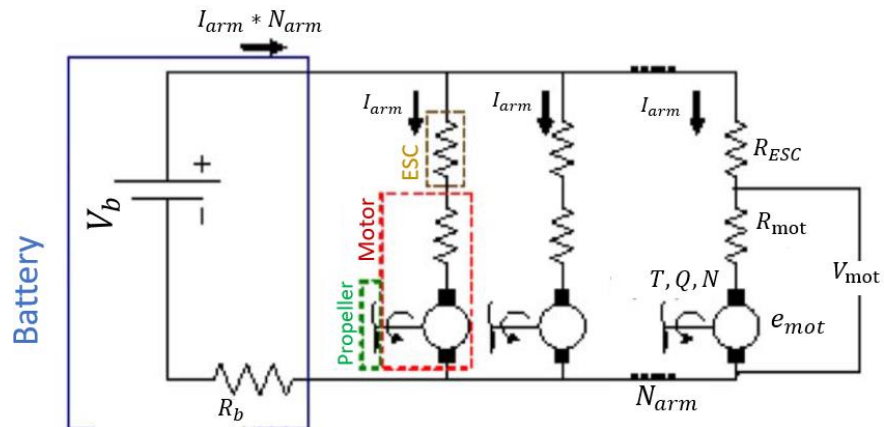
Figure 2.6 The propulsion system physical model in (Ampatis and Papadopoulos, 2014).

In (Mauro Gatti, 2015; Gatti, 2017), based on Raymer's fixed-wing aircraft design process (Raymer, 2012), an algorithm similar to Wang's is proposed. Compared with Wang's algorithm, this algorithm is an improvement in several ways. First, it defines a specific mission, including take-off, hovering, forward flight and landing. It then adopts Raymer's rotary wing aircraft equations to calculate the multicopter's power consumption in these situations. Second, it develops databases for the components and attempts correlate simple relationships between the performance parameter and their mass. This method is more integrated for the optimisation algorithm than selecting components from a candidate pool. Last, it introduces an empty-frame-vs-$MTOM$ factor, which makes it possible to consider the frame design. Gatti also discusses separating the conceptual design process from the further preliminary and detailed design processes. At the end, a thorough discussion on battery design and how battery capacity influences the total endurance is provided.

Winslow, Hrishikeshavan and Chopra (2017) propose a sizing algorithm based on conventional sizing methods for large-scale rotary-wing vehicles (Stepniewski, 1983). It is similar to the process of Raymer and Wang while also having its differences (see Figure 2.7). The basic logic is still to calculate the power and torque first (under both hover and forward flight conditions) and then select each component. Other than the design requirements, the algorithm adds some pre-defined design parameters. Then, by changing the initial $GTOW$ guess, it performs a simple optimisation to achieve the minimum valid $GTOW$. For the components selection, it uses a technique similar to the RTL sizing methods (Stepniewski, 1983) to fit the mass and size estimation equations for components based on their databases. Furthermore, it includes a determination of two types of motors: brushless and brushed. While their paper focusses on small-scale UAVs (30–1000 g), the algorithm is validated using five existing UAV products with an estimation error of less than 20% for each component and less than 4% for the overall $GTOW$.
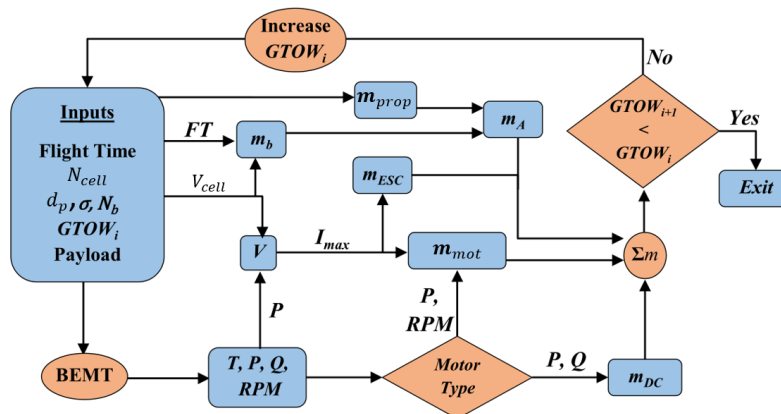
Figure 2.7 Sizing algorithm proposed by Winslow et al.
(Winslow, Hrishikeshavan and Chopra, 2017a)

In (Vu, Dang & Dinh, 2019), the conceptual design procedure for a heavy agriculture multicopter is proposed (see Figure 2.8). This algorithm follows logic similar to Wang, Gatti and Winslow but includes the consideration of atmosphere conditions and the propeller tip velocity Mach number. The component sizing regression uses the same method as Gatti, and the optimisation target is

to minimise the $GTOW$. This algorithm is verified using one commercial platform and is tested in designing a prototype.
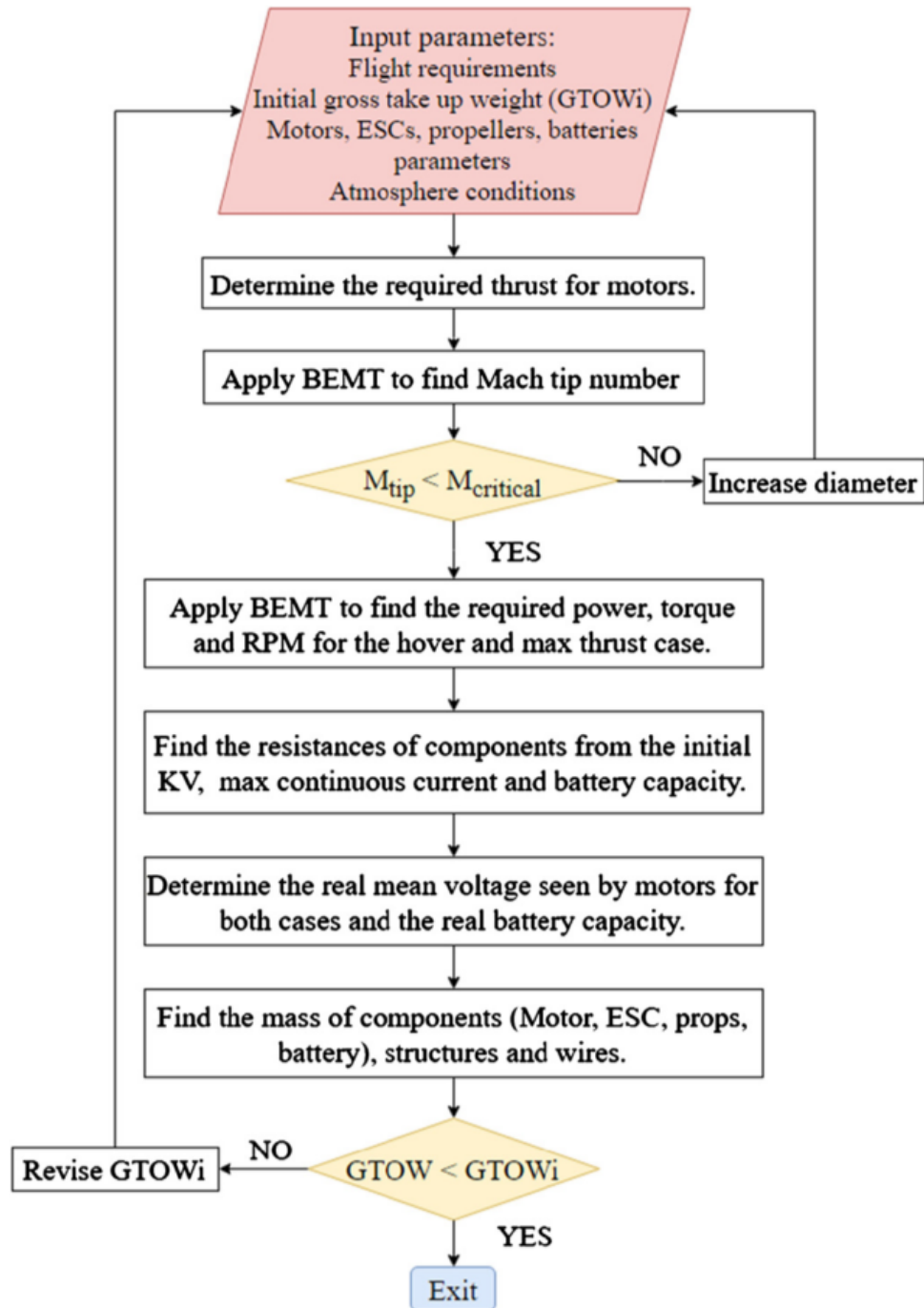
Figure 2.8 Propulsion system sizing algorithm in (Vu, Dang and Dinh, 2019)*.*

2.3 Components Modelling

2.3.1 Frame Design and Simulation

(Nie, 2017) first proposes a design based on experience and then uses ANSYS to perform the simulation on a 1/4 model (which contains only one arm and ¼ body of a multicopter). He stops when the simulation results reveal that the material and structures are safe. (Song and Luo, 2019)

performed a similar FEM analysis for their heavy lift multicopter, while (Liu *et al.*, 2018) pushed the process further. After the proposed design was evaluated, they optimised the arms and central plate by changing the number and angle of the carbon fibre layers and performing FEA simulations for all the combinations.

It can be found from the three studies that the FEA method is time consuming. It is more suitable for the evaluation of a decided structure during the preliminary design phase or the detailed optimisation of the structure during the detailed design phase.

Instead of using FEA methods, the basic material mechanics equations are introduced in the optimisation of the arms. It quickens the calculation process and makes it possible to consider multiple cross-sections and materials. This theory can be used because the arms of multicopters are normally symmetric and of standard shapes. This theory is suitable for the conceptual design phase.

2.3.2 Components Regression Analysis

The regression of components is important for drawing empirical conclusions from the database. This is the typical solution for the conceptual design of fixed-wing aircraft and large rotorcraft; however, such information does not exist for multicopters (Theodore, 2018), so people must collect their own database and achieve the results on their own.

In (Ampatis and Papadopoulos, 2014), the logic of the components sizing is unique. Instead of estimating the components' mass, size and price based on their desired performances, this algorithm introduces feature dimensions for the components. The feature dimensions of all components are part of the vector of design parameters (the input of the optimisation). The author correlates all the parameters of components to their feature dimensions. For example, with a brushless motor, its featured size—say, the diameter—is first guessed, and then its characteristics such as mass, maximum power, resistance, torque constant, KV and maximum rotation speed are estimated with the featured size. Here, the regression equations use the power function. This regression method is unique and is effective to some extent.

Mauro Gatti (2015) provides the most detailed regression of all the important systems, including the motors, propellers, ESCs and batteries; the database contains more than 2,000 models. Linear functions are used for the regression.

In (Winslow, Hrishikeshavan and Chopra, 2017a), the regression is done for the motors, batteries, propellers, electronic speed controllers (ESCs) and frames. However, they followed a different approach. A mixed power function and logarithmic function are used for the regression. The main characteristics and performance parameters of each component are used for these multiple-variable regressions. For example, to estimate the mass of the motor, the KV, output power and maximum current are used as the variables.

In (Russell, Theodore and Sekula, 2018), propeller weight versus diameter, motor weight versus maximum torque, and fuselage weight versus $GTOW$ are concluded. The power function is used for the regression. Although the quantity of data points is too few (only four or five points for each regression), the trend is revealed.

In (Vu, Dang and Dinh, 2019), the regression of the motors and the ESCs used linear functions against the maximum power of the motor and the maximum current of the ESC, and the regression of the propellers used cubic polynomial functions against the diameter. The regression of the battery is special; the battery mass is correlated against the maximum capacity rather than the maximum energy.

2.3.3 Random Forest Technique for Regression

For some complicated regression problems, if they are of high dimension, the random forest technique is traditionally introduced (Ho, 1995; Zhu, Zeng and Kosorok, 2015). Compared with common regression techniques such as the polynomial or Gaussian processes, the random forest technique has the following advantages:

- ability to deal with a high-dimension data set (more than two variables);
- ability to judge the importance of different features (variables) automatically;
- ability to judge the interactions between features;
- not easy to get overfitting;
- easy to realise, and the training speed is fast.

To understand the random forest technique, the definition of decision tree must first be understood. A decision tree is the method of classifying a group of data with a certain measurement. For example, a group of job offers can be divided into several smaller groups (see Figure 2.9). At the end of each tree are the leaf nodes, and the data in each leaf node corresponds to a specific regression function. Therefore, for a given input vector, the tree will first locate the leaf node and then calculate the result using the regression function of that specific leaf node.
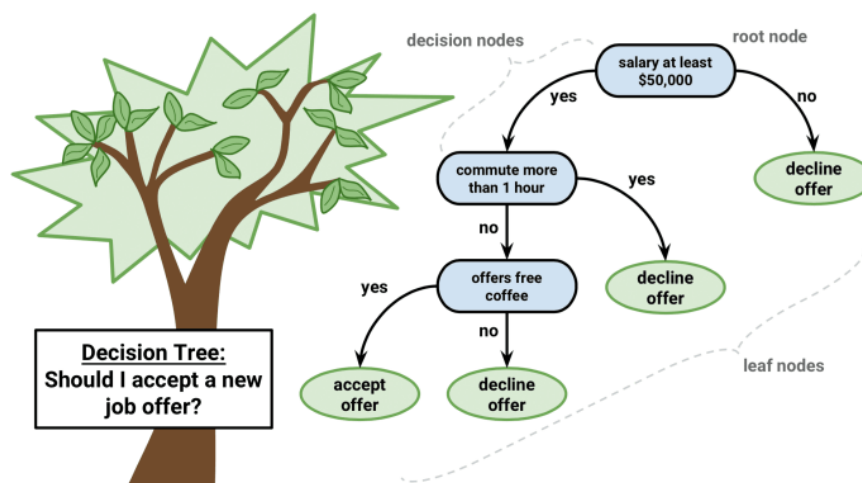
Figure 2.9 An example of decision tree.
Image source: https://towardsdatascience.com/decision-tree-hugging-b8851f853486

17

Briefly speaking, the random forest is used to generate many decision trees randomly for the same data set; the trees are independent from one another. For each tree, the samples and decision nodes are selected randomly. With the given input vector, each tree will produce an estimation result, and the final result of the forest will be the mean prediction.

2.4 Optimisation

There are three levels of optimisations throughout the conceptual design process. At the bottom is the optimisation of each sub-system, in the middle is the process of finding the valid $MTOM$, and at the top is the optimisation of various multicopter configurations.

2.4.1 Sub-System Optimisation

(Liu *et al.*, 2018) introduced the optimisation of the design of the arms and central plate. It is a non-linear, single-target, multiple-variable optimisation process. The main calculation is performed by the ANSYS software, but due to the high computation cost of each run, there are only limited groups of input variables. The optimised result is manually selected from the pool of valid results.

(Weiand *et al.*, 2020) introduced the optimisation of the rotor planform, rotor twist and fuel mass. The COBYLA algorithm is used for the rotor planform optimisation, since it is a constrained problem. For the latter two problems, a trim calculation is performed to determine the rotor twist that requires the least power to hover and the least fuel mass to satisfy the range requirement.

2.4.2 $MTOM$ Optimisation

In the classic design process, an iteration-based method is normally used to find the valid $MTOM$ (Raymer, 2012; Winslow, Hrishikeshavan and Chopra, 2017a; Vu, Dang and Dinh, 2019; Weiand *et al.*, 2020). However, for a certain group of design parameters, the only input is the initial guessed $MTOM$, and after a series of calculations, the only output is the estimated $MTOM$. By taking the difference between the two $MTOM$s as the optimisation target, this problem becomes a non-linear, single-variable, single-objective optimisation process.

2.4.3 Multicopter Configuration Optimisation

Each converged $MTOM$ produces a valid design which corresponds to a particular group of design parameters (Winslow, Hrishikeshavan and Chopra, 2017a; Vu, Dang and Dinh, 2019), called a 'configuration'. One ability of the conceptual design is finding the most suitable configuration for a certain mission. The common design parameters include the rotor diameters, number of rotors and battery number of cells, among others. The main design parameters are normally discrete integers and have a finite number of candidate values. Then, there is a series of combinations of different design parameter values. The $MTOM$ is then calculated for each combination. If the $MTOM$ can converge and the results satisfy all the constraints, then this configuration is considered valid. A list of valid configurations is then determined, and each has different performances for $MTOM$, price, endurance, maximum speed and total energy consumption. Optimisation is then performed by ranking one selected performance parameter for

a single-objective optimisation or ranking multiple performance parameters for a multiple-objective optimisation.

The algorithm proposed by Ampatis and Papadopoulos (2014) is an exception to the aforementioned procedure. This algorithm does not include the iteration-based $MTOM$ convergence process; alternatively, it uses the design parameters directly as the input and then determines all the parameters of each component and finally the target parameter to be optimised. The 'fmincon' algorithm is used to perform a constrained optimisation. By doing so, the scale of automation is increased, and it can more easily be used. When the range of the design parameters is decided, the algorithm can automatically run until it finds the optimal result; however, the drawbacks are apparent. The required number of calculation tasks is much more than in the traditional approach. To avoid the $MTOM$ convergence process, it must introduce several more parameters as the input. Moreover, some of the parameters are of a continuous range. These conditions cause the number of calculations to grow exponentially. Therefore, although unique and effective, this algorithm is not suitable for conceptual design.

In most of the studies, the optimisation of the configuration is for a single objective. However, a multicopter can be evaluated by many performance parameters, of which the common ones include the $MTOM$, price, endurance, maximum speed and total energy consumption. When considering more than one parameter, the pareto front appears (Hassanzadeh and Rouhani, 2010). For example, with mass and price, cheaper and lighter designs are preferred; however, for some designs, it is no longer possible for both parameters to be optimised. That is, for design configuration A, a cheaper and lighter design configuration B does not exist, yet there could exist cheaper but heavier, or more expensive but lighter solutions C and D. Then, a vector containing A, C and D becomes the objective vector, and the vector includes all the points similar to A, C and D. The shape of this vector is the pareto front.

Zhang, Xue and Gong (2005) reviewed the main optimisation methods for multiple-objective aircraft design and optimisation. When there are multiple optimisation targets, the following methods can be used. Most attempt to convert the original problem with multiple objectives into a single-objective optimisation problem.

1. Linear scalarisation
2. The compromising (ϵ constraints) method
3. Classify the objectives by importance, then solve the problem one after another.
4. Develop an overall function which considers all objectives and their preferred value.
5. No-preference methods

In the realisation of the multiple-objective optimisation, the genetic algorithm (GA) is used in a particular aircraft design problem. The single-objective and multiple-objective optimisation results are then compared. The proposed algorithm is validated, and the results suggest that single-objective optimisation can produce the optimal solution for a single objective, though normally in

sacrifice of other performances, while multiple-objective optimisation can ensure overall satisfaction.

2.5 Conclusions

It can be seen from the literature that there exist a mature design process and tools for the fixed-wing aircraft and rotorcraft. It is during the conceptual design that design configurations are compared and the most suitable solution for further design phases is determined. However, the condition is different for the design of multicopters.

1. The design process of multicopters is gradually reaching perfection. Different approaches are available, but a typical and efficient approach is similar to the traditional procedure. In different literature, the proposed design procedures have different emphases, and hence do not consider the entire aircraft. Thus, a complete conceptual design procedure which combines the advantages from the various literature is proposed.

2. One obstacle of introducing large-scale rotorcraft design tools into the design of multicopters is that the empirical conclusions are not suitable for the scale of multicopters. This can be solved by collecting information and making new regressions. The regression results of some key literatures are reviewed, and it can be found that different approaches are utilised. In this thesis, information was collected, and my own databases were built. The regression results from previous literature are validated by the databases. A problem was found and was solved by introducing the random forest technique for regression. The new technique improved the accuracy of estimation and expanded the applicable range of component models.

3. In the literature, the design of the frame and arms is completed with the help of FEA tools such as ANSYS. Although more accurate, such an approach is more time consuming and thus is not suitable for the conceptual design phase. For this reason, a mathematical optimisation tool based on basic material mechanics principles is proposed for the design and optimisation of the arms. This tool simplifies the problem and is faster.

4. Most of the literature focusses on the optimisation of a single target, either the $MTOM$ or the maximum endurance. In this thesis, the proposed algorithm considers up to five targets. Although the optimisation process is still single objective, the result is a valid design configuration pool. It is possible for further multi-objective optimisation analysis.

5. The most discussed flight condition is hovering, and not many studies considered other flight conditions, such as forward, ascending and mixed forward-ascending. In this thesis, the proposed algorithm considers all possible flight conditions.

Chapter 3 Parametric Design

The main procedure of the parametric design is introduced in this chapter. A flow chart is presented first, followed by a detailed discussion of the individual parts. Finally, the appropriate range and impact of parameters are discussed.

3.1 Introduction to the Design Framework

This procedure begins with the requirements and follows a two-layer optimisation. At the top layer, the design parameters change to form different combinations, called configurations. At the second layer, for each specific configuration, a constrained optimisation is completed to find the optimal $MTOM$ which leads to the minimum $MTOM$ error (convergence). When coding, a third layer is added for the general functions called by the second-layer process.

The requirements include three elements: mission requirements (constraints), mission descriptions (waypoints and behaviours) and constants. The layer_1 process reads in the requirements and loops through all the configurations (combinations of all possible values of the design parameters). For each configuration, an optimisation process is proceeded, calling the layer_2 function (see Figure 3.1). There may be one or no valid solution for each layer_2 function that is run. After proceeding through all the configurations, a pool of valid candidates is created, and the optimum design for any given target can be selected from the pool.
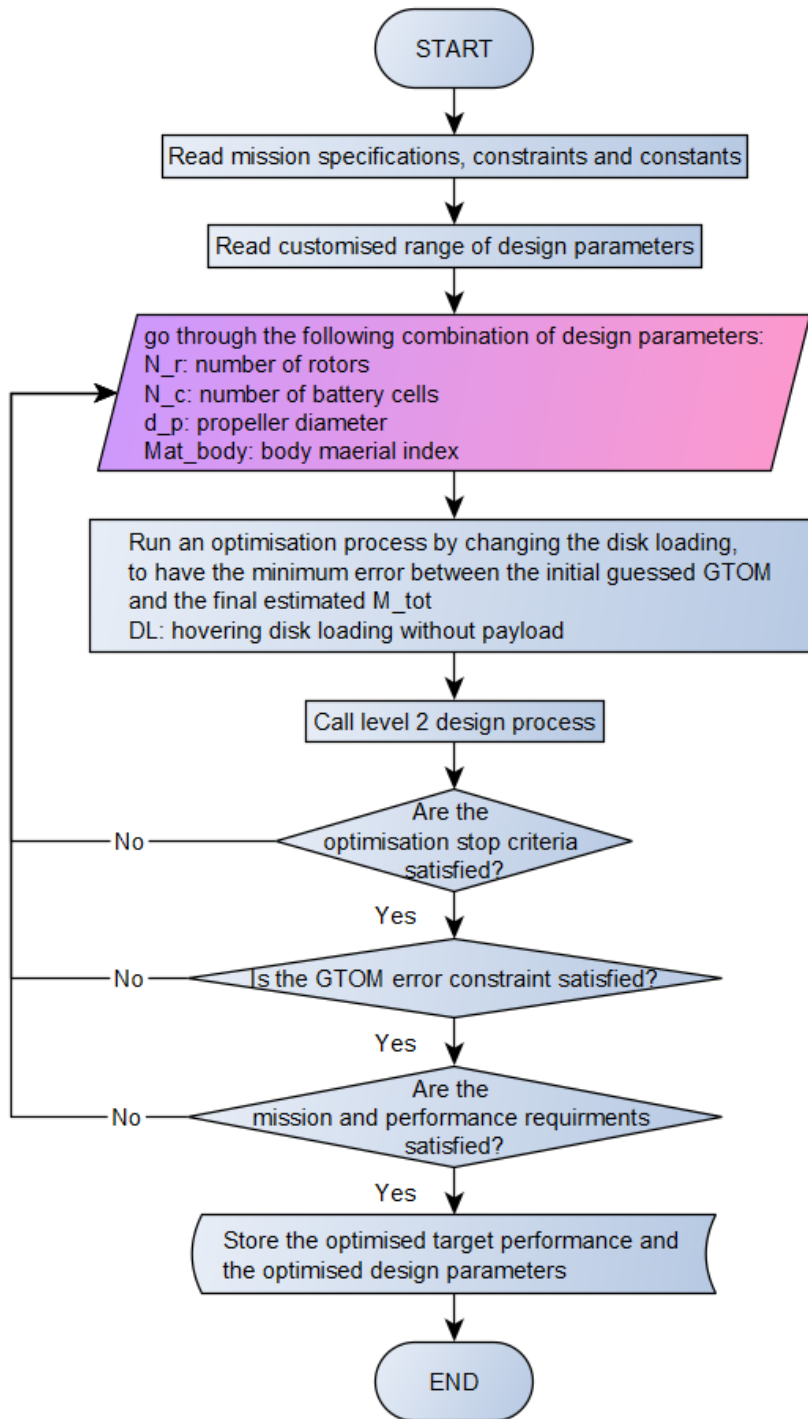
Figure 3.1 Level One design process: get optimised design parameters.

In each layer_2 process, the calculation chain follows an outside-in sequence, as follows: initial guessed $MTOM \rightarrow$ basic parameters calculated from a specific group of design parameters $\rightarrow$ aircraft movement $\rightarrow$ propeller performance $\rightarrow$ motor performance $\rightarrow$ electrical condition in the system $\rightarrow$ battery performance $\rightarrow$ mechanical conditions $\rightarrow$ frame design $\rightarrow$ whole aircraft (see Figure 3.2). The final estimated $MTOM$ subtracted from the initial guessed $MTOM$ is the $MTOM$ error. Only when the $MTOM$ error is close to 0 and the middle parameters pass all the constraints checks is the configuration considered valid.
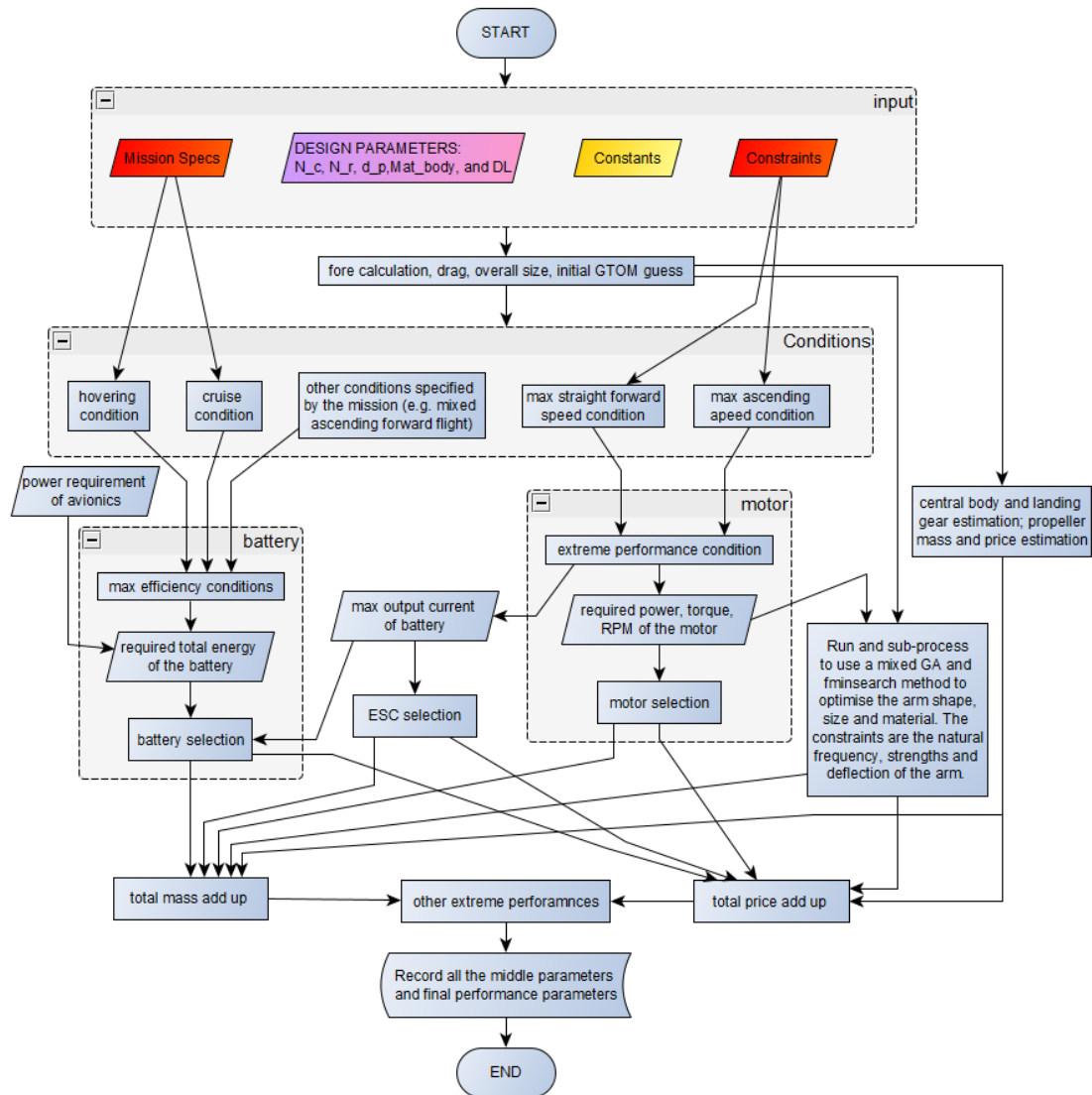
Figure 3.2 Level Two design process: the optimisation of $MTOM$ and price.

Three types of input must be explained. Provided below is a brief introduction, and more detailed lists can be found in Section 3.3.1.

- Mission requirements, also known as constraints.

The mission requirements form the foundation of the entire design process; they are the start points and evaluation standards of the design. The requirements should include three parts: 1. A list of performance specifications, which include but are not limited to the maximum forward velocity, maximum ascending velocity, maximum tilt angle, maximum endurance for a certain operation condition, maximum payload, range of permitted $MTOM$, size and cost, and maximum service ceiling, among others. 2. An example of the mission process, which is divided into phases by action, such as take-off, hovering, cruising and so on. The payload and aircraft speed on two axes should be specified. 3. The optimisation target: $MTOM$, cost, endurance or consumed energy.

- Design parameters

The design parameters are key for the design of a multicopter; by changing them, the multicopter's appearance, performance and characteristics will be altered. The four main design parameters considered in the process are 1. the number of rotors, 2. the number of battery cells, 3. the diameter of propellers and 4. the material of the body. Of course, there are more parameters necessary for designing a multicopter, but according to the five key studies, these four parameters are considered to most significantly influence the final result. The other independent parameters considered in this process are the cross-section shape of the arms, the dimensions of the arms and the material of the arms. Each parameter has a variety of options; it would be too time consuming to consider all possible options, so switches are set up for each option. Then, the algorithm can only go through the turned-on parameter values. The remaining parameters are in the following category.

- Constants

Three types of constants are used in the proposed design process. 1. Physical constants, which include the standard gravitational acceleration, air density at standard sea level and 15°C, Young's modulus, shear modulus and density of selected materials, among others. 2. The engineering coefficients, which are primarily empirical numbers that help with engineering calculations, such as the voltage per cell of Li-Po batteries, propeller efficiency and motor efficiency, among others. Some less significant design parameters are normally detailed parameters of certain parts and influence the coefficients used for design. For examples, the pitch, chord and number of blades of a propeller determine its coefficients of thrust, coefficient of power and solidity. These coefficients then influence the efficiency of the propeller; thus, once the propeller efficiency is assumed, the detailed design of the propeller is no longer necessary to consider in this stage. After all, the conceptual design phase focusses more on the performance and characteristics of the aircraft as a whole, proposing only the requirements for subsystems. The detailed design of subsystems, such as propellers, motors and body, among others, should be saved for later design phases. 3. Some of the important design parameters can be treated as constants, such as the ratio between the adjacent propellers' tip distance and the propeller diameter. This ratio is used to calculate the minimum arm length from the propeller diameter. This parameter is important because when the two adjacent propellers are too close, the air between them might become turbulent flow, which causes power loss of the propeller or a possible unexpected accident. Empirically, the minimum number of this ratio is near constant in many sources, so in this algorithm, it is treated as a constant coefficient (see Section 4.3.1).

The use of empirical coefficients is to avoid an unnecessarily complex model in the conceptual design stage; by doing so, the calculations are simplified. The sacrifice of accuracy can be kept within an acceptable range given reasonable values of these coefficients based on certain assumptions. The determination of the values of these coefficients is explained, and the sensitivity of the design process to these coefficients is analysed later in this chapter.

3.2 Tools Introduction

3.2.1 Programming Tool

MATLAB is the main tool used for programming the entire process. As it has abundant libraries (such as Math, Statistics and Optimisation) and community support, it provides powerful graphics tools. The structure of the program is as follows: The start-up file reads all the input from an Excel file and then calls the corresponding functions to perform the optimisation. The aforementioned Level One and Level Two processes are two independent function files. Level Three functions typically involve the detailed calculation, such as the power consumption in the hover condition, which is called in the Level Two process. The code has been uploaded to GitHub for version control.[1]

3.2.2 Database Built-Up

Since many models of multicopter components exist in the market, it is possible to proceed the design process using a statistical method. Then, a component database is necessary.

The data used to construct this database came from two main sources:

3.2.2.1 Existing Databases

a. OscarLiang's database

This is a personal blog. The blogger himself collected the information and made a spreadsheet database of the electronic components on a multicopter. This up-to-date database includes 168 entries of ESC,[2] 138 flight controllers,[3] 78 video transmitters (VTX)[4] (video transmitter) and 93 first-person-view (FPV) cameras.[5] The focus of this database is on micro UAV, and the mass of the components is mostly less than 30 g.

b. A Li-Po battery database shared by user andrew_c80 on rcgroups.com.[6] This database contains 437 battery models from multiple manufacturers; however, the database is somewhat out of date, since it stopped being updated in May 2008.

c. QuickCode (previously called ScrapperWiki) is a cloud web crawler service provider. In the past, it had a community for users to share the data they gathered. There was an anonymous user who shared a database containing 355 motors and 827 batteries from Hobbykign.com in 2012.[7] One drawback of this database is that it does not provide the manufacturer and brand info for all entries.

d. Some model calculator software came with their own databases. An up-to-date database was extracted from DraveCalc and contains 310 batteries, 260 ESC,

---

[1] https://github.com/rechalsunshine/Multicopter-Preliminary-Design-Tool

[2] https://docs.google.com/spreadsheets/d/1SYzJWKTu2vFVL99mt5tQxc2sTiHCXNAEZyGodfy3uE0/edit#, last updated: 01/02/2019

[3] https://docs.google.com/spreadsheets/d/1VuBpQVZflz5zVNUG43gKTg4Mkwt-cTssWvb1CGgskQk/edit#gid=0, last updated: 01/02/ 2019

[4] https://docs.google.com/spreadsheets/d/1YD3765S2pcZbyNis_38R2RCZ7TEfM1g-hvfXmU3pX2E/edit#gid=0, last updated: 01/02/ 2019

[5] https://docs.google.com/spreadsheets/d/1SFix5Wn8JDl5O6t0xeb-lngUiH41K2OIkpptk8hzAm4/edit#gid=0, last updated: 01/02/ 2019

[6] https://www.rcgroups.com/forums/showthread.php?742175-Lipo-and-LiMn-Searchable-Database-ver1-3-UPDATED, last updated: 12/05/2008

[7] This service is no longer available now, and the publisher can no longer be found.

260 motors and 349 propellers. Another incomplete database was extracted from XcopterCalc, which includes 9132 motor models; however, due to the website's copyright protection, these entries only provide the mass and output power of the motors.

e. Other small groups of data were shared on hobby forums. Due to the small quantity of entries, they were all added into my own database. Although their sources are not traceable, they have been manually checked, as with the other self-collected entries.

f. There is a flight review website supported by the PX4 team.[8] Users of Pixhawk autopilot can upload their flight log data to the database for further analysis. This database contains more than 20,000 flight logs since 2016.

3.2.2.2 Self-Collected

Most data was collected manually or using crawler/spider tools from mainstream hobby stores and top brands' official sites, such as Hobbykings.com, Banggood.com, rotorrating.com, flybrushless.com and tmotor.com.

The tool used to automatically crawl data from these websites is LocoySpider. The basic mechanism of this tool is to find a pattern of a certain type of data (such as the price) in the source code of its webpage by going through the webpages of all the products and recording the price of each.

This tool makes it possible to gather much data over a short time, but it can be difficult to avoid incorrect data being recorded. This might occur for several reasons, such as the website itself providing incorrect data or a specific webpage having changes in the source code which cause the spider to record data at the wrong place. Despite these errors, most of the data is correct. After the data was collected, a sampled manual review was conducted, in which 'odd' entries were checked.

The self-collected database currently contains a total of 2,033 batteries, 187 ESC, 1496 motors, 363 propellers, 104 frames, 92 flight controllers and three landing gears.

In addition to the database of components, there is a database of commercial multicopter products. This database includes all information about a multicopter, such as the basic information of the size, mass, price, main performances and detailed geometry parameters. It also includes the components used by the multicopter, and the components are connected to the components database by calling the specified component ID. Most of the information came from the official product specification, and some review and test articles were considered when the data is not included in the specification. Since there is no uniform format of the specifications from different manufacturers, it is difficult to autonomously collect these data, so this data-recording

---

[8] https://review.px4.io/browse, still in service.

work is completely manual. Two windows were created to simplify this work (see Figure 3.3 and Figure 3.4).

Figure 3.3 The "Add Entry" window.

Figure 3.4 The "Add Shape Parameters" window.

27

3.3 Level One Design Process

The Level One process comprises four tasks: 1. reading data, 2. looping through turned-on design parameter options, 3. proceeding an optimisation for the selected group of parameters and 4. recording the result and determining the optimal design.

3.3.1 Input Data[9]

3.3.1.1 Mission Specification

There should first be a mission specification, which includes two parts: the mission description and required performance (constraints).

A mission description describes what happens during the mission and how the multicopter should behave; an example is provided in Table 3.1. In this mission, the multicopter takes off (vertical ascent) for 15 s, reaching the height of 30 m. It then flies to the target location, forward 600 m for 120 s. Afterwards, it performs a surveillance mission, hovering at this location for 600 s. Finally, it returns and lands. During all the phases, it carries the same payload, which is a passive unit not powered by the multicopter. Since multicopter aerial carrier configuration and aerial delivery are potential applications, the payload and its power draw may change over the phases in some missions. The payload is defined as any device onboard that is not necessary for ensuring the aircraft to fly but is useful for the mission. Typical payloads include a camera, goods for delivery, gripper or water tank, among others.

Table 3.1 An example mission description.

Phase	1	2	3	4	5
Behaviour	take-off	forward flight	hover	forward flight	landing
Flight Time/s	15	120	600	120	15
Horizontal Displacement/m	0	600	0	600	0
Vertical Displacement/m	30	0	0	0	-30
Payload/ kg	0.5	0.5	0.5	0.5	0.5
Payload power/ W	0	0	0	0	0

The flight time and payload to be carried determine how large and heavy the final aircraft is. Based on the flight time and displacement in a phase, the average velocity in vertical and horizontal directions can be calculated. The velocities are used to work out the required power, which is then combined with the flight time to determine the required amount of energy. The total energy required through all phases finally determines the size and mass of the battery.

Here, the average velocity is used as a simplification of real movement (see Section 3.4.5.1 for justification), so only the average performance of the motors is reflected. To decide on the extreme performance of the motors, there must be more technical requirements, which leads to the table of constraints (see Table 3.2).

---

[9] The ISO unit system (m, s, kg…) is used through the algorithm. But in the analysis, for convenience, other units may be used, and they will be specified.

Table 3.2   List of constraints.

Name	Symbol	Unit	Reference values or range	Default
Maximum $MTOM$	$MTOM_{max}$	kg	0.1-20	inf
Maximum Size	d_{max}	m	0.1-2	inf
Maximum Cost (Budget)	pr_{max}	$	100-10000	inf
Maximum Forward Velocity	v_{f_max}	m/s	10-30	0
Maximum Ascending Velocity	v_{a_max}	m/s	3-10	0
Including max payload in maximum velocity forward or upward flight?			0 or 1	0
Endurance for Hovering	E_h	s	180-2400	0
Endurance for Cruising	E_c	s	180-2400	0
Standard Payload Mass	m_{PL_std}	kg		0
Standard Payload Power	P_{PL_std}	W		0
Standard Cruising Speed	v_{cr_std}	m/s	3-12	5
Avionics Power	P_{av}	W	2-20	2
Avionics Mass	m_{av}	kg	0.05-0.5	0.05
Landing Gear Height	h_{lg}	m		0
Landing Gear Mass	m_{lg}	kg		0
Thrust to Weight Ratio Range	TrW		1.4-15.4	
Disc Loading Range	DL	N/m^2	14.2-134.3	
Optimisation Target	$MTOM$, total price, total energy consumption, total endurance, maximum speed, etc.			

The typical values and range of the constraints are only for reference. They are concluded either from market surveys or from existing multicopters in the database. By default, there are no limits to these parameters (set to value '0', for the upper boundary constraints, use '0' to represent 'infinity'), unless there is a requirement. This table must be determined prior to design. The following are explanations of the above constraints:

- The first three constraints are the upper boundary constraints established by the user based on his or her budget, preference and the operation scenario. They are not involved in the calculation but are used to filter out satisfactory results (see Section 3.4.5.3). From a practical point of view, the $MTOM$ and size may be limited by aviation regulations and the terrain and space of the application. To clarify, $MTOM$ refers to the maximum take-off mass, which includes all the components and the maximum possible payload. $GTOM$ refers to gross take-off mass and represents the mass of a fully functional aircraft without any payload. The size of a multicopter is measured by the axial distance between two diagonal motors.

- The maximum forward velocity and maximum ascending velocity directly join the calculation of the extreme performance of the propulsion system (see Section 3.4.4). They are the requirements of the user and significantly impact the final design. By default, in the maximum velocity mode, the payload is not included in the calculation, but the switch can be turned on by the users.

- The expected endurances (for hovering and cruising, with or without the payload) are equivalent to single-phase missions, in which the multicopter should only hover or cruise. These parameters indicate the endurance ability of a multicopter based on various aspects. They serve as additional information to understand the performance of a multicopter. Compared with the full mission description, which might be complicated, the

endurances are more straightforward, presenting an overall requirement for the power source. The expected endurances serve as constraints; after the total energy is calculated from the mission description, available endurances are calculated for comparison with the expected values. The standard payload mass, payload power and cruise speed are necessary parameters for determining the power consumption in the endurance calculation.

- Avionics are defined as the necessary electronic components, except for motors and ESCs, that ensure the multicopter flies. They include only the autopilot, IMU sensors, signal receiver and antenna, power distribution board or power module, and the battery elimination circuit (BEC). Any other components are considered part of the payload (such as a camera, video and OSD[10] transmitter). Although they are involved in the main calculation process, they are kept the same throughout different design parameters (i.e. the avionics should be decided before the algorithm, and the mass and power should be known in advance).

- The main purpose of the landing gear is to provide sufficient clearance for the payload. Its height varies greatly with the size of the payload rather than the size of the frame. It is best for the landing gear to be decided prior to the design process. As with the avionics, its mass remains unchanged throughout all the design parameter combinations, but it is involved in the main calculation process.

- The thrust-to-weight ratio is one of the algorithm results. It is calculated based on the maximum total thrust and the $MTOW$ (see Section 4.3.7). From the aircraft database, the range of typical thrust-to-weight ratio is concluded. This range is used as a constraint to check whether the result is reasonable. Normally, this number will not likely exceed the upper boundary, but if this number is too small and exceeds the lower boundary, this indicates that the design lacks basic manoeuvrability and therefore is not valid.

- The hovering disc loading is the only variable of the Level Two process. Based on its definition, it is equivalent to the initial guessed $GTOM$ (see Section 4.3.8). Furthermore, it can indicate the loading condition on a propeller. For different purposes, the disc loading of an aircraft varies. However, when the disc loading is too large, the propeller may be under serious burden, the efficiency may be greatly reduced and the model used in the algorithm may fail. Thus, a reasonable range is necessary. Since disc loading is the variable of the Level Two function, the upper and lower boundaries are set up in the optimiser options before the Level Two function is called.

- The optimisation target is a flag for the algorithm to select the corresponding solution. This flag is also useful for the sub-optimisation process of the arm, since the optimisation for the minimum mass and lowest cost are two different processes.

---

[10] OSD: On Screen Display

The maximum tilt angle, maximum angular velocity and angular acceleration are other important performance indicators. They are often provided in the specification of multicopter products; however, they are not constrained in this conceptual design algorithm. In this algorithm, the maximum tilt angle is determined by the maximum thrust (see Section 4.3.9), while the maximum thrust is determined by the maximum speed (see Section 3.4.3). When the maximum speed is constrained, the parameters on this chain are all constrained. The angular velocity and acceleration are related to the moment of inertia of the frame; while this parameter concerns the frame's shape and configuration, it has little influence on the $MTOM$ and total size. For a motor, only the extreme performance is required to determine its mass and price. Thus, the angular velocity and acceleration are unnecessary parameters for motor calculation, as well.

There are other actual requirements for each mission, but due to the lack of influence on the design parameters, they are listed here but are not considered in the design process. This is due to their own nature and the fact that they are not included in the algorithms of the five key studies. They can be thoroughly considered in further design stages. To simplify the conceptual design process, unless specified, the multicopter is assumed to be operated in a wind-free space of 15°C.

- Maximum operational wind speed
- Operational range of temperature
- Hovering accuracy (drifting rate)—decided more by the accuracy of sensors and the control system rather than the mechanical structure.
- Appearance (for conceal purpose or specific preference)
- Communication range (communication device could simply be considered a payload)

3.3.1.2   Design Parameters

The design parameters are structural parameters of a multicopter which determine how the multicopter looks. A multicopter may have many design parameters, but in this algorithm, only the most important six parameters are considered (see Table 3.3). The design parameters are given in the form of switches so that users can turn off the unwanted options to reduce the size of the candidate pool and thus reduce the calculation time. The first four parameters are looped, exterior to the optimisation process (i.e. the optimisation would run for each given combination of design parameters). The last two parameters are used in the layer_3 arm optimisation sub-process.

From the six main design parameters, with the help of some empirical constants, most of the design parameters can be determined, and the structural design of the aircraft can then be decided; however, this design is simply a standard design, sufficient for the conceptual design stage. In later design stages, more design parameters can be introduced to design a certain part in detail. For example, the number of propeller blades is an important parameter for propeller design, affecting the solidity ($\delta = \frac{A_{blades}}{A_{disk}}$) of the rotor, which influences the FM and efficiency of the propeller. However, in the conceptual design stage, only the diameter and efficiency of the propeller are necessary to the algorithm; thus, the empirical constants of FM and η_p allow the

calculation to be far simpler without losing much accuracy. The desired efficiencies then become the propeller's design requirements. Based on the requirements, users can select or design any satisfactory products.

3.3.1.3   Constants

Due to the large number of constants, they are not introduced here. A full list can be found in Appendix A. In the following sections, the constants are introduced in detail as they are used in the calculation.

The material characteristics are presented in the second part of the list. Among the four materials, only carbon fibre has relatively complete pricing information on certain cross-section shapes. In the algorithm, only carbon fibre has a price estimation.

3.3.2 Optimisation and Constraints Check

When all the inputs are loaded, before the design parameters are looped, the optimisation method options are set up; the 'fminsearchcon' method is used here. 'fminsearchcon' is a nonlinear programming solver which searches for the minimum of a constrained multivariable function using a derivative-free method. 'fmincon' and 'ga' are the two most commonly used optimisation algorithms. Due to the complexity of this aircraft design question, 'fmincon' can hardly converge to the correct minimum. Compared with 'fminsearchcon', 'ga' is too time consuming, and the optimisation results are not necessarily the minimum. Thus, 'fminsearchcon' is the most appropriate method for this question.

The options of 'fminsearchcon' include the function to be called, the upper and lower boundary of the variable, the start point and the stop criteria. The function to be called is the layer_2 function, which is the most significant process in this algorithm. The layer_2 function accepts DL as the only variable and returns the error ratio ($err_{percent}$) between the initially guessed empty mass ($GTOM_0$) and the finally estimated empty mass (m_{tot}). The boundary of the variable is the range of DL specified in the constraints list. The starting point is the minimum boundary, as there exist multiple local minimums (see Figure 4.5), but only the left-most one (minimum $GTOM_0$) is the desired result. Starting from the minimum boundary can ensure that the solver converges at the correct solution. The stop criteria include the maximum iteration and minimum accuracy of the change between two iterations. When the solver converges, if the error of the outputs between two iterations is smaller than the minimum accuracy, the optimisation will stop. If the solver cannot converge, it will also stop when the maximum iteration is reached. The stop criteria determine how long the optimisation process will take.

Ideally, $err_{percent}$ should be equal to zero for a best-fit design. However, in reality, the algorithm cannot always achieve this result. Hence, an absolute threshold of 5% is set for $err_{percent}$. When the M_{tot} is larger, the design parameters are not sufficient for fulfilling the requirements. In this situation, the threshold ensures that the gap is not too large and can be easily covered in later design stages.

Table 3.3   List of multicopter design parameters.

Name	Symbol	Typical values or range			Comment
Number of Rotors and Arms	N_r, N_{arm}	Number of rotors		Coaxial?	The number of rotors directly decide the total thrust and the disc loading, and it has a large influence on the hovering stability. For coaxial configurations, there are two motors on each arm. The number of arms is related to the total size of the aircraft. There are in total six configuration candidates, they are non-coaxial Quadcopters, Hexacopters and Octocopters, and coaxial Exacopters, Quadcopters, and Hexacopters. Although introduced here, the calculation of coaxial rotor system is not included in the algorithm yet. It will be left to future works.
		4		0	
		6		0	
		6		1	
		8		0	
		8		1	
		12		1	
Number of battery cells	$N_c = \dfrac{U}{U_c}$	Centre		Range	In this design algorithm, Li-Po battery is by default used. The voltage of a single Li-Po cell is a constant, thus, the total voltage of the system is decided by the number of cells. To increase the voltage can effectively reduce the maximum current in the system as well as increase the maximum thrust. Appropriate numbers should be estimated in advance according to the mission requirement. The candidates are determined by "Canter $\pm$ Range". As in the left example, the candidates would be 2,3,4,5,6,7.
		4		2	
Propeller diameter	d_p	Min	Max	Step	Larger propeller has better propeller efficiency, but the propeller should also match the motor to have a better motor efficiency. In design, a suitable combination of propeller and motor need to be decided so that they can provide enough thrust in the most efficient way. The candidates are given as a range and step. As in the left example, the candidates would be 5,7,9,11 inches.
		5	11	2	
Body Material		Index	Material		Different material has different density, unit price and mechanical characteristics. To reach the desired strength, the material could be "light and expensive" or "cheap but heavy". Different material would be selected for different purposes. There are currently four candidates. Carbon Fibre and Glass Fibre are the two most commonly used materials in the market.
		1	Carbon Fibre		
		2	Glass Fibre		
		3	ABS plastic		
		4	Aluminium		
Arm Shape		Index	Material		The cross-section shape of an arm would have a great influence on its mechanical performance. There are eight candidates for the arm optimisation subprocess. The most commonly used arm cross-section shapes are rectangular and hollow oval.
		1	rectangular		
		2	hollow rectangular		
		3	hollow oval		
		4	T section		
		5	channel		
		6	L section		
		7	I section		
		8	H section		
Arm Material		Index	Material		Normally the arms use the same material as the body, but mixed material design are also an option. The arm material candidates are the same as the body material.

DL is the only variable that changes during the optimisation process; however, many other parameters are involved in the calculation, such as the design parameters, constants and mission descriptions. These parameters remain constant in a single optimisation run but may change between different runs. Due to the requirement of 'fminsearchcon', the called function can have only a single output; however, many other middle parameters are of interest. For the aforementioned reasons, several global parameters are defined to transfer data between functions in different levels (see Table 3.4).

After the options are set, the candidates of the four main design parameters are proceeded through by a four-layer loop structure. For each combination, the optimisation runs once, producing $err_{percent}$, err_{flag} and FUN_{output}. err_{flag} is a series of Boolean-form data, with each entry representing a type of error. If a constraint is not meet, the corresponding entry is set to 1. If $err_{percent}$ is larger than the threshold (design parameter does not fit the mission requirement), or the sum of err_{flag} is larger than 0 (exist constraints errors), the result is invalid. Otherwise, the results from FUN_{output} are recorded in the matrix parameter $results$.

Table 3.4   The main global parameters.

Symbol	Comments
C	Constants, $n \times 1$ vector, defined in layer_1 function and being used in all sublevel functions.
$DsPm$	Design Parameters, $n \times 1$ vector, defined in layer_1 function and being used in layer_2 function.
$Cstr$	Constraints, $n \times 1$ vector, defined in layer_1 function and being used in all sublevel functions.
MP	Material properties table, $n \times m$ matrix, defined in layer_1 function and being used in all sublevel functions. m is the number of materials.
MPr	Material prices table, $n \times m$ matrix, defined in layer_1 function and being used in all sublevel functions. m is the number of materials.
	Trained motor estimation forest models.
err_{flag}	Error flags, $1 \times n$ vector, defined in layer_2 function and being checked in layer_1 function.
FUN_{output}	Function outputs, including all the necessary middle parameters, such as the detailed mass and price of each component, and their performances. $1 \times n$ vector, defined in layer_2 function and being checked in layer_1 function.

At the end of the function, all the design parameters' combination candidates are calculated, and all valid results are recorded. Finally, the best design (such as the lightest design or cheapest design) is selected based on the optimisation target.

3.4   Level Two and Level Three Design Processes

3.4.1 Brief Intro and Process

The Level Two design process begins with a guess of disk loading (DL), which reflects the $GTOM_0$ and ends with two equations: (1) and (2). They are simply a summation of the mass and price of all components:

$$m_{tot} = N_r \cdot \left(m_p + m_m + m_{ESC}\right) + N_{arm} \cdot m_{arm} + m_{body} + m_b + m_{av} + m_{lg} \tag{1}$$

$$pr_{tot} = N_r \cdot \left(pr_p + pr_m + pr_{ESC}\right) + N_{arm} \cdot pr_{arm} + pr_{body} + pr_b \tag{2}$$

In the above equations, m_{tot} is the calculated gross take-off mass (total mass without payload), N_r is the number of rotors, m_p is the mass of a propeller, m_m is the mass of a motor, m_{ESC} is the mass of an ESC, N_{arm} is the number of arms (for coaxial configurations, $N_r \neq N_{arm}$), m_{arm} is the mass of an arm, m_{body} is the mass of the central body frame, m_b is the mass of the battery, m_{av} is the mass of all avionics, m_{lg} is the mass of the landing gear and pr_x is the price of a component.

From the constants, constraints, given design parameters and guessed DL, the detailed performances are calculated for each specific flight condition and determine the requirements for the components, such as the maximum power consumption, required current, torque and RPM, among others. The flight conditions include the following:

- Straight forward flight with cruising speed.

- Straight ascending.

- Straight descending.

- Hovering with normal payload.

- Mixed forward ascending flight.

- Mixed forward descending flight.

- Straight forward flight with maximum speed.

- Straight ascending with maximum speed.

- Hovering with the maximum payload.

All the flight conditions can be divided into two categories. The first category considers extreme flight conditions. It is useful for estimating motors and ESCs and influences the maximum discharge rate of the battery. The second category considers the most efficient flight conditions, and hence is useful for estimating the total battery energy.

The mass and price of each component are then estimated based on these required performances using layer_3 functions. The components include propellers, motors, ESCs, batteries, avionics, arms, the central body and the landing gear (Valavanis and Vachtsevanos, 2015). Afterwards, they are summed, and finally, the percentage error between $GTOM_0$ and m_{tot} is used as the output. During the above process, the constraints are checked to produce err_{flag}. All the necessary middle parameters are recorded in FUN_{output}.

The layer_3 functions are all detailed functions that can solve the most specific questions, such as determining the power consumption of a certain flight condition or estimating the mass and price of a certain component. Among all the components, the arm design requires a sub-optimisation process. The other components are estimated using a statistic method, in which databases are built for these components, and relation equations are correlated between the mass or price and the requirements.

In the following sections, to clearly explain every component, the introductions to the layer_2 and layer_3 calculations are presented together.

3.4.2 Fore Calculation

3.4.2.1   General Parameters

With a DL and the given design parameters, the following parameters can be calculated. In Equations (3)–(8), As is the disc area of a single rotor, $r_p = \frac{d_p}{2}$ is the radius of the propeller, A is the total disc area, N_r is the number of rotors, $GTOW_0$ is the initially guessed gross take-off weight, $GTOM_0$ is the initially guessed gross take-off mass, $MTOM$ is the guessed maximum take-off mass, $m_{pl,max}$ is the maximum payload, U is the output voltage of the battery, U_c is the voltage per cell of Li-Po batteries and is a constant, and N_c is the number of battery cells:

$$As = \pi r_p^2 \tag{3}$$

$$A = As \cdot N_r \tag{4}$$

$$GTOW_0 = A \cdot DL \tag{5}$$

$$GTOM_0 = GTOW_0/g \tag{6}$$

$$MTOM = GTOM_0 + m_{pl,max} \tag{7}$$

$$U = U_c \cdot N_c \tag{8}$$

3.4.2.2   Diagonal Distance

The total size L_d is measured by the distance between the axes of two diagonal motors and is also known as the diagonal distance. In this algorithm, L_d is determined by the propeller diameter d_p and the number of arms N_{arm}, as the gap ratio gr_p between two adjacent propellers is considered a constant (see Section 4.3.1 for a detailed explanation). This relationship is presented in Figure 3.5.
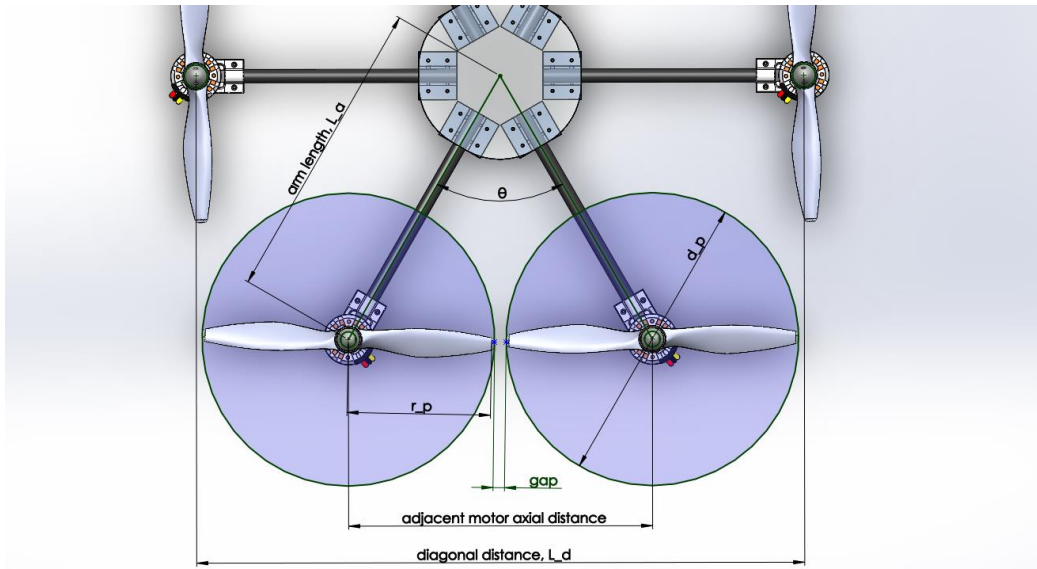
Figure 3.5 Relationship between total size and propeller size.

There are the following relations:

$$gr_p = gap/d_p \tag{9}$$

$$\sin\left(\frac{\theta}{2}\right) = \frac{(2r_p + gap)/2}{L_a} = \frac{d_p + gap}{L_d} \tag{10}$$

$$\theta = \frac{2\pi}{N_{arm}} \tag{11}$$

Combining Equations (9)–(11) yields the following:

$$L_d = \frac{d_p \cdot (1 + gr_p)}{\sin(\frac{\pi}{N_{arm}})} \tag{12}$$

36

3.4.2.3 Central Body

The mass and price of the central body are estimated according to the volume of the material (V_c), given the density and unit price as constants (layer_3_body function).

In this algorithm, the central body uses a simplified model. It ignores any connector or fastener and is comprised of only multiple layers of round plates (normally two layers). To calculate the volume, the diameter (d_c) and thickness (th_c) of the plate must be known (see Equation (13)). In the equation, N_{layer} is the number of plates and is a pre-determined constant.

$$V_c = \frac{\pi d_c^2}{4} \cdot th_c \cdot N_{layer} \tag{13}$$

d_c and th_c thus are related to L_d (the diagonal distance of the multicopter). By analysing 18 multicopters in the aircraft database, the diameter of the central body d_c correlates with the diagonal distance L_d (see Figure 3.6 and Equation (14)). Not all central bodies of multicopters have a round shape; since rectangular and polygonal are the most common shapes, the diagonal length (also known as the circumcircle diameter) is taken as an equivalent central body diameter. These kinds of dimensions are normally not included in the specification of a product, so all the dimensions are manually measured based on the product pictures.
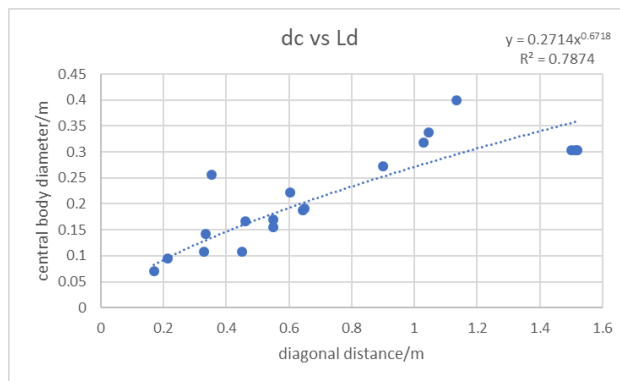
Figure 3.6 The relationship between d_c and L_d.

$$d_c = 0.2714 \cdot L_d^{0.6718} \tag{14}$$

Compared with the diameter, it is much more difficult to obtain the information of the thickness of a central body plate; it is not even possible to measure the thickness from the pictures. At the end, in the database, only five models contain the thickness of the central body, and the range of L_d covers only 110 mm to 625 mm (see Figure 3.7). This relation is valid only for carbon fibre frames. This is not a very accurate estimation, but it is sufficient for the conceptual design.
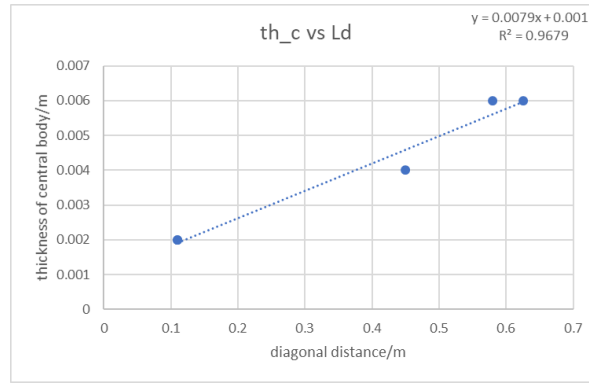
Figure 3.7 The relationship between th_c and L_d.

$$th_c = 0.0079 \cdot L_d + 0.0011 \qquad (15)$$

3.4.2.4   Avionics and Landing Gear

The landing gear and avionics should be determined prior to running the algorithm. Their mass (m_{av}, m_{lg}) and the power of avionics (P_{av}) are considered constants in the calculation.

Avionics form the brain of the multicopter; they are responsible for navigating the aircraft, automatically adjusting the altitude, processing the command from the pilot and converting the command into signals to control the ESCs. Typical avionics include the receiver, antenna, autopilot, IMU sensors, GPS, current sensor, power module, distribution board and wirings (see Figure 3.8).

The main purpose of landing gear is to provide enough space for the payload. Meanwhile, the landing gear is responsible for absorbing impact and maintaining balance during landing. The landing gears are of different types, such as four curved legs, four short sticks, strong skids, retractable skids, etc (see Figure 3.9). The landing gear should be determined based on the mission requirement. Due to the variety of landing gear types and the uncertainty of the payload, it is unrealistic to estimate the mass and price of the landing gear. Thus, it is better to determine them in advance. However, it is assumed that for a given aircraft size, the landing gear should not exceed a maximum height; otherwise, the CoG of the aircraft would be too high and thus cause instability. The maximum landing gear height is then estimated using the layer_3_lg function, which is one of the err_{flag} entries. The maximum landing gear height H_{lg} is correlated with the diagonal distance L_d (see Figure 3.10) based on 46 multicopters from the database.

For reference, in (Russell, Theodore and Sekula, 2018), a 1% $MTOM$ is used for the motor mount mass estimation, and a 4% $MTOM$ is used for the landing gear mass estimation. The avionics mass is a given number, namely 0.354 kg.
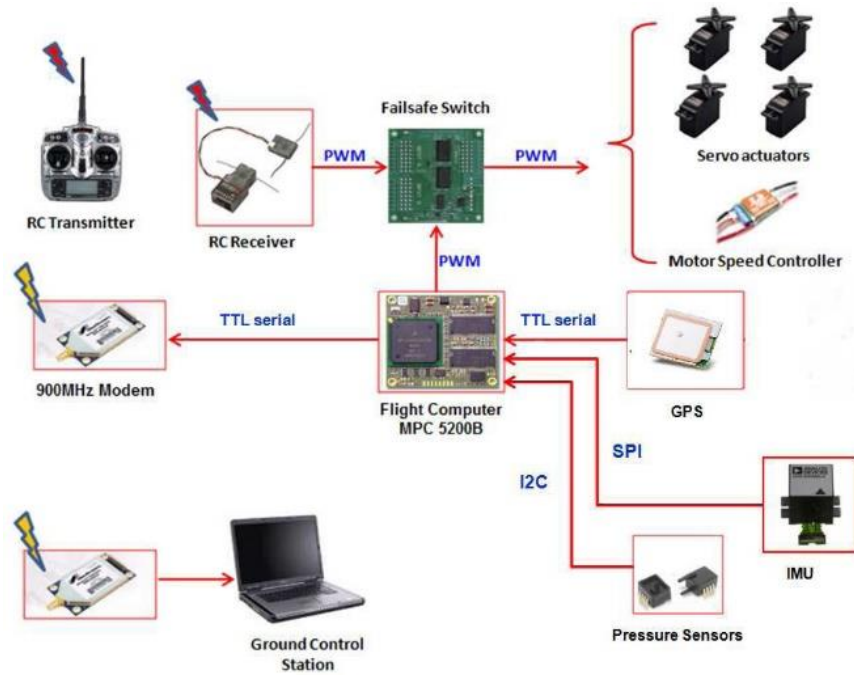
Figure 3.8 A typical avionics configuration[11].

Figure 3.9 Different types of multicopter landing gears[12,13,14,15,16].
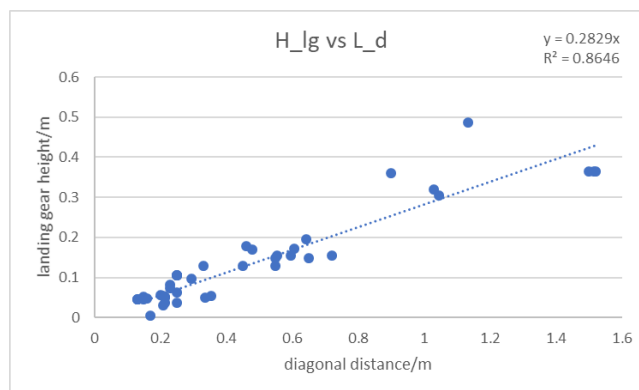
Figure 3.10   The relationship between H_{lg} and L_d.

[11] http://wolfuas.com/wp-content/uploads/2015/04/avionicsarchitecture.jpg
[12] https://hobbyking.com/en_us/extended-landing-skid-set-for-sk450-quadcopter-frame.html
[13] http://rcduniya.com/product/f450-450-quadcopter-multicopter-frame-kit-whitered-tall-landing-gear-and-integrated-pcb
[14] https://www.amazon.com/Xiangtat-multicopter-Anti-Vibration-Multicopter-Quadcopter/dp/B06XBSJQHJ
[15] https://www.tester.co.uk/media/catalog/product/cache/2/image/1800x/05346a985a93e33e9004a4119d1ea6fd/d/j/dji-inspire-2-front-angled.jpg
[16] https://hobbyking.com/en_us/hobbykingtm-robocat-270mm-true-carbon-racer-quad-yellow.html

3.4.3 Flight Calculation

3.4.3.1 Flight Conditions and Categories

The multicopter can fly in different conditions. Under these conditions, the multicopter has different performances and thus different requirements for the components. Some typical flight conditions include hovering, cruising, taking off, landing, maximum forward flight, maximum ascending and forward ascending flight. These flight conditions are divided into two categories: the extreme performance category and the most efficient category (Quan, 2017).

- The propulsion system of the multicopter has different efficiency under different flight conditions. From the design point of view, the multicopter should operate under the best efficiency for the longest time so that the proper multicopter can be used on a specific mission. Otherwise, power is wasted, and the performance is poor. The most efficient situations should be decided based on the main task of the mission, which is normally hovering or cruising. For example, if the mission is to hover for 10 min, then the propulsion system should be designed to work most efficiently for hovering. If the mission requires the multicopter to move 3 km in 300 s, then the propulsion system should be designed to work most efficiently for cruising at 10 m/s.

- Other than completing the mission, emergencies might occur for the multicopter, such as wind or turbulence. To eliminate these emergencies, the motors may consume more power to produce more thrust. The worst situations in which the multicopter can still fly are considered the extreme performance situations. In these situations, the motors should output their maximum power to support the multicopter in performing extreme movement, such as flying at maximum speed or making a sudden change in velocity.

It should be noticed that the calculation of each flight condition focusses on only equilibrium conditions. Equilibrium occurs between the gravity force, thrust force and drag force (see Figure 3.11). For a certain movement phase, it must include three stages: acceleration, constant-speed flight and deacceleration (there may be more stages for an acrobatic or racing drone, but they are not considered in this algorithm for now). Since a multicopter is not a stable-equilibrium system, in reality, the thrust of each motor is adjusted by the autopilot at each moment to maintain the altitude of the aircraft. When the multicopter is transferring from hovering to forward flight, the thrust of the front motors is reduced, and the thrust of the rear motors is increased. The torque produced by the thrust difference then rotates the multicopter forward (increases the pitch angle). The thrust of each motor is dynamically adjusted so that the rotation deaccelerates until the target tilt angle and the aircraft accelerate forward. When the speed increases, the drag is increased, causing the acceleration to be reduce until the drag, weight and thrust achieve an equilibrium state. Finally, the multicopter flies forward under a constant speed. This procedure takes place over a short period compared with the constant-speed phase (see Section 3.4.5), and every parameter changes rapidly during this phase, so it is not an ideal condition to study. This is the main reason for focussing on the equilibrium state.
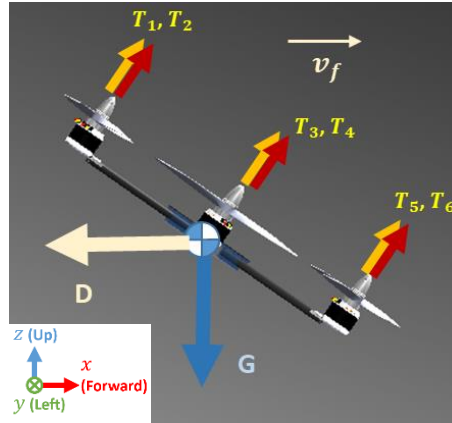
Figure 3.11   Equilibrium state in forward flight.

For the most efficient situations, only the average power matters in a movement phase (see Section 3.4.5). The average power can be calculated only from the equilibrium condition. However, for extreme performance situations, the maximum power is calculated from the maximum thrust (see Equation (47)), which can then be calculated from either the maximum acceleration (see Equation (16)) or the maximum velocities (see Equation (17)–(19)). The maximum velocity is selected for the following reasons. A) It is conventional to use the maximum velocity as an indicator for the maximum performance of a multicopter, which can be found from the specifications of most commercial multicopter products. This may be because the maximum velocity is a more specific concept than acceleration and thus is easier to understand by non-professional consumers. B) From the design point of view, the maximum velocity offers more certainty than acceleration. When the maximum velocity is determined, assuming the multicopter is in the equilibrium condition, everything else can be calculated; however, given the acceleration, this could occur in many different situations, which is unfavourable for the standardisation of the algorithm.

$$\vec{F} = m \cdot \vec{a} \tag{16}$$

$$q = \frac{1}{2}\rho v_f^2 \tag{17}$$

$$D = C_d q A_d \tag{18}$$

$$\sum \vec{F} = \vec{D} + \vec{G} + \vec{T} = 0 \tag{19}$$

3.4.3.2   Power Transmission

The power transmission is presented in Figure 3.12. The battery provides all the power. The main part is consumed by the propulsion system, while a small part is consumed by the payload and avionics. The propulsion system is comprised of multiple rotors; for each rotor, the power moves through the components in the following order: battery → ESC → motor → propeller → aircraft movement. To clarify, the naming rule of the power is 'P' plus a subscript of the initial component to represent the output power of the component. For example, P_{mot} is the output power of the motor and equals the input power to the propeller (assuming there is no loss on the cable). There is power loss on each component, so the powers have the following relationship: $P_{prop} < P_{mot} < P_{esc} < P_{bat}$.
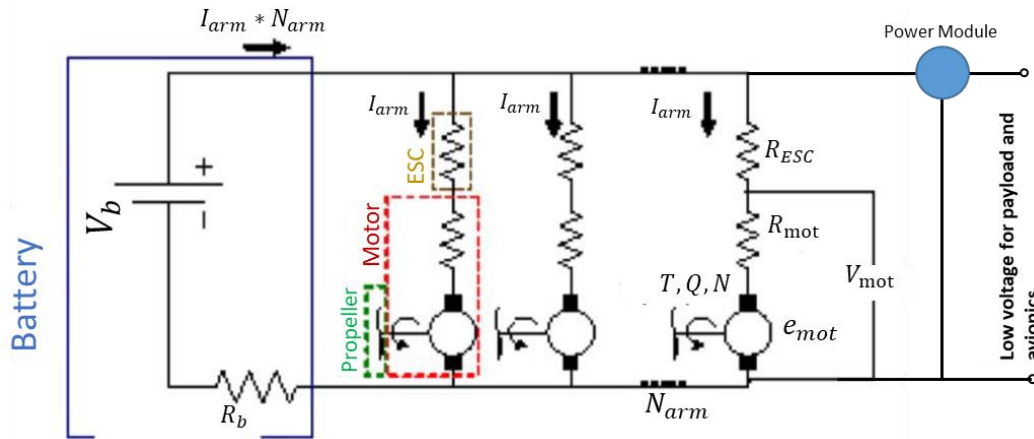
Figure 3.12   The propulsion system physical model in (Ampatis and Papadopoulos, 2014)*.*

$\sum P_{prop,i}$ is the total rotor output power that maintains the movement of the aircraft. Thus, conversely, in the flight calculation step, P_{prop} should be calculated.

3.4.3.3   Compare Different Sources and Methods

The calculation of the propulsion system of multicopters is primarily based on two theories: momentum theory and blade element theory. These two theories are widely used in the propulsion system design of helicopters and fixed-wing aircraft. These theories are introduced in several books (McCormick, 1979; Johnson, 1980; Leishman, 2006; Seddon & Newman, 2011; and Raymer, 2012); in the core literature on multicopter design, the methods for calculating the hovering power are the same (see Equation (26)), while the methods for calculating the forward flight and vertical flight conditions are different.

Ampatis and Papadopoulos (2014) introduced a unique approach, employed the basic momentum theory to determine the hovering condition, and then used a constant ratio (similar to TrW) to estimate the maximum thrust condition. In (Quan, 2017), momentum theory is used to calculate four working conditions. Winslow, Hrishikeshavan and Chopra (2017b) and Vu, Dang and Dinh (2019) followed the algorithm from (Leishman, 2006), and Vu et.al developed the algorithm to a mixed momentum-blade-element theory and included the propeller design parameters. Finally, Raymer's algorithm on vertical and forward flight conditions is used in (Mauro Gatti, 2015; Gatti, 2017).

In this thesis, Leishman's calculation method is used for all the flight conditions. It calculates the induced velocity in any condition and hence is more accurate. Raymer's method is a simplification of the actual condition so that it can eliminate the complex calculation of the induced velocity. In the forward flight power calculation, the rotor is treated as a round wing, and the wing's Oswald efficiency factor is used instead of the propeller efficiency to estimate the propeller's input power. As a result, Raymer's method is valid only for a short range of forward speed; otherwise, the error is too large. Leishman's method is introduced in detail in Section 3.4.3.4, Raymer's method is introduced in Appendix B and a comparison between the two methods is presented in Appendix C.

3.4.3.4   Detailed Calculation of the General Condition

The layer_3_general function provides an algorithm to determine the thrust, rotation speed and power of the rotor based on the given flight conditions. It accepts three inputs, v_x, v_y and $GTOM$ and considers two situations based on whether there is movement perpendicular to the propeller disc plane.

1. **Hovering.** $(v_x = v_y = 0)$

Let cross-section 0 denote the plane far upstream of the rotor, where in the hovering case, the fluid is quiescent (i.e. $v_0 = 0$). The rotor disc area is denoted by A with radius R. Cross-sections 1 and 2 are the planes just above and below the rotor disc, respectively, and the far wake is denoted by cross-section ∞ with radius r_∞ (see Figure 3.13).
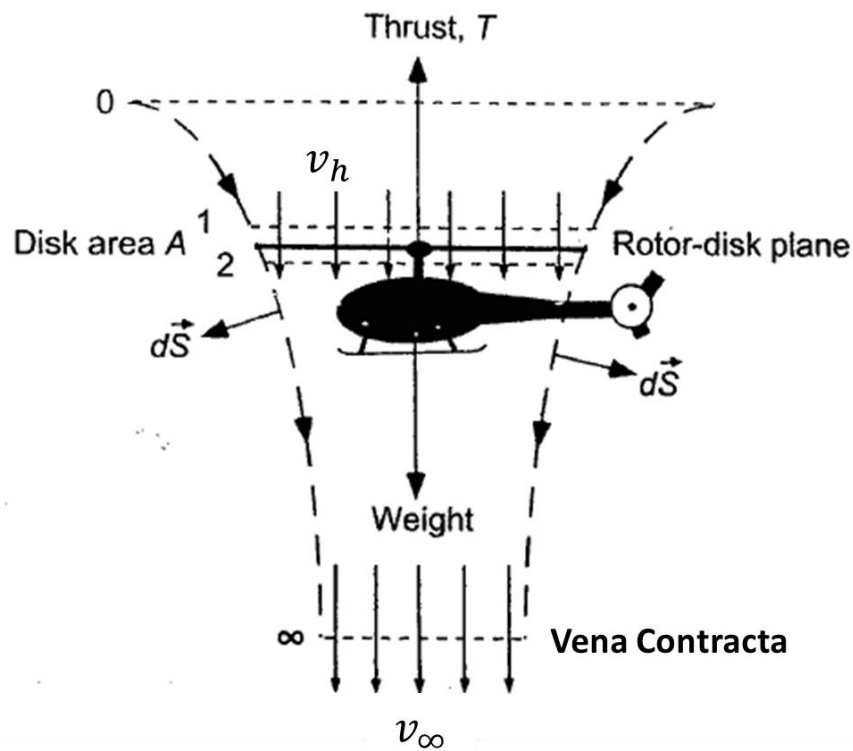
Figure 3.13   Flow model for momentum theory analysis of a rotor in hovering flight.
(Leishman, 2006).

Based on energy and momentum conservation theory and due to the incompressible fluid assumption (Leishman, 2006), the relationship between the induced velocity in the plane of the rotor (v_h) and the velocity in the vena contracta (v_∞) is given as follows:

$$\dot{m} = \rho A_\infty v_\infty = \rho A v_h \tag{20}$$

$$T = \dot{m} v_\infty \tag{21}$$

$$T v_h = \frac{1}{2} \dot{m} v_\infty^2 \tag{22}$$

$$v_\infty = 2 v_h \tag{23}$$

$$r_\infty = \frac{R}{\sqrt{2}} \tag{24}$$

where ρ is the density of the air, and $\dot{m}$ is the mass flow rate of the air. As a conclusion, the air velocity is twice the hovering induced velocity, and the radius of the cross-sectional area of the far wake below the rotor is $\frac{1}{\sqrt{2}}$ of the rotor disc's area. By substituting Equation (23) into Equation (22), the power and rotation speed can be calculated by Equations (25)–(28). It is clear that the power is consumed to propel the air to keep the multicopter flying against gravity.

$$T_{h,tot} = T_{h,s} \cdot N_r = GTOW \tag{25}$$

$$P_{h,s} = T_{h,s} v_h = \frac{(GTOW/N_r)^{\frac{3}{2}}}{\sqrt{2\rho \cdot A}} \tag{26}$$

$$T_{h,s} = C_{T0} \rho n^2 d_p^{\ 4} \tag{27}$$

$$n_h = \sqrt{\frac{T_{h,s}}{C_{T0} \rho d_p^{\ 4}}} \tag{28}$$

In the above equations, $T_{h,tot}$ is the total thrust in hover, $T_{h,s}$ is the single rotor thrust in hover and C_{T0} is the propeller static thrust coefficient, which is determined by the design of the propeller and is considered a constant here.

2. **Other Conditions.** $(v_x \neq 0 \ or \ v_y \neq 0)$

This situation includes five conditions; for each, air is moving into the propeller, and the calculation remains the same:

- Straight forward flight $(v_x \neq 0 \ and \ v_y = 0)$
- Straight upward flight $(v_x = 0 \ and \ v_y > 0)$
- Straight downward flight $(v_x = 0 \ and \ v_y < 0)$
- Forward upward flight $(v_x \neq 0 \ and \ v_y > 0)$
- Forward downward flight $(v_x \neq 0 \ and \ v_y < 0)$

Consider the forward upward flight as the general condition (see Figure 3.14); then, the following equations can be derived (see Equations (29)–(33)). All other conditions are special conditions of the general condition.

$$\tan(\gamma) = \frac{v_y}{v_x} \tag{29}$$

$$v_{inf} = \sqrt{v_x^2 + v_y^2} \tag{30}$$

$$q = \frac{1}{2} \rho v_{inf}^2 \tag{31}$$

$$D = C_d \cdot q \cdot A_d \tag{32}$$

$$\alpha = \beta + \gamma, \ \alpha \in [0, \frac{\pi}{2}] \tag{33}$$
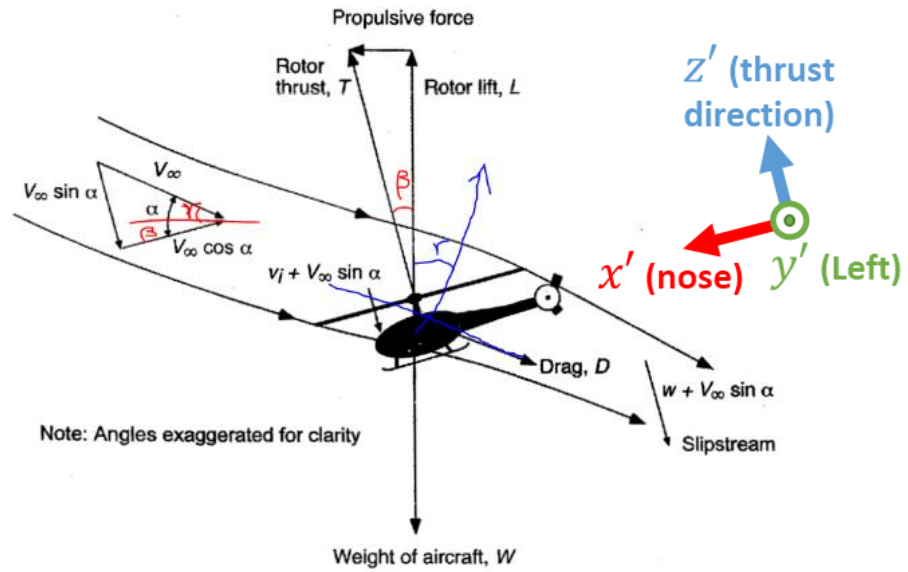
Figure 3.14   The forward upward flight condition of a helicopter (Leishman, 2006).

As displayed in Figure 3.14, α is defined as the propeller angle of attack. When there is dynamic air flow into the disc area, then $\alpha = \frac{\pi}{2}$ for perpendicular flow, and $\alpha = 0$ for parallel flow. β is the tilt angle of the aircraft and is defined as the angle between the motor axes and the vertical up direction. γ is the climb angle, v_{inf} is the relative velocity of the coming flow and D is the drag.

3.   Drag Assumption

The drag is calculated by Equation (32), in which q is the dynamic air pressure, C_d is the drag coefficient and A_d is the effective drag area.

The value of C_d is set to be 0.9, which is a typical value for the drag coefficient of a cube with an arbitrary orientation relative to the wind. This selection of C_d corroborates with the work by Moyano Cano (2013) and Christian and Lawrence (2016).

The drag area A_d is explained in Figure 3.15. A_1 is the top area, A_2 is the front area and A_d is the projected drag area. These values are calculated by Equations (34)–(36), in which A is the total disc area, and A_c is the area of the central body, which are introduced previously. In the event of overlap between the propellers' disc and the central body, a fix coefficient C_{ol} is introduced, which is a constant. Another constant is the ratio between the top area and the front area C_{tf}. The default value of the constants can be found in Appendix A.

$$A_d = A_1 \sin(\alpha) + A_2 \cos(\alpha) \qquad (34)$$
$$A_1 = (A + A_c) \cdot C_{ol} \qquad (35)$$
$$A_2 = A_1 / C_{tf} \qquad (36)$$
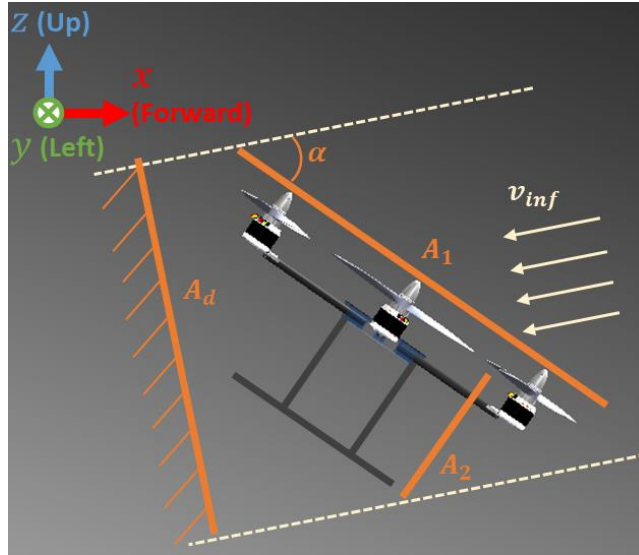
Figure 3.15   The explanation to the drag area.

4.   Calculation of α

In Figure 3.14, regarding the multicopter's own coordinate system (x'-y'-z'), there are

$$T\cos(\alpha) = GTOW\cos(\gamma) \tag{37}$$

$$T\sin(\alpha) = D + GTOW\sin(\gamma) \tag{38}$$

By substituting Equations (32) and (34) into Equations (37) and (38), α can be presented as follows:

$$\frac{C_d q}{GTOW\cos(\gamma)}[A_1\sin(\alpha) + A_2\cos(\alpha)] + \tan(\gamma) - \tan(\alpha) = 0 \tag{39}$$

Then, set $f(\alpha) = \frac{C_d q}{GTOW\cos(\gamma)}[A_1\sin(\alpha) + A_2\cos(\alpha)] + \tan(\gamma) - \tan(\alpha)$

Then, α can be solved using the Newton-Raphson method (see Equation (40)). Given γ, q and $GTOW$, α can be solved in the Layer_3_alpha function. As α is known, T and D can be calculated.

$$x_{n+1} = x_n - \frac{f(x_n)}{f'(x_n)} \tag{40}$$

5.   Calculation of v_i

When $v_{inf} \neq 0$, Equations (21) and (23) are still valid, but part of the flow influences the production of thrust because the mass-flow ratio is changed (see Equations (41)–(46) and Figure 3.16).

$$\dot{m} = \rho A_s v_{through} \tag{41}$$

$$v_{through} = \sqrt{v_{inf,p}^2 + (v_{inf,v} + v_i)^2} \tag{42}$$

$$v_{inf,v} = v_{inf}\sin(\alpha) \tag{43}$$

$$v_{inf,p} = v_{inf}\cos(\alpha) \tag{44}$$

$$T = 2\dot{m}v_i = 2\rho A_s v_i \cdot \sqrt{v_{inf,p}^2 + (v_{inf,v} + v_i)^2} \tag{45}$$

46

Equation (45) can be rewritten as follows:

$$v_i^4 + 2v_{inf} \sin(\alpha)v_i^3 + v_{inf}^2 v_i^2 - \left(\frac{T}{2\rho A_s}\right)^2 = 0 \qquad (46)$$

Then, set $f(v_i) = v_i^4 + 2v_{inf} \sin(\alpha)v_i^3 + v_{inf}^2 v_i^2 - \left(\frac{T}{2\rho A_s}\right)^2$

Then, v_i can be solved using the Newton-Raphson method (see Equation (40)). Given α, v_{inf} and T, v_i can be calculated from the Layer_3_ vi function.
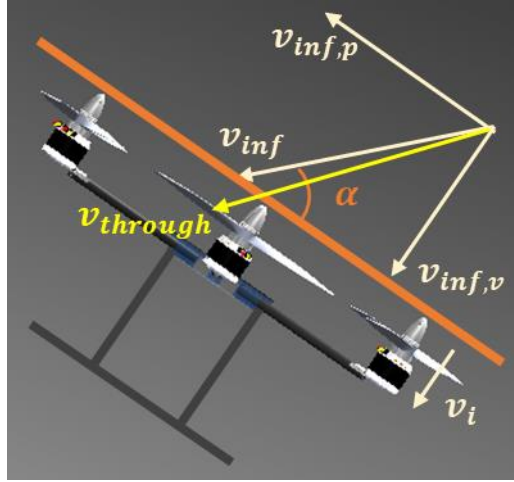
Figure 3.16   The flow model for momentum theory analysis in ascending *(Leishman, 2006)*.

6.   Power and Rotation Speed

With everything required, the power and rotation speed can be calculated (see Equations (47)–(50)). It can be seen that the power is consumed in two parts: one part is converted to the works made by the movement, while the other is to propel the air to produce thrust. The calculation of the rotation speed introduces the concept of advance ratio J (Brandt *et al.*, 2015). It will be discussed in more details in Section 4.3.2.4.

$$T_{g,s} = \frac{T}{N_r} \qquad (47)$$

$$P_{g,s} = T_{g,s} \cdot v_{inf,v} \qquad (48)$$

$$J = \frac{v_{inf,v}}{nd_p} \qquad (49)$$

$$n = \frac{v_{inf,v}}{Jd_p} \qquad (50)$$

7.   Propeller Efficiency

The power calculated in the previous section is the propeller output power. To know the propeller input power (motor output power), the propeller efficiency (η_p) is introduced (see Equation (51)). The efficiency of a propeller is a coefficient to represent the overall loss of the propeller. By analysis, since a multicopter is a low-speed aircraft, the efficiency difference between the cruising flight and maximum speed flight are nearly the same, so η_p is considered constant for all the flight conditions. Due to the definition of efficiency, the efficiency of a propeller in the hovering condition

is zero, and the coefficient figure of merit (FM) is then introduced (see Equation (52)). FM and η_p are considered constants in this algorithm (see Appendix A). The parameters of the propellers and the values of the propeller efficiencies are explained in Section 4.3.4.

$$P_m = \frac{P_p}{\eta_p} \tag{51}$$

$$P_m = \frac{P_p}{FM} \tag{52}$$

8. Fuselage Downwash

Other than the propeller efficiency, another factor must be considered to estimate the motor output power from the propeller input power.

$$T_{actual} = T_{ideal} \cdot C_f \tag{53}$$

This factor is called the fuselage downwash (Raymer, 2012) or the download penalty (Leishman, 2006). Because there exists an arm and motor hub underneath the propeller, the actual power consumed should be larger than that under the ideal condition. This influences the calculation of P_{useful} and P_i (or P_h). The discussion on the value of this factor can be found in Section 4.3.3.

3.4.3.5 Special Conditions

The above method is valid for the calculation of most flight conditions, save for the descending condition. In low-speed vertical descending ($-2 < \frac{v_c}{v_h} < 0$), the rotor operates in the vortex ring state (VRS). This is an unstable state in which the rotor cannot effectively produce thrust (Leishman, 2006) and should be avoided at all times. The rotor states and the VRS flow condition are presented in Figure 3.17. Two approaches to avoid the VRS state are 1. descending at a higher velocity and 2. descending and flying forward simultaneously.
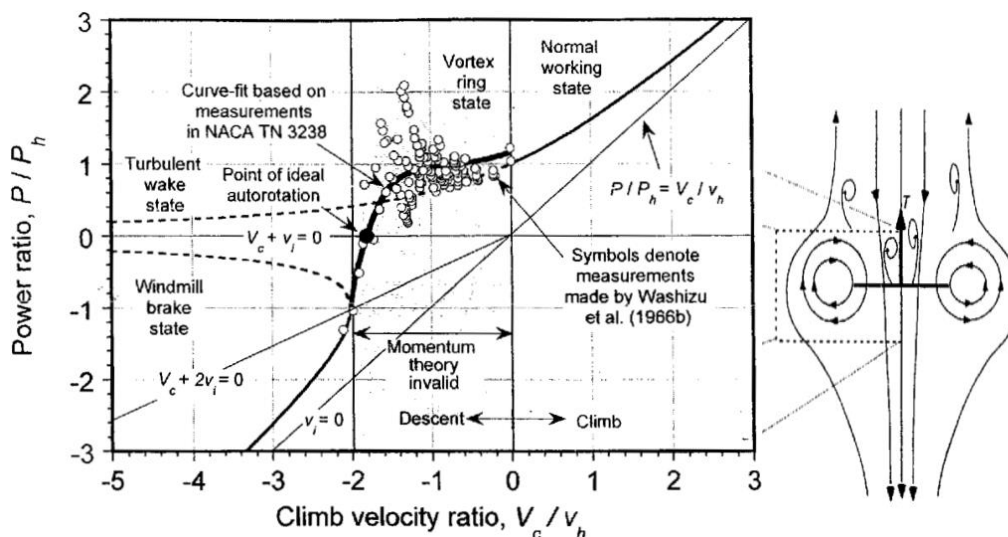
Figure 3.17   The required power vs vertical velocity, and the flow condition of VRS state.
(Leishman, 2006)

When $\frac{v_c}{v_h} < -2$, the rotor is in the windmill brake state, in which the power required to maintain the descending is reduced. There is a point called the ideal autorotation condition when the required power is zero, which is the maximum descending velocity. The descending velocity is checked in the algorithm as a constraint.

3.4.4 Extreme Performance Calculation

There exist several situations in which a multicopter might be operated in extreme performance mode. These situations include hovering with the maximum payload and forward or upward flight under the maximum velocity. In these conditions, the motors and propellers are normally working at their worst efficiency, but the rotor can provide the maximum thrust. Using the Layer_3_general functions, given different variables (v_x, v_y, M), the three flight conditions can be calculated. The algorithm first reviews the constraints list to obtain the maximum forward and vertical velocity. If these values are not specified or if they are smaller than the velocities from the mission description, the latter ones are used as the maximum velocities. In the hovering situation, although not specified, the multicopter should have the least manoeuvrability, so the actual maximum power should be corrected by multiplying the hovering power with the minimum thrust weight ratio (see Section 4.3.7). By default, $MTOM$ is used for the hovering calculation, and $GTOM$ is used for maximum velocity calculation because it is a convention of the manufacturers to measure the maximum velocity without the payload. However, if the users prefer to specify the maximum velocity with the payload, there is the option to switch on.

The layer_3_general function returns the thrust, power and rotation speed of the rotor. Among the results of the three flight conditions, the maximum results (P_{max}, T_{max} and n_{max}) are selected as the extreme performance. The extreme performance flight condition is not necessarily the maximum velocity forward flight condition. The relationship between the rotor power and the forward velocity is presented in Figure 3.18. It can be found that in the low forward speed condition, the power is actually smaller than the hovering power.
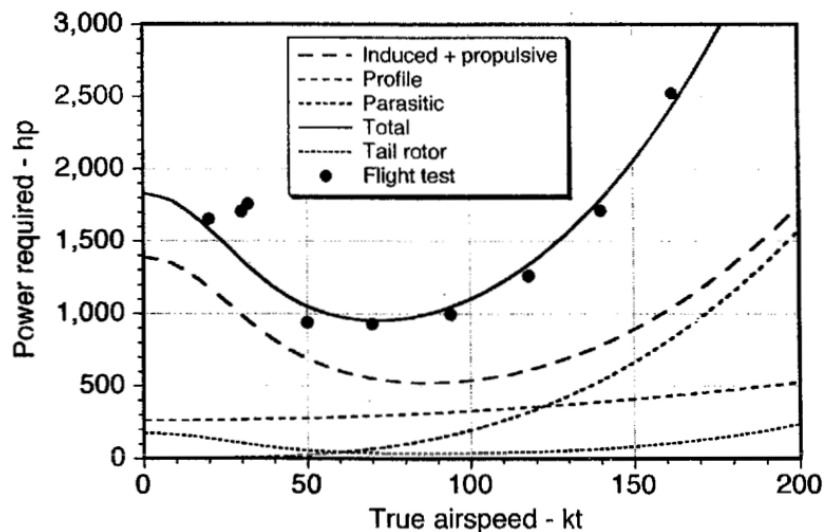
Figure 3.18   Predictions of helicopter main rotor power in forward flight.
Figure source: Leishman (2006), Data source: Ballin (1987).

With the extreme performance parameters, the actual maximum TrW can be determined from the maximum total thrust (see Equation (54)). It is checked by the allowed range of TrW in the list of constraints (see Section 3.3.1.1 and Section 4.3.7).

$$TrW_{max} = \frac{T_{max}}{GTOW} \tag{54}$$

Next, the propulsion system components (the mass and price of propellers, motors and ESCs) can be estimated using the extreme performance parameters (maximum thrust, power and rotation speed of one rotor system).

3.4.4.1 Propeller Selection

For the propeller estimation, there is an assumption that only a fixed-pitch, two-bladed, one-piece propeller is used. In the current algorithm, the propellers are estimated based on only the diameter. The layer_3_prop function accepts the d_p as input and returns the mass (m_p) and price (pr_p) of the propeller. In this function, the unit of d_p is inches, and the unit of m_p is kg.

1. **Mass**

The propeller mass is given by Equation (55):

$$m_p = \frac{0.00369 d_{pi}^3 - 0.021 d_{pi}^2 + 0.93 d_{pi}}{1000} \tag{55}$$

This equation is correlated from 145 RC propeller products in the market (see Figure 3.19). The regression is validated by the other 48 products (see Figure 3.20). The curve fitting is performed by a MATLAB application called Curve Fitting Tool. This tool can return the goodness of fit and the prediction interval of different levels. The goodness of the validation is given in Table 3.5.

Goodness of fit:
SSE: 1.453e+04
R-square: 0.931
Adjusted R-square: 0.9301
RMSE: 10.11
Goodness of validation:
SSE: 1866
RMSE: 6.23499
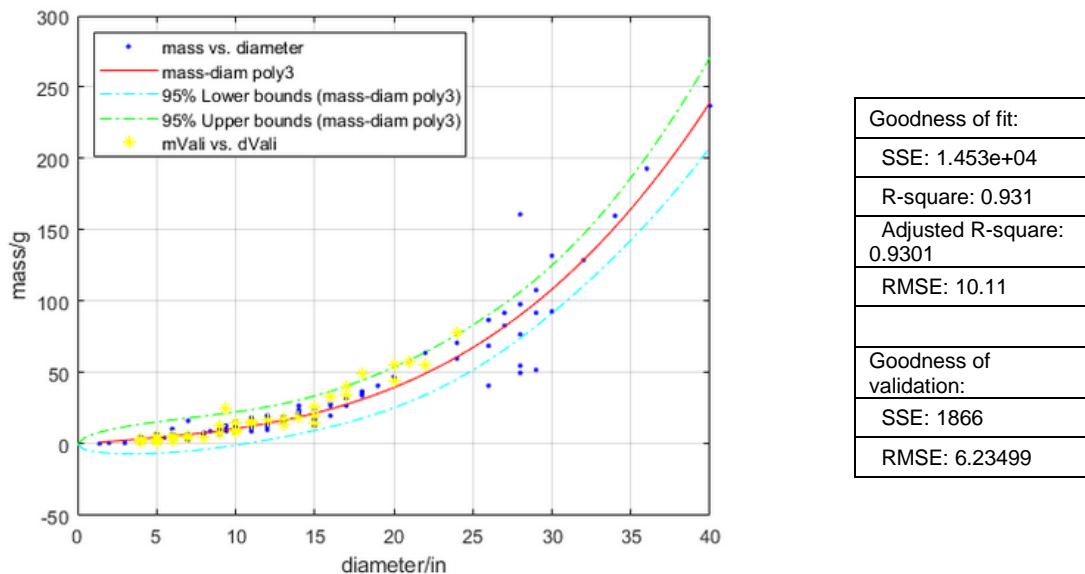
Figure 3.19   The regression of the relationship between propeller mass and diameter.
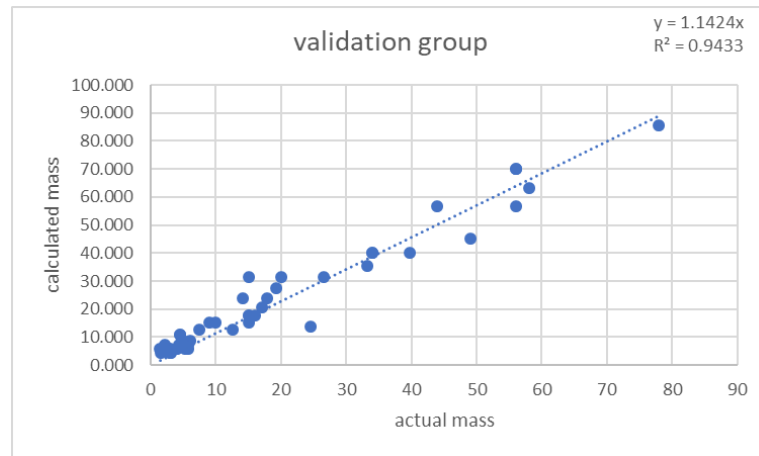
Figure 3.20   Propeller mass estimation equation validation.

Table 3.5   The goodness of validation of the propeller estimation function.

	Absolute Error	Error Ratio
Max	10.86693	2.907905
Min	-16.2702	0.009551
Average	-4.10927	0.54703
Standard Deviation	4.625375	0.594839
Variation Coefficient	-1.1256	1.087397

The validation group data are examined to determine whether they fall into a given prediction interval (the dashed line in Figure 3.19); the result is shown in Appendix D. The prediction interval is a range which displays the possibility of the estimation result. For example, 95% PI indicates that the estimation of new data has a 95% chance to be within the estimated interval.

The two validation methods agree that the regression is trustworthy. It is understandable that the mass is linearly related to the volume, while the volume is the third power of the dimensions. The variance may occur due to different materials and designs, but it is maintained at an acceptable level.

1. **Price**

The above propellers are used for the price estimation regression; however, as different manufacturers price their products using their own standards, two propellers of the same size but with different designs and materials may greatly differ in terms of price. Thus, the MATLAB Curve Fitting Tool can no longer work out a proper regression (see Figure 3.21). Finally, an algorithm called random forest is used to model the data, as introduced in Section 2.3.3. In total, 248 RC propellers are fed into the algorithm to formulate a prediction model. The model is validated against the other 81 products (see Figure 3.20), and the statistics of the validation results are presented in Table 3.6 .

Results

General model Exp2:
    f(x) = a*exp(b*x) + c*exp(d*x)
Coefficients (with 95% confidence bound
    a =   1.623
    b =   0.1371
    c =   0
    d =   0.1371

Goodness of fit:
    SSE: 1.021e+05
    R-square: 0.6943
    Adjusted R-square: 0.6905
    RMSE: 20.46

Goodness of validation:
    SSE: 28200.5
    RMSE: 18.6589
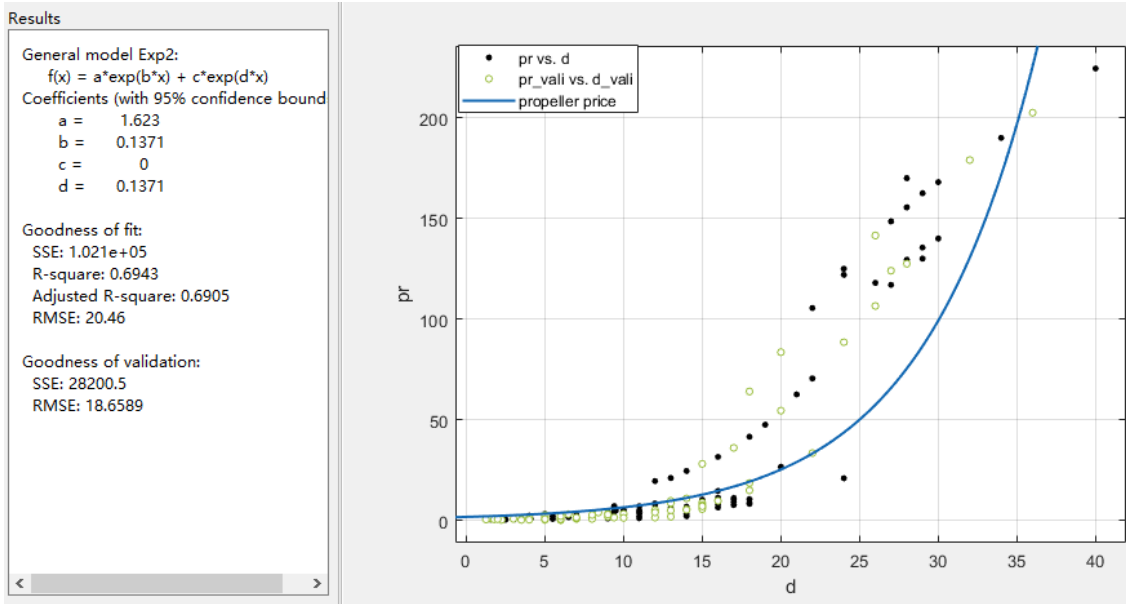
Figure 3.21   The best regression result of propeller price using Curve Fitting tool.

Table 3.6   *The goodness of the validation to the random forest model.*

	absolute error	error ratio
min	-57.7	0.1%
max	30.8	276.5%
average	4.041773	50.6%
standard deviation	10.58488	57.5%
Variance coefficient	2.618871	1.136918
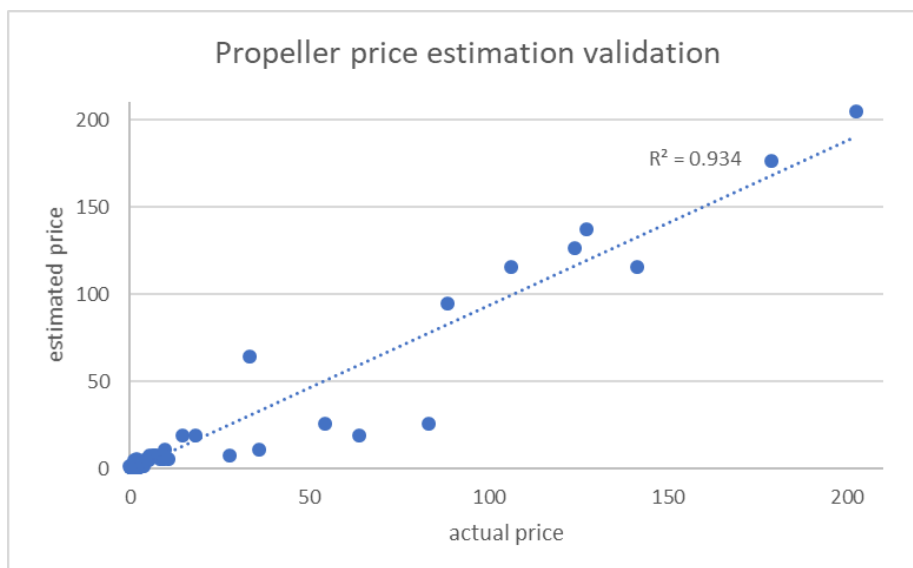
Figure 3.22   Propeller price estimation validation.

52

3.4.4.2   Motor Selection

1. **Mass**

    A) Estimation results validation

The random forest technique is used for the regression of the motor mass (see Section 2.3.3 for a review of this technique and Section 4.3.4 for more details on why it is used). The Gaussian process is used for the regression of every leaf node on all the trees. After a simple optimisation process, the number of trees and the model type of each leaf are determined to achieve the most accurate estimation. The model is trained with 214 motors and is validated by 71 models. The optimum number of trees is 13, the optimum model type is squared exponential and the optimum method is the minimum sd corrected by the $m_{m,tot}/MTOM$ ratio. The validation of the regression is presented in Table 3.7 and Figure 3.23.

Table 3.7   The goodness of the validation of motor mass estimation method.

	Error	Error ratio
Min	-551.978	0.00%
Max	244.9293	67.35%
Average	27.14075	14.81%
Standard Deviation	71.02233	13.76%
Variation Coefficient	2.616815	0.928509
R_2	0.871643	
RMSE	75.8637	
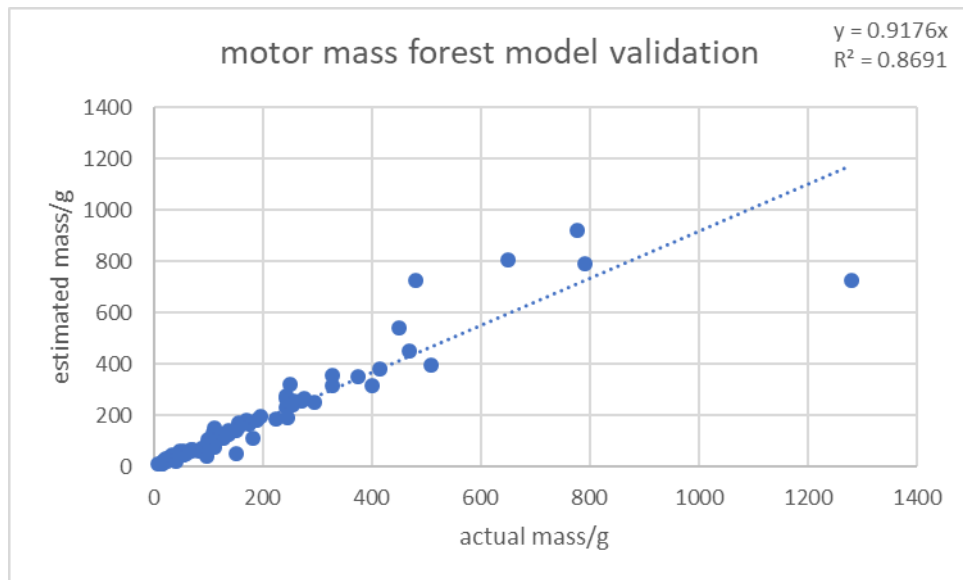
Figure 3.23   The validation of the motor mass forest model.

B) Explanation of the $\frac{m_{m,tot}}{MTOM}$ ratio

$m_{m,tot}$ is the total mass of the motor, as described in Equation (56).

$$m_{m,tot} = N_r m_m \tag{56}$$

By evaluating 45 commercial multicopter products, it is found that for most multicopters, the $\frac{m_{m,tot}}{MTOM}$ ratio is between 10%–15%. By focussing on 20–2000 g multicopters, the range becomes wider: 10%–30%. The average is then used.
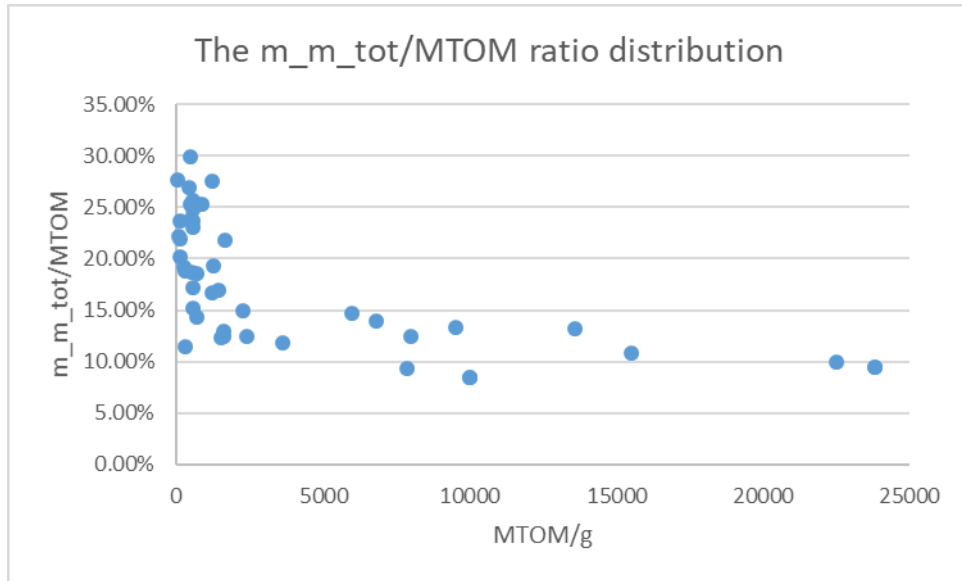
Figure 3.24   The distribution of the $\frac{m_{m,tot}}{MTOM}$ ratio.
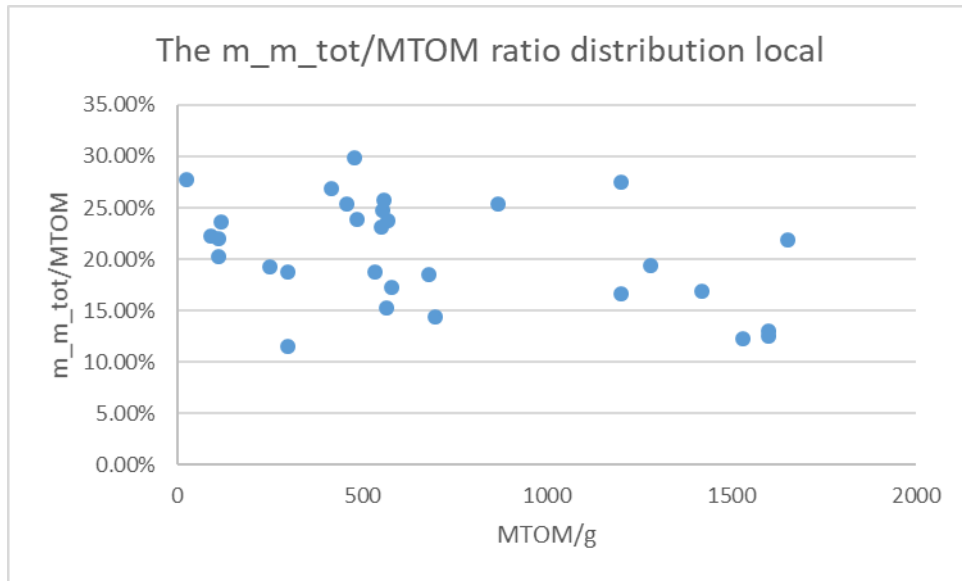
Figure 3.25   The zoomed in view of the distribution of the $\frac{m_{m,tot}}{MTOM}$ ratio.
(for $MTOM<2000$ g multicopters)

Table 3.8   The statistics of the $\frac{m_{m,tot}}{MTOM}$ ratio.

Min	8.40%
Max	29.87%
Average	17.56%
Standard Deviation	6.12%

2. Price

The random forest method is used also for the motor price estimation (see Section 2.3.3).

The model is trained with 214 motors and is validated by 69 models. The optimal number of trees is 87, the optimal model type is squared exponential and the optimal method is the weighted combination of the results from all the trees. The validation results are presented in Figure 3.26, and the goodness of the validation is presented in Table 3.9.

Table 3.9   The goodness of the validation of the motor price estimation.

Min	-125.14	1.15%
Max	33.7461	100.10%
Average	15.55291	27.17%
Standard Deviation	28.45059	25.63%
Variation Coefficient	1.829278	0.94335
R^2	0.929884	
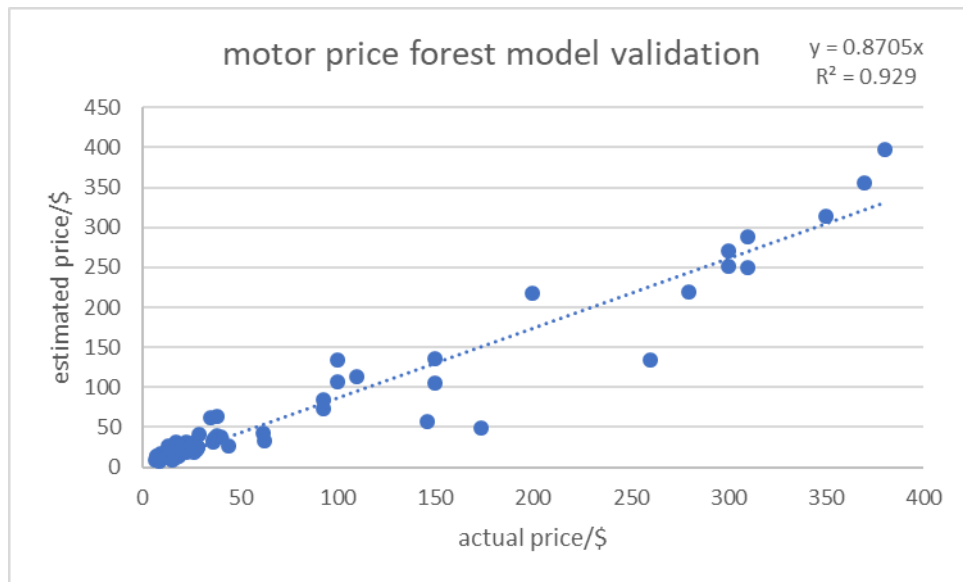
Figure 3.26   The validation of the motor price estimation method

3.4.4.3   ESC Selection

1. Mass

The ESC has the following characteristics (see Equations (57) and (58)). When the motor output power ($P_{m,input}$) is decided, the ESC output power can be determined using the empirical motor efficiency, discussed in Sections 4.3.5 and 4.3.6. Here, for the extreme performance condition, also the minimum motor efficiency (η_m) is used. Between the ESC and the motor, the ESC converts the DC current into a three-phase current. $I_{esc,output}$ is the RMS current of the actual waveform.

$$P_{esc,output} = P_{m,input} = \frac{P_{m,output}}{\eta_m} \tag{57}$$

$$I_{esc,output} = \frac{P_{esc,output}}{U} \tag{58}$$

Then, the total battery output power is calculated, and with the battery output voltage, the maximum output DC current from the battery can be calculated:

$$P_{esc,input} = \frac{P_{esc,output}}{\eta_{esc}} \tag{59}$$

$$\eta_{esc} = \frac{P_{esc,output}}{P_{esc,output} + P_{esc,loss}} \tag{60}$$

$$P_{b,output,max} = N_r P_{esc,input,max} + P_{av} + P_{pl} \tag{61}$$

$$I_{b,output,max} = \frac{P_{b,output,max}}{U} \tag{62}$$
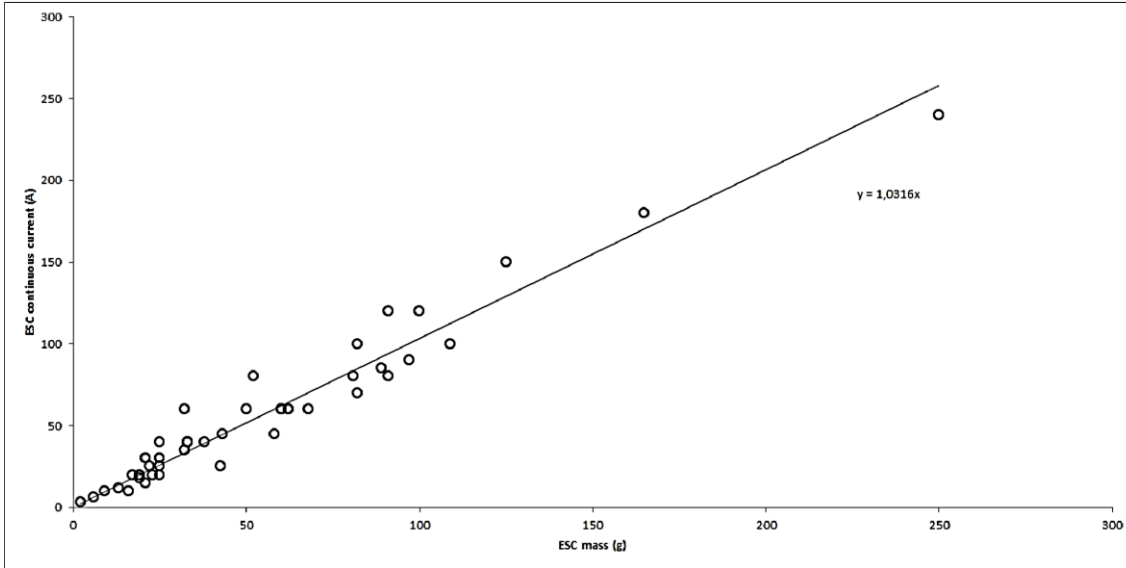
Figure 3.27   ESC specified current as a function of ESC mass (Mauro Gatti, 2015).

$$m_{esc} = \frac{I_{esc,output}}{1.0316} = 0.969 I_{esc,output} \tag{63}$$

Gatti's method of ESC mass regression is validated with my own database; in my database, various types of ESCs differ in terms of mass and price. ESCs are sold in different types: pure chips that customers must solder by themselves, suitable for small drones, or integrated frames for which the wire mass can be saved. This type of ESC does not include any heat sink; customers must add the heat sink according to the actual working condition. Half wired has only three wires on the motor side and require customers to solder the power wire. This type is suitable for larger frames in which the power wire length is not determined. Finally, there are fully wired products, and there exist more compact 4in1, 6in1 or 8in1 configurations integrated to the power distribution board. This kind of design can save a large part of the mass budget. In this algorithm, only the fully wired products are used for the regression and validation.

Finally, only the fully wired ESCs are selected from the database, of which 50 are used for regression (see Figure 3.28), while the remaining 20 are used for validation (see Figure 3.29 and Table 3.10). The estimation equation is given in Equation (64):

$$m_{esc} = 0.9121 \cdot I_{esc,output} \tag{64}$$
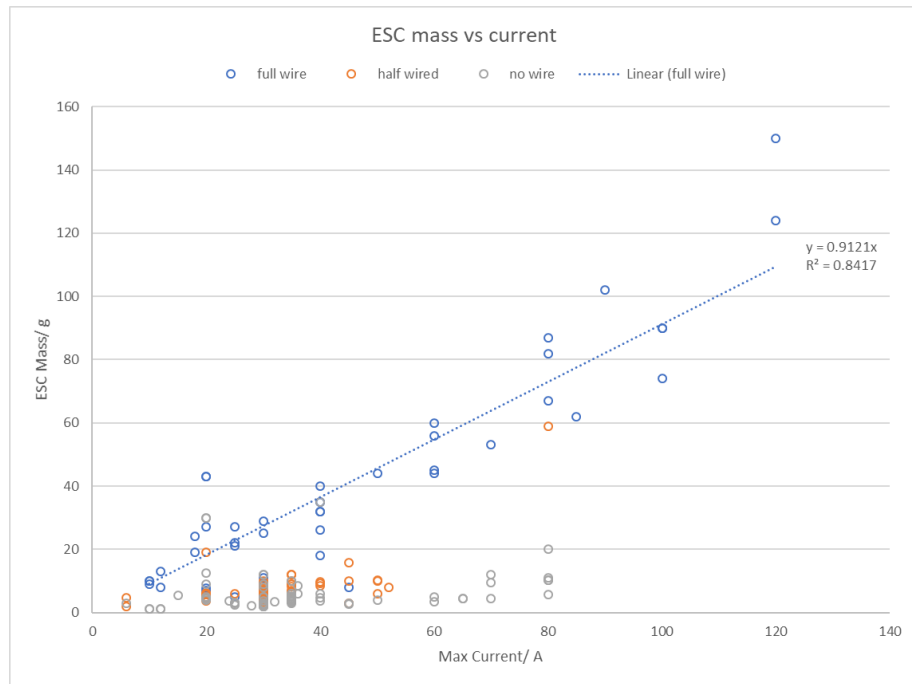
Figure 3.28   ESC mass regression.
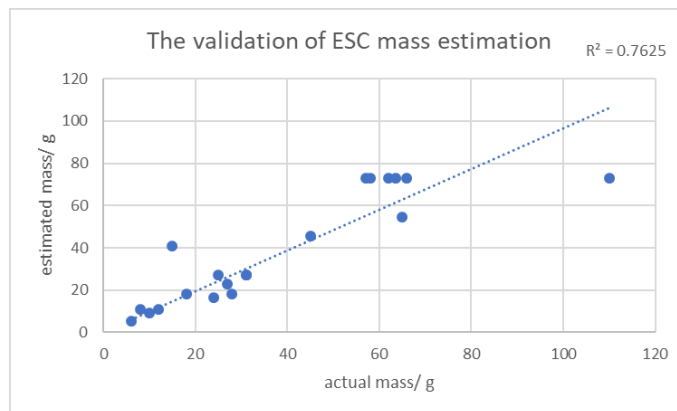
Figure 3.29   The validation of the ESC mass estimation.

Table 3.10 The goodness of the validation of ESC mass estimation.

	Absolute Error	Error Ratio
Max	26.04	173.63%
Min	-37.03	1.34%
Average	0.60	25.04%
Standard Deviation	12.77	36.63%
Variation Coefficient	21.36	1.46

2. Price

All the single ESCs are selected for the price regression. From the database, 115 ESCs are used for the regression, and the results are validated by the other 35 ESCs. The results and validation are presented in Figure 3.30, Equation (65), Figure 3.31 and Table 3.11.

$$pr_{esc} = 1.9318 \cdot I_{esc,output}^{0.5878}$$
(65)

The ESC price vs max amp plot $y = 1.9318x^{0.5878}$
$R^2 = 0.4485$
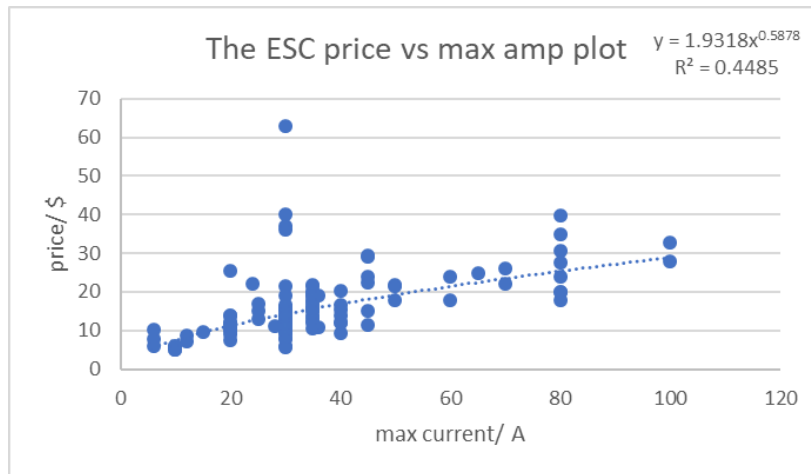
Figure 3.30   The ESC price regression.

The validation of ESC price estimation $R^2 = 0.4732$
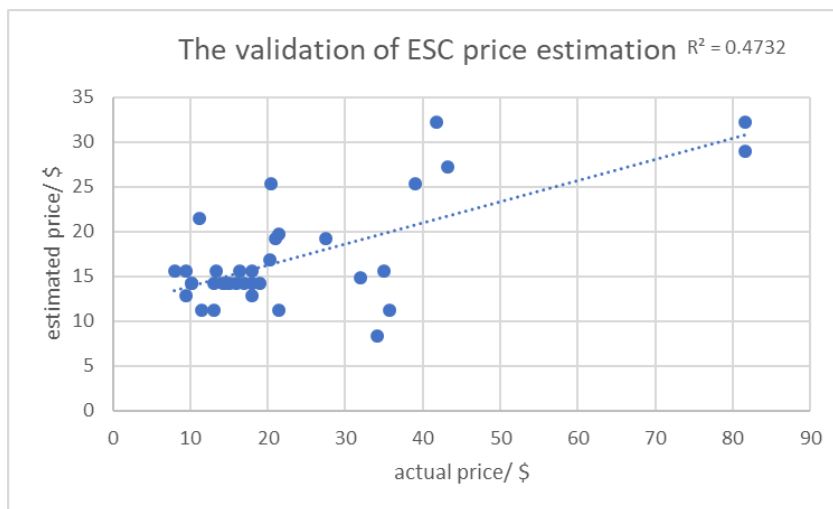
Figure 3.31   The validation of the ESC price regression.

Table 3.11 The goodness of the validation of the ESC price estimation.

	Absolute Error	Error Ratio
Max	10.23	95.44%
Min	-52.65	0.37%
Average	-6.66	32.70%
Standard Deviation	14.00	26.16%
Variation Coefficient	-2.10	0.80

3.4.5 Total Energy Consumption Calculation

3.4.5.1   Energy Workout Simplification

In reality, the movement of a multicopter from one location to another follows an accelerating-constant speed moving-deaccelerating process. However, in this algorithm, the average velocity in each phase is used to calculate the average power as a simplification. This simplification assumes that the multicopter is operated at low speed and takes little time to accelerate to the required velocity. Compared with the time of constant-velocity flying, it is negligible. Consider the

mission presented in Section 3.3.1.1 as an example: assuming the $MTOM$ is 2 kg including the payload (it is a reasonable number for carrying 0.5 kg of payload, see Table 4.23), the thrust used for accelerating is 1.5 times the $MTOW$ (TrW, see Section 4.3.7), and the tilt angle when forward accelerating is 10° (β, see Section 4.3.9). The ascending and forward flight condition details are presented in Table 3.12.

Table 3.12 The acceleration and energy consuming details of an example mission.

Parameters	Unit	Ascending	Forwarding
$MTOM$	kg	2	2
Thrust	N	29.4	29.4
Force of accelerating	N	9.8	5.105256
Acceleration	m/s^2	4.9	2.552628
Target velocity	m/s	2	5
Time of acceleration	s	0.408163	1.958765
Displacement of acceleration	m	0.408163	4.896914
Total energy considering average velocity	J	294	3063.154
Total displacement considering acceleration	m	29.18367	590.2062
Total energy considering acceleration	J	286	3013.154
Percentage Error		2.80%	1.66%

According to the mission description, the ascending phase and forwarding phase are calculated as two examples. Assuming the force for acceleration is constant (in reality, as the velocity increases, the drag increases, while the increasing incoming flow to the propeller reduces the induced velocity. As a result, the acceleration gradually reduces). According to Newton's law, during the accelerating and deaccelerating period, the actual displacement is half the displacement calculated using the average velocity. The total displacement is calculated for the entire accelerating-constant speed-deaccelerating phase. By comparison, in the example mission, the error of total consumed energy in a phase is less than 3%, which is reasonable to be neglected.

It is worth mentioned that the assumed TrW and β are close to their lower boundary, indicating that the calculated energy errors are close to their maximum. Furthermore, it can be noticed that when the average velocity in a phase is high while the total flight time of a phase is short (i.e. the constant speed period counts less significantly in a phase), the error may increase. However, this situation seldom occurs during a general-purpose multicopter mission; it is more likely to be the case for a racing drone, which must change speed and direction rapidly all the time. The latter situation is not included in the consideration of this algorithm. Moreover, the impact of the error is to overestimate the energy consumption, resulting in a heavier design. This impact, when limited to a low percentage, is not undesirable for a conceptual design. It allows for more space for further detailed component design stages without producing ridiculous estimations.

3.4.5.2 Total Energy Workout

The calculation of the total energy consumed by the system is given by Equation (66), in which $P_{tot,i}$ is the total power in phase i, and FT_i is the flight time of phase i. FT_i is specified in the mission description, while $P_{tot,i}$ is comprised of the power consumed in all sub-systems during a flight phase (see Equation (67)):

$$E_{tot} = \sum P_{tot,i} \times FT_i \qquad (66)$$

$$P_{tot,i} = N_r \times P_{ESC,i} + P_{pl,i} + P_{av,i} \qquad (67)$$

The $P_{ESC,i}$ is the input power of one ESC in mission phase i. The calculation of this parameter is given in Equation (68). In each mission phase, due to the various flight conditions, the input may vary, and as explained previously, the multicopter is designed for the mission, so the propulsion system and power system should be operated at their highest efficiency. In Equation (68), $\eta_{m,max}$ and $\eta_{esc,max}$ are used. The discussion on motor efficiency can be found in Section 4.3.4, and the discussion on ESC efficiency can be found in Section 4.3.6.

$$P_{ESC,i} = \frac{P_{m,i}}{\eta_{m,max}\eta_{esc,max}} \qquad (68)$$

$$P_{m,i} = level3\_general(v_{x,i}, v_{y,i}, GTOM_i) \qquad (69)$$

3.4.5.3 Power Source

Various types of power sources exist, such as IC generators, chemical batteries, solar cells and hybrid-technique power sources. In this algorithm, a lithium polymer (Li-Po) battery is used as the power source because it has a relatively high energy density, stable discharge rate and voltage output (Linden and Reddy, 2002; Amadori *et al.*, 2010). It is the most popular power source for today's multicopters. The power source is modelled as an equivalent circuit with a fixed voltage source and an internal resistance (see Figure 3.12). This model is slightly simplified, but with some corrections it is acceptable for the conceptual design. The more accurate models consider temperature and dynamic effects, but they would be too complicated for the multicopter optimisation process for the little benefit they provide. In reality, there is loss consumed on the internal resistor. During discharge, the actual voltage also gradually reduces (see Figure 3.32), and when the battery has discharged about 80% of the full capacity, the voltage experiences a sudden drop (Linden and Reddy, 2002). This phenomenon is expressed by a coefficient called the depth of discharge (η_{dod}), while the internal loss and gradual voltage decreasing are involved in the efficiency of the battery (η_b) and are considered constant. The total energy of the battery $E_{b,full}$ can then be calculated by Equation (70)–(71):

$$E_{b,useful} = \frac{E_{tot}}{\eta_b} \qquad (70)$$

$$E_{b,full} = \frac{E_{b,useful}}{\eta_{dod}} \qquad (71)$$
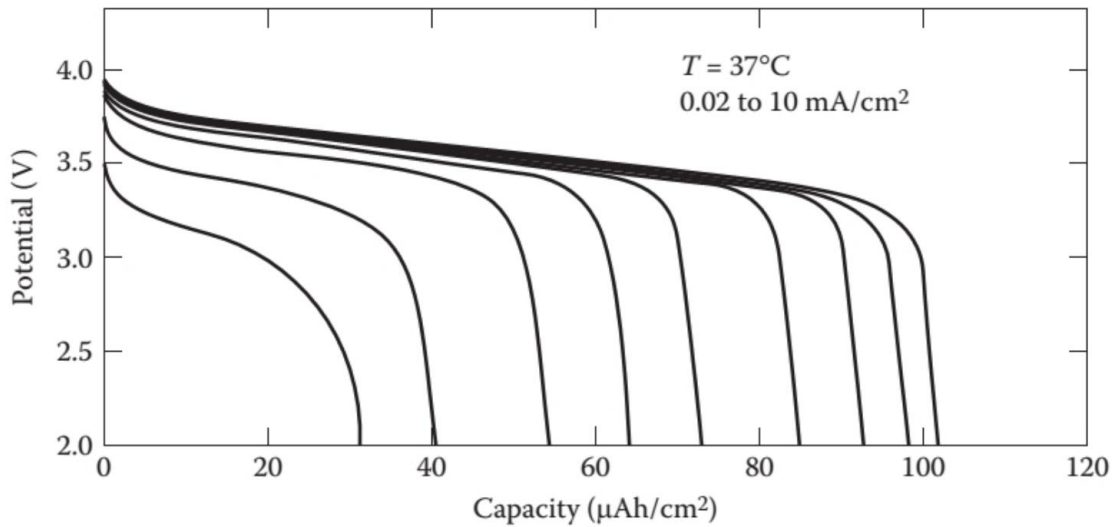
Figure 3.32   Example of Li-Po battery discharge curves (Jha, 2016).

For reference, in (Russell, Theodore and Sekula, 2018), the maximum discharge depth is 80% of the total energy, and the discharge efficiency is 98%.

3.4.5.4   Battery Selection

3.   **Mass**

The batteries are normally estimated by their total energy. Gatti's regression is described by Equation (72) and Figure 3.33:

$$m_b = \frac{E_{b,full}}{138.04} = 0.007244 \cdot E_{b,full} \tag{72}$$
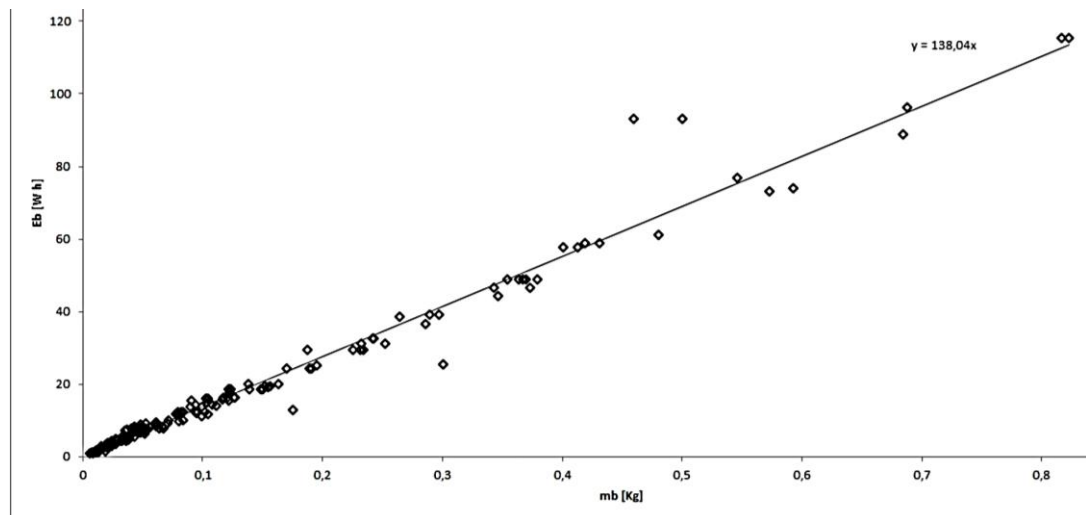
Figure 3.33   Battery capacity as a function of battery mass trend line (Mauro Gatti, 2015).

This regression is validated with my own database: 678 models for regression, 381 for validation. See Equation (73), Figure 3.34, Figure 3.35 and Table 3.13 for the regression results and validation details. An extra prediction interval validation is presented in Table 3.14.

$$m_b = 0.006703 \cdot E_{b,full} = \frac{E_{b,full}}{149.2} \tag{73}$$
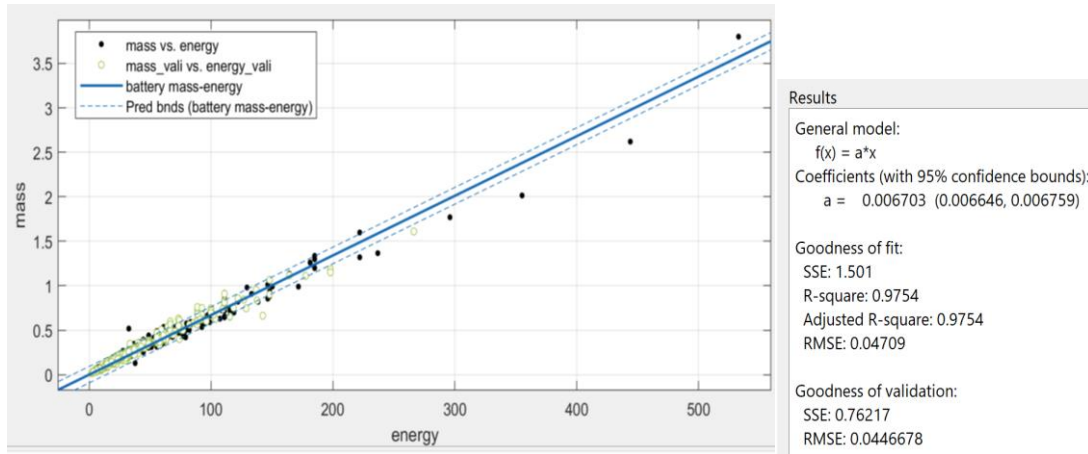
Figure 3.34   The regression between battery mass and energy.
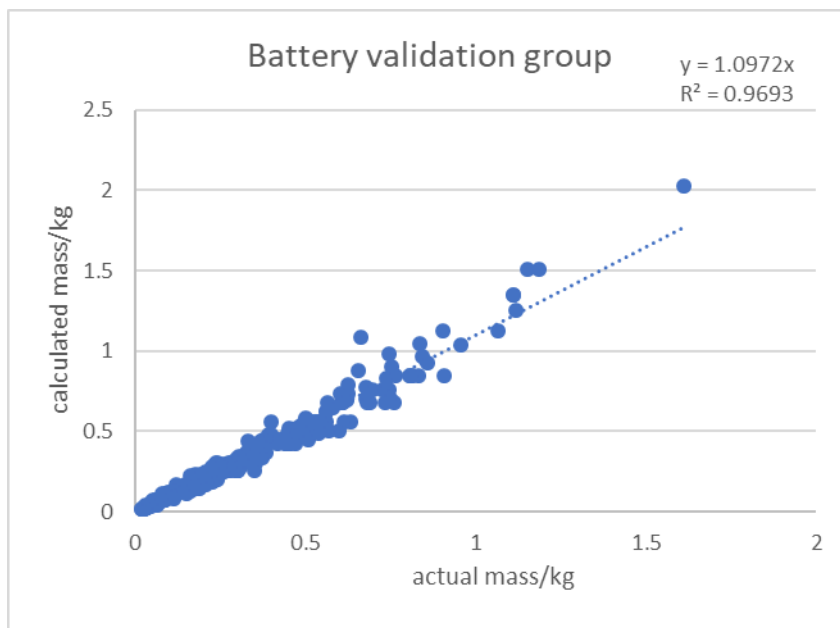
Figure 3.35   The validation of the battery mass regression.

Table 3.13 The goodness of validation of the battery mass estimation.

	Absolute Error	Error Ratio
Max	0.421	63.48%
Min	-0.095	0.02%
Average	0.018	9.99%
Standard Deviation	0.058	9.02%
Variation Coefficient	3.21	0.90

Table 3.14 The actual ratio of validating models that fall into the prediction interval.

Prediction Intervals	99%	95%	90%	80%	67%	35%	10%
Actual Ratio	96.00%	93.50%	91.50%	86.00%	83.00%	61.00%	30.50%

4. Price

The price of the battery is correlated with models from the database: 310 models for regression, 157 for validation. See Equation (74), Figure 3.41, Figure 3.42 and Table 3.15 for the regression results and validation details. An extra prediction interval validation is presented in Table 3.16.

$$pr_b = 0.6337 \cdot E_{b,full} \tag{74}$$

General model:		
f(x) = a*x		
Coefficients (with 95% confidence bounds):		
a =	0.6337 (0.6141, 0.6533)	
Goodness of fit:		
SSE: 5.734e+04		
R-square: 0.8517		
Adjusted R-square: 0.8517		
RMSE: 13.62		
Goodness of validation:		
SSE: 24283.8		
RMSE: 12.4368		
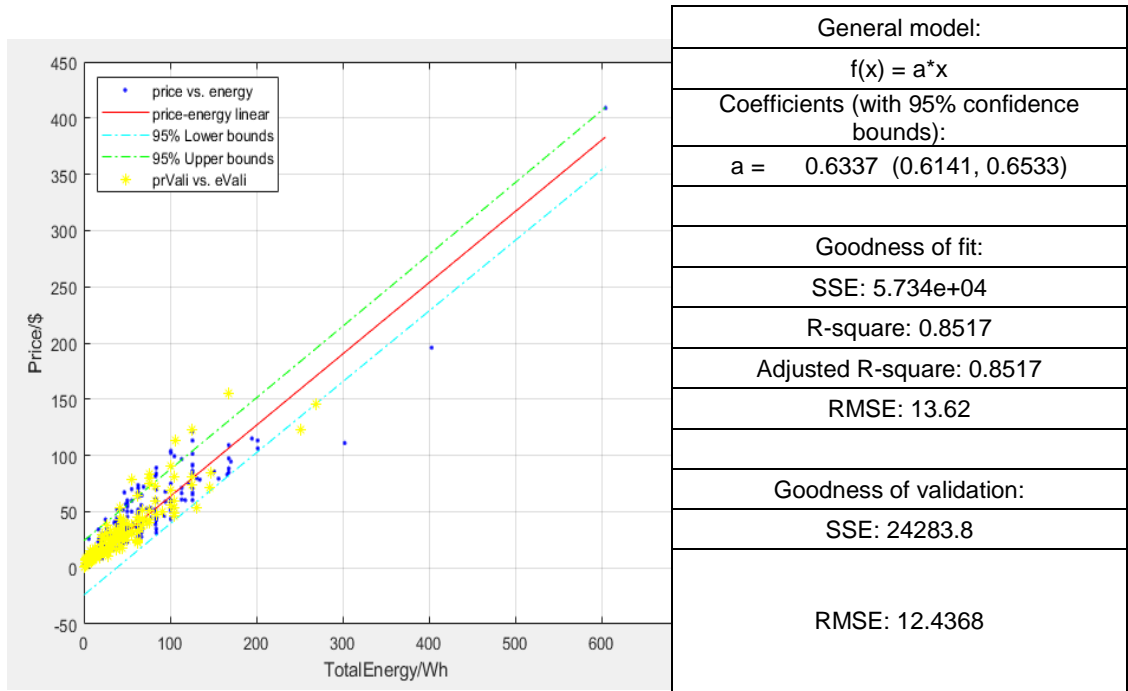
Figure 3.36   The validation of the battery mass regression and its goodness.
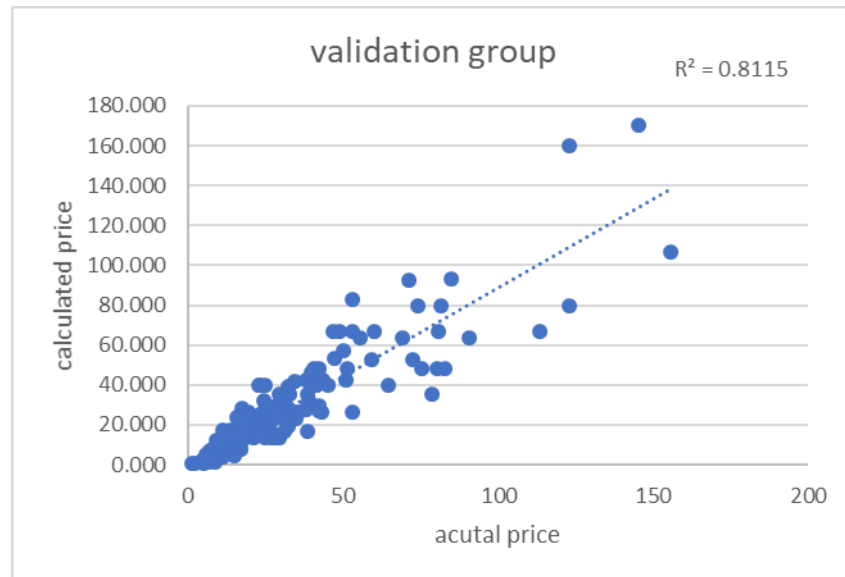
Figure 3.37   The validation of the battery mass regression.

63

Table 3.15 The actual ratio of validating models that fall into the prediction interval.

	Absolute Error	Error Ratio
Max	36.65	82.26%
Min	-49.21	0.54%
Average	-3.22	27.51%
Standard Deviation	12.05	20.36%
Variation Coefficient	-3.74	0.74

Table 3.16 The actual ratio of validating models that fall into the prediction interval.

Prediction Intervals	99%	95%	90%	80%	67%	35%	10%
Actual Ratio	98.28%	94.83%	91.38%	89.66%	82.76%	56.90%	27.59%

3.4.6 Arm Optimisation

The layer_3_armopt function accepts the maximum single rotor thrust, maximum torque of a motor and minimum arm length as inputs and determines the optimised cross-section shape (including its width, height and wall thickness) that causes the arm to have the minimum mass or price. The involved theories and equations of material mechanics are introduced in Appendix I. A detailed analysis of the optimisation function is presented in Section 4.3.10.

3.4.6.1 Structure of the Function

GA is used for this multi-input nonlinear constraints problem optimisation. The materials, shapes and dimensions are the variables for the optimised function. The output is either the mass or price of the arm. The forces and torques on the arm are involved in the calculation as global parameters.

Nonlinear constraints are set for the GA solver:

- Natural frequency
- Stress and shear stress
- Deformation

The variables are the material type, cross-section shape, cross-section width, cross-section height and thickness of the material. They are adjusted by the optimisation process and passed to the called function (layer_3_ armcalc) for material properties calculation. In this function, the mass and price of the arm are determined, and the performance parameters are checked by the constraints. In the end, the optimised arm should have the least mass or price when it satisfies the requirement for strength. (The basic knowledge of material mechanics can be found in Appendix I)

3.4.6.2 Price Optimisation

The price is calculated as the unit price times the total volume of arms.

This requires another optimisation command to call for a wrap function which uses the price of the arm as the optimisation target.

3.5   Constraints Check and Storage

Once all the components are calculated, the total mass and price can be summed. The mass error is calculated to return to the optimisation function.

Meanwhile, a series of error flags is recorded once an abnormal number of parameters appears. The appeared odd number does not stop the optimisation process, but the flag gets recorded in the exported data for further reference.

The checked parameters are as follows:

Table 3.18 The table of error flags.

$err_{flag}(1)$	Diagonal distance exceeds max size constraint
$err_{flag}(2)$	Exceed max landing gear height constraint
$err_{flag}(3)$	Not meet max forward velocity requirement
$err_{flag}(4)$	Not meet max ascent velocity requirement
$err_{flag}(5)$	Not meet hovering endurance requirement
$err_{flag}(6)$	Not meet cruising endurance requirement
$err_{flag}(7)$	Exceed max $MTOM$ constraint
$err_{flag}(8)$	Warning: motor max rotation speed exceeds the arm's first order natural frequency
$err_{flag}(9)$	Prop tip velocity exeeds Mach0.7
$err_{flag}(10)$	Descending velocity not appropriate, need to adjust mission specs
$err_{flag}(11)$	Exceed max advance ratio mu
$err_{flag}(12)$	Not meet mission forward velocity requirement
$err_{flag}(13)$	Not meet mission ascending velocity requirement

After testing all the combinations, the most suitable (normally the result with the lowest $MTOM$ or cost) result is selected from all the valid results. According to the optimisation target, the optimal design can be selected.

Chapter 4 Algorithm Validation and Results

As mentioned in (Weiand *et al.*, 2020), the conceptual design phase can evaluate various configurations quickly, but the calculations and estimations are largely based on empirical conclusions, which significantly contribute to the uncertainty of the algorithm (Chen, 2017). The purpose of conceptual design is to determine a trustworthy configuration for further design phases. The higher the confidence of the configuration, the easier it becomes for further design (Raymer, 2012).

4.1 Validation

In this thesis, the proposed algorithm is validated from four aspects, each reflecting one source of uncertainty:

- Components regression: Can the estimation functions of all components accurately estimate the component mass and price given the required performance?
- Design tools: Given the mission requirement and actual design parameters, can the layer_2 function accurately determine the required performances of each component?
- layer_2 function accumulative errors: Can the function provide an accurate estimation of the total mass, and hence, is the total mass estimation accurate?
- Optimisation process: What is the influence of the optimisation on the results?

4.1.1 Components Estimation

For each component, there exists a database of models. Approximately 70% of the models are used to determine the estimation function, while the remainder are used as the validation group. In previous sections, the validations of the estimation functions are introduced together with the functions and are included below in Table 4.1.

Due to the data limit, the estimation models of the central body frame geometry parameters and arm parameters are not validated. However, in the following section, they are included in the total mass estimation for comparison with actual multicopters.

This result reveals that save for the ESC price (explained in Section 3.4.4.3), the other components estimation models are trustworthy. Thus, the layer_3 functions can accurately estimate the mass and price of components based on given required performances.

Table 4.1   The conclusion of the validation of the component's estimation models.

Component	Initial Group	Validation Group	Regression method	Regression R^2	Validation R^2	Absolute Average Error	Absolute Max Error	RMSE
Propellers Mass	145	48	Poly3	0.93	0.94	54.70%	290.79%	59.48%
Propellers Price	248	81	Random forest	/	0.93	50.6%	276.5%	57.5%
Motors Mass	214	71	Random forest	/	0.87	14.81%	67.35%	13.76%
Motor mass against actual multicopter	Same as above	11	Same as above	/	0.98	22.57%	65.00%	18.58%
Motors Price	214	69	Random forest	/	0.93	27.17%	100.10%	25.63%
ESCs Mass	50	20	Linear	0.84	0.76	25.04%	173.63%	36.63%
ESCs Price	115	35	Exponential	0.45	0.47	32.70%	95.44%	26.16%
Batteries Mass	678	381	Linear	0.98	0.97	9.99%	63.48%	9.02%
Batteries Price	310	157	Linear	0.85	0.81	27.51%	82.26%	20.36%
Arms mass & price	/	/	sub-optimisation process	/	/	/	/	/
Central body diameter	18	/	Power	0.79	/	/	/	/
Central body thickness	5	/	Linear	0.97	/	/	/	/

4.1.2 Total Mass Estimation

Five commercial multicopter products have been selected (see Figure 4.1). From small to large, they are GEPRC Hummingbird 110,[17] Lisam 210,[18] 3DR Iris,[19] DJI Matrice 100[20] and DJI Spreading Wing 1000.[21] Their mission requirements, actual design parameters and actual middle parameters are fed into the algorithm. The calculated mass of each component and the total mass are then compared with the actual masses to validate the components estimation of the algorithm.

*Figure 4.1 The selected commercial multicopter platforms.
Images from web.*

[17] https://cn.bing.com/th?id=OIP.9zPr6qcuGUO_ZeldNNmmeQHaHa&pid=Api&rs=1

[18] https://cn.bing.com/th?id=OIP.DsiT38WZb3ESqTENktBUjAHaEK&pid=Api&rs=1

[19] https://cn.bing.com/th?id=OIP.15QB7GFrmWFpHpVqrkDv0QHaDa&pid=Api&rs=1

[20] https://cn.bing.com/th/id/OIP.SuWCPEi--WMK3nXT_baSegHaEQ?pid=Api&rs=1

[21] https://cn.bing.com/th?id=OIP.-8pJSNca-xknFeEEweG-9gHaHa&pid=Api&rs=1

The $GTOM$ of the five selected multicopters ranges from 120 g to 6000 g. The design parameters, such as the propeller diameter, number of rotors and body size, among others, are fixed and identical to the candidates. The mission requirements, constraints and some constants are also changed accordingly. Then, the required power and other middle parameters for estimating the components are calculated, and finally, the mass of all the components is estimated. The calculation results are presented in Table 4.2, and the details can be found in Appendix H.

The terms in this table are explained as follows:

- All units are in grams (g).
- For each model, the table lists its actual single-component mass, estimated single-component mass, absolute total error (e.g. the multicopter has four arms, the total error is the single-arm error multiplied by the number of arms) and the error ratio. The error ratio is colour labelled.
- The table is divided into three main parts: the $GTOM$, the body and the propulsion system.
- The $GTOM$ is the full mass of a multicopter without the payload. The fixed $GTOM$ is explained later.
- The 'frame total' is the total frame mass, including the unloaded body and unloaded arms. This data is normally given by the all-in-one frame, in which the arms and body are manufactured from a single piece of carbon fibre board (see Figure 4.2).
- The loaded central frame mass includes the mass of the avionics and landing gear.
- The loaded arm mass includes the mass of the propulsion system: a propeller, motor and ESC.

Figure 4.2 The all-in-one frame of Lisam-210[22].

Table 4.2   The validation of the components' mass estimation of the algorithm.

Component		Nr	GTOM	GTOM fixed	frame total	central body loaded	central frame loaded	single arm loaded	single arm	prop mass	motor mass	ESC mass	battery mass
GEPRC.. Hummingbird	actual	4	118.72	118.72	34	\	\	\	\	0.78	7.10	2.80	42
	estimated		157.37	124.81	28.07		14.11		3.49	1.81	12.56	10.94	28.04
	abs total error									4.13	21.85	32.56	13.96
	error ratio		32.55%	5.13%	-17.44%	\	\	\	\	132.44%	76.94%	290.68%	-33.25%
Lisam...210	actual	4	550		90					4	28	36	155
	estimated		548.87		97.81		64.22		8.40	4.60	24.07	31.96	156.55
	abs total error									2.40	15.72	16.14	1.55
	error ratio		-0.21%		8.68%					15.01%	-14.03%	-11.21%	1.00%
3DR...Iris	actual	4	1282			410 g	202	121 g	53	6.3	62	31	262
	estimated		1363.52			402 g	193.80	163 g	51.34	12.61	62.25	26.5	310.40
	abs total error									25.24	1.02	17.87	48.40
	error ratio		6.36%			-2.00%	-4.06%	34.24%	-3.12%	100.17%	0.41%	-14.41%	18.47%
DJI.. Matrice 100	actual	4	2355							19	106	43	600
	estimated		2554.03				226.77		30.43	16.65	168.29	51.24	560.83
	abs total error									9.39	249.15	32.95	156.67
	error ratio		8.45%							-12.36%	58.76%	19.15%	-6.53%
DJI.. Spreading wings S1000	actual	8	5945			1330 g	610	325 g	119	13	158	35	2015
	estimated		6404.37			1410 g	689.99	361 g	100.45	21.67	179.52	35.78	2109.24
	abs total error									69.39	172.20	6.24	94.24
	error ratio		7.73%			6.01%	13.11%	10.97%	-15.59%	66.72%	13.62%	2.23%	4.68%

From Table 4.2, it can be found that the estimation of the $GTOM$ is considered accurate (less than a 20% error, as explained below) for four of the five candidates. The estimations of components are mostly accurate, but there are some outstanding items:

- There is a brief explanation of the validation results. The regression function of all the components represents the average performance in the entire market (i.e. for a BLDC motor whose maximum power is 1000 W, KV is 2700, and the maximum operation voltage is 21 V; then, the estimation of its mass of 35 g is only the mean standard in the market). Due to the differences in terms of brand, materials used and techniques used, among others, there must exist lighter or heavier models of the same performance. Thus, in the validation, an error between the mass of the actual model used and the estimated mass is common, so long as it is within a reasonable range. The 20% error threshold results from the analysis of the components database. According to Table 4.2, the average error ratio of the components estimation ranges from 14% to 54%, which reflects the variance of products in the market. Thus, in this validation, when the total error ratio is less than 20%, it is possible that the actual multicopter uses a component of similar performance but different in mass. The DJI Matrice 100 is a suitable example; its motor estimation is slightly poor, but the total mass estimation is acceptable.

- The estimation of the components of very small multicopters is mostly inaccurate, especially the estimation of the ESC. This is because very small multicopters tend to integrate the electronic circuits on the frame, so the ESC can be made very small and light, while the algorithm still estimates the ESC as though they are independent components. The estimations of other components are not as poor (the absolute error is not large), and when considering the actual ESC mass, the fixed $GTOM$ error is acceptable; however, at this scale, even a 1 g mass matters. As a result, before further studies, the algorithm is currently not valid for the multicopter design in this level ($GTOM$ < 120 g).

- For the 3DR Iris, the estimation of the mass is not very accurate, as the actual arm is in a truss form (see Figure 4.3). This shape is not modelled in the arm estimation algorithm, so a simple hollow rectangular is used instead.

Figure 4.3 The arm of 3DR-Iris[23].

---

[23] https://cn.bing.com/th/id/OIP.2h_k65LKj6ErYrHYaL0EsgHaHa?pid=Api&rs=1

- The propeller estimations of the 3DR Iris and DJI SW 1000 have relatively larger error ratios, but the error numbers are quite small compared with other components. Consider DJI SW 1000, for which the comparison of all the component errors is presented in Figure 4.4. This figure also indicates that the motors and battery are the two heaviest components and should be considered more than other components if the optimisation target is $GTOM$.
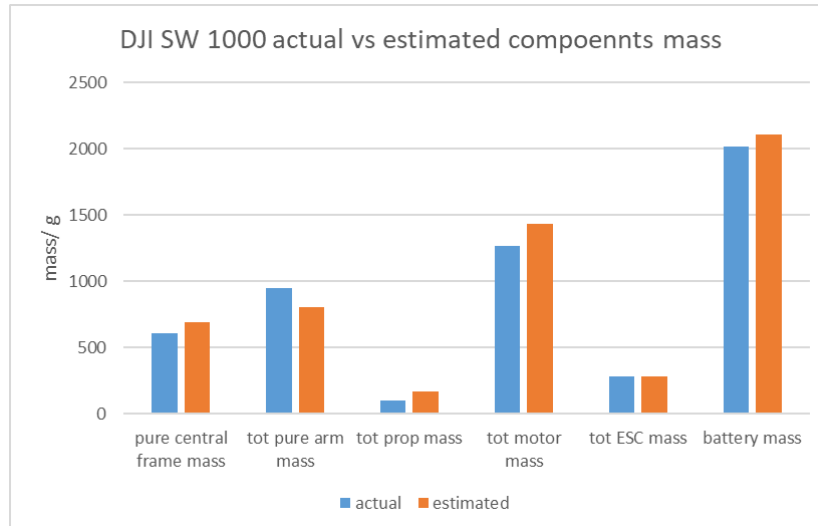
Figure 4.4 The comparison of the estimation errors of different component.

4.1.3 Layer_2 Function Results

4.1.3.1   Output-Input Plot.

In the layer_2 function, all the necessary parameters are calculated from the given design parameters and DL. An inappropriate DL value may return invalid results, in which the error between the initial $GTOM$ and the estimated total mass is too large to be fixed in further design stages (this threshold is 2% in this algorithm). The layer_1 function uses the fminsearch method to find the optimum DL for which the error is as close as possible to zero. By scanning the DL for a given group of design parameters, an input (DL)-output ($err_{percent}$) graph can be plotted. The five selected multicopters are used for this plot (see Figure 4.5). In the textboxes, the comparison between the actual multicopter data and the optimised result is listed. The coordinate of the point is written inside parentheses, (DL, percentage error), and is followed by the $GTOM$. The following can be concluded from the figure:

- 3DR and Lisam are quite close to the theoretical optimum. Thus, their design is valid according to the calculation of this algorithm.
- The other three multicopters suffer from larger differences between the actual and optimised DL and $GTOM$. From the algorithm point of view, they are invalid designs, but as this algorithm is based on statistics results and several assumptions, this is because the manufacturer used better technology on some components (same performance but lighter). Thus, it is clear the algorithm is based on the average performance of

components from the market and develops a design that addresses the average requirement. On the other hand, the overestimation is a safety factor as well; thus, starting with the design made by the algorithm, there is always the potential for improvement.

The actual and estimated mass of five multicopters on the error-DL plot
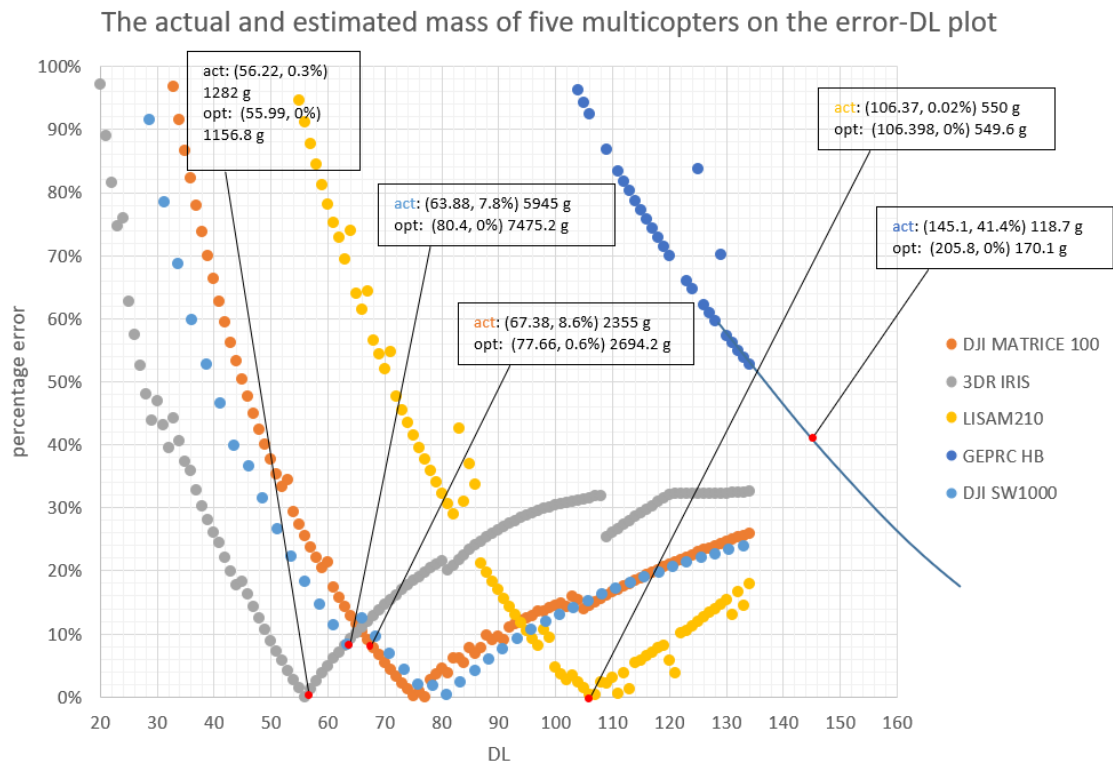
Figure 4.5 The layer_2 function output-input plot.

4.1.3.2   Discontinuity

The role of the 'fminsearch' method is to find the minimum point on the curve. It can be noticed that the curve is not continuous, caused by the forest model of the motor. The forest is comprised of several tree; each tree includes multiple leaves, and each leaf models a certain range of motors. When the layer_3_motor function is called and the performance requirement of the motors is known, each tree model first locates the correct leaf and then develops a candidate answer with its confidence. Based on this answer and its confidence, the forest then selects the most suitable answer. From this procedure, it can be seen that the forest model is not always linear, which causes the discontinuity of the error-DL plot. To prove that discontinuity is indeed caused by the motor model, two other motor estimation methods, from (Mauro Gatti, 2015) and (Winslow, Hrishikeshavan and Chopra, 2017a), are tested. It can be seen in Figure 4.6 that the error-DL curves of the two comparison methods are smooth. Figure 4.7 presents the zoomed-in view close to the optimum point. The selected multicopter for comparison is the DJI SW 1000.

4.1.3.3   Invalid Zone

It can be seen in Figure 4.5 that the GEPRC Hummingbird drone does not have a valid optimisation result within the range of DL. The main concern of the DL value is that a larger DL indicates a larger pressure on the propeller blade. Thus, the upper boundary of the DL range is

determined by the strength of the blade (see Section 4.3.8 for the determination of the DL range). The GEPRC is a racing drone; it uses a three-bladed propeller, which has larger solidity than two-bladed ones, so it can withstand an extremely large DL value and provide enough thrust to accelerate the multicopter.
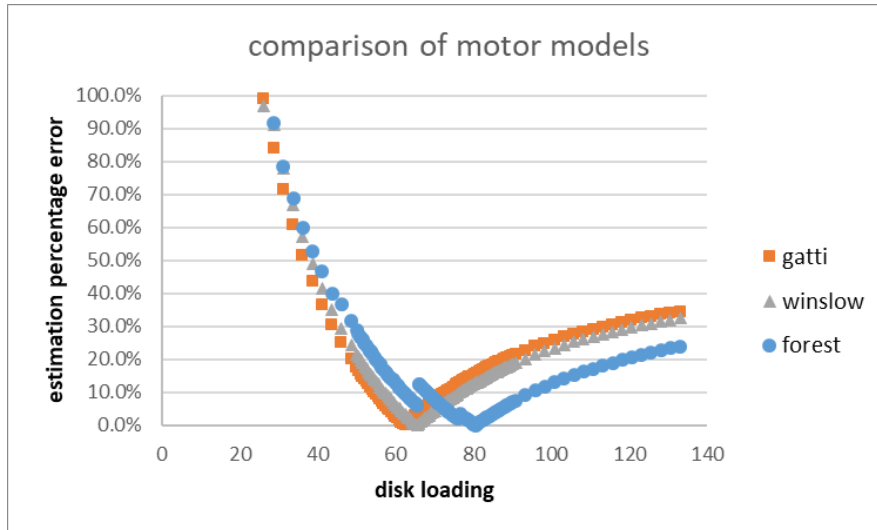
Figure 4.6 The comparison of three motor mass estimation methods.
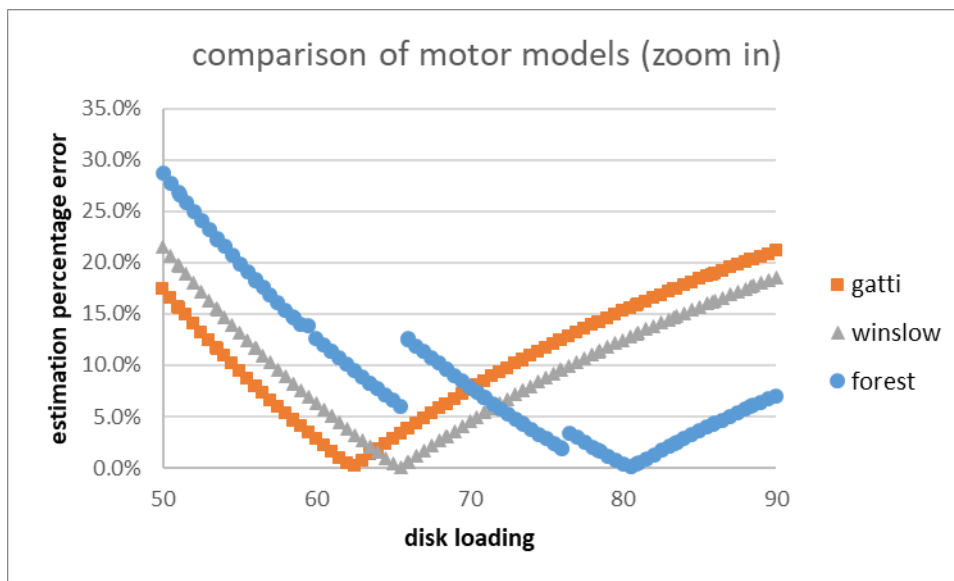
Figure 4.7 The zoomed in view of the error-DL plot.

In the previous two sections, the design parameters are fixed according to the multicopter; however, in the design process, all the design parameter combination candidates are considered. When the range of DL is defined, for a group of design parameters, the optimised point falls outside the range, and the parameters are considered an invalid design.

Considering the DJI SW 1000 as an example, the three main design parameters are tested to determine how they influence the invalid zone (see Table 4.3).

74

Table 4.3   The optimised percentage error changes with design parameters.

Number of rotors, N_r	number of battery cells, N_c	propeller diameter, d_p	Thrust weight ratio, TrW	Disk Loading, DL	total no payload mass, M_tot,g	err_percent
Only change N_r						
4	6	15	1.4	134.3	6776.868	8.5%
6	6	15	1.4	101.5864	7083.656	0.0%
8	6	15	1.4	80.40062	7475.159	0.0%
Only change N_c						
8	1	15	1.4	100.3655	9331.376	0.0%
8	2	15	1.417499	72.72288	6761.33	0.0%
8	3	15	1.438106	70.90406	6592.234	0.0%
8	4	15	1.456617	69.32298	6445.21	0.0%
8	5	15	1.449452	69.92923	6501.599	0.0%
8	6	15	1.4	80.40062	7475.159	0.0%
8	7	15	1.4	79.05022	7351.684	0.0%
8	8	15	1.4	78.59275	7307.077	0.0%
8	9	15	1.4	76.88501	7148.304	0.0%
8	10	15	1.4	76.53123	7115.408	0.0%
8	11	15	1.4	76.29221	7093.176	0.0%
8	12	15	1.4	76.0363	7069.374	0.0%
8	13	15	1.4	76.04775	7070.456	0.0%
Only change d_p						
8	6	4	1.4	134.3	3855.077	334.2%
8	6	5	1.4	134.3	4638.818	234.4%
8	6	6	1.4	134.3	4501.212	125.3%
8	6	7	1.4	134.3	4478.977	64.7%
8	6	8	1.4	134.3	4691.891	32.1%
8	6	9	1.4	134.3	4960.974	10.4%
8	6	10	1.4	134.3	5762.21	3.8%
8	6	11	1.4	113.9471	5697.28	0.0%
8	6	12	1.4	93.71245	5576.189	0.0%
8	6	13	1.4	84.36837	5891.748	0.0%
8	6	14	1.4	77.35548	6265.093	0.0%
8	6	15	1.4	80.40062	7475.159	0.0%
8	6	16	1.473033	72.94125	7716.001	0.0%
8	6	17	1.615199	66.47456	7938.365	0.0%
8	6	18	1.739038	62.23838	8332.625	0.0%
8	6	19	1.822178	60.60114	9039.983	0.0%
8	6	20	1.961319	56.44928	9330.337	0.0%
8	6	21	2.061061	54.39681	9912.678	0.0%
8	6	22	2.154559	52.69155	10538.15	0.0%
8	6	23	2.186433	53.11396	11610.3	0.0%
8	6	24	2.302314	50.69666	12066.47	0.0%
8	6	25	2.654723	42.60696	11003.7	0.0%

It can be seen from the table above that the propeller diameter has the largest influence on the invalid zone, followed by the number of rotors. Meanwhile, the number of battery cells has the least influence. Regarding the propeller diameters (see Figure 4.8), it is clear that a smaller propeller diameter results in a larger DL; when the propeller is smaller than a size, the optimisation results fall within the invalid zone.
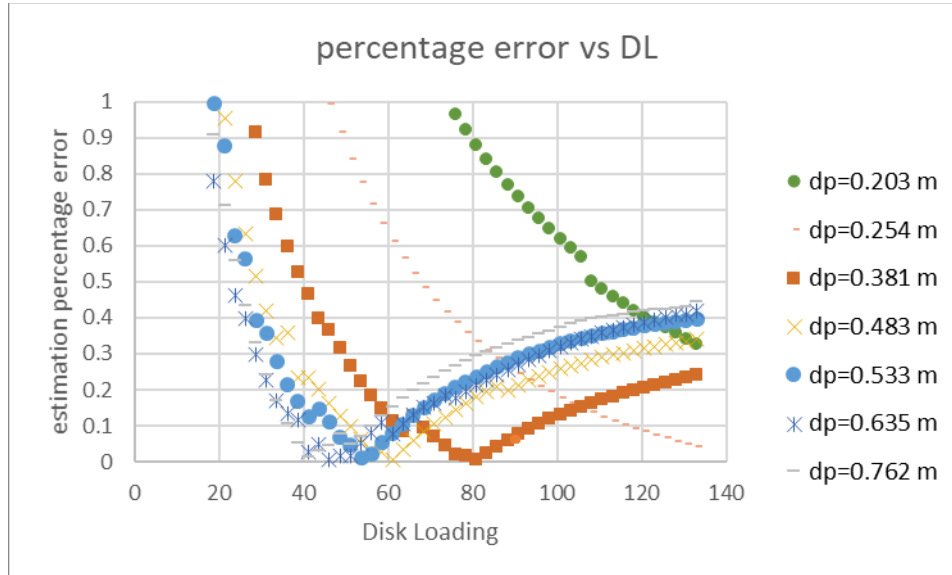
Figure 4.8 The output-input plot for different propeller diameters.

4.1.4 Total Cost

Costs in rotorcraft design typically include three sources: (Johnson, 2010)

- The aircraft purchase price (CAC, in dollars) consists of the airframe and mission equipment package (MEP).
- The flight control electronics (FCE) costs.
- The direct operating cost (DOC, in cents per available seat mile [ASM]) is the sum of the maintenance cost (C_{maint}, in dollars per flight hour), flight crew salary and expenses, fuel and oil cost, and depreciation.

The costs are estimated using statistical models based on historical aircraft price and maintenance cost data, with appropriate factors to account for technology impact and inflation.

However, there currently does not exist such a database for multicopters. Instead, the price can be estimated only by summing the price of all the components. In this thesis, the purpose of the conceptual design algorithm is to help in deciding the most suitable multicopter configuration for certain missions. To be specific, the algorithm would be used to compare different designs. Cost is one of the factors considered in the comparison. Given that for both designs the price is estimated using the same method, such a comparison is meaningful and can be used as a reference for decision making.

Most of the optimisation targets share the same procedure; however, when the optimisation target is the minimum total cost, the layer_2 function calls a different layer_3_arm_price function to minimise the cost of the arms. The main difference is that the layer_3_arm_price function tends to select cheaper materials even though it may become larger and heavier.

Presented below is the price estimation based on the results from Section 4.1.2 The price is in $.

Table 4.4   The estimated component price of DJI SW 1000.

Nr=8		motor price	ESC price	propeller price	arm price	battery price	body price	total price
	unit price	65.42	10.87	7.69	43.07			
	total price	523.34	86.98	61.54	344.55	302.82	100.05	1419.27

The price values for the components of the DJI SW s1000 are not officially specified, but according to information online,[24] the total price of the multicopter ranges from $1,200 to $1,440 for a pure aircraft without the RC controller and any accessories (see Figure 4.9).
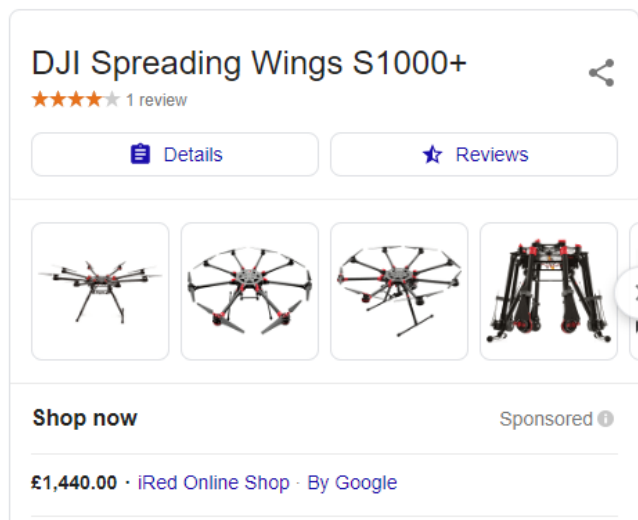
Figure 4.9 Price of DJI SW 1000 online.

4.2   Optimisation Process Validation

The DJI SW 1000 is selected to perform a full optimisation, in which all design parameters can be changed, including the number of rotors (N_r), number of battery cells (N_c), propeller diameter (d_p), arm cross-section shape and arm materials. The body material is still fixed to carbon fibre. The arm parameters are independent of the main parameters and are functional in the sub-optimisation process. Thus, by proceeding through the three main design parameters—$3(N_r) \times 7(N_c) \times 5(d_p) = 105$ combinations—the algorithm produces 89 valid results and 16 invalid designs (optimised point falls into the invalid zone).

---

[24] https://thewiredshopper.com/dji-spreading-wings-s1000/

The results of the $GTOM$ distribution are plotted in Figure 4.10, Figure 4.11 and Figure 4.12. The actual multicopter is located on the chart. All the valid designs can theoretically complete the mission. In terms of mass, several designs exist that have a lighter $GTOM$ than the actual product. The 3D plot presents the results clearer (see Figure 4.13). To generate the plot in MATLAB, the invalid designs must be included in the data matrix. To distinguish them, they are covered.
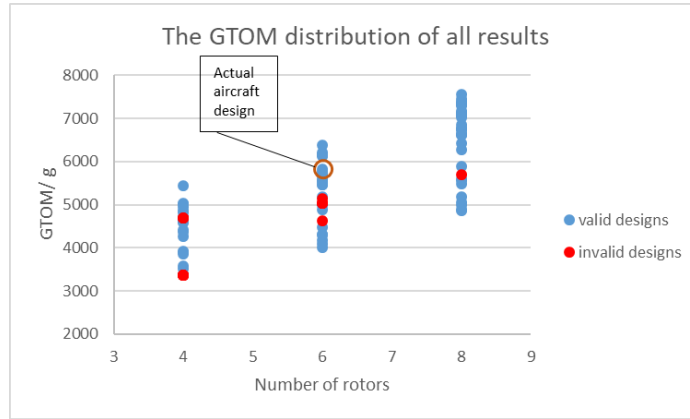
Figure 4.10   The $GTOM$ distribution against number of rotors.
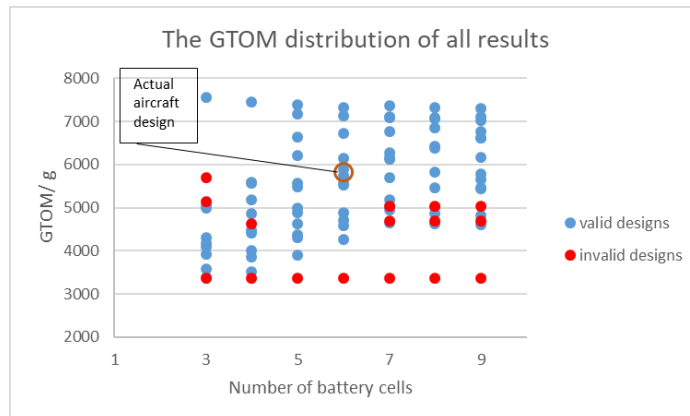
Figure 4.11   The $GTOM$ distribution against number of battery cells.
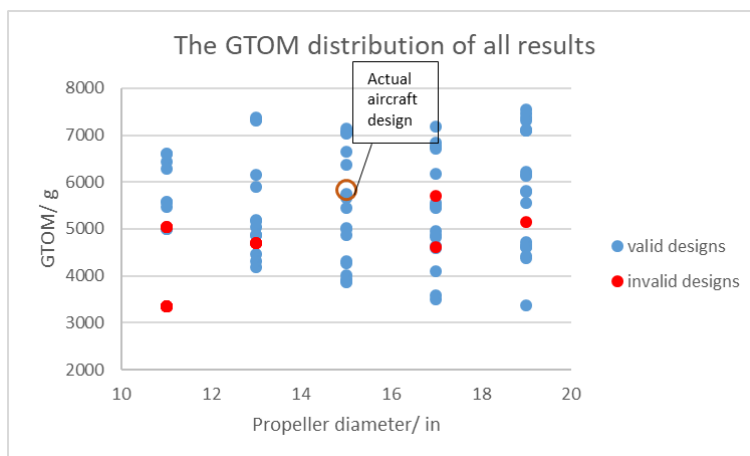
Figure 4.12   The $GTOM$ distribution against propeller diameters.
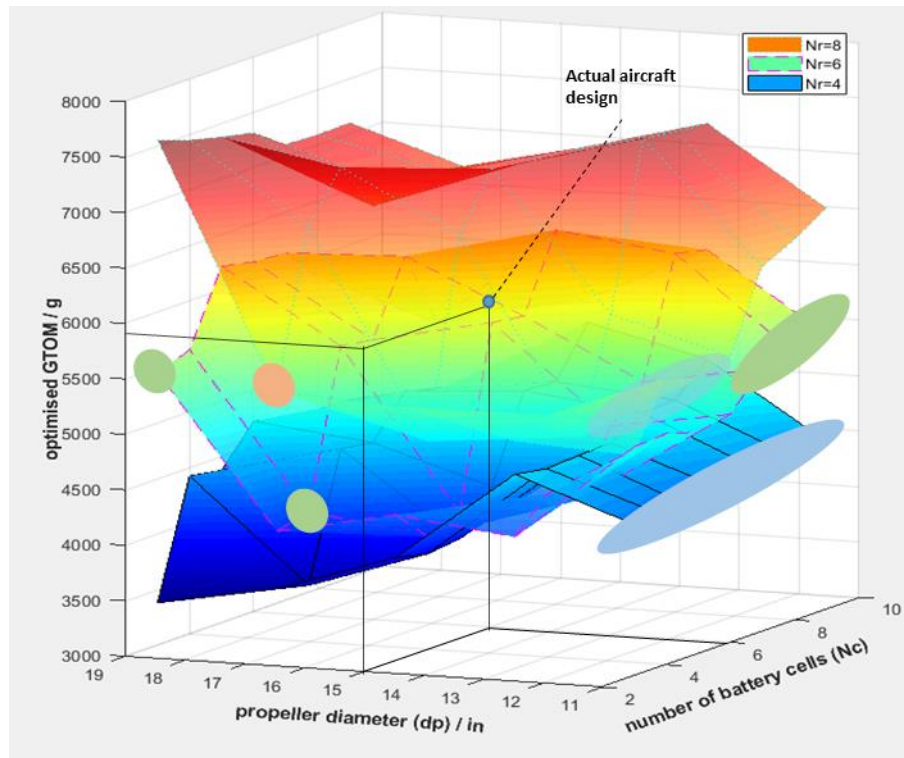
Figure 4.13   The 3D plot of the GTOM distribution.

The detailed data is given in Table 4.5. Invalid designs are listed as zero. Each sub-table maps one layer in Figure 4.13 above and are also plotted in Figure 4.14, Figure 4.15 and Figure 4.16..

Table 4.5   The optimised GTOM distribution against three main design parameters.

GTOM		N_c						
N_r	d_p	3	4	5	6	7	8	9
4	11	0	0	0	0	0	0	0
	13	4749.061	4698.26	4716.684	4729.633	0	0	0
	15	3928.43	3861.056	3895.978	4263.648	5029.008	5007.31	5443.045
	17	3575.171	3506.843	4635.374	4591.236	4951.34	4864.128	4818.608
	19	3381.58	4422.721	4372.996	4714.097	4652.098	4617.829	4607.935
6	11	5064.941	5084.413	4996.684	5053.903	0	0	0
	13	4184.508	4471.873	4311.857	4878.188	5176.069	6231.812	6164.844
	15	4311.305	4015.915	4123.453	5741.999	5699.817	6376.158	5653.677
	17	4095.551	0	5562.193	5517.068	6173.008	5469.542	5459.158
	19	0	5559.288	6212.385	6151.852	6128.836	5816.225	5793.002
8	11	4988.533	5587.118	5476.133	5575.687	6284.508	6425.618	6612.013
	13	5048.266	5184.392	4876.88	5888.1	7375.154	7325.6	7307.066
	15	5289.001	4871.691	6640.124	7131.314	7081.243	7063.487	7028.312
	17	0	6742.435	7174.682	6720.471	6760.206	6845.874	6760.684
	19	7555.051	7451.269	7379.299	7315.104	7108.677	7096.483	7103.038
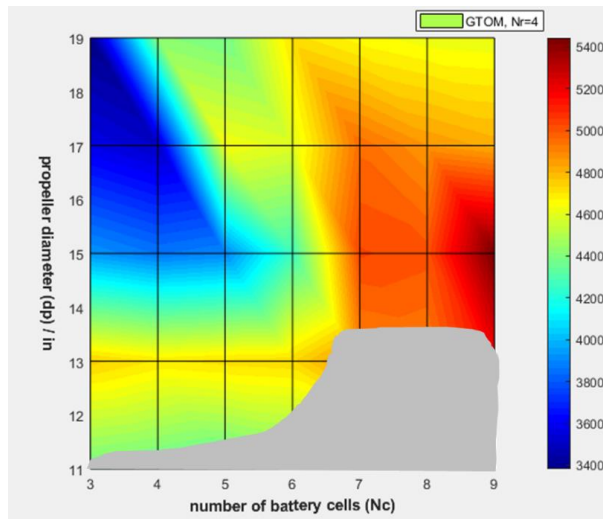
Figure 4.14   The $GTOM$ distribution for $N_r = 4$ designs.
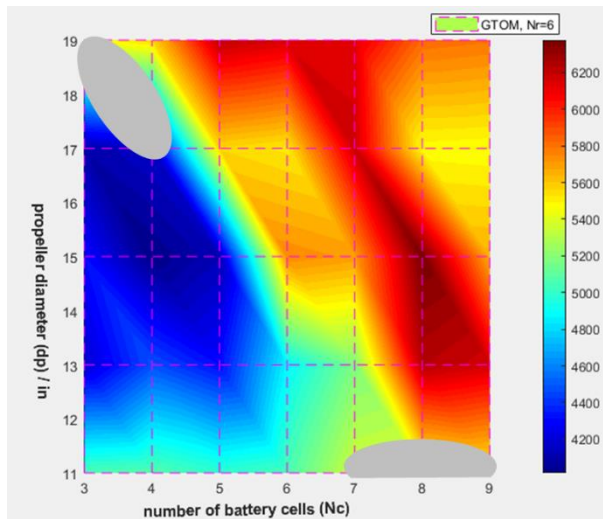
Figure 4.15   The $GTOM$ distribution for $N_r = 6$ designs.
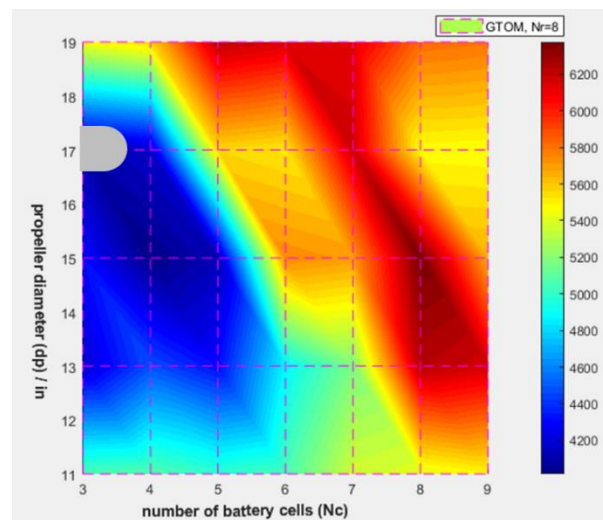
Figure 4.16   The $GTOM$ distribution for $N_r = 8$ designs.

In the results, for each design entry, the algorithm recorded its main middle parameters, normally the performance; $GTOM$ is only one of them. Similar plots have been applied on the two other main performance parameters: the total cost and the total energy consumption (see Figure 4.17 to Figure 4.24, Table 4.6 and Table 4.7).
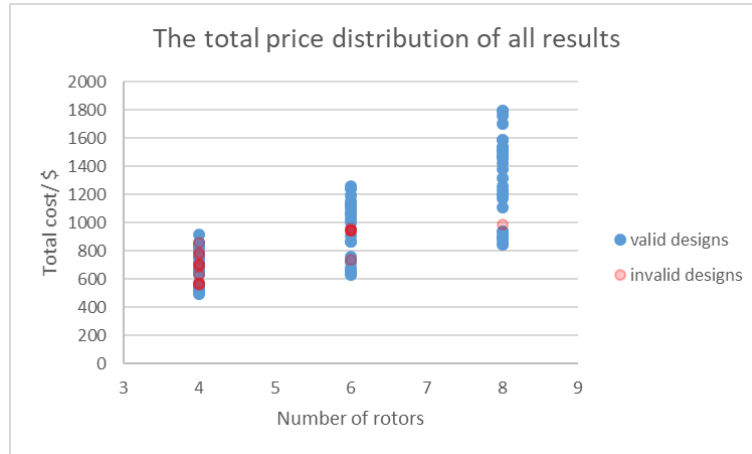
Figure 4.17   The total cost distribution against number of rotors.
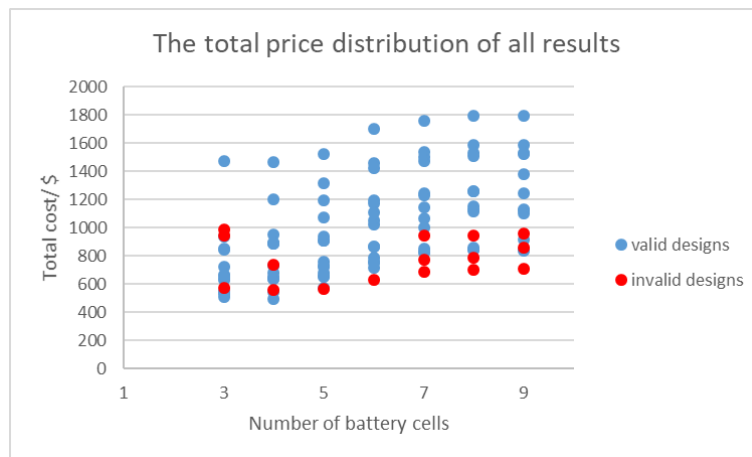
Figure 4.18   The total cost distribution against number of battery cells.
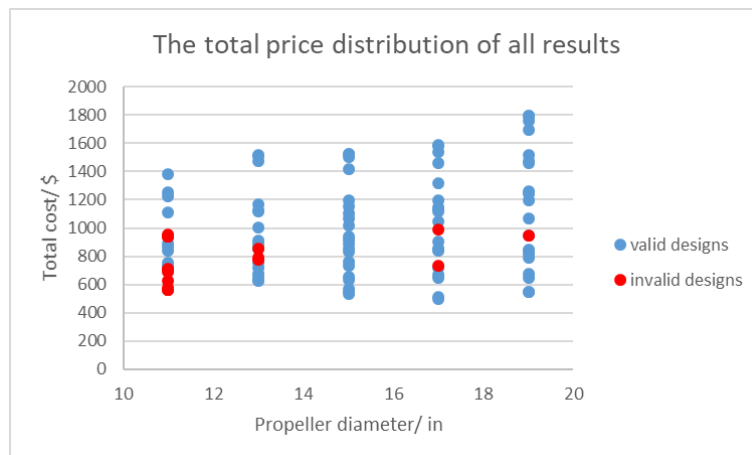
Figure 4.19   The total cost distribution against propeller diameters.
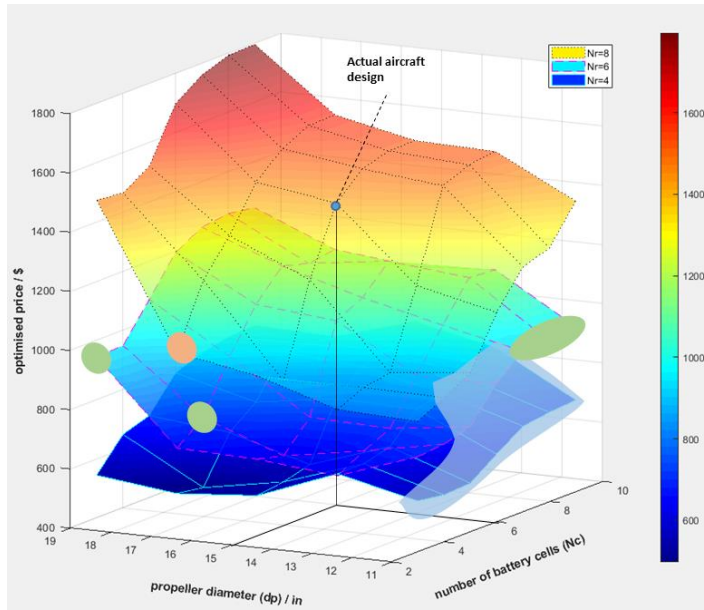
Figure 4.20   The 3D plot of the total cost distribution.

Table 4.6   The optimised total cost distribution against three main design parameters.

GTOM		N_c						
N_r	d_p	3	4	5	6	7	8	9
4	11	0	0	0	0	0	0	0
	13	635.7112	635.2971	658.7336	751.5715	0	0	0
	15	533.192	545.2949	569.7536	758.4188	832.0916	856.062	915.947
	17	511.5203	497.4887	649.574	718.132	853.6051	844.6009	836.896
	19	544.7695	648.5834	677.8173	788.1482	821.0373	841.7056	847.16
6	11	5064.941	5084.413	4996.684	5053.903	0	0	0
	13	4184.508	4471.873	4311.857	4878.188	5176.069	6231.812	6164.844
	15	4311.305	4015.915	4123.453	5741.999	5699.817	6376.158	5653.677
	17	4095.551	0	5562.193	5517.068	6173.008	5469.542	5459.158
	19	0	5559.288	6212.385	6151.852	6128.836	5816.225	5793.002
8	11	841.2717	887.474	936.4328	1107.756	1225.862	1256.619	1380.443
	13	852.8221	893.0094	908.5659	1169.144	1472.312	1508.342	1519.563
	15	937.8028	886.9102	1193.684	1419.273	1500.227	1527.169	1527.375
	17	0	1198.597	1314.223	1461.276	1539.66	1583.833	1585.686
	19	1474.814	1463.5	1520.959	1698.218	1760.701	1792.814	1795.651
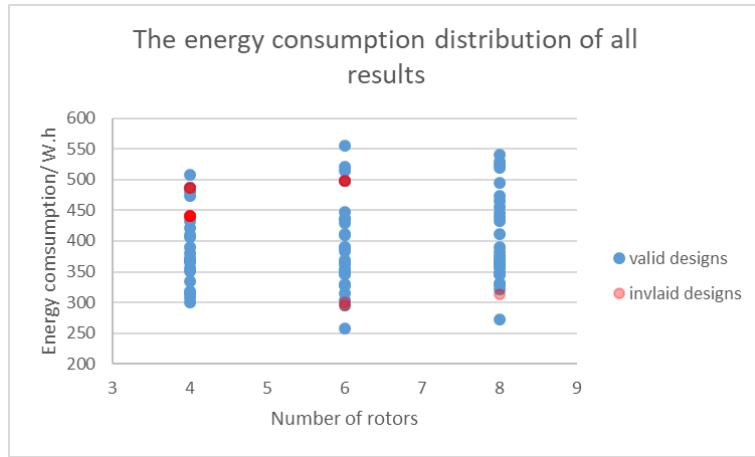
Figure 4.21   The total energy consumption distribution against number of rotors.
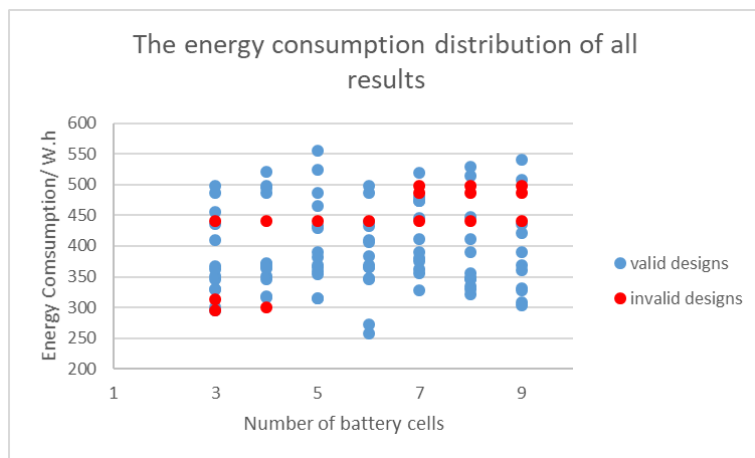
Figure 4.22   The total energy consumption distribution against number of battery cells.
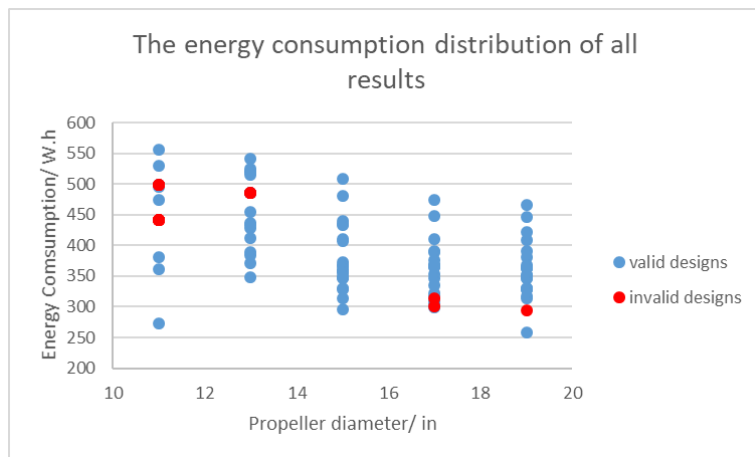
Figure 4.23   The total energy consumption distribution against propeller diameters.

83
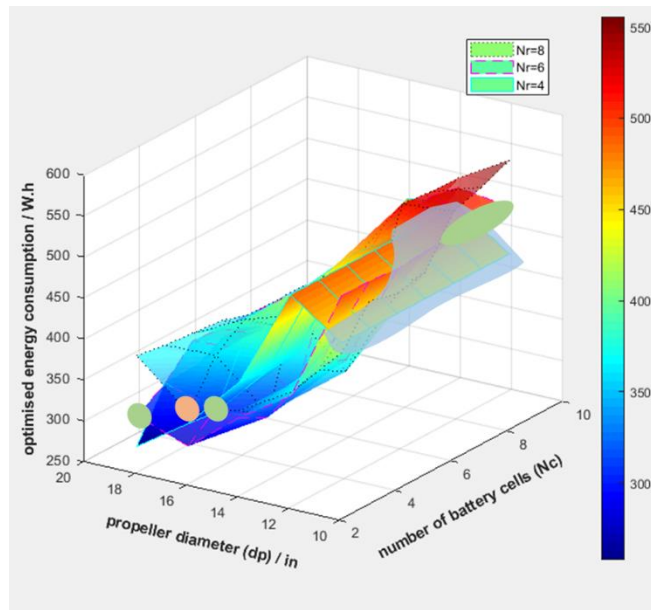
Figure 4.24   The 3D plot of the total energy consumption distribution.

Table 4.7   The optimised total energy consumption distribution.

GTOM		N_c						
N_r	d_p	3	4	5	6	7	8	9
4	11	0	0	0	0	0	0	0
	13	485.8498	485.8498	485.8498	485.8498	0	0	0
	15	364.7823	359.9008	362.4281	389.3918	447.5607	445.875	480.1431
	17	299.8039	295.5421	368.5106	365.5564	389.89	383.9481	380.859
	19	257.7565	317.3183	314.3802	334.7204	330.9917	328.9364	328.3436
6	11	498.6479	498.6479	495.2311	498.6479	0	0	0
	13	361.4784	381.6536	370.3741	410.7992	432.6195	514.9888	507.7077
	15	321.2969	303.5127	314.2103	412.0971	409.3139	454.7071	406.2754
	17	272.3064	0	353.4836	350.8805	389.3346	348.1471	347.5506
	19	0	316.3931	350.7235	347.4919	346.2657	329.7578	328.5407
8	11	428.6142	474.1669	465.6044	473.2829	529.1478	540.5166	555.6568
	13	366.8535	375.5345	356.0224	421.4796	524.2346	520.6911	519.3675
	15	329.8402	308.6103	409.8458	439.6324	436.5636	435.4771	433.3281
	17	0	364.961	390.5611	366.1844	368.296	372.8626	368.3209
	19	368.3403	363.226	359.6948	356.5544	346.5189	345.9297	346.2462

Finally, the optimised designs are presented in Table 4.8. Each optimised design is, in some aspect, superior to not only the theory result of the same design as the actual multicopter but also the actual product. It is possible to achieve even better performance than the optimised result if more appropriate components are selected and if the system is designed towards the required capability in later design stages.

Table 4.8   The actual product and the optimised designs.

	Number of rotors	number of battery cells	prop diameter, in	Thrust weight ratio	Disk Loading	Arm cross section shape	diagonal distance, mm	$GTOM$, g	total cost, $	Total energy consumption, W.h
Actual Product	8	6	15	2.78	63.88	Hollow Oval	1045	5495	/	403.2
Same design as actual product	8	6	15	1.4	80.4	Hollow Oval	1045	7475.2	1321.7	411.2
Smallest design	4	4	13	1.4	134.30	L	490.14	4698.26	635.30	635.30
Cheapest and most efficient design	4	4	17	1.4	58.73	L	640.96	3506.84	497.49	295.54
Lightest design	4	3	19	1.4	45.34	L	716.36	3381.58	544.77	257.76

Based on the figures and data presented above, the following conclusions can be made:

- By comparing with the actual multicopter, the results confirmed the conclusion formed in the previous section—that the algorithm is based on the statistical average performance of components from the market. The optimised designs by the algorithm are also average performance designs. There is room to improve certain components to obtain greater performance (i.e. the algorithm tends to slightly overestimate the $GTOM$, price or other target parameters).

- The above figures are useful to examine whether the design is optimised for a certain target, and it reveals how to improve the performance. For example, if the optimisation target is $GTOM$, then the fewer rotors the better, and the number of battery cells must be appropriate for the mission. Alternatively, if the target is the total cost, then the fewest number of rotors, fewest number of battery cells, and cheapest materials form the cheapest design, but as a compromise, the $GTOM$ and energy consumption may be large. If the target is the total energy consumption, then efficiency becomes the most important factor, and among the three main design parameters, only the propeller diameter would significantly impact the efficiency.

- These figures prove the practical capability of the algorithm in the multicopter conceptual design stage. Multiple valid designs can be developed that are suitable for different optimisation targets. Furthermore, the algorithm provides clues regarding how to change the design parameters to form a balanced performance in the event that there are multiple optimisation targets.

4.3   Discussion of Constants and Constraints

4.3.1 Propeller Spacing

The propeller spacing problem can be traced back to the tandem propeller helicopter study (Dingeldein, 1954; Sweet and Langley, 1960). When two propellers move closer together, the vortex at the tip would influence each other and hence result in an efficiency drop. However, when they continue to move and begin to overlap, there exists a certain range of positions for which the vortex interaction can slightly increase the efficiency.

This research is interested in the minimum distance between two adjacent propellers, and the overlapping conditions are not considered. According to more recent literature (Aleksandrov and Penkov, 2012; Ramasamy, 2013; Brazinskas, Prior and Scanlan, 2016; Theys *et al.*, 2016), in the study of tandem propellers, the conditions with the setting of $\frac{d_a}{d_p} > 1$ are also covered. d_a is the distance between two propeller axes, and d_p is the propeller diameter. Harrington (2011) has visualised this phenomenon in an experiment. By using a smoke plume to visualize the airflow, it can be clearly observed that when the space between propellers (gap_p) varies from $0.05d_p$ to $0.5d_p$, each propeller has an independent vortex without affecting propeller performance (see Figure 4.25).
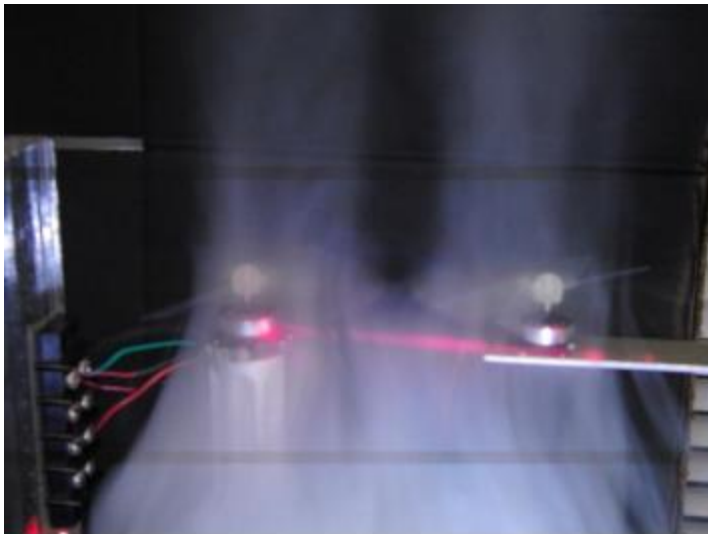
Figure 4.25   Two micro rotors operating side-by-side.
(Harrington, 2011)

As a common conclusion of the above studies, $1.05 < \frac{d_a}{d_p} > 1.2$ is considered a safe gap distance, and the influence from neighbouring propellers is reduced to an acceptable level. Nie (2017) designed a heavy lift octo-copter and used 0.083 as the $\frac{gap_p}{d_p}$ ratio. In this thesis, the $\frac{gap_p}{d_p}$ ratio is set to 0.124 as a constant.

4.3.2 Propeller Design and Performance Parameters

In Section 3.4.3.4, four important coefficients for propellers are used in the algorithm: the static thrust coefficient (C_{t0}), static figure of merit (FM), advance ratio (J) for certain efficiency, and overall efficiency (η_p). In this algorithm, a 'rubber propeller' is used, so for different-sized propellers, these parameters are all considered constants. In addition, they are the requirements for further detailed propeller design. If the user knows the performance parameters of their own propellers, these parameters can be changed accordingly.

4.3.2.1   Static Thrust Coefficient

The thrust coefficient is used for the calculation of thrust (see Equation (27)). In this algorithm, it is used reversely; it is the rotation speed to be calculated based on a known thrust.

C_{t0} changes slightly within a small range (the sensitivity is studied in Section 4.4.1). A typical example of a C_{t0} curve is displayed in Figure 4.26.
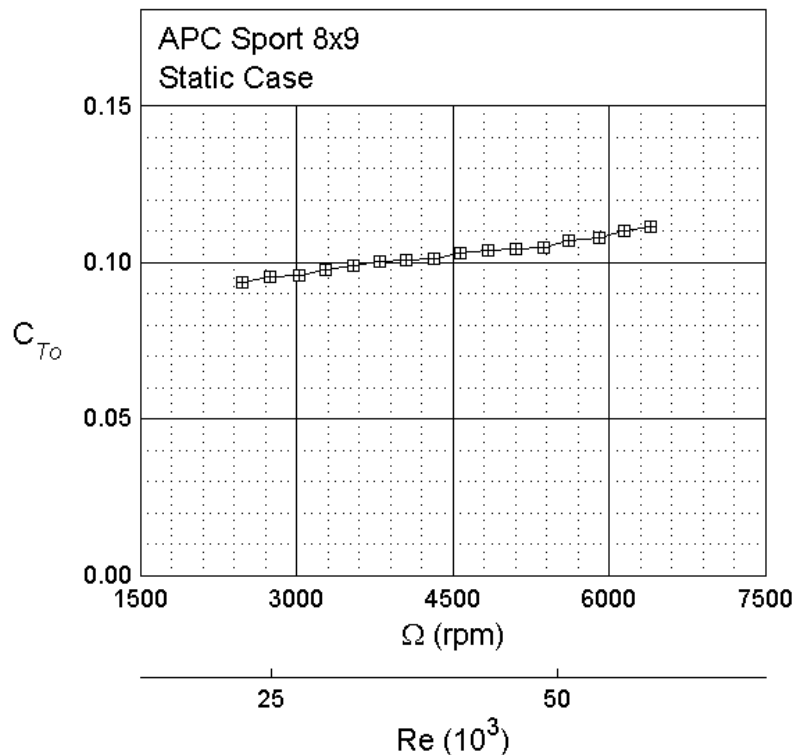
Figure 4.26   *The C_{t0} curve of the APC sport 8x9 propeller* (Brandt *et al.*, 2015).

The data in the UIUC propeller database[25] are extracted (65 models) and analysed (see Appendix E). It is found that for a given propeller diameter, by changing the pitch angle, C_{t0} can be adjusted (see Figure 4.27). Thus, C_{t0} is set to a constant 0.1 (Table 4.9), assuming that there exist certain propeller designs for any diameter that has the required performance.

---

[25] https://m-selig.ae.illinois.edu/props/propDB.html
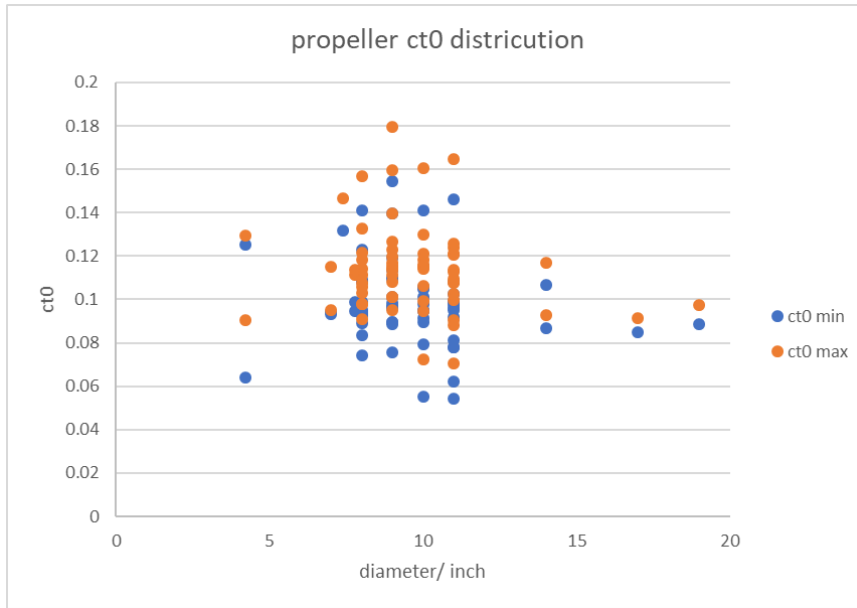
Figure 4.27   The distribution of the C_{t0} of 65 propellers.

Table 4.9   The statistics of the C_{t0} of 65 propellers.

Max	0.1672
Min	0.06225
Average	0.106175
Standard deviation	0.019834
Variation coefficient	0.186802
Median	0.1047
Skewness	0.793459

4.3.2.2   Efficiency in Static Flow Situation

During hovering, there is no movement, so there is no useful power (which is defined as the power consumed to do work, see Section 3.4.3.4 -1); rather, there are only the induced power (P_h) and profile power ($P_{0,h}$). The induced power is the part used to maintain the hovering, while the profile power is consumed by the drag on the propeller as it rotates; it is pure loss. In this situation, the figure of merit (FM) is introduced to describe the efficiency of the rotor during the hovering condition (see Equations (75)–(79)).

$$FM = \frac{P_h}{P_{input}} \tag{75}$$

$$P_{input} = P_h + P_0 \tag{76}$$

$$P_{0,h} = C_{p0,h} \cdot \rho \cdot n^3 \cdot d_p^5 \tag{77}$$

$$C_{p0,h} = \frac{1}{8} \cdot \sigma \cdot C_{d0} \tag{78}$$

Recalling Equation (26),

$$FM = \frac{\frac{C_T^{\frac{3}{2}}}{\sqrt{2}}}{\frac{\kappa C_T^{\frac{3}{2}}}{\sqrt{2}} + \frac{\sigma C_{d0}}{8}} \tag{79}$$

In this equation, κ is an empirical coefficient to fix the error between the measured C_T and actual C_T, σ is the solidity of the propeller and C_{d0} is the drag coefficient of the propeller blades. C_{d0} is determined based on the air foil of the propeller cross-section. The solidity is defined in Equation (80), where N_b is the number of blades, R_p is the propeller radius and c is the average chord.

$$\sigma = \frac{blade\ area}{disk\ area} = \frac{N_b c R_p}{\pi R_p^2} = \frac{N_b c}{\pi R_p} \tag{80}$$

4.3.2.3 Efficiency in Dynamic Flow Situation

The efficiency of a rotor when it is moving is defined as follows:

$$\eta = \frac{P_{useful}}{P_{input}} \tag{81}$$

$$P_{useful} = P_p + P_c = T_{g,s} \cdot v_{inf,v} \tag{82}$$

$$P_{input} = P_{useful} + P_i + P_0 \tag{83}$$

$$P_0 = C_{p0} \cdot \rho \cdot n^3 \cdot d_p^5 \tag{84}$$

$$C_{p0} = \frac{\sigma C_{d0}}{8} \cdot (1 + K\mu^2) \tag{85}$$

$$\mu = \frac{v_{inf,p}}{\Omega R_p}, \qquad \Omega = 2\pi n \tag{86}$$

The useful power refers to the power consumed to make any movement. Under the general flight condition, the useful power includes two parts: one part removes the drag and flies towards the wind-coming direction (known as the parasitic power, $P_p = D v_{inf}$), and the other part removes the gravity and climbs higher ($P_c = GTOW v_{inf} \sin(\gamma)$). Equation (82) can be derived from Equation (48). In addition to the useful power, there are the induced power (P_i) and profile power (P_0). The induced power is the power that propels the air and produces thrust. It is the required power; however, it is not directly involved in the movement. As described in Equation (85), the profile power coefficient is related to the solidity (σ) of the propeller, the drag coefficient of the blades (C_{d0}) and the helicopter advance ratio (μ). ΩR represents the tip velocity of the propeller, so the helicopter advance ratio reflects the forward movement velocity. The higher the velocity parallel to the disc plane, the higher the profile power (see Figure 4.28). Equation (85) is valid only for $\mu < 0.5$. At higher μ, P_0 increases more quickly. Once the rotation speed is determined, the value of μ is checked as a constraint in the algorithm. Here, K varies from 4.5 to 5 based on various assumptions, in which the compressibility losses, tip relief and reverse flow may be considered (Leishman, 2006).
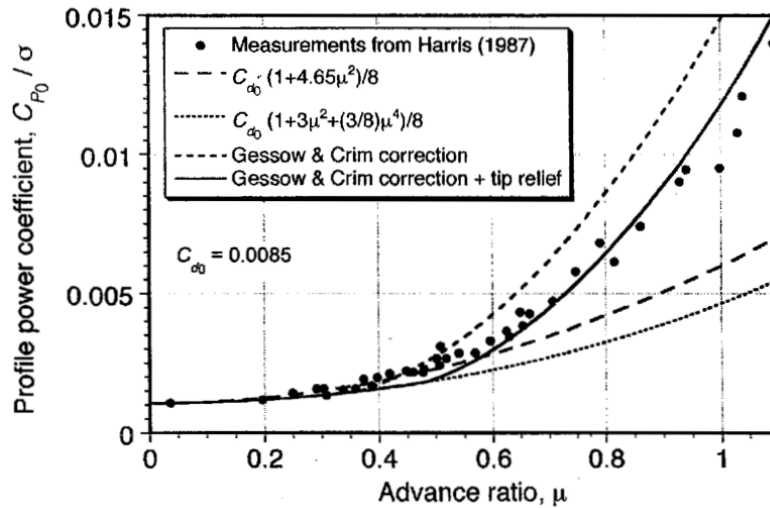
Figure 4.28   The profile power coefficient vs advance ratio chart (Leishman, 2006).

4.3.2.4   Dynamic Advance Ratio

Different missions may have different requirements for multicopters and propellers. Consider the APC propellers as an example: APC divides its products into various types, such as thin electric, slow fly and sport, and each type is suitable for a specific range of flight speed. The dynamic efficiency curve is illustrated in Figure 4.29.
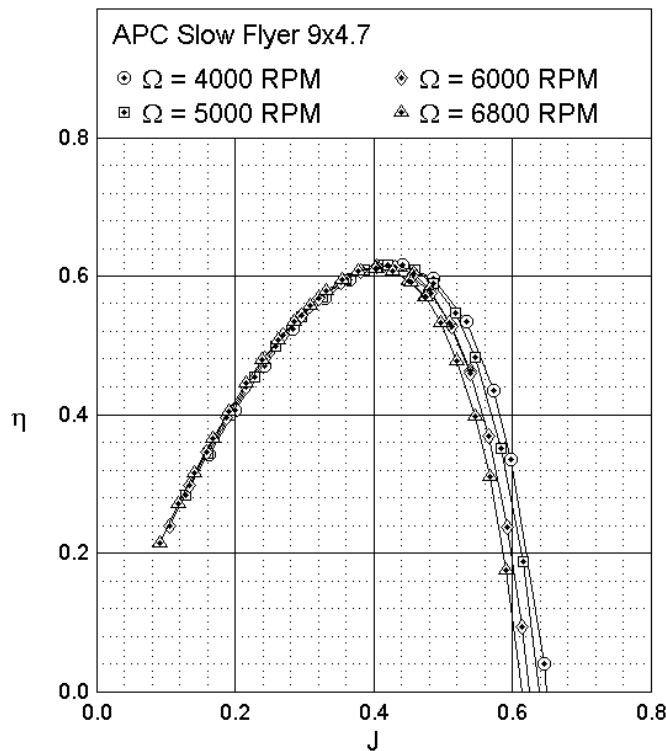
Figure 4.29   The efficiency curve of APC SF 9x4.7 propeller (Brandt *et al.*, 2015).

If the propeller is operated at a certain rotation speed, according to Equation (49), the advance ratio J is positively related to the perpendicular flow velocity. The propeller has the highest efficiency when $J = 0.4$; as the incoming flow velocity is increased or decreased, the efficiency lowers.

By adjusting a propeller's design parameters, the efficiency curve can be changed. For example, for a fixed-diameter propeller, if its pitch is changing, the efficiency curve takes the form displayed in Figure 4.30.
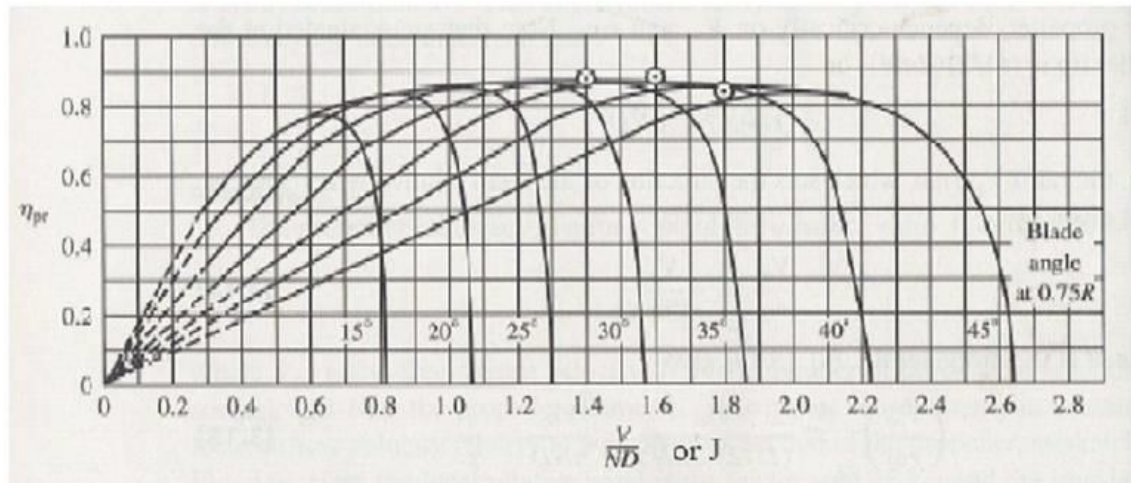
Figure 4.30   The efficiency chart of a variable pitch propeller (McCormick, 1979).

The advance ratio at which the propeller has the highest efficiency is defined as J_0. In this algorithm, a 'rubber propeller' model is utilised, so J_0 is considered a constant. It is assumed that for any diameter, the propeller can be designed to have the maximum efficiency at a certain J_0.

By analysing 65 propellers in the UIUC database (see Appendix E), J_0 is determined to be 0.58 (see Figure 4.31 and Table 4.10).
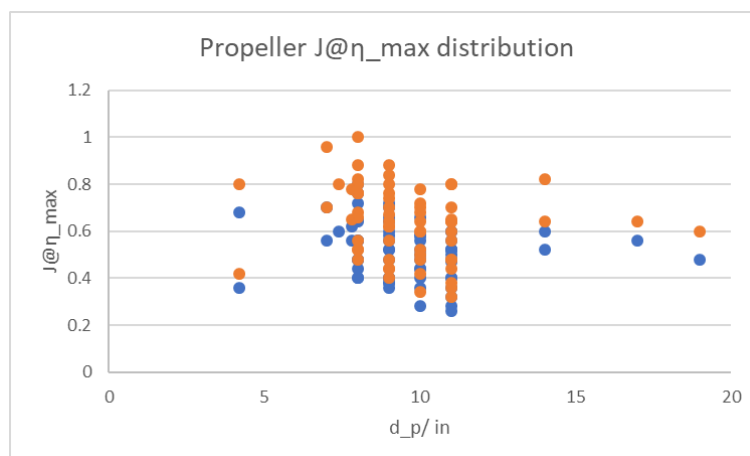
Figure 4.31   The distribution of the J_0 of 65 propellers.

Table 4.10 The statistics of the J_0 of 65 propellers.

Max	0.9
Min	0.29
Average	0.576385
Standard deviation	0.137924
Variation coefficient	0.239292
Median	0.58
Skewness	-0.02753

In Section 3.4.3.4 6, J is used for the rotation speed calculation, and it becomes clear that J differs between the two categories of flight conditions. Under the most efficient conditions, $J = J_0$. Under extreme performance conditions, as the velocity of the multicopter increases, the change in J is worth discussing. Considering the APC SF 8x3.8 propeller as an example, whose dynamic characteristics are presented in Figure 4.32, assuming the multicopter is forward cruising when the propeller is operated under the highest efficiency and rotates at 4,000 rpm, the aircraft information can be estimated as described in Table 4.11. Then, the detailed performance of the propeller under different incoming flow velocities is given in Table 4.12, in which step 1 and step 6 are the throttle increase steps. When the throttle is increased, the propeller's rotation speed and produced thrust increase, and the aircraft begins to accelerate. However, this step is considered to occur instantaneously, so the aircraft velocity has not yet changed. At this moment, the advance ratio is reduced, causing the efficiency to drop and thrust coefficient to increase. During the other steps, assuming the propeller rotation speed remains constant and the aircraft velocity is increased to a specific value, the real-time thrust and drag are examined to check the states of the aircraft. It can be concluded that when the velocity is increasing, the advance ratio is increasing and thus causes the efficiency to first increase and then decrease, the thrust coefficient to decrease, the thrust to decrease and the drag to increase. This condition persists until the forward projection of the total thrust is equal to the drag.
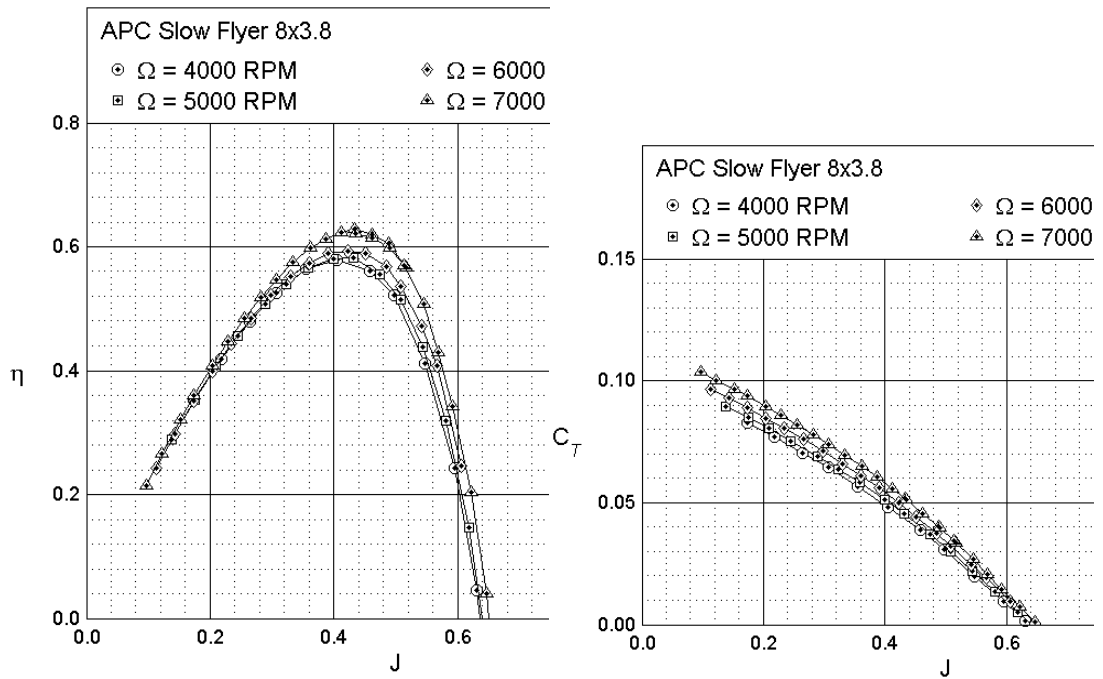
Figure 4.32   The efficiency and thrust coefficient chart of APC SF 8x3.8 propeller.
(Brandt *et al.*, 2015)

Table 4.11 The aircraft details and parameters in cruising flight.

Items	Value	Comment	Items	Value	Comment
$v_0(m/s)$	5.96	Incoming flow velocity	$\rho(kg/m^3)$	1.225	Air density
J_0	0.44	Advance ratio	$d_p(in)$	8	Prop diameter
η_{max}	0.58	Prop efficiency	$d_p(m)$	0.2032	Prop diameter
$n_0(rpm)$	4000	Prop rotation speed	C_d	0.9	Multicopter drag coefficient
$n_0\ (rev/s)$	66.67	Prop rotation speed			
C_t	0.04	Prop thrust coefficient	N_r	4	Number of rotors
$T_0(N)$	0.37	Prop thrust	$MTOW(N)$	1.46	$MTOW$
$T_0 \cdot sin(\alpha) \cdot Nr$	0.26	Total thrust projected on the forward direction	$A_1(m^2)$	0.04	Top view area
$\alpha_0(°)$	10	Tilt angle	$A_2(m^2)$	0.01	Front view area
$\alpha_0(rad)$	0.17	Tilt angle			
$q(m/s)$	21.76	Dynamic pressure			
$A_0(m^2)$	0.01	Total drag area			
$D_0(N)$	0.26	Drag			
Action	equilibrium				

Table 4.12 The detailed propeller parameters in different rpm and forward speed.

Item	step 1 $\frac{n_1}{n_0} =$	step 2 $\frac{v_2}{v_0} =$	step 3 $\frac{v_3}{v_0} =$	step 4 $\frac{v_4}{v_0} =$	step 5 $\frac{v_5}{v_0} =$	step 6 $\frac{n_2}{n_0} =$	step 7 $\frac{v_6}{v_0} =$	step 8 $\frac{v_7}{v_0} =$	step 9 $\frac{v_8}{v_0} =$
	1.5	1.5	1.6	1.7	1.8	3	3	3.5	4
$v_i(m/s)$	5.96	8.94	9.54	10.13	10.73	5.96	17.88	20.86	23.84
J_i	0.29	0.44	0.47	0.50	0.53	0.15	0.44	0.51	0.59
η_i	52%	58%	57%	54%	53%	28%	70%	64%	53%
$n_i(rpm)$	6000	6000	6000	6000	6000	12000	12000	12000	12000
$n_i\ (rev/s)$	100	100	100	100	100	200	200	200	200
C_t	0.045	0.05	0.04	0.035	0.025	0.1	0.05	0.04	0.02
$T_i(N)$	0.94	1.04	0.84	0.73	0.52	8.35	4.18	3.34	1.67
$T_i \cdot sin(\alpha) \cdot Nr$	3.46	3.91	3.00	2.53	1.49	33.38	16.64	13.29	6.52
$\alpha_i(°)$	67.10	69.50	64.04	59.99	45.55	87.49	84.98	83.72	77.36
$\alpha_i(rad)$	1.17	1.21	1.12	1.05	0.79	1.53	1.48	1.46	1.35
$q(m/s)$	21.76	48.96	55.71	62.89	70.51	21.76	195.85	266.57	348.17
$A_i(m^2)$	0.04	0.04	0.04	0.04	0.03	0.04	0.04	0.04	0.04
$D_i(N)$	0.75	1.71	1.90	2.09	2.05	0.77	6.95	9.47	12.37
Action	continue accelerate	continue accelerate	continue accelerate	continue accelerate	exceed maximum speed	continue accelerate	continue accelerate	continue accelerate	exceed maximum speed

Based on Table 4.12, the following conclusions can be made:

- By increasing the rotation speed, the efficiency and thrust coefficient curves are slightly changed, causing the propeller to be more efficient and produce more thrust under the same advance ratio.
- Most of the general multicopters are low speed compared with fixed-wing aircraft. The propeller efficiency changes little between cruising flight and maximum speed flight. Thus, η_p is considered constant for all flight conditions.
- When the rotation speed is increased, the aircraft begins to accelerate until a new equilibrium is reached. In the new equilibrium, the advance ratio is slightly increased. Based on the above analysis, the J_{max}/J_0 ratio is determined to be 1.2. Thus, in the calculation of the extreme performance flight conditions, J_{max} rather than J_0 should be used to estimate the maximum rotation speed.

4.3.3 Fuselage Downwash

In (Raymer, 2012), the recommended value for C_f is 1.02. The definition of C_f is discussed in (Leishman, 2006) and is based on the valid disc area (see Equation (87)). Leishman does not provide an exact value of C_f, but he recommends that $\frac{A_{frame}}{A_{disk}} < 0.1$, which is equivalent to $C_f < 1.11$.

$$C_f = \frac{A_{disk}}{A_{valid}} = \frac{A_{disk}}{A_{disk} - A_{frame}} = \frac{1}{1 - \frac{A_{frame}}{A_{disk}}} \tag{87}$$

An example of this relationship is provided in Figure 4.33. Because multicopters differ slightly helicopters in terms of configuration, the value of C_f may also differ. Thus, 12 commercial multicopters are examined. By rebuilding their models in SolidWorks using top-view pictures, the relative areas and C_f of these models are found (see Table 4.13). The average value of C_f is 1.068, and it is set as its default value in the list of constants.
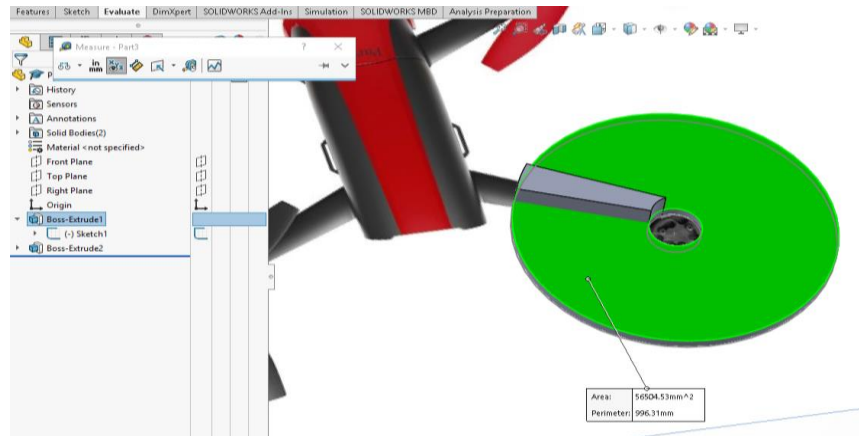
Figure 4.33   An example sketch of the fuselage and the propeller disc.

Table 4.13 The C_f value of some typical commercial multicopters.

No	Model	A_disk	A_frame	C_f		Max f
1	DJI PHANTOM 4	0.6831	0.0619	1.084367		1.121538
2	PARROT ANAFI	1.4013	0.1289	1.071911		Min f
3	BEBOP2	5.6504	0.2935	1.054789		1.033026218
4	BREEZE	4.673	0.5064	1.121538		Average f
5	MD-200	17.1879	0.655175	1.039629		1.067692805
6	MD3000	8.4775	0.4907	1.061439		
7	FLAME WHEEL 550	9.8882	0.7266	1.079309		
8	MAVIC	15.491	0.495253	1.033026		
9	3DR IRIS	3.41	0.2915	1.093474		
10	MK8 3500	2.8242	0.09312	1.034096		
11	SOLO	3.6282	0.2971	1.08919		
12	YUNEEC H520	5.4888	0.2591	1.049544		

4.3.4 Motor Mass Regression

4.3.4.1 Problem in Motor Estimation

Mauro Gatti (2015) created a motor mass versus output power regression using his own database (see Figure 4.34), but the goodness of the regression is unknown. The estimation function is provided as Equation (88):

$$P_{out,m,max} = 4140.8 \cdot m_m \qquad (88)$$
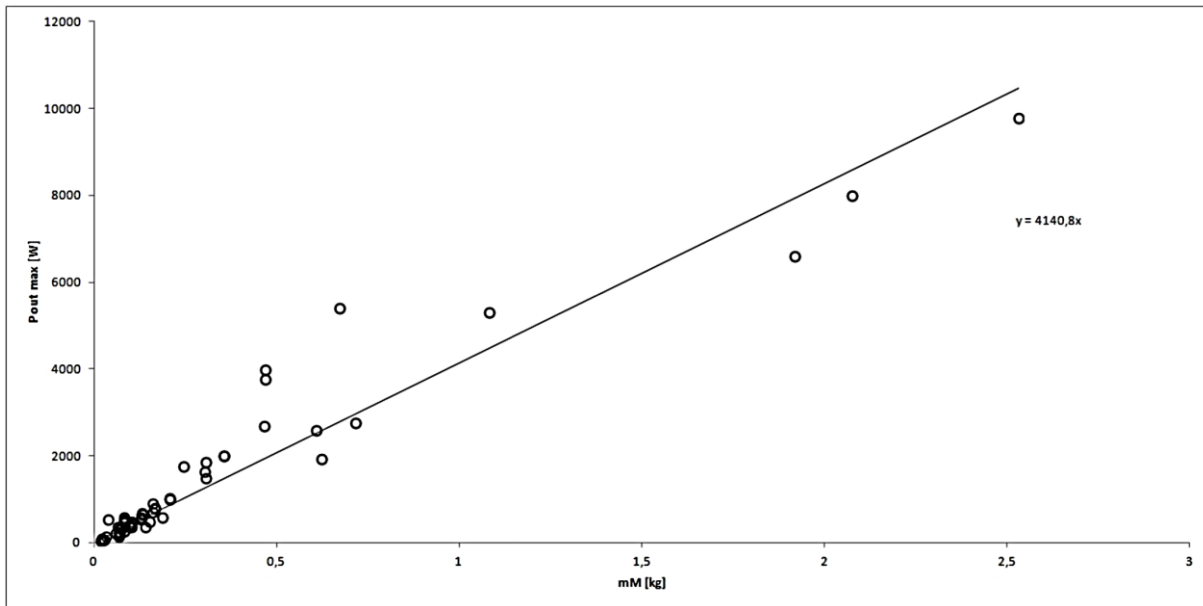
Figure 4.34   Motor maximum output power as a function of motor mass.
(Mauro Gatti, 2015)

When the motor database is built up, a similar regression is performed. The result reveals a good value for R^2 (see Figure 4.35); however, when zoomed in, the motors between $20\ g$ to $50\ g$ are outstanding, as many motors of this mass can provide a very high power (see Figure 4.36 and Figure 4.37). Such motors are widely used for racing drones. Compared with Gatti's regression, although the slopes are slightly different, the overall estimation is similar. Using Gatti's method to estimate the motor mass would have large errors for the motors in the above range.
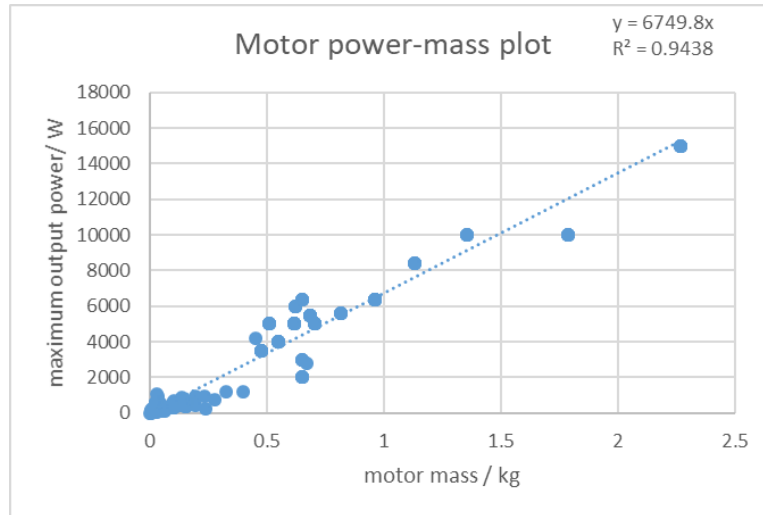
Figure 4.35   Motor mass vs output power regression.
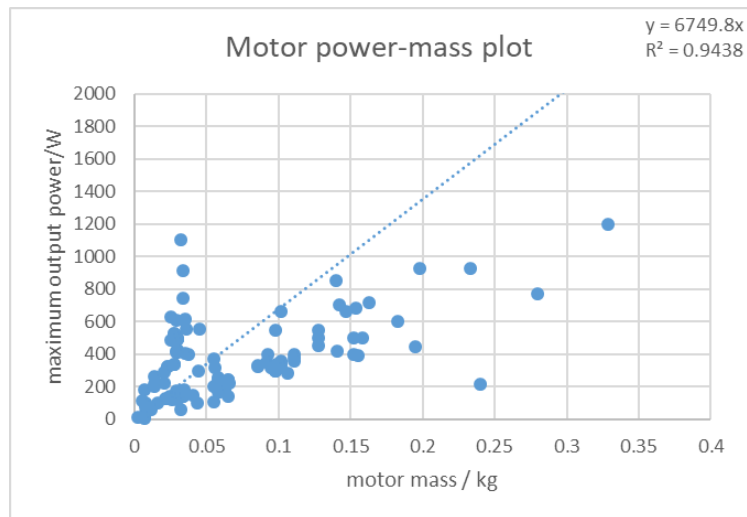
Figure 4.36   The zoomed in view of the regression details.
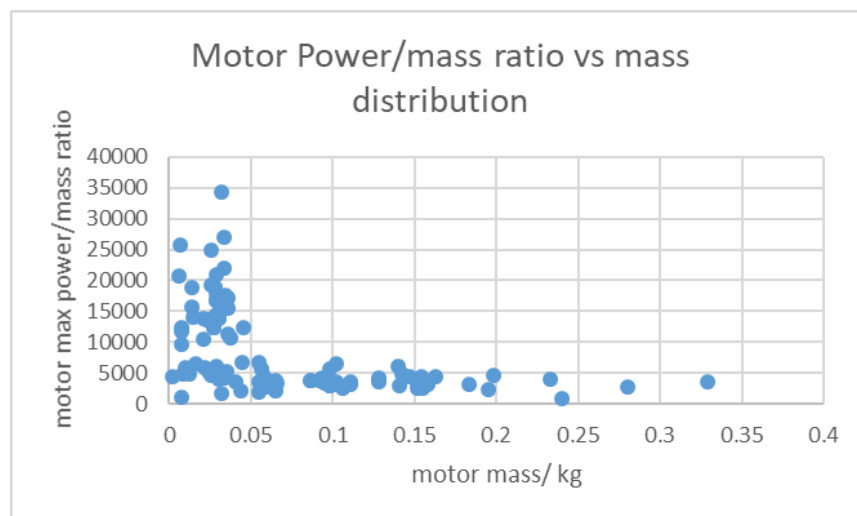
Figure 4.37   The zoomed in view of the $\frac{P}{m}$ vs m plot.

The motors from 10 commercial multicopters are used to validate Gatti's method. The results reveal that this method has good accuracy for large motors and a large error for small motors (see Table 4.14 and Figure 4.38).

Table 4.14 The detailed data of the validation of Gatti's motor estimation method.

Model description	MTOM/g	actual motor mass/g	Gautti's method mass estimation/g	absolute error/g	error ratio
DJI..MG-1S	23800	280	203.47	-76.53	27.3%
DJI..Matrice 600	15500	280	260.18	-19.82	7.1%
GS..1000	8000	248	65.69	-182.31	73.5%
DJI..Matrice 100	3600	106	137.21	31.21	29.4%
Speedy..Gonzalas	570	33.8	363.08	329.28	974.2%
Stigg..195	560	36	190.94	154.94	430.4%
Diatone..GT M200	554	32	240.96	208.96	653.0%
Eachine..Wizard X220S	535	25	76.76	51.76	207.1%
Furibee..Darkmax 220	487	29	187.09	158.09	545.1%
VXR..190	479.4	35.8	449.22	413.42	1154.8%
ARC..200	458	29	112.77	83.77	288.9%

	absolute error/g	error ratio
min	-182.311	7.08%
max	413.415	1154.79%
average	155.462	399.16%
Standard deviation	173.595	396.50%
Variance coefficient	1.117	0.993337
r2	0.029	
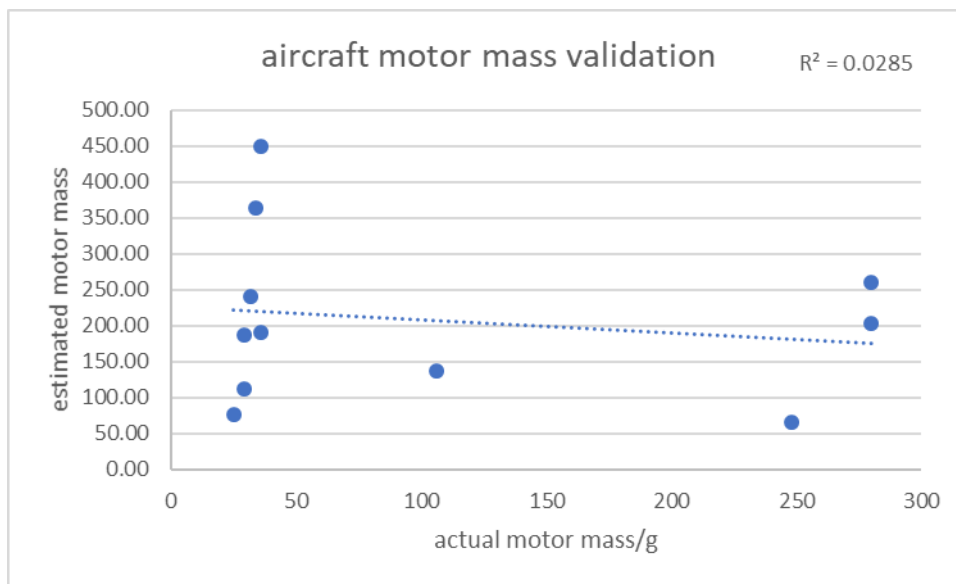
Figure 4.38   The validation of Gatti's estimation method using ten multicopters.

Winslow (2017b) used a different approach; he correlated the mass of the motor to I, P and KV. His method is validated using 10 multicopters, and the result reveals that it is superior to Gatti's result but still has a relatively large error for small motors (see Figure 4.39 and Table 4.15).

Table 4.15 The detailed data of the validation of Winslow's motor estimation method.

Model description	MTOM/g	actual motor mass/g	Gautti's method mass estimation/g	absolute error/g	error ratio			absolute error/g	error ratio
DJI..MG-1S	23800	280	230.72	-49.28	17.6%		min	-132.642	2.02%
DJI..Matrice 600	15500	280	274.35	-5.65	2.0%		max	236.325	660.13%
GS..1000	8000	248	115.36	-132.64	53.5%		average	108.662	278.13%
DJI..Matrice 100	3600	106	159.80	53.80	50.8%		Standard deviation	108.846	237.55%
Speedy..Gonzalas	570	33.8	238.68	204.88	606.2%		Variance coefficient	1.002	0.854121
Stigg..195	560	36	152.37	116.37	323.2%		r2	0.101	
Diatone..GT M200	554	32	180.93	148.93	465.4%				
Eachine..Wizard X220S	535	25	74.84	49.84	199.3%				
Furibee..Darkmax 220	487	29	151.52	122.52	422.5%				
VXR..190	479.4	35.8	272.13	236.33	660.1%				
ARC..200	458	29	104.05	75.05	258.8%				
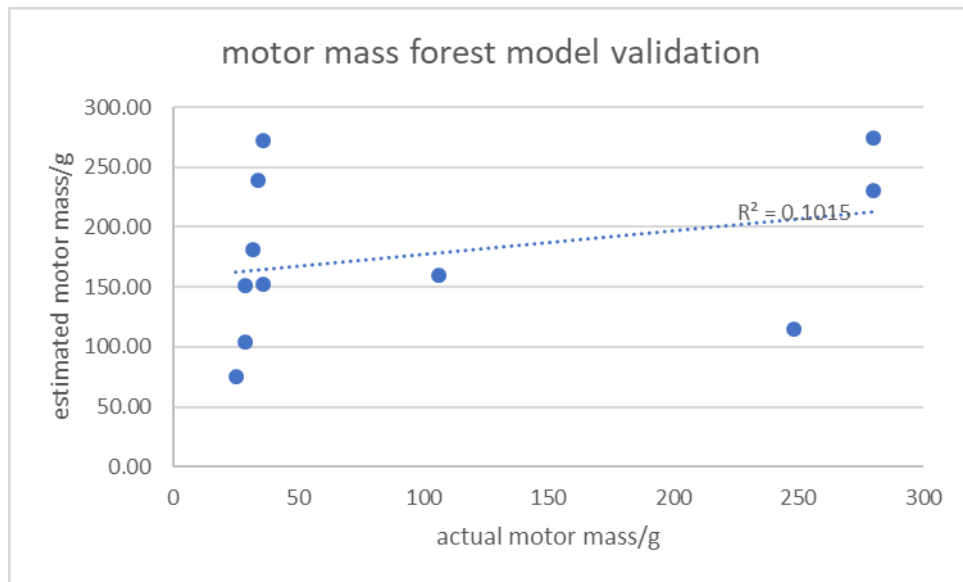
Figure 4.39   The validation the Winslow's motor estimation method.

4.3.4.2   Solution

The reason for the inaccurate estimation is the characteristics of motors. Power is not the only parameter used to measure a motor; more important parameters are the torque the rotation speed, which are a pair of negatively correlated parameters (see Section 4.3.4. Briefly speaking, the torque-speed characteristics determine how fast the motor can spin under a given power and load. For a propeller, the faster it rotates, the more thrust it produces; on the contrary, it also produces reversed torque to the motor. When the ESC adjusts the input current to the motor, it is actually adjusting its torque to form an equilibrium with the rotating propeller. Small motors can provide high power, but the efficiency is quite low. Thus, to properly correlate the motor mass, the necessary parameters must be determined.

Several methods are tested, such as correlating the motor mass against its dimension, poly fitting the mass to the power and KV, attempting to build a possibility distribution function (PDF) for the power/mass ratio and attempting to divide the entire range into several short ranges and then correlating different models for each range. This method clearly increases the estimation accuracy, but it is difficult to address the data at the boundary of each range. Finally, the random forest technique is used to develop a model (Section 2.3.3), and a similar algorithm is used for the propeller price estimation.

Finally, the parameters are decided to be the maximum power (P_{max}), maximum bearable voltage (U) and noted KV. P_{max} is one of the extreme performances determined in Section 3.4.3, U is determined in Section 3.4.2.1, and the noted KV is explained below.

The noted KV is calculated from KV_{min}, and KV_{min} is calculated by Equations (89) to (90):

$$RPM = KV * U \tag{89}$$

$$KV_{min} = \frac{RPM_{max}}{U} = \frac{n_{max} \cdot 2\pi}{U} \tag{90}$$

According to the Brushless Direct Current (BLDC) Motor principles (Zhao, July and Yangwei, 2011), the calculation of torque is given by Equation (91).

$$T = Km * I = 2FR \tag{91}$$

$$Km = 2 * N * B * L * R_{stator} \tag{92}$$

$$F = BILsin\,(\theta) \tag{93}$$

$$T\omega = VI * \eta \tag{94}$$

$$Km = \frac{T}{I} = \frac{V}{\omega} = KV \tag{95}$$

*Km motor constant, N number of coils, B strength of magnetic field, L stator length, R_{stator} stator radius

4.3.4.3   Explanation to Noted KV

The noted KV of a motor is measured under the no-load condition. According to the torque RPM[26] characteristics of BLDC motors (see Figure 4.43 in Section 4.3.4), as the load increases, the maximum RPM should decrease (i.e. $RPM_{max,loaded} < RPM_{max,unloaded}$). Thus, with $RPM_{max,loaded}$, only the minimum required KV_{min} can be determined. By evaluating 20 models, the noted KV and the calculated KV_{min} present a relatively constant relationship (see Figure 4.40). The average ratio number is 1.308 (see Table 4.16), which is used as a constant for the estimation of the noted KV (see Equation (96)).

---

[26] RPM: Revolution per Minute
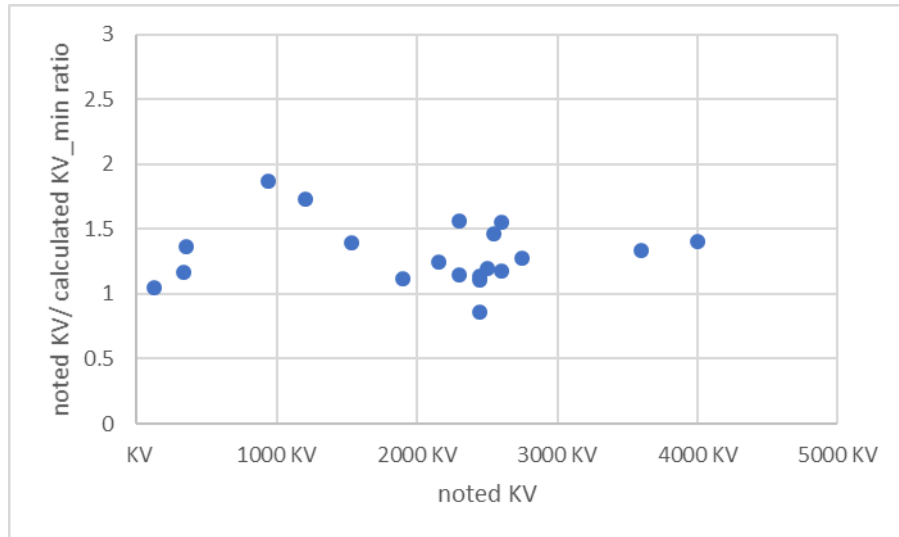
Figure 4.40 The $\frac{KV}{KV_{min}}$ ratio plot vs KV.

$$KV = 1.308 \cdot KV_{min} \tag{96}$$

Table 4.16 The statistics of the $\frac{KV}{KV_{min}}$ ratio.

Min	0.857
Max	1.870
Average	1.308
Standard Deviation	0.243
Variation Coefficient	0.185974

4.3.4.4 Validation of the Proposed Regression

As introduced in Section 3.4.4.2, the random forest technique is used for the regression of the motor mass. As with Gatti and Winslow's regression method, this proposed regression is also validated by the 10 multicopters. The results presented in Table 4.17 and Figure 4.41 demonstrate better accuracy.

Table 4.17 The validation of the random forest model for motor mass estimation.

Model description	MTOM/g	actual motor mass/g	Gautti's method mass estimation/g	absolute error/g	error ratio
DJI..MG-1S	23800	280	348.74	68.74	24.5%
DJI..Matrice 600	15500	280	304.42	24.42	8.7%
GS..1000	8000	248	295.91	47.91	19.3%
DJI..Matrice 100	3600	106	158.68	52.68	49.7%
Speedy..Gonzalas	570	33.8	27.41	-6.39	18.9%
Stigg..195	560	36	12.60	-23.40	65.0%
Diatone..GT M200	554	32	28.81	-3.19	10.0%
Eachine..Wizard X220S	535	25	23.18	-1.82	7.3%
Furibee..Darkmax 220	487	29	31.50	2.50	8.6%
VXR..190	479.4	35.8	27.21	-8.59	24.0%
ARC..200	458	29	25.45	-3.55	12.2%

	absolute error/g	error ratio
min	-23.402	7.28%
max	68.740	65.00%
average	22.108	22.57%
Standard deviation	30.100	18.58%
Variance coefficient	1.361	0.8232175
r2	0.983	
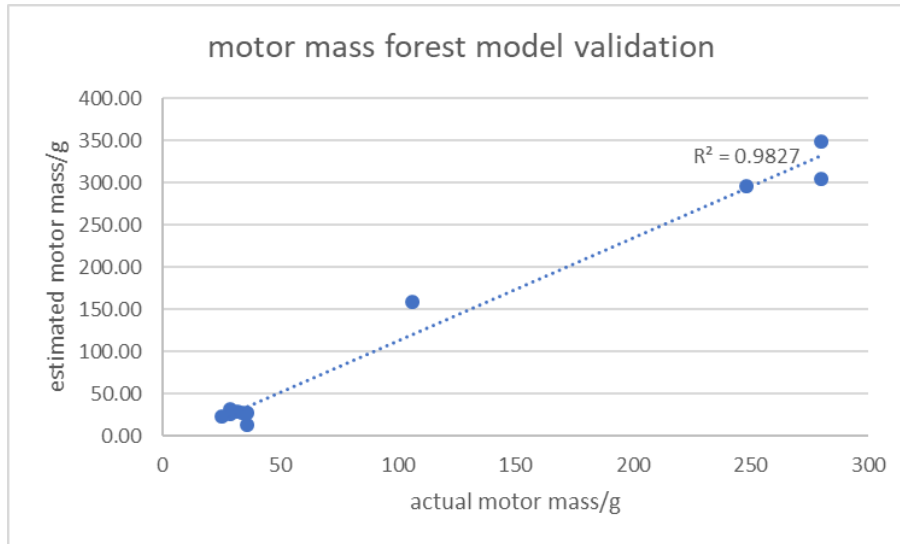
Figure 4.41   The validation result of the motor mass forest model using ten multicopters.

4.3.5 Motor Efficiency

Due to the limited time and the purpose of this algorithm, a brushless DC motor is taken as the only source of motion. This is because brushless motors are one of the most efficient methods for creating mechanical power from another form of energy. It is the most popular option used in current multicopters. Brushless motor efficiency is high compared with combustion engines, with values averaging between 70% and 90% (Amadori *et al.*, 2010; Harrington and Kroninger, 2013; Song and Luo, 2019).

The motor efficiency is defined in Equation (97), in which the motor output power is equal to the propeller input power:

$$\eta_m = \frac{P_{m,output}}{p_{m,output} + P_{m,loss}} \qquad (97)$$

There are two types of power loss in a BLDC motor: 1. The power consumed by the inner resistance (also called the iron loss), and 2. The back EMF (electromotive force) caused by the moving coil in the magnetic field, (also called the copper loss). The efficiency of BLDC motors gradually reduces as the input current increases (see Figure 4.42).
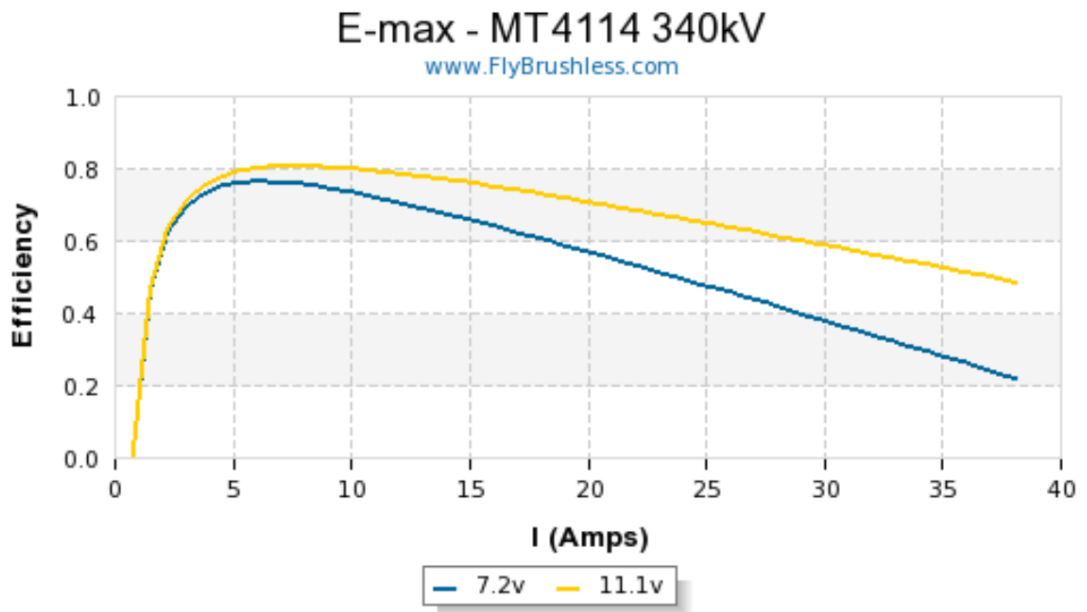
Figure 4.42   The efficiency curve of an Emax MT4114 motor[27].

Figure 4.43 illustrates how the torque and rotation speed change when the throttle is gradually pushed up (Amadori *et al.*, 2010; Harrington and Kroninger, 2013).

Based on the literature, the efficiency of a BLDC motor is typically between 50% and 80% (Amadori *et al.*, 2010).
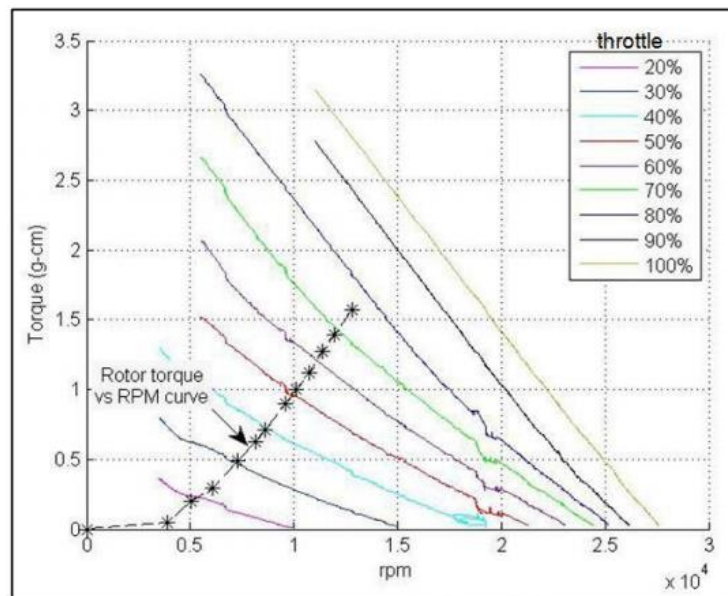
Figure 4.43   Torque vs RPM at various throttle for an example motor.
*The stars indicate the actual working conditions.(Harrington and Kroninger, 2013)

---

[27] www.flybrushless.com

103

4.3.6 ESC

The ESC efficiency is defined in Equation (98). Most of the power loss out of the ESC is from conduction loss (Green and McDonald, 2015). The efficiency of ESCs is relatively more stable, and an example is presented in Figure 4.44. A range of commercial ESCs was tested by Gong and Verstraete (2017). Combined with other studies, the efficiency of a common ESC is between 80% and 90% (Amadori *et al.*, 2010; Harrington and Kroninger, 2013; Green and McDonald, 2015)

$$\eta_m = \frac{P_{m,output}}{p_{input}} \qquad (98)$$
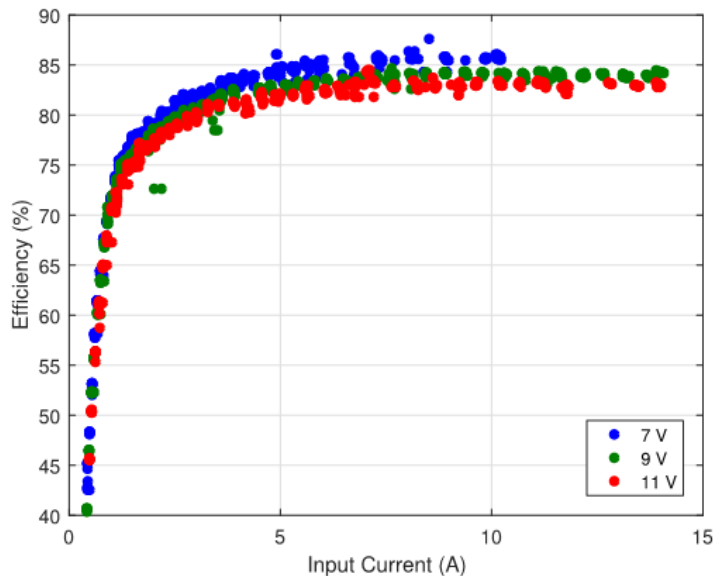
Figure 4.44   The test result of an Aerostar 30A ESC.

4.3.7 Maximum Thrust to Maximum Weight Ratio

For rotorcraft design, such as for helicopters and multicopters, the capability of the maximum available thrust is often more than simply hovering the aircraft. There must be excess power to fulfil the manoeuvrability requirement (accelerating, maximum-speed flight, rolling and turning, among others) and maintain stability in wind and gust. Thus, a key parameter to reflect the manoeuvrability of multicopters is introduced: the maximum thrust to maximum weight ratio (TrW).

This ratio is defined by Equation (99), in which T_{max} is the total maximum thrust of all motors, and $MTOM$ is the maximum take-off weight, which is defined as the summation of the $GTOW$ and the weight of the maximum payload (see Section 3.4.2.1).

$$TrW = \frac{T_{max}}{MTOW} \qquad (99)$$

Typical range of TrW

Amateurs typically assemble their multicopter following the 'half throttle' rule, in which the TrW is roughly 2[28,29,30] (Admin, 2016). For reference, in (Russell, Theodore and Sekula, 2018), for a heavy lifting drone, a TrW of 2.5 is used.

Given the various purposes of the aircraft, the thrust-weight ratio may vary. For example, for heavy lifting drones, this number is normally less than 2 due to the lower requirement for manoeuvrability, while for racing drones, this ratio can reach up to 10:1. A higher thrust makes the drone faster, but a high thrust-to-weight ratio makes the drone more difficult for the pilot to control, since a tiny change in throttle has a large effect.

According to the aircraft database, the typical range and distribution of TrW is concluded based on 30 actual multicopter platforms in the market (see Table 4.18, Figure 4.45 and Figure 4.46 for details). It is found that only the racing drones tend to have a large TrW, for the purpose of achieving high velocity and good manoeuvrability. The maximum TrW is 15.4. All the drones for other general purposes have an average TrW of 2.2. Furthermore, it is clear that smaller drones are more likely to have a larger TrW. In this algorithm, 1.4 is used as the minimum boundary of TrW for all drones to ensure basic movement.

Table 4.18 The range of drones TrW based on different samples.

Samples	All 30 drones	18 drones, excluding 12 racing drones
min	1.436364	1.436364
max	15.3859	4.764706
average	5.015415	2.189635
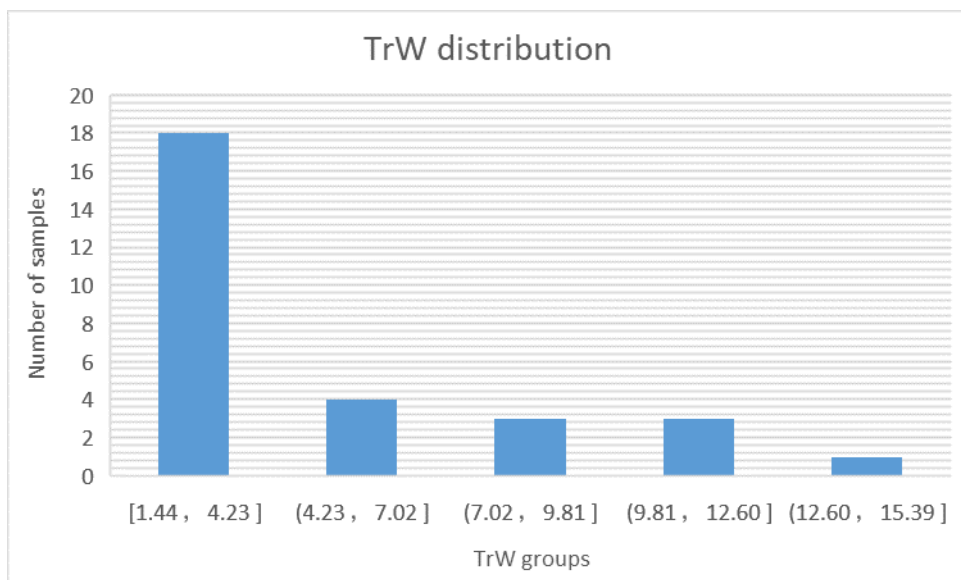
Figure 4.45   The distribution of TrW of the 30 samples.

---

[28] https://filmora.wondershare.com/drones/drone-motors.html
[29] http://www.rcdronegood.com/calculate-quadcopter-power-consumption/
[30] *http://ardupilot.org/copter/docs/advanced-multicopter-design.html#motors-propellers-and-escs*
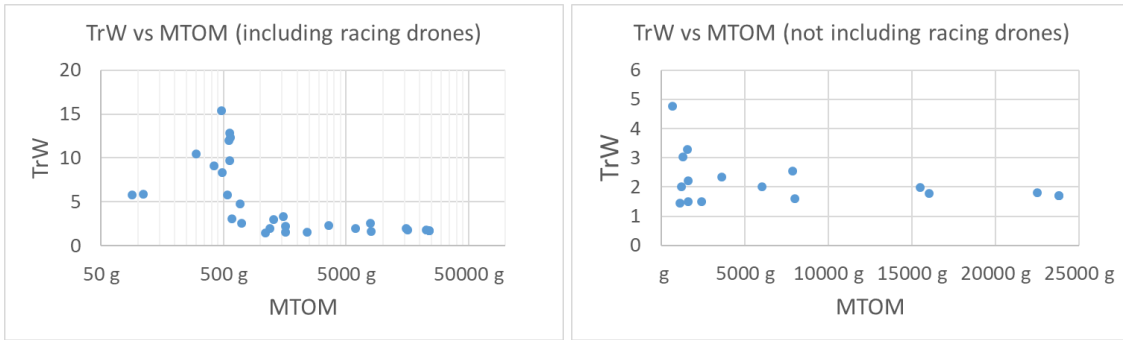
Figure 4.46   The TrW vs $MTOM$ plots of different samples.

Influence of TrW

A larger TrW indicates that the rotor is more powerful and can produce more thrust. In this multicopter optimisation algorithm, TrW is not involved in the calculation but is a medium parameter for reference. For a given mission, when several valid designs are developed, TrW is a straightforward and important indicator of the required performance of the rotor system. If the value of TrW is between 2 and 3, this design requires a general propulsion system. If it is larger than 3, a more powerful propulsion system is necessary to accomplish the mission (compared with the general systems of its own $MTOM$ level). However, it should be noted that, for a certain $MTOM$-level multicopter, the propeller size is typically limited, and so the more powerful propulsion system indicates that the disk loading would be larger. However, if the value is close to the minimum value (1.4 in this algorithm), then the mission duty is light, and the maximum power is close to the hovering power.
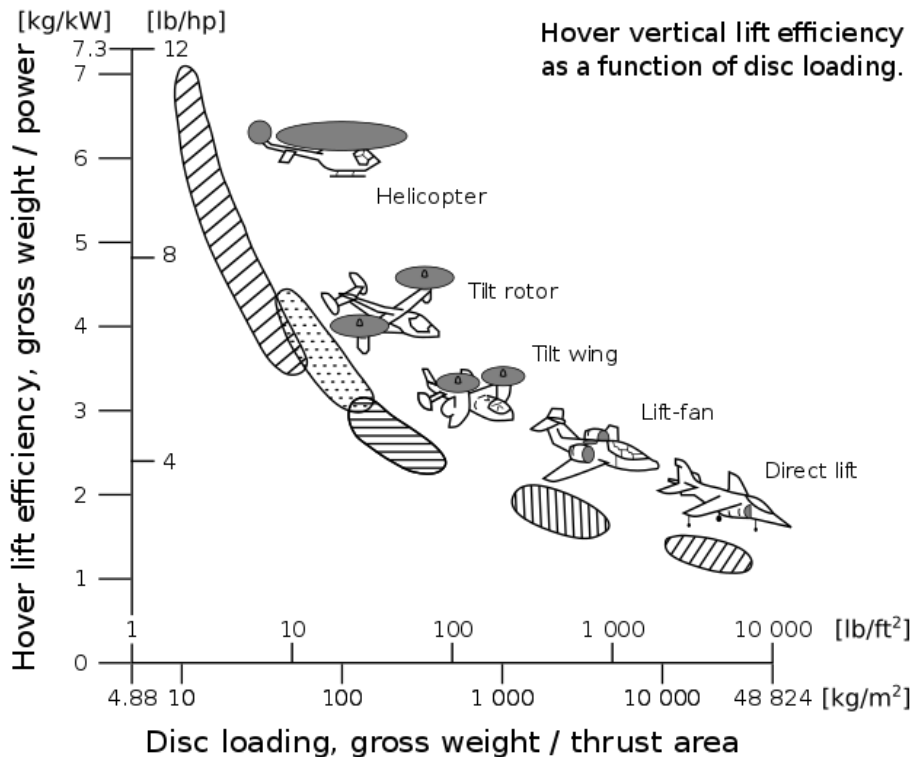
Figure 4.47   Different purpose aircraft have different DL.
(Raymer, 2012)

4.3.8 Hovering Disc Loading

Hovering disc loading is defined by Equation (100), in which $GTOW$ is the gross take-off weight (i.e. the empty take-off weight without the payload).

$$DL = \frac{GTOW}{A_{tot}}$$

(100)

The normal range for multicopters is between 14.2 and 134.3 N/m^2. This number comes from the statistic results of 71 multicopters in the database and is supported by Figure 4.47.

4.3.9 Maximum Tilt Angle, Angular Velocity and Acceleration

The maximum tilt angle can be calculated by Equation (101), considering the multicopter is flying forward with maximum thrust. According to Figure 3.11, in the equilibrium state, the projection of the thrust on the vertical axis (axis z) is equal to the $GTOW$.

$$\alpha = arccos \frac{GTOW}{T_{max}}$$

(101)

The standard tilt angle is normally around 10°–40°[31],[32] (Russell, Theodore and Sekula, 2018). However, this range is limited by the control system for the purpose of stability, while the actual maximum tilt angle calculated using the above equation is much larger than this range. For most DJI products, such as Inspire2,[33] the specification notes that the maximum tilt angle has different values for different operation modes. Meanwhile, the manual for Ardupilot,[34] an open-source autopilot, has the Acro mode, in which 'the throttle is completely manual with no compensation for tilt angle'. Acrobatic drones operated in this mode can perform a flip-over, which requires tilting more than 90°. For most of the racing drones, the autopilot allows for a large tilt angle (up to 70° −80°) so that the aircraft can best take advantage of the thrust. Figure 4.48 displays the tilt condition of a Diatone GT200 racing drone flying under maximum speed. The QuadStar drones series[35] consider the large tilt angle for the frame design (see Figure 4.49 and Figure 4.50).

Figure 4.48   A racing drone under maximum forward velocity[36].

---

[31] https://www.rcgroups.com/forums/showthread.php?2439905-Multirotor-generally-speaking-most-efficient-tilt-angle-for-max-range
[32] https://phantompilots.com/threads/maximum-pitch-values.17191/
[33] https://www.dji.com/uk/inspire-2/info#specs
[34] http://ardupilot.org/copter/docs/acro-mode.html
[35] https://quadstardrones.com/portfolio/
[36] https://www.youtube.com/watch?v=fls_Web9idE

Figure 4.49   Quad Star VXV prototype[37].
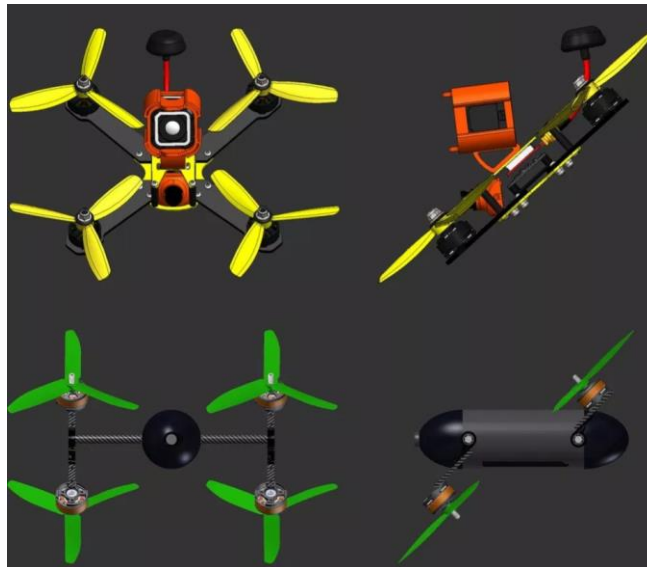
Figure 4.50   Concept Design of Quad Star C1 compared with a general quadcopter[38].

According to the aircraft database, when operated under the maximum thrust and when in the equilibrium state in forward flight, the calculated maximum tilt angle is as presented in Appendix G. It can be concluded that the actual maximum tilt angle is mostly larger than the autopilot-allowed maximum tilt angle.

The angular velocity and acceleration can be calculated by Equations (102) and (103). This algorithm focusses more on the equilibrium state, so the angular velocity and acceleration are not thoroughly considered. When the extreme performance of the motors is determined, it is the response time and accuracy of the control system that are more important.

$$\overrightarrow{\omega_t} = \overrightarrow{\omega_0} + \vec{\beta} \cdot t \qquad (102)$$

$$\vec{I} \times \vec{\beta} = \vec{M} \qquad (103)$$

In the above equations, $\vec{\omega}$, $\vec{\beta}$ and $\vec{M}$ are 3x1 vectors, representing the angular velocity, angular acceleration and torque around the three axes. $\vec{I}$ is a 3x3 matrix and represents the moment of inertia of the frame. Taking the frame as a coordinate system with the centre of gravity as the origin, the torque is then determined solely by the difference of the thrust of all the motors.

---

[37] https://quadstardrones.com/vxv/
[38] https://quadstardrones.com/air-drag-and-cross-sections/

4.3.10   The Analysis of the Arm Optimisation

4.3.10.1   Parameters Determination

GA setting:

Two parameters are used to evaluate the performance of the GA: the average result difference from the best individual and the time elapsed. Two sets of optimisation input parameters are used (see Table 4.19).

Table 4.19 Load input and important parameters.

Set	Hovering Power (W)	Maximum Power (W)	Propeller Diameter (m)	Minimum Arm Length (m)	Motor Mass (kg)
1	76	156	0.2286	0.1937	0.056
2	125	230	0.2286	0.1937	0.076
3	536	1084	0.4318	0.36639	0.168

By running the optimisation 97 times of the first problem and 92 times for the second problem. The influence of three key setting parameters are analysed.

1.   Population and generations required to converge

A lower population consumes less time for each generation but leads to a less accurate convergence result, and it normally requires more generation to converge. A larger population can converge closer to the real minimum and reduce the required generation to converge, but a larger population requires more time for each generation (see Figure 4.51).

By analysing the simulation results, it is found that a population of 100 is feasible. It consumes relatively the shortest time and can converge close to the real minimum.
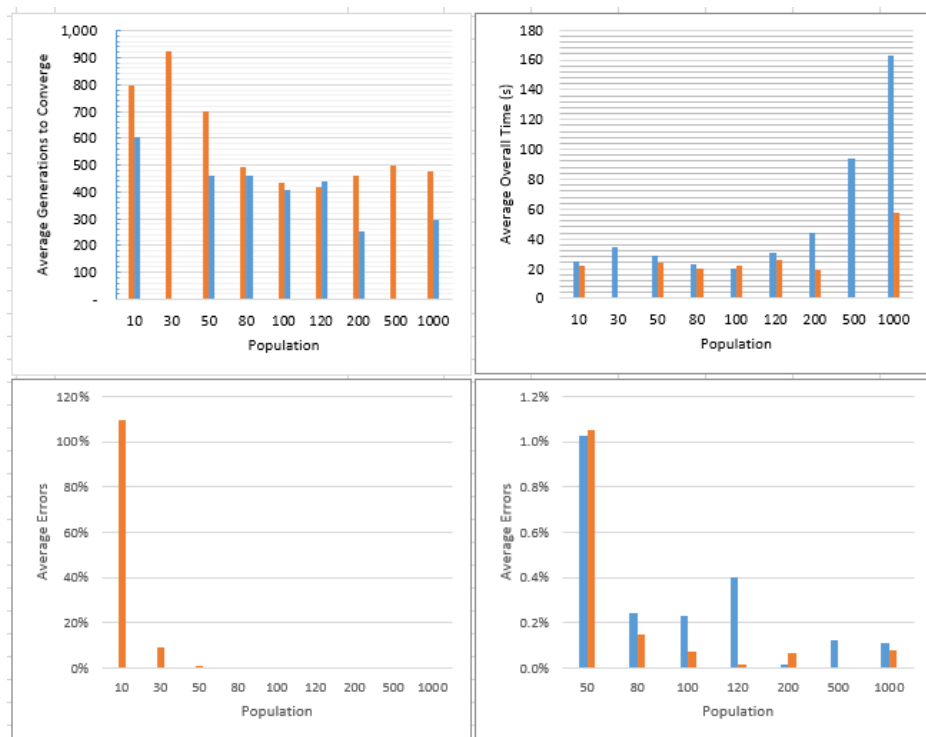
Figure 4.51   The GA performance for different population for two sets of input.

109

2. Stopping criteria

The stopping criteria used in this code include the function tolerance, maximum generation and stall generation. The function tolerance refers to the acceptable score difference between two generations. If the change in the best score in two generations is smaller than this parameter, the new generation is considered a stall generation. When the stall generation exceeds the limit, the optimisation is considered to converge, while if the overall generation reaches the limit, the optimisation finishes without convergence. Sufficient margin should exist for the maximum generation and stall generation, while the function tolerance should be small enough so that the optimisation can converge as close as possible to the real minimum.

4.3.10.2 Result Analysis

The following are found based on the optimisation results of the above runs:

1. A T-section shape can produce enough strength and fulfil all the constraints while having the minimum mass.
2. Under the objective of minimum mass, carbon fibre is the best option of the four materials.
3. The thickness tends to approach the lower boundary. Thus, the minimum thickness can provide enough strength under the given load.
4. The arm length also tends to approach the lower boundary; this is understandable, since under this given load, the motor frequency is lower than the first natural frequency. Hence, the arm is shorter the farther the natural frequency is from the motor rotation frequency.
5. Validation. After each run of the optimisation, it yields an optimal set of parameters that can produce the minimum armlength. Using these parameters in the constraints function reveals that the constraints are really fulfilled. From the validation of more than 100 results, it is found that all the constraints are fulfilled (value < 0) save for the deflection. The deflection errors are mostly positive, but the result is still valid because the values are very small, smaller than the allowed constraints tolerance (which is set as 1e-6 in the program). Thus, the result is actually on the edge. This result from the other aspect reveals that it is the deflection constraints that limit the minimum size of the cross-section.
6. Compared with (Thomas *et al.*, 2016), the optimisation results are similar, ending up with a vertical plate.

4.3.10.3 Contour Plot

See Appendix K.11 to Appendix K.18 for the source code. By calculating a series of cross-section geometry parameters, width and height, the result satisfies all the constraints only for certain combinations. The optimisation can find the minimum objective combination, while the contour plot helps us to understand how the constraints influence the design parameters.

In the code, the parameter 'level' is a key parameter and defines the accuracy of the contour. A larger 'level' requires more time to calculate. Figure 4.52 and Figure 4.53 provide a comparison of the plot quality between level = 100 and level = 500.
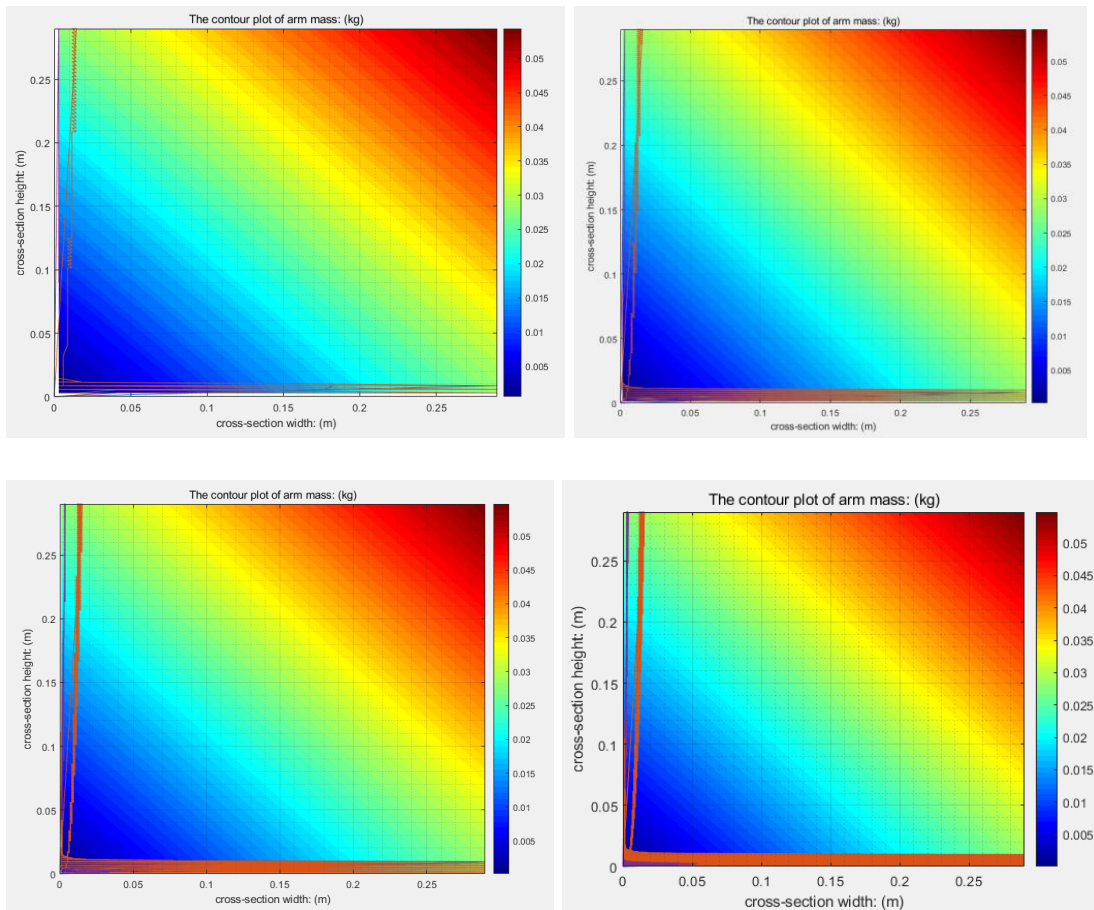
Figure 4.52   The comparison of plot quality of the constraints region.
(in order, level=100,200,300,500)
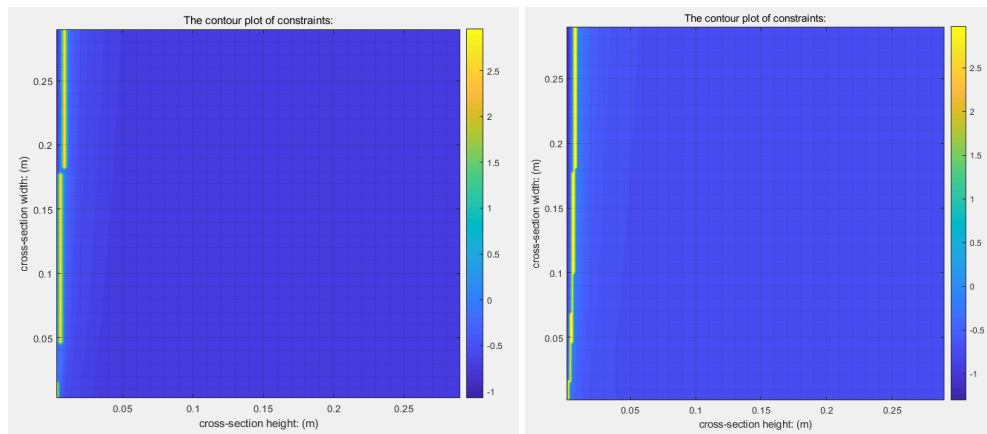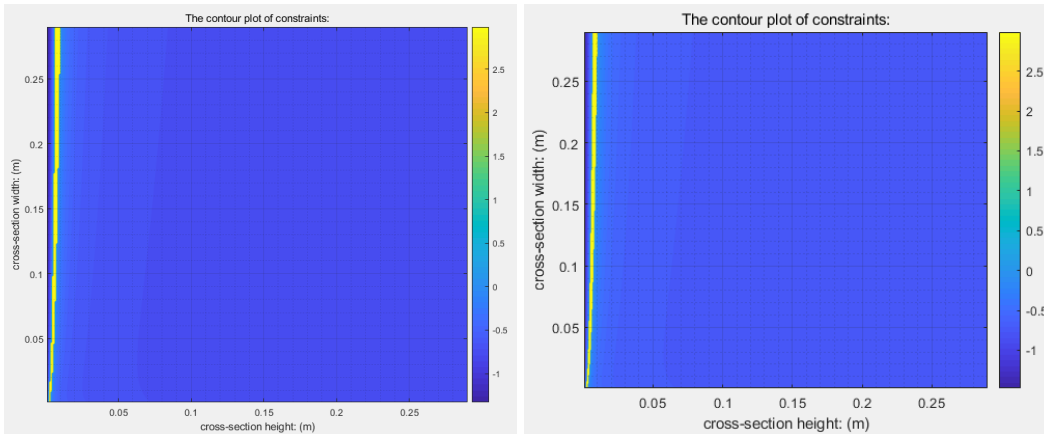
Figure 4.53 The comparison of plot quality of y axis 1st order natural frequency contour. (in order, level=100,200,300,500)

Since there are so many constraints, it is difficult to separate them on the combined plot (see Figure 4.54), so separate plots are provided, from Figure 4.55 to Figure 4.65. In these plots, the dark red regions represent the invalid region, while all other regions fulfil the constraints. From the combined plot, it can be concluded that a smaller width and smaller height results in a smaller mass and weak structure. The different-order natural frequency constraints are separate. The minimum geometry combination is located where the rotor frequency is between the first- and second-order frequencies for the y-axis, so the width can be small. The third- and fourth-order natural frequencies are far from the rotor frequency and hence have less influence on the parameters than does the maximum deflection. The constraint that has the most influence on the height parameter is the maximum deflection.
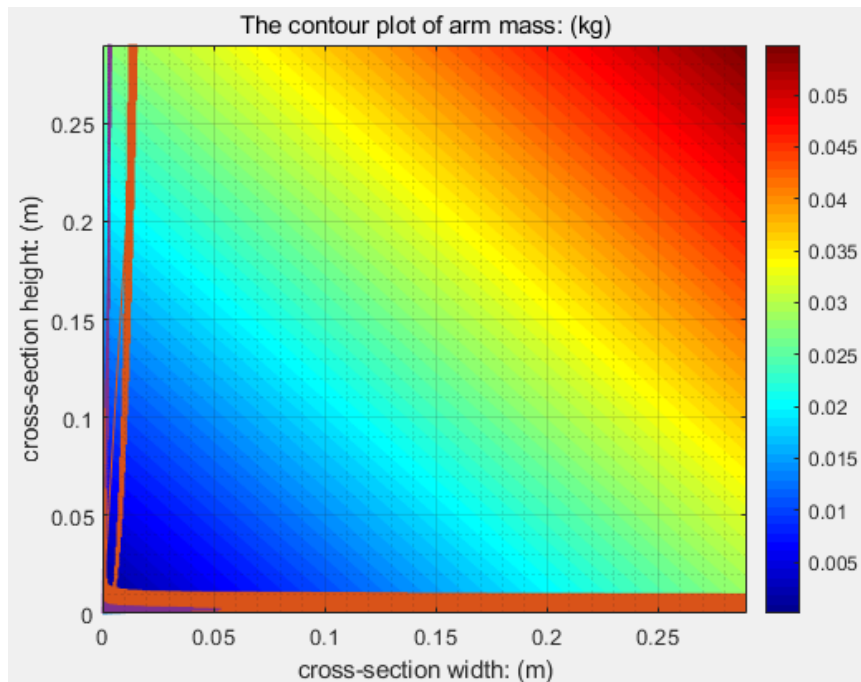
Figure 4.54 The contour plot of arm mass of cross-section geometry including constraints.
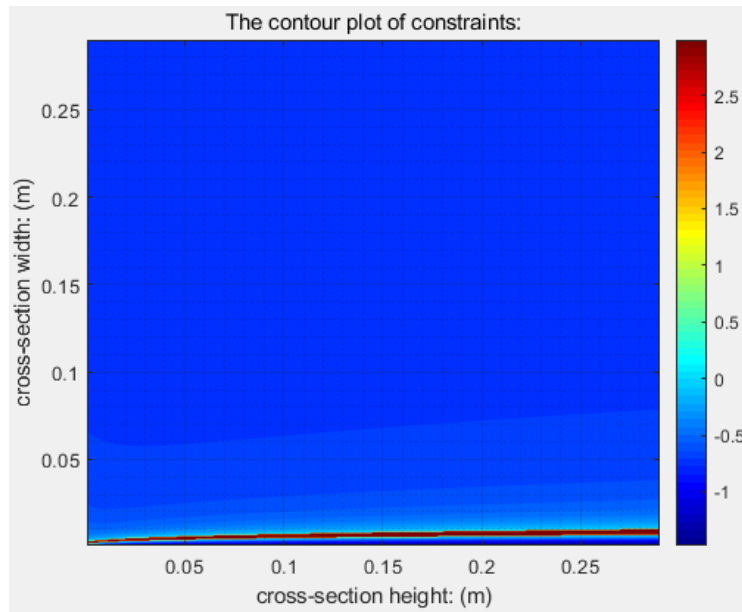
Figure 4.55   The contour plot of constraint- x axis first order natural frequency.
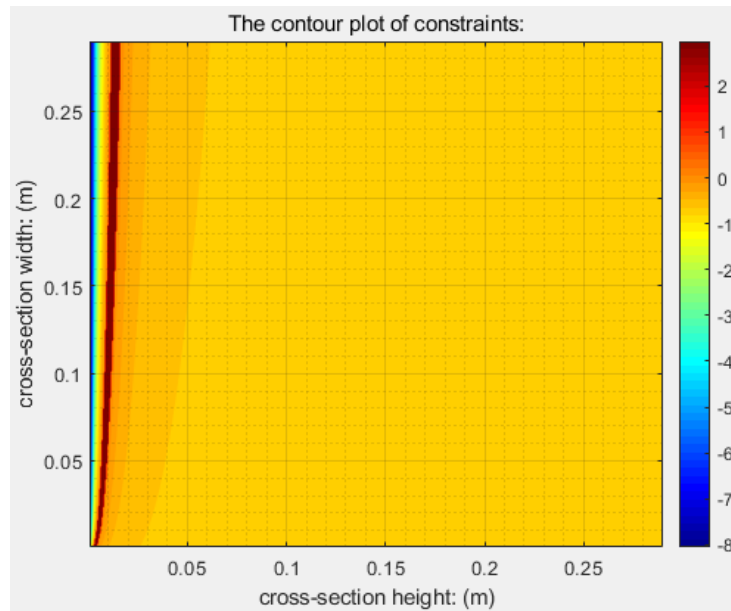
Figure 4.56   The contour plot of constraint- y axis first order natural frequency.
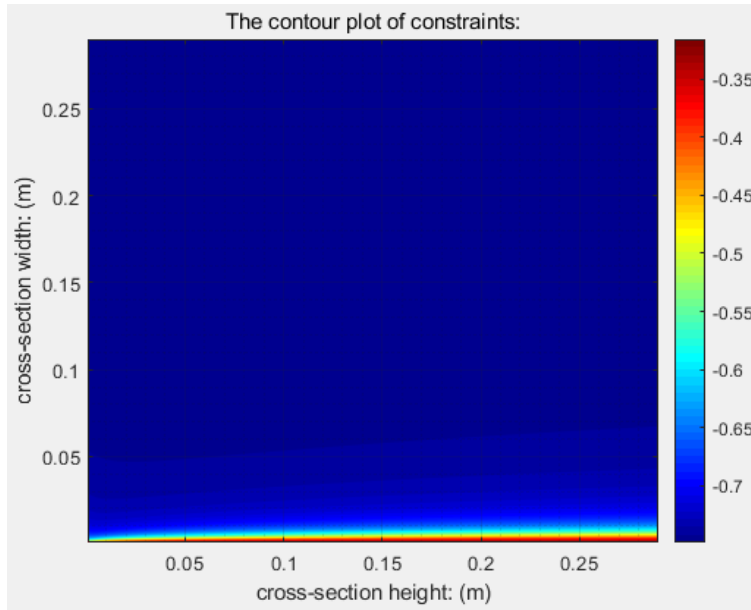
Figure 4.57   The contour plot of constraint- x axis 2nd order natural frequency.
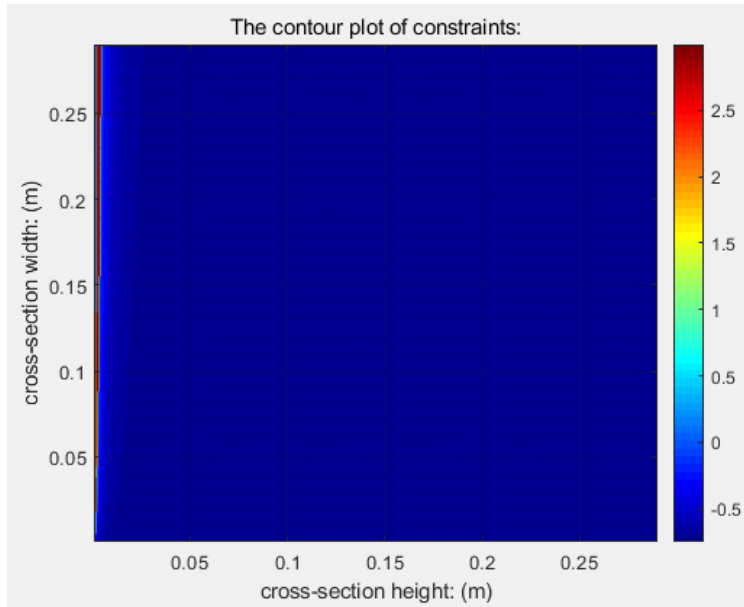
Figure 4.58   The contour plot of constraint- y axis 2nd order natural frequency.
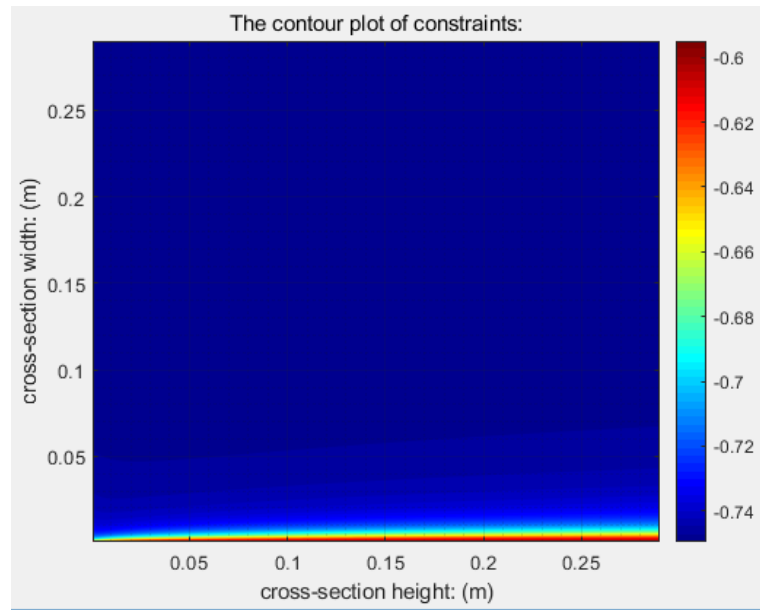
Figure 4.59   The contour plot of constraint- x axis 3rd order natural frequency.
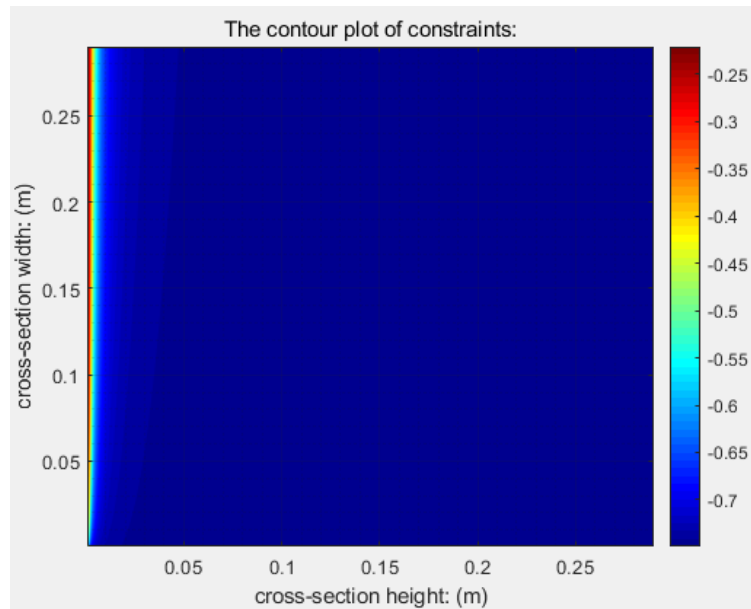
Figure 4.60   The contour plot of constraint- y axis 3rd order natural frequency.
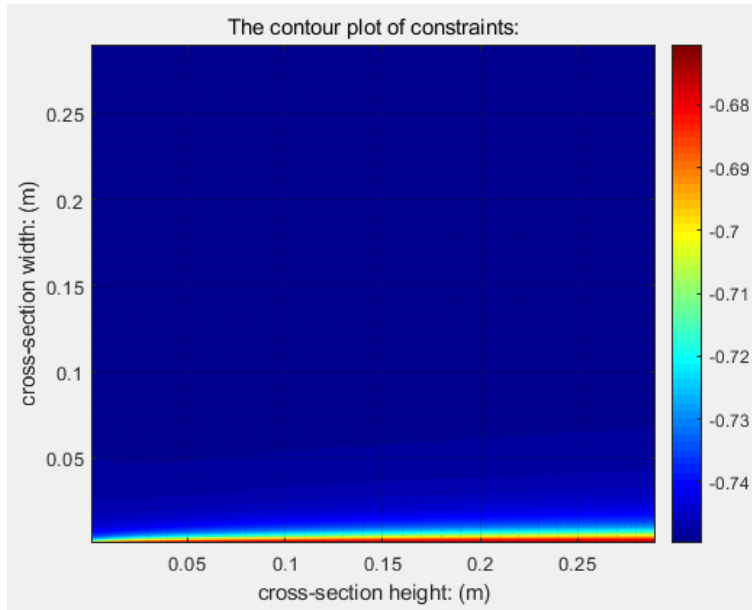
Figure 4.61   The contour plot of constraint- x axis 4th order natural frequency.
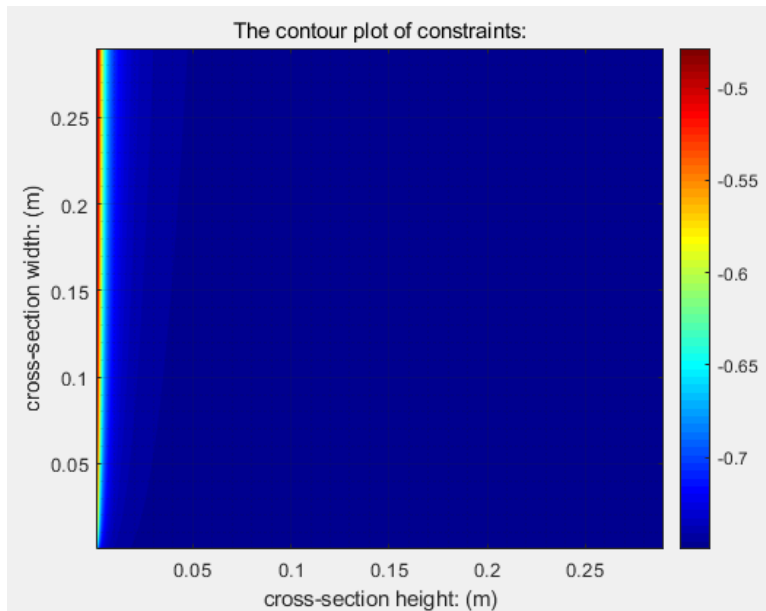
Figure 4.62   The contour plot of constraint- y axis 4th order natural frequency.
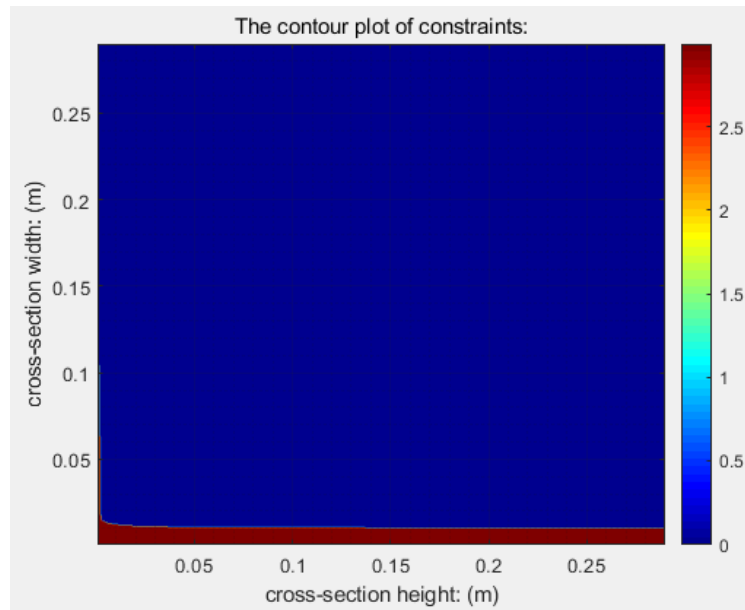
Figure 4.63   The contour plot of constraint- overall maximum deflection error.
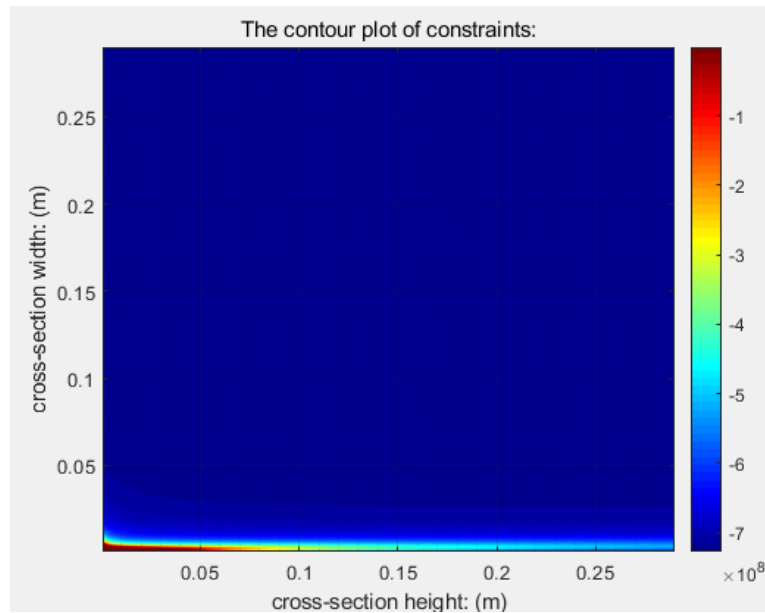
Figure 4.64   The contour plot of constraint- maximum tensive strain error.

117
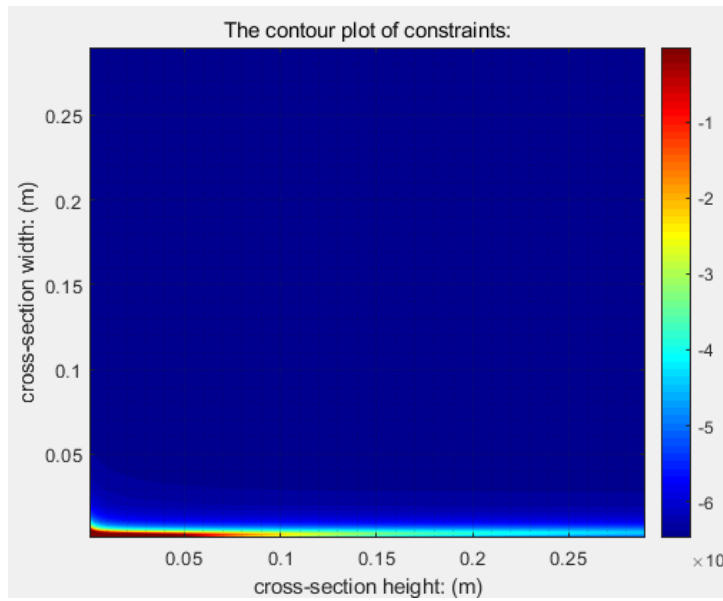
Figure 4.65   The contour plot of constraint- maximum compressive strain error.

4.4   Sensitivity Analysis

In this section, the sensitivity features of some selected key parameters are studied. The sensitivity features describe the impact on the optimisation results when a parameter is changing. For comparison, all the sensitivity studies are based on the DJI SW100 model, and the control group is the result introduced in Section 4.1.3.1 . The main parameters are listed in Table 4.20.

Table 4.20   The initial value and test range of the observed constants.

Main parameters	Symbol	Initial Value	Test range low	Test range high	Number of samples
Propeller Figure of Merit	FM	0.75	0.6	0.8	11
Minimum motor efficiency	$\eta_{m,min}$	0.6	0.6	0.8	11
The $\frac{m_{mot}}{MTOM}$ ratio		0.1756	0.1	0.3	11

4.4.1 Constant--Propeller Figure of Merit

The impact of the propeller figure of merit is presented in Figure 4.66 to Figure 4.68. The propeller FM is used to determine the motor output power from the propeller power under the hovering condition (see Section3.4.3.4-1), so the value of FM influences only the hovering power calculation and thus the total energy consumption, battery mass and price (see Figure 4.67). In addition to the reduction of $GTOM$ caused by battery mass decreasing, the required maximum power is slightly increasing (see Figure 4.68); this is the reverse condition, as discussed in the payload impact (see Section 4.5.1). However, the influence is so small that the motor mass remains unchanged. The mass and price of the ESCs and the arms slightly increase accordingly; however, this is difficult to observe in the figure, so detailed data is provided in Table 4.20 (the mass unit is g, and the price unit is $\$$).

118

Figure 4.66   The optimised $GTOM$ and components mass vs prop FM.

Figure 4.67   The optimised $GTOM$ and components mass vs prop FM.

Figure 4.68   The impact of FM on power consumption and motor-related features.

119

Table 4.21 The mass and price table against different propeller FM.

propeller FM	GTOM	total motor mass	total esc mass	total arm mass	battery mass	total price	total motor price	total esc price	total arm price	battery price
0.6	9342.21	1933.14	461.52	653.36	4710.81	1845.76	680.10	130.70	367.40	505.97
0.62	9016.05	1933.14	463.72	647.66	4388.14	1808.56	680.15	131.31	364.20	471.32
0.64	8747.35	1933.14	465.46	648.90	4116.46	1761.95	661.54	131.79	364.90	442.14
0.66	8517.29	1933.14	466.89	652.65	3881.22	1738.02	660.37	132.19	367.01	416.87
0.68	8313.50	1933.14	468.12	655.89	3672.96	1716.71	659.26	132.53	368.83	394.50
0.7	8131.54	1933.14	469.19	658.72	3487.11	1697.58	658.22	132.82	370.42	374.54
0.72	7967.94	1933.14	470.11	661.21	3320.09	1680.31	657.23	133.07	371.82	356.60
0.74	7819.95	1933.14	470.93	663.41	3169.08	1656.87	648.55	133.30	373.06	340.38
0.76	7685.34	1933.14	471.65	665.38	3031.78	1642.59	647.71	133.50	374.16	325.63
0.78	7562.34	1933.14	472.30	667.15	2906.37	1629.51	646.92	133.67	375.16	312.16
0.8	7449.46	1933.14	472.87	668.75	2791.32	1617.47	646.18	133.83	376.06	299.81

4.4.2 Constant—Minimum Motor Efficiency

The impact of the minimum motor efficiency is presented in Table 4.22 (the mass unit is g, and the price unit is \$), but this parameter is insignificant. In the algorithm, the minimum motor efficiency is used to determine the ESC output power from the motor output power under extreme flight conditions. Based on the quality of the selected motor, this value changes between 0.5 and 0.8 and represents the capability of a motor under extreme working conditions. However, it does not influence the motor estimation but only the mass and price of the ESC. Rather, the propeller efficiency is responsible for influencing the motor output power, which would be used to estimate the motor parameters. The ESC mass has a minor contribution to the $GTOM$, so the $GTOM$ slightly reduces. Along with $GTOM$, the motors, arms and battery also slightly change accordingly.

Table 4.22 The mass and price table against different minimum motor efficiency.

motor's lowest efficiency	GTOM	total motor mass	total esc mass	total arm mass	battery mass	total price	total motor price	total esc price	total arm price	battery price
0.6	12677.25	2798.94	1816.11	1187.15	5171.57	3686.59	1175.27	1109.28	667.57	555.46
0.62	12631.58	2798.94	1770.44	1187.15	5171.57	3574.45	1175.27	997.14	667.57	555.46
0.64	12589.29	2798.94	1728.14	1187.15	5171.57	3480.75	1175.27	903.44	667.57	555.46
0.66	12550.02	2798.94	1688.87	1187.15	5171.57	3401.65	1175.27	824.34	667.57	555.46
0.68	12335.25	2801.00	1543.29	1188.59	5098.89	3328.15	1175.00	758.12	668.38	547.66
0.7	12272.88	2801.84	1509.41	1189.17	5068.99	3267.53	1174.89	700.48	668.71	544.44
0.72	12214.59	2802.60	1477.69	1189.71	5041.11	3214.76	1174.78	650.52	669.01	541.45
0.74	12159.97	2803.31	1447.94	1190.22	5015.03	3168.52	1174.68	606.89	669.29	538.65
0.76	11742.04	2630.49	1421.28	1169.84	4816.95	3083.73	1159.22	570.30	657.84	517.37
0.78	11692.83	2630.46	1394.91	1170.19	4793.80	3047.31	1159.13	536.26	658.03	514.89
0.8	12014.99	2805.15	1368.81	1191.54	4946.02	3044.56	1159.71	504.57	670.04	531.24

4.4.3 Constant— $\frac{m_{m,tot}}{MTOM}$ Ratio

The impact of $\frac{m_{m,tot}}{MTOM}$ is illustrated in Figure 4.69 and Figure 4.70. In the algorithm, $\frac{m_{m,tot}}{MTOM}$ is used as a standard to select the motor estimation results produced by different trees (see Section 3.4.4.2). From Figure 4.70 through Figure 4.77, it is clear that the impact of $\frac{m_{m,tot}}{MTOM}$ is purely on the motor mass and price estimation. Given the same initial guessed $GTOM$, the larger the $\frac{m_{m,tot}}{MTOM}$, the larger the estimated motor mass. It can be noticed that after $\frac{m_{m,tot}}{MTOM}$ = 0.18, the motor mass no longer changes. If the target $\frac{m_{m,tot}}{MTOM}$ ratio is called r_{m0}, the $\frac{m_{m,tot}}{MTOM}$ values calculated from the estimated motor mass by different trees are indexed as $r_{m1}, r_{m2}, r_{m3} \dots r_{mx}$. The random forest method then selects the result whose r_{mx} is closest to r_{m0}. In this study, all the r_{mx} values are smaller than 0.18; so as long as $r_{m0} > 0.18$, the algorithm can only pick the largest r_{mx}. The motor mass increase causes the increase in $GTOM$, after which the changes take place, including the arms, ESCs and battery (see Figure 4.69).

Figure 4.69   *The optimised $GTOM$ and components mass vs $\frac{m_{m,tot}}{MTOM}$.*

Figure 4.70   *The impact of $\frac{m_{m,tot}}{MTOM}$ on power consumption and motor features.*

4.5   Analysis to the Other Parameters

As discussed in Section 4.2 by knowing the impact of parameters on a certain optimisation target, the design can be adjusted accordingly to achieve more desirable performance. In this section, the impact of some other parameters is analysed. The parameters include design parameters and constraints and are listed in Table 4.23.

Table 4.23 The initial value and test range of the observed parameters.

Main parameters	Symbol	Initial Value	Unit	Test range low	Test range high	Number of samples
Payload	PL	3550	g	0	6000	11
Maximum forward speed	$v_{f,max}$	16.6	m/s	0	30	11
Hovering Endurance	FT	900	s	180	1800	10
Number of battery cells	N_c	6		2	12	11
Propeller diameter	d_p	15	in	7	25	10

4.5.1 Constraint—Payload

The impact of payload is presented in Table 4.24, Figure 4.71 and Figure 4.72.

Table 4.24 The optimised $MTOM$ that satisfy the payload requirement.

payload mass/g	total no payload mass/g	$MTOM$/g	$\dfrac{PL}{MTOM}$
0	4334.38	4334.38	0.0%
600	4514.26	5114.26	11.7%
1200	4713.39	5913.39	20.3%
1800	5270.71	7070.71	25.5%
2400	5818.98	8218.98	29.2%
3000	6711.34	9711.34	30.9%
3600	7216.91	10816.91	33.3%
4200	7545.37	11745.37	35.8%
4800	7894.52	12694.52	37.8%
5400	8281.26	13681.26	39.5%
6000	8712.38	14712.38	40.8%

Some points must first be explained:

- Since this study is based on an existing multicopter, all the design parameters are fixed. The result reflects only the impact of the payload on this specific design. The propeller diameter is fixed to $15\ in$, which decides the overall size of the multicopter; hence, the body mass is constant. In addition, the mass of the avionics and landing gear are also constants. Summing the three components yields a result of $1.41\ kg$. Although they are not considered part of the payload by the algorithm, they contribute a significant constant part to the total mass. The role of the propulsion system and power system is to lift and hover both the payload and the aforementioned constant parts. Thus, the multicopter

weighs more than $4\ kg$ when there is no payload. If a full optimisation can be done on this study (due to limited time, it is not done), more appropriate designs can be developed to lift a given payload.

- When the payload increases, the $\frac{PL}{MTOM}$ ratio also increases because, for this multicopter model, the increase of the components' mass is slower than the increase of the payload. A statistic result from (Mauro Gatti, 2015) yields the regression equation of $\frac{PL}{MTOM}$ (see Equation (104), the unit is kg), which can be rewritten as Equation (105). It can be derived from the equation that the range of $\frac{PL}{MTOM}$ is (0,0.565). The data in Table 4.24 agrees with the equation.

$$MTOM = 1.7691PL + 1.5311 \tag{104}$$

$$\frac{PL}{MTOM} = \frac{1}{1.7691 + \dfrac{1.5311}{PL}} \tag{105}$$
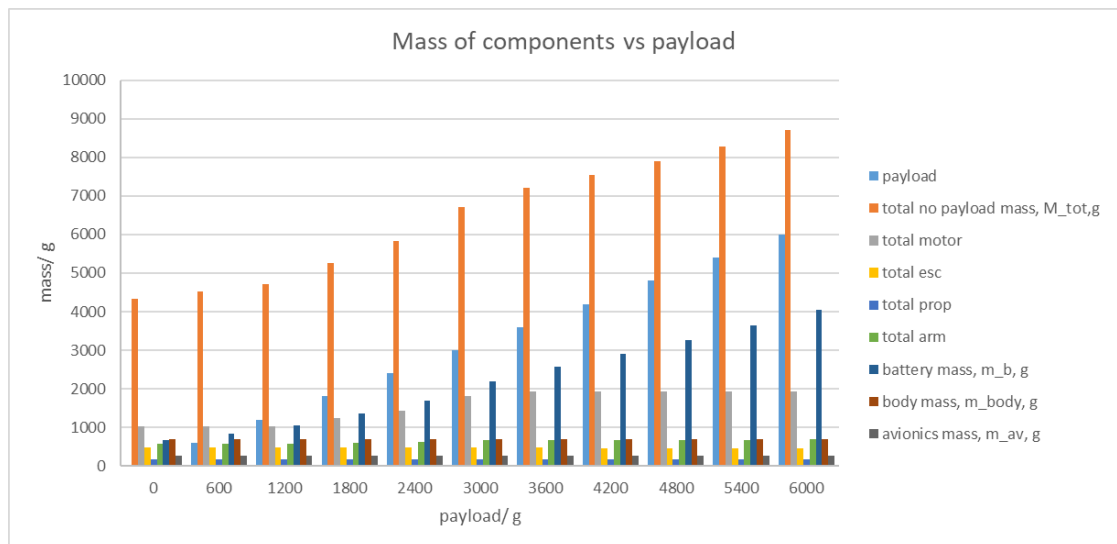
Figure 4.71   The optimised $GTOM$ and components mass vs payload requirement.
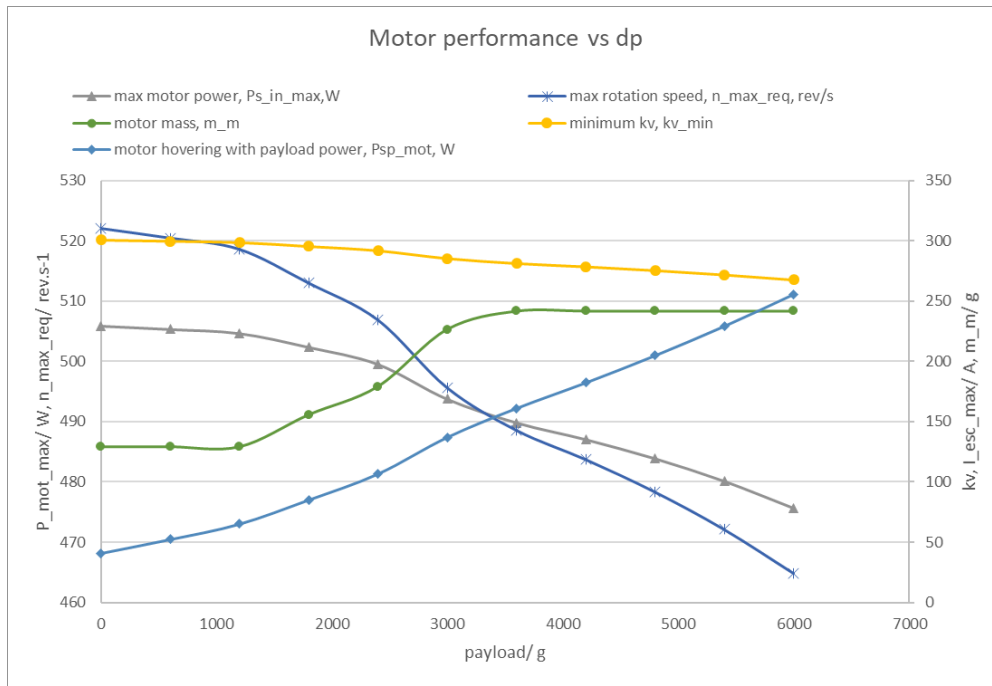
Figure 4.72   The impact of payload on power consumption and motor-related features.

The following points are concluded from the above table and figures:

- The increase of the payload causes the increase of the hovering power consumption and hence the total energy consumption. However, the maximum power consumption is barely influenced. As a result, the payload has the most direct impact on the battery mass and little influence on the other components until the hovering power exceeds the maximum forward flight power.

- The motor mass is estimated based on three parameters: the maximum power, minimum KV and maximum voltage. The estimation process employs the random forest method and hence is a black box for users. It is not known how exactly the three factors determine the estimated mass, but generally speaking, a higher power, higher voltage and smaller KV tend to result in a larger motor mass.

- It can be seen from Figure 4.72 that with the payload increase, the maximum power of the motor reduces. This is caused by the method in which the maximum forward flight power is calculated. As presented in Figure 4.73, in the maximum forward flight condition, the multicopter is in equilibrium between the gravity, drag and thrust. When the $GTOM$ increases, G increases, causing the tilt angle α to decrease. α then influences the value of the drag force, which is related to the speed and drag area. Now that the speed should be the same (it is the mission requirement), the reduction in α causes the drag area reduction (see Figure 4.74), and the drag force decreases. Finally, a new thrust is required to form a new equilibrium. This is a comparison between two multicopters of the same design but with different $GTOM$ values. It is noticed that the amount of drag force change depends on the value of the tilt angle. Thus, under certain circumstances, the required thrust may be smaller when the $GTOM$ is larger.
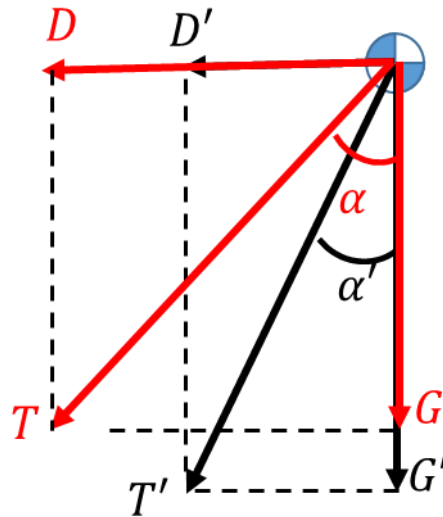
Figure 4.73   The comparison of two similar multicopters in equilibrium state.
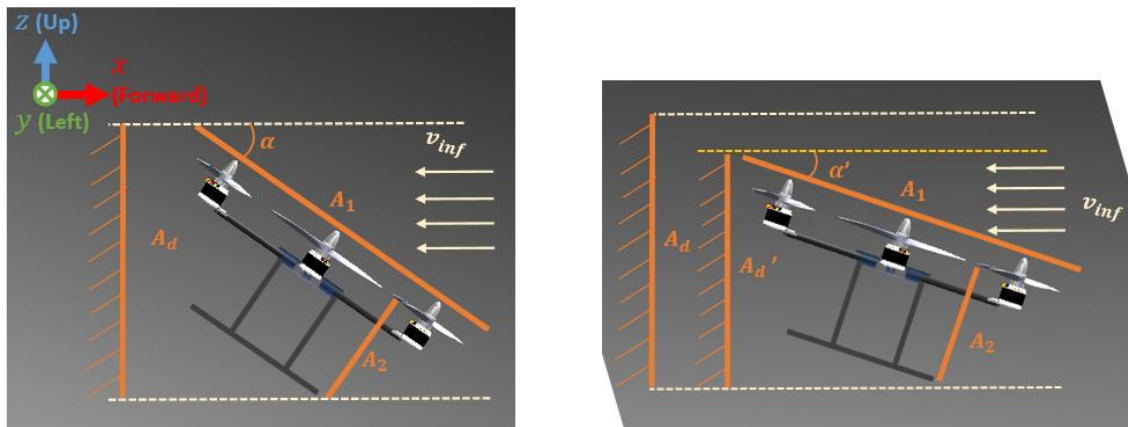
Figure 4.74   The drag area is reduced when the tilt angle is reduced.

4.5.2 Constraint—Maximum Forward Speed

The impact of the maximum forward speed is shown in Figure 4.75 to Figure 4.79.

The impact of the maximum forward speed is presented in Figure 4.75 through Figure 4.79.

From Figure 4.77, it is clear that after a certain speed, DL and TrW begin to increase. This is because, if the maximum speed is smaller than a threshold, the maximum required forward flight power would be smaller than the (TrW-modified) hovering power. Hence, TrW remains minimum. From Figure 4.78 and Figure 4.79, the increase of the maximum forward speed causes the increase of the maximum required power and maximum current through the propulsion system (the voltage is almost constant). As a result, the ESC mass and price are influenced the most, and a clear increase can be observed. Over, the motors reveal an increasing trend, but due to the non-linear property of the random forest estimation method, the increase is accompanied by fluctuation. The increase of the maximum motor thrust causes the arm strength to increase, as well. Finally, the overall increase of $GTOM$ requires more hovering power, and hence, the battery capacity must increase. These changes are clearly illustrated in Figure 4.75 and Figure 4.76.

Regarding the arm optimisation, in Figure 4.75 and Figure 4.76, the trend of the arm appears to be inconsistent; this is because the arm is selected via a sub-optimisation process. The related arm data of this study is presented in Table 4.25. It can be seen that the cross-section dimension (width, height and thickness) continues to increase. However, the optimal cross-section shape varyies. The hollow circle and hollow rectangular shape are regular shapes, while the 'L' and 'n' shapes are irregular. Thus, the carbon fibre tubes of the latter shapes are relatively more expensive than the former shapes.
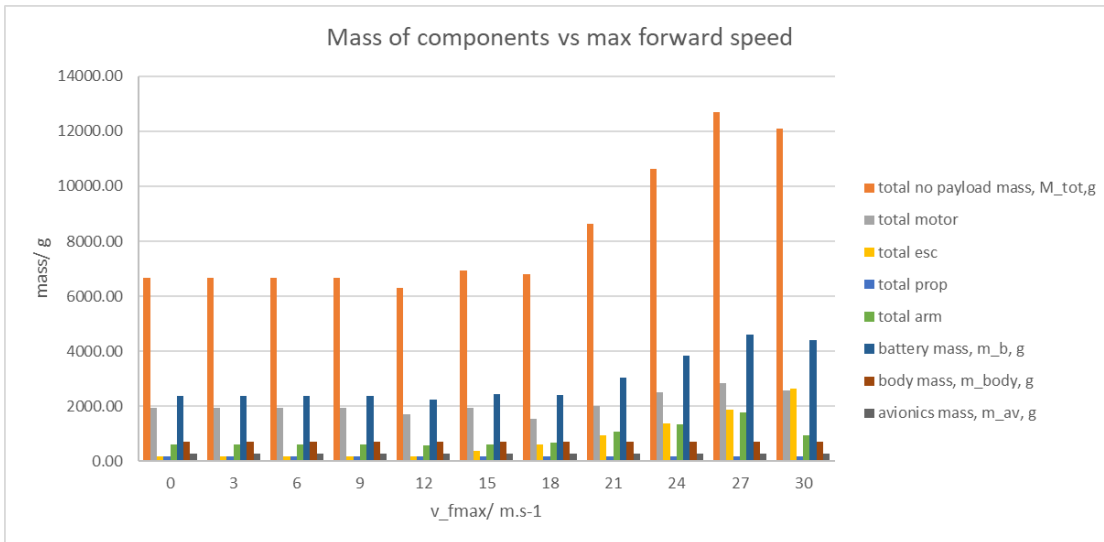
Figure 4.75   optimised $GTOM$ and components mass vs speed requirement
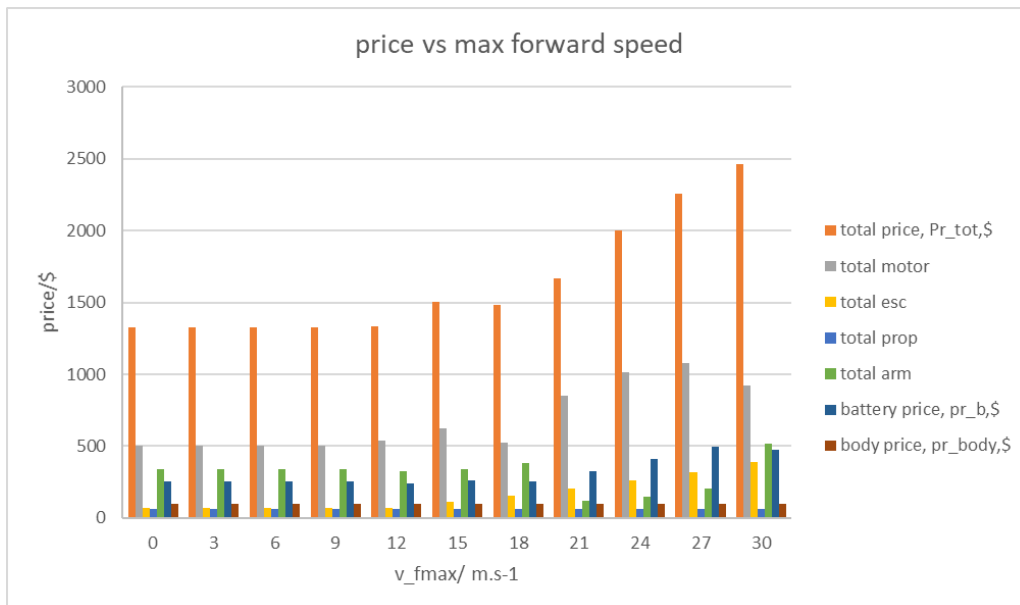
Figure 4.76   The impact of max forward speed on components price.
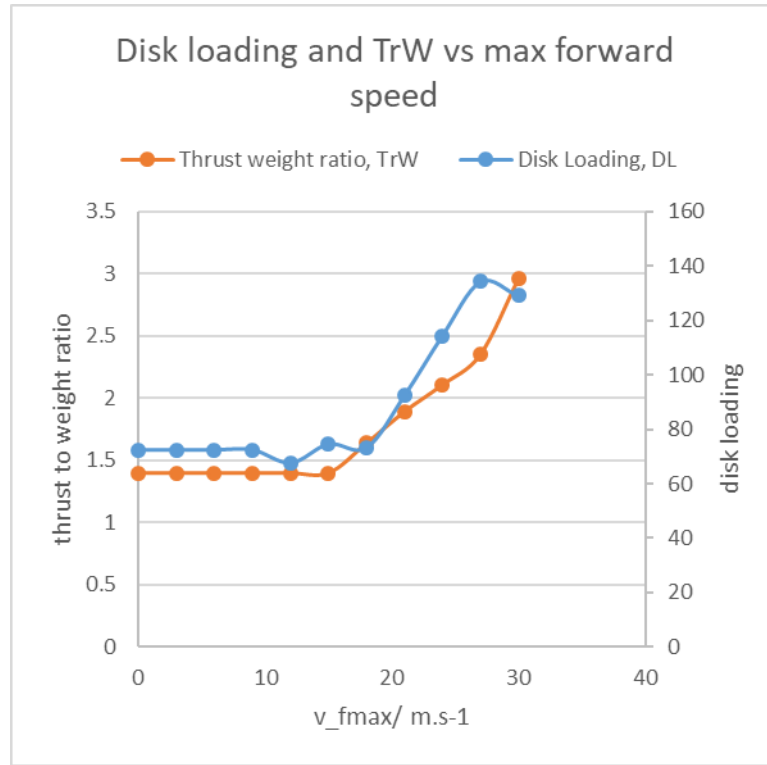
Figure 4.77   The impact of max forward speed on DL and TrW.
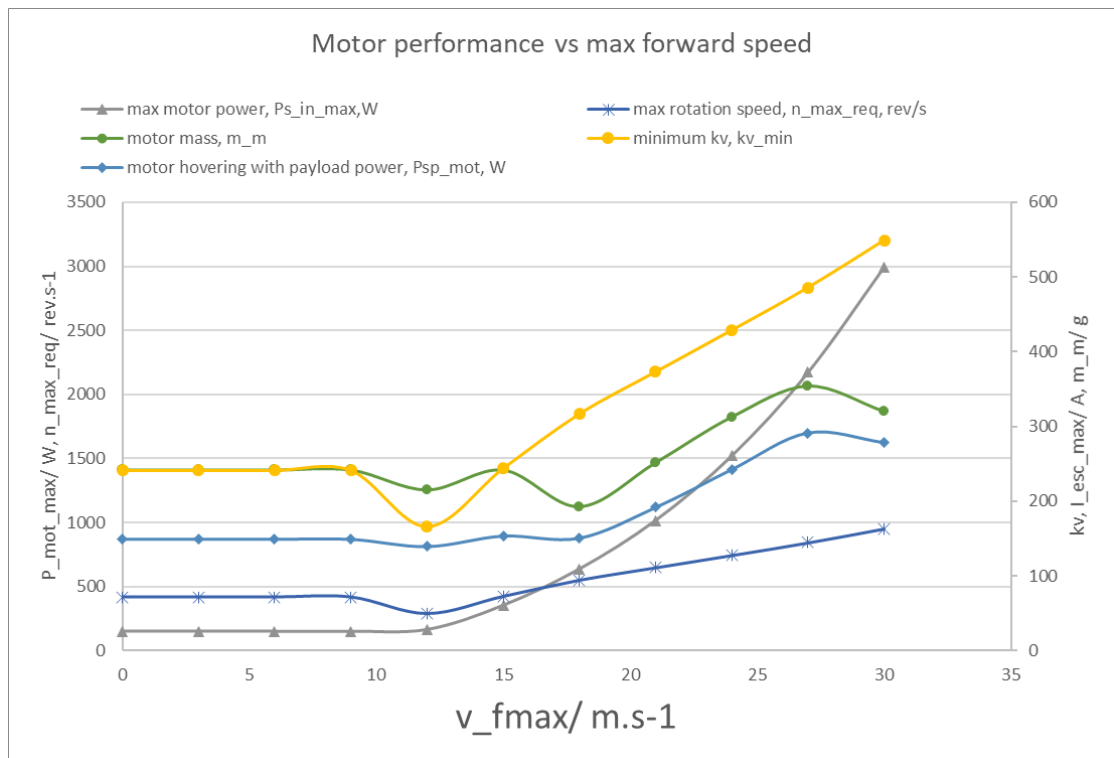
Figure 4.78   The impact of max forward speed on motor-related features.
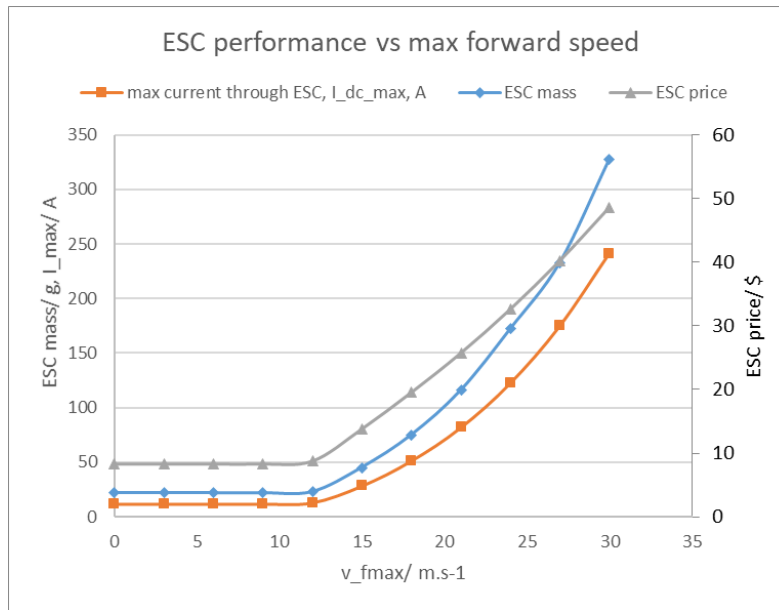
Figure 4.79   The impact of max forward speed on ESC-related features.

Table 4.25 The data of optimised arm against different maximum forward speed.

v_fmax, m/s	arm cross section shape	Unit Price, $/m3	arm cross section width, mm	arm cross section height, mm	arm cross section thickness, mm
0	6: corner "L" shape	562.33	55.89	55.89	0.80
3	6: corner "L" shape	562.33	55.89	55.89	0.80
6	6: corner "L" shape	562.33	55.89	55.89	0.80
9	6: corner "L" shape	562.33	55.89	55.89	0.80
12	6: corner "L" shape	562.33	53.06	53.06	0.80
15	6: corner "L" shape	562.33	56.30	56.30	0.80
18	6: corner "L" shape	562.33	62.66	62.66	0.80
21	3: hollow circle	113.48	62.60	62.60	0.80
24	2: hollow rectangular	113.48	61.96	61.96	0.80
27	2: hollow rectangular	113.48	65.40	65.52	1.02
30	5: channel "n" shape	562.33	46.28	62.53	0.80

4.5.3 Constraint—Endurance

The impact of required hovering endurance is displayed in Figure 4.80 and Figure 4.81. The impact of endurance is quite similar to the impact of the payload. It has the greatest influence on the battery, while the other components are barely changed, since the extreme performance requirement is not changed.
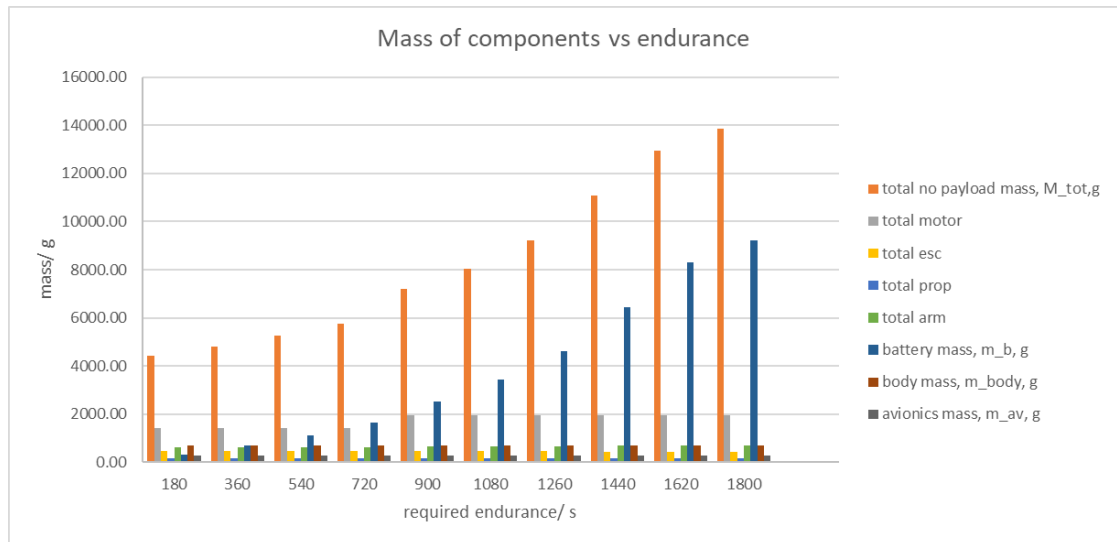
Figure 4.80   The optimised $GTOM$ and components mass vs endurance requirement.
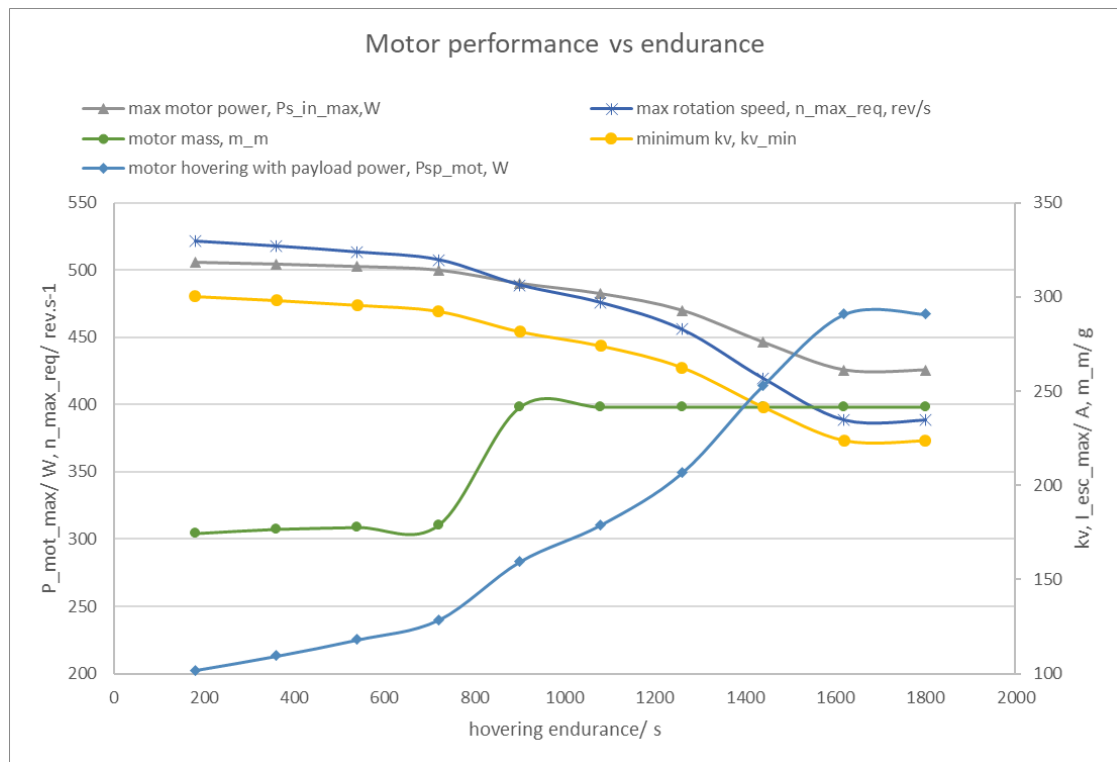
Figure 4.81   The impact of endurance on power consumption and motor-related features.

4.5.4 Design Parameter—Propeller Diameter

The impact of the propeller diameter is displayed in Figure 4.82 to Figure 4.86. A larger propeller is heavier and more expensive. The first impact of the propeller diameter change is the change of the overall size and hence the mass and price of the arms and the central body (see Figure 4.82 and Figure 4.83). The increasing $GTOM$ also causes an increase of the mass and price of the motors and ESCs (see Figure 4.84 and Figure 4.85). It is noteworthy that the growth of the body and propeller also causes the projection drag to increase; thus, unlike the study of the payload, the maximum motor power also increases. Theoretically, larger propellers should have

129

better efficiency and hence reduce the required hovering power, total energy consumption and battery mass and price. However, the $GTOM$ increase caused by the growth of the body and arms is so significant that additional power is consumed to lift the increased mass. As a result, the total energy consumption reveals a fluctuated curve (see Figure 4.86).
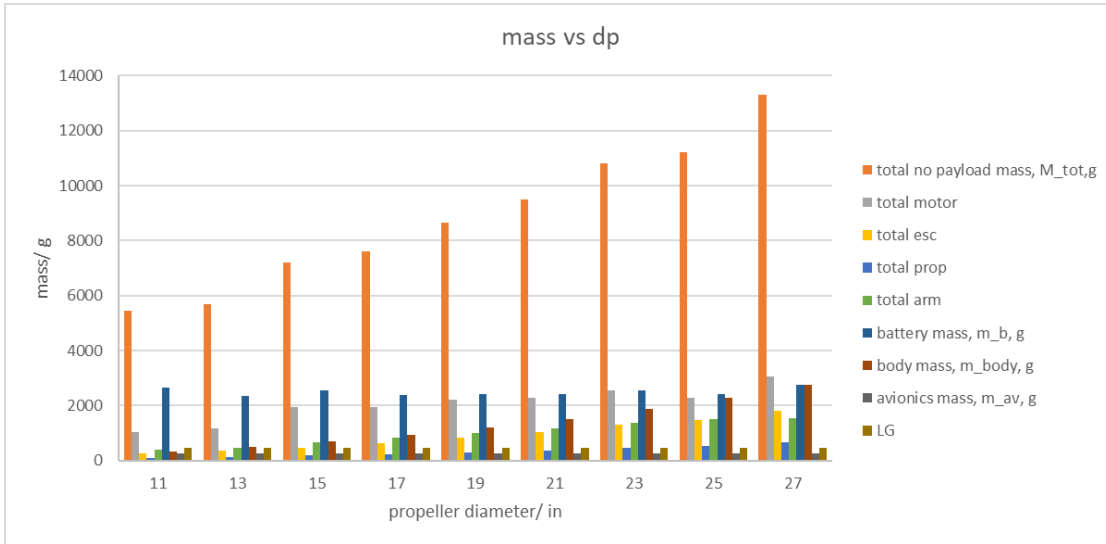
Figure 4.82   The optimised $GTOM$ and components mass vs propeller diameter.
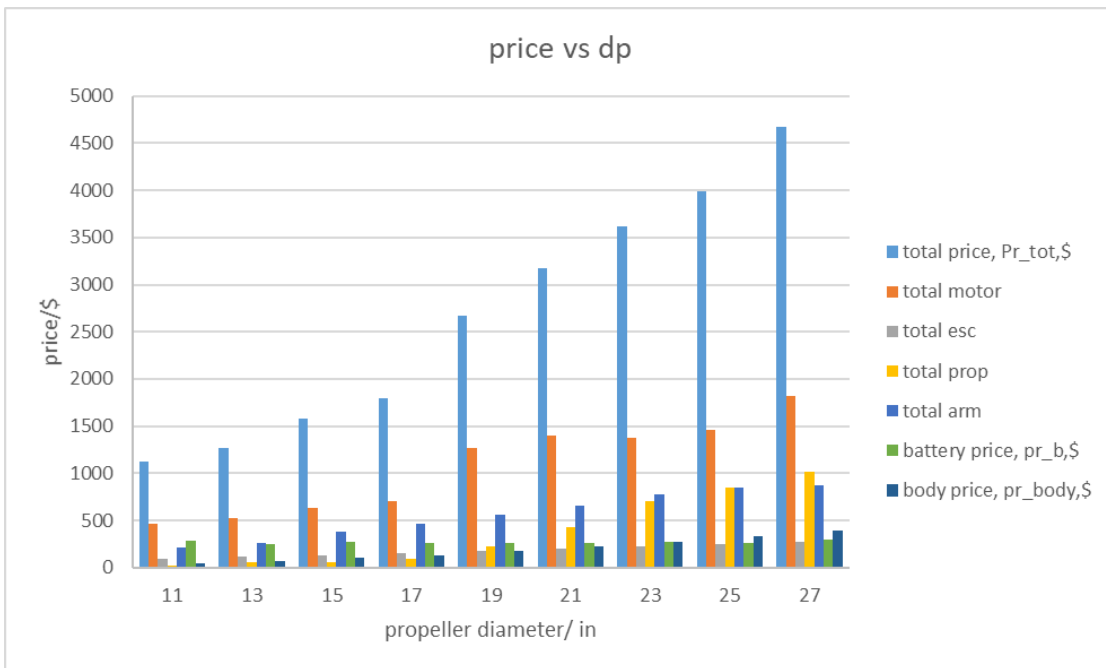
Figure 4.83   The optimised price and components mass vs propeller diameter.
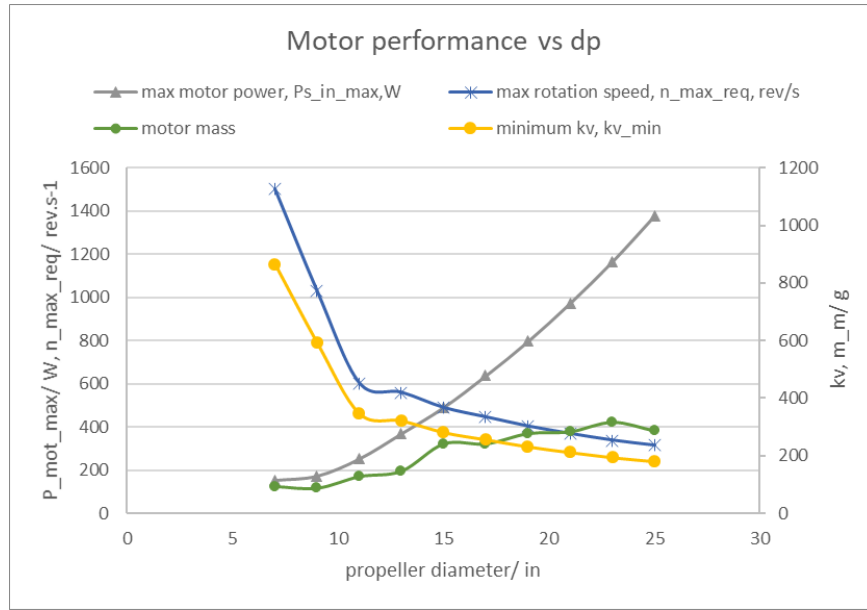
Figure 4.84   The impact of propeller diameter on power consumption and motor features.
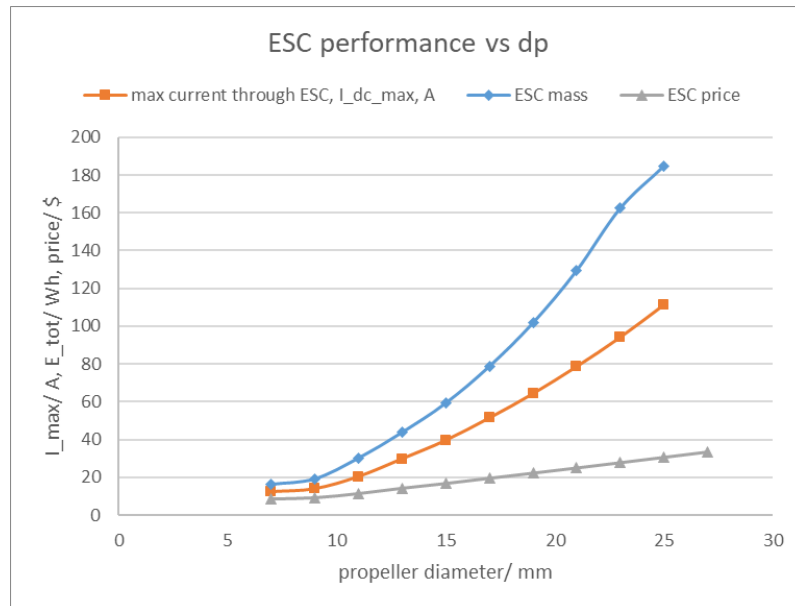
Figure 4.85   The impact of propeller diameter on ESC-related features.

131
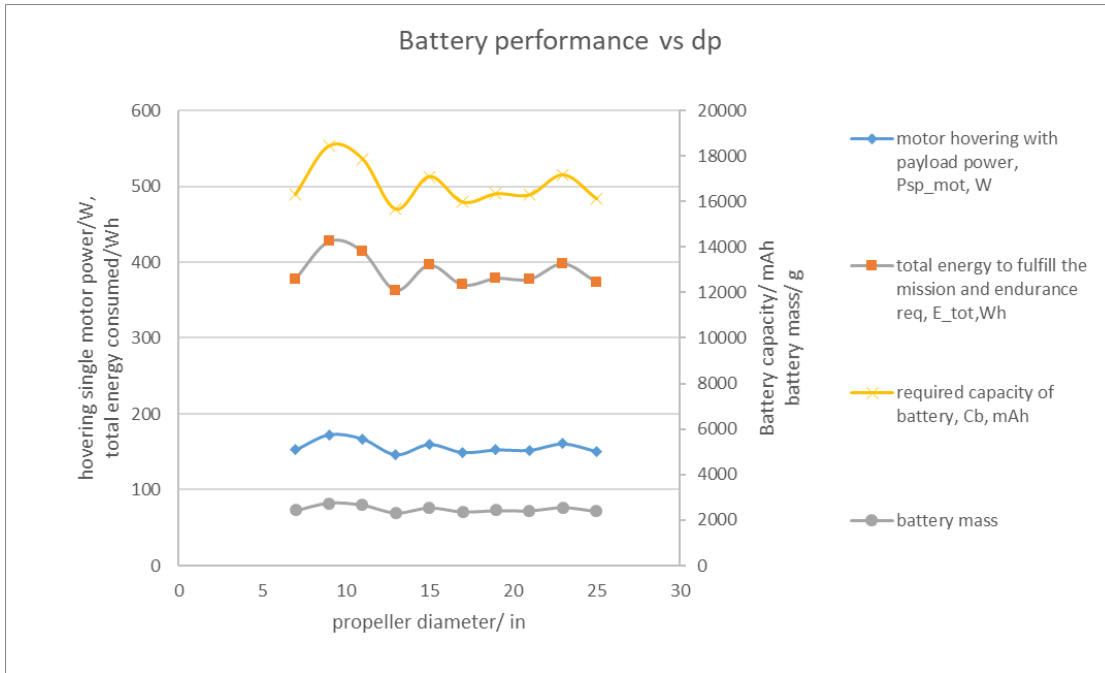
Figure 4.86   The impact of propeller diameter on battery-related features.

4.5.5 Design Parameter—Number of Battery Cells

The impact of the number of battery cells is presented in Figure 4.87 through Figure 4.90. As the number of cells increases, the output voltage increases. The power consumption is barely influenced and the hovering power is almost constant (see Figure 4.89), while the maximum power changes in conjunction with the change in $GTOM$ (see Figure 4.90). As a result, the current through the system is reduced, which directly causes the mass and price of the ESC to decrease (see Figure 4.87 and Figure 4.88). The reduction in current also causes the required battery capacity to drop; however, it has little influence on the mass and price of the battery, as they are linearly related to the required total energy, which is almost unchanged (see Figure 4.89).

Another significant impact is on the price of the motor. The maximum voltage is the necessary parameter to determine the KV (see Equation (90)), and both belong to the three key parameters used to estimate the motor mass and price via the random forest method. The exact estimation procedure of the random forest model is unknown, but the result reveals that the price of the motor increases as the voltage increases and KV reduces, while the mass changes slightly in the same pattern as the maximum rotation speed and the $GTOM$ (see Figure 4.90).
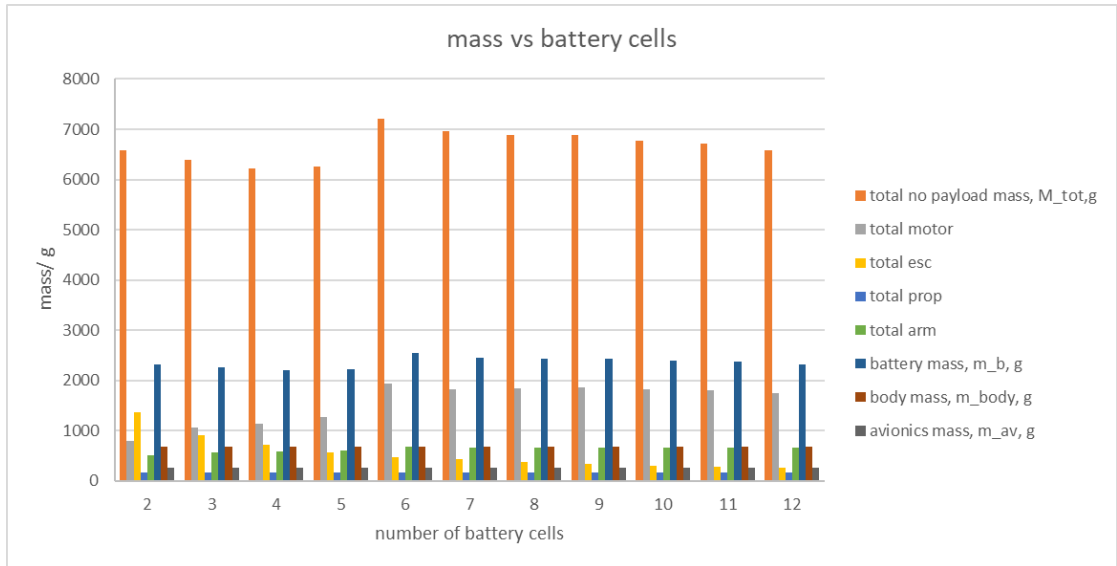
Figure 4.87 The optimised $GTOM$ and components mass vs payload requirement.
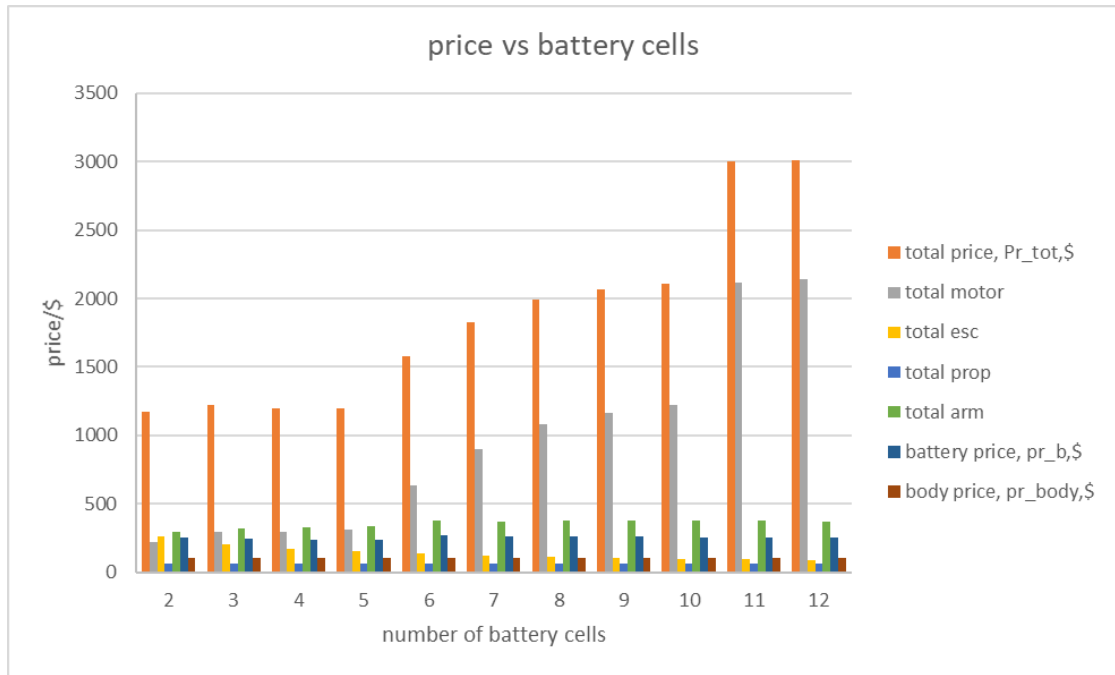
Figure 4.88 The impact of payload on components price.
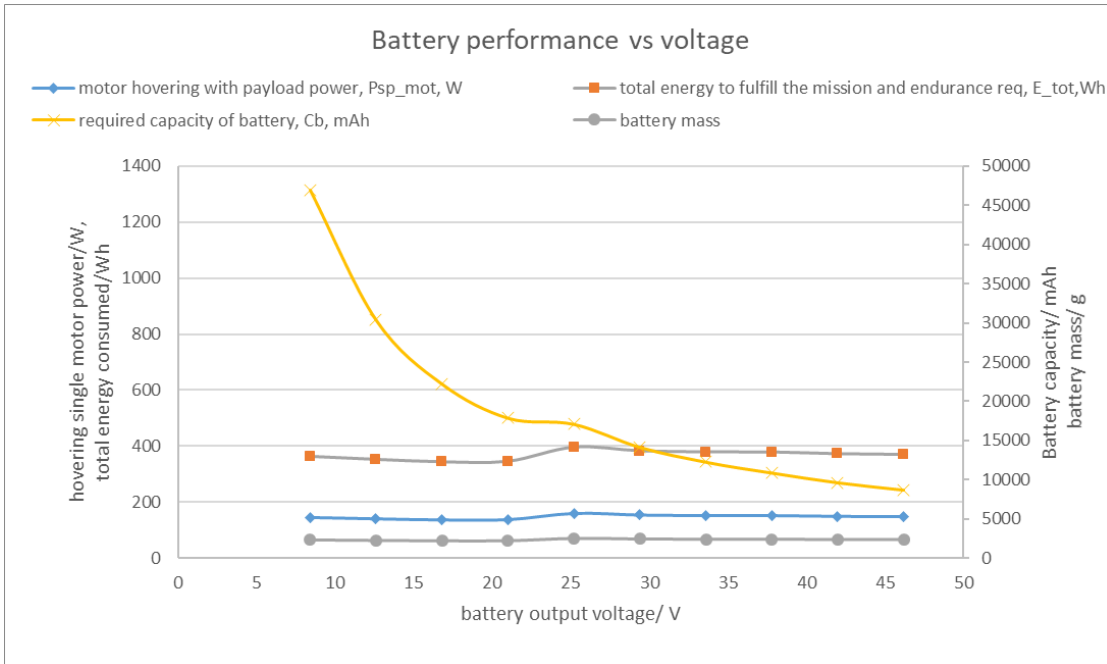
Figure 4.89   The impact of payload on battery-related features.
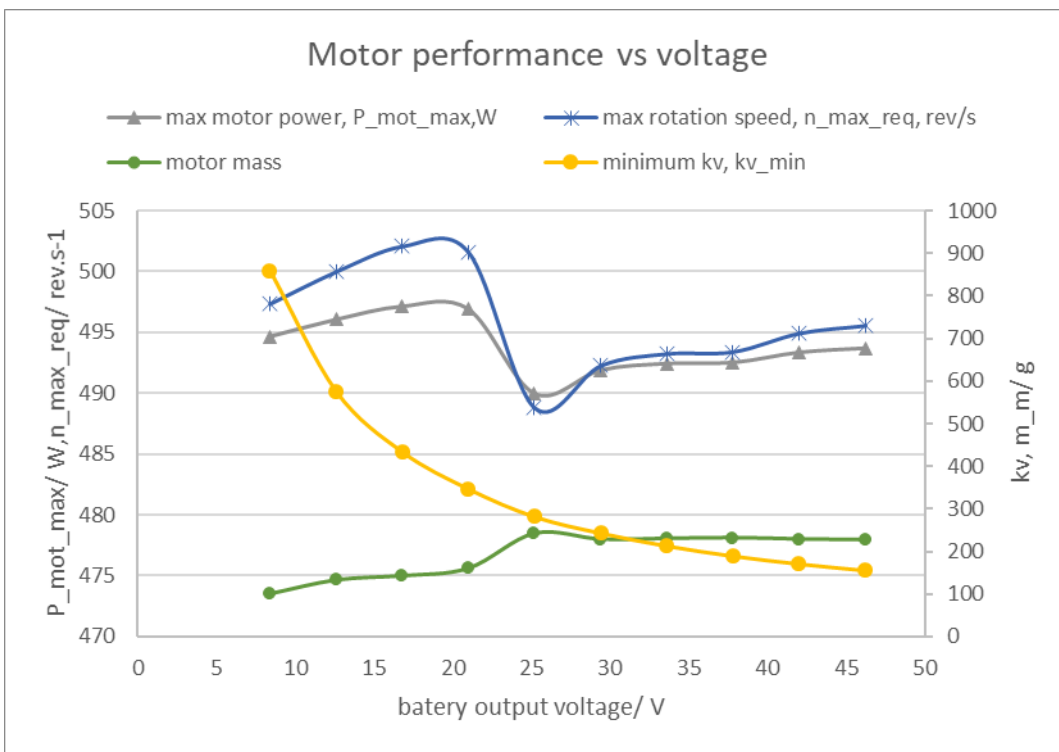
Figure 4.90   The impact of payload on power consumption and motor-related features.

4.6   Conclusion

In this chapter, the conceptual design algorithm is validated based on four aspects: the components estimation, total mass estimation, layer_2 function output-input plot and full optimisation process validation. Then, the value determination of some constants is explained and discussed. Finally, the sensitivity feature of some selected parameters is studied. In conclusion, this algorithm makes designs based on average performance components. The final

optimisation results still have the room (errors between estimation results and actual multicopters) and possibility (errors are within an acceptable range and can be recovered via detailed design and replacing components) to be improved for certain targets. Based on this, the algorithm is considered accurate and trustworthy, and it is proven to be valid as a tool for multicopter conceptual design and the numerical analysis of multicopter application scenarios.

Chapter 5 Application

The proposed algorithm can be used to analyse certain scenarios and provide foundations for further decision making. In (Ampatis and Papadopoulos, 2014), the influences of the payload and number of motors on the design and performance are studied, while in (Gatti, 2017), the relationship between the multicopter endurance and the battery weight was analysed using the proposed algorithm. In this chapter, a mission of long-range communication and surveillance which requires the cooperation of several multicopters is considered.

5.1 Brief Introduction to the Mission

Assume that for a mission, a remote location must be searched. Suppose that for some reason, the road is blocked by an earthquake, it is located in a hostile region or maybe the location is in an environment harmful to humans, such as a radiation-polluted factory. A preferred feature in this mission is the real-time surveillance of the target area. Thus, this mission proposes the requirement that the drone should be capable of transmitting the video signal back to base, which is called BRLOS (beyond radio line of sight) communication.

An EMW (electromagnetic wave) can transmit more information as the frequency is higher. However, a higher-frequency EMW also has higher attenuation and worse penetration. To transmit real-time video, the UHF (ultra-high frequency) band, ranging from 300 MHz to 3 GHz, or a higher frequency band is normally used. The typical transmission range is from 300 m to 3 km. The actual range is influenced by many factors, such as the transmitter (Tx) power, gain of the antennae, sensitivity of the receiver (Rx), weather condition and obstacles between the Rx and Tx. A longer transmission distance and better video quality indicate more expensive, more powerful and heavier equipment (see Appendix J for a benchmark study of video transmitters for multicopters). Moreover, the noted range on the product specification generally only applies to an ideal open-space condition, and most are exaggerated. When obstacles are between the transmitter and receiver, the communication range is greatly reduced.

Under this circumstance, a cooperative multiple-multicopter solution is proposed. The multiple aircraft can form a chain network and repeat the video signal from the frontier to the base. The distance between each aircraft can be maintained at an acceptable level; thus, cheaper and lighter equipment can be used. This solution can be accomplished following three different methods, and in this section, the methods are modelled, compared and evaluated based on various aspects using the previously proposed multicopter conceptual design algorithm.

5.2 Scenarios and Mission Requirements

5.2.1 Description to the Standardised Scenario

The mission is described by a model. As presented in Figure 5.1, the base is at point $'O'$, the mission target is at point $'E'$, the best communication range between two aircraft is $'d'$ and the

altitude of the trajectory is $'h'$. The process follows that the multicopters take off from $'O'$, lift to altitude $'A'$ and fly forward at speed $'v'$. One multicopter will stop and remain at a middle point, such as $'B'$, $'C'$ or $'D'$, and act as a signal repeater. The communication network is then built to support the long-range signal link. The final multicopter arrives at the mission target and proceeds with the mission for time $'T'$. The '…' between $'C'$ and $'D'$ indicates that more segments can be inserted to extend the total range. The mission data is presented in Table 5.1.

Two assumptions must be clarified:

1. The first multicopter stops at point $'B'$. The base is equipped with a larger high-sensitivity receiver, so the communication range to the base is longer.
2. A highly dynamic and highly robust ad-hoc network is between the multicopters; one node can search for the nearest two nodes and build up a connection over a negligible time.
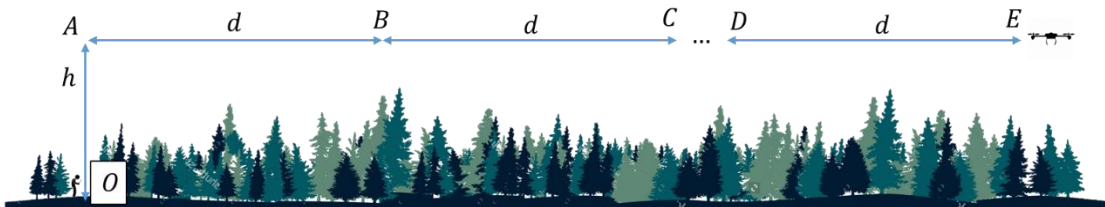
Figure 5.1 The description of the mission.

Table 5.1 The data of the mission.

Term	Altitude	Communication range	Fly speed	Mission duration
Symbol	h	d	v	T
unit	m	m	m/s	s
Value	300	500	10	400

The multicopters can be organised into three configurations, as introduced below.

1. 'Chain'
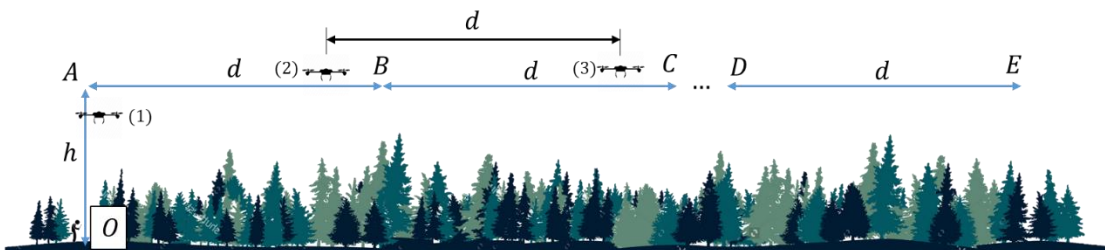
Figure 5.2 The description of the "Chain" configuration.

As displayed in Figure 5.2, the multicopters are organised as follows: the multicopter (3) takes off, lifts to point $'A'$, then flies forward. When it has a distance of $'h'$ to point $'B'$, the multicopter (2) takes off. The forward velocity and ascending velocity are the same, which ensures that multicopters (3) and (2) arrive at points $'B'$ and $'A'$ at the same time. They continue to move forward, and since their velocity is the same, the distance between them no longer changes. When the multicopter (2) has a distance of $'h'$ to point $'B'$, multicopter (1) takes off. In this

sequence, one after another, as though pulling a chain, the multicopters form the network until the multicopter arrives point $'E'$ and proceeds with the mission. Once the mission is finished, the multicopters fly back and land in the reverse sequence. Since the process is similar to pulling a chain, this configuration is called 'Chain'.

2. **'Mother and Children'**
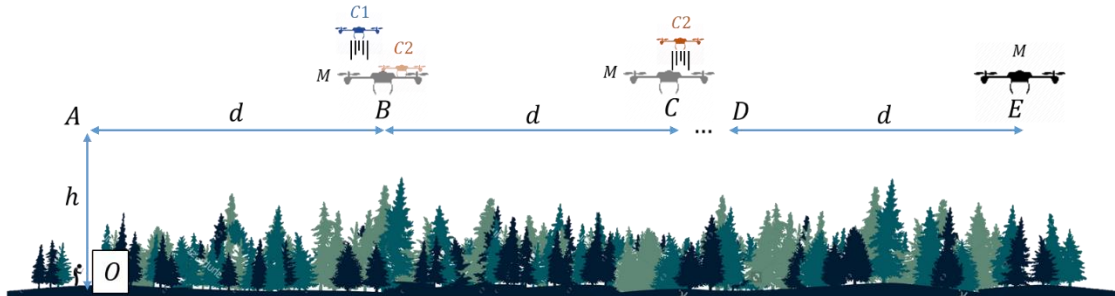
Figure 5.3 The description of the "Mother & Children" configuration.

This configuration uses a large mother multicopter to carry all the children multicopters and transport them to each stop along the way. The mother then launches a child at one stop, and the child remains at the point and acts as a node in the network. At point $'B'$, C1 is launched; the mother and the other child were there previously, but now they have moved forward, so they are presented as partially transparent. C2 is launched at point $'C'$, and finally, M arrives at the mission target. Once the mission is finished, M flies back and recovers each child along the way. The key to this configuration is that the children are supposed to only hover. Thus, it is acceptable for them to be poor at moving.

3. **'Russian Doll'**
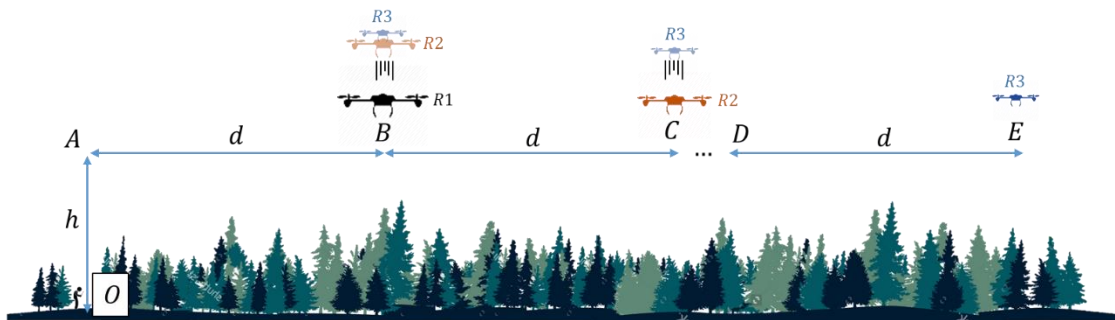
Figure 5.4 The description of the "Russian Doll" configuration.

The 'Russian Doll' is similar to the 'Mother and Children' approach; however, in this case, at each stop, it is the outmost multicopter who detaches and remains as a repeater. The inner multicopters take off from the shell and continue onward. Finally, the innermost multicopter arrives at the target and proceeds with the mission.

5.2.2 Brief Analysis

Through an analysis of the three configurations, at the first glance, the 'Chain' configuration appears to be the most efficient. This configuration ensures that the multicopters do not waste any energy (i.e. they are doing just the right amount of work). This is difficult to assess for the 'Mother and Children' configuration, since it wastes some extra energy during the launching and recovering actions, however, since the children do not require strong manoeuvrability, this may save some mass and price. Moreover, instead of several aircraft flying forward together, this configuration has only one aircraft moving forward. When the forward velocity is the same, it is the drag area that determines the forward flight power consumption. The mother multicopter is certainly larger because it carries all the children, so it is worth comparing whose total drag area is larger. Until it is calculated by the design algorithm, the answer to this question is not known. The 'Russian Doll' configuration wastes even more energy. For the first multicopter, for most of the time, it is hovering, but its extreme performance is greatly enhanced because it should be able to transport all the other multicopters. However, unlike in the 'Mother and Children' approach, the drag area of this configuration continues to reduce, so this configuration is also worth calculating.

Two optimisation sessions are performed:

- In the first session, a range of $1500\,m$ is specified, so the number of multicopters is determined to be three. The multicopters of the three configurations are optimised, and their performances are evaluated. In addition, they are compared with the single-multicopter condition.
- In the second session, the 'Chain' and 'Mother and Children' approaches are selected to study the influence of range. It is interesting to know whether the performance of the two configurations would change when the mission range differs.

5.3   Optimisation Session 1

5.3.1 Brief Intro of Setting

In Session 1, 10 independent optimisations are performed for each multicopter in each configuration and also for the single multicopter, since each multicopter has a different flight time and hovering time. Due to the difference between the configurations, the constrains and design parameter ranges also vary and are specified in Table 5.2, while the exact flight time of each mission phase is specified in Table 5.3.

In Table 5.2, the avionics with a standard COM device weighs 0.07 kg. For Chain (3), M and R3, an extra camera is required to proceed with the mission, so their avionics weighs 0.19 kg and consumes more power. Moreover, because of the camera, the landing gear of Chain (3) and M are larger. During the recovery phase, a docking mechanism is required to guide and connect the two multicopters. The docking mechanism typically is two pieces and is installed on both the mother and child multicopters. For C1, C2 and R3, they have a docking mechanism rather than landing gear, since they are to be recovered by the mother multicopter. Meanwhile, R1 and R2

have two systems: the mother-side docking mechanism to recover the child multicopter and the landing gear or the child-side docking mechanism (see Table 5.4 and Table 5.5 for the components break-down). It should be noticed that the launching and recovery are calculated as the take-off and landing. When the child in launching, the mother multicopter is considered as hovering. For simplification, the docking mechanisms are all passive (no power consumption), and their influence is reflected only by the mass of the landing gear.

Table 5.2 Design parameters options and constraints of multicopters.

	N_r options	N_c options	d_p options	Number of total results	Max velocity m/s	Avionics mass kg	Avionics power W	Landing gear mass kg
Chain (1)	3 (4,6,8)	9 (1,2,3,4,5,6,7,8, 9), 5 (3,4,5,6,7)	3 (3,4,6) 5 (5,7,9,11,13)	156	15	0.07	2.5	0.05
Chain (2)	3 (4,6,8)	9 (1,2,3,4,5,6,7,8, 9), 5 (3,4,5,6,7)	4 (2,3,4,6)5 (5,7,9,11,13,15)	183	15	0.07	2.5	0.05
Chain (3)	3 (4,6,8)	9 (2,4,6,8,9,10,11, 12,13), 5 (2,3,4,5,6,7,8)	5 (4,5,6,7,8), 5 (7,9,11,13,15)	219	15	0.19	4	0.2
C1	3 (4,6,8)	4 (1,2,3,4)	4 (2,3,4,5)	48	0	0.07	2.5	0.05
C2	3 (4,6,8)	4 (1,2,3,4)	6 (2,3,4,5,6,7)	72	0	0.07	2.5	0.05
M	3 (4,6,8)	7 (1,3,5,7,9,11,13)	7 (4,7,10,13,16,19,22)	147	15	0.19	4	0.3
R1	3 (4,6,8)	7 (3,4,5,6,7,8,9)	6 (11,13,15,17,19,21)	126	15	0.07	2.5	0.25
R2	3 (4,6,8)	5 (3,4,5,6,7)	6 (9,11,13,15,17,19)	90	15	0.07	2.5	0.25
R3	3 (4,6,8)	7 (2,3,4,5,6,7,8)	4 (5,6,7,8)	84	15	0.19	4	0.1
Single	1 (4)	10 (1,3,4,5,6,7,8,9,1, 13)	18 (4,6,7,8,9,10,11,12,13,1 4,15,16,17,18,19,20,22, 24)	180	15	0.3	8	0.3

* In the table, 3 (4,6,8) means there are three candidates, and they are (4,6,8). Two brackets mean the same problem is run under two group of dataset.

Table 5.3 The flight time of each mission of the multicopters.

Phases	Forward Flight Time	Hovering Time	Launching	Recovering	Take Off	Landing
Chain(1)	300	400			30	30
Chain(2)	200	400			30	30
Chain(3)	100	400			30	30
C1		610	5	5		
C2		500	5	5		
M	300	420			30	30
R1	100	620			30	30
R2	100	510	5	5		
R3	100	400	5	5		
Single	300	400			30	30

*The unit for time is s

Table 5.4   The avionics break-up.

	General (auto pilot, GPS, IMS, etc.)	Standard COM	Camera	Advanced COM
Mass (g)	0.05	0.02	0.12	0.13
Power (W)	2	0.5	1.5	4.5

Table 5.5   The landing gear mass break-up

	Landing Gear	**Docking Mechanism Mother**	**Docking Mechanism Child**
Chain(1)	0.2		
Chain(2)	0.05		
Chain(3)	0.05		
C1			0.05
C2			0.05
M	0.2	2*0.05	
R1	0.1	0.15	
R2		0.1	0.15
R3			0.1
Single	0.3		

*The unit for mass is kg

5.3.2 Results Analysis

The algorithm offers several valid designs for each multicopter. Based on accomplishing the mission, some outstanding designs are selected and displayed in Table 5.6. For each multicopter, multiple valid designs can accomplish the mission; a standard is required to make the comparison between multicopters. Thus, the total mass (g), total cost ($\$$) and total energy consumption ($W \cdot h$) are selected as the three main factors for evaluating each design. For each multicopter, if a design has one or more of the three main factors for which the value is the smallest, its details are recorded in the table. Finally, each configuration as a whole is compared with one another. Based on the results, the following discussions can be made:

- The 'Single' configuration is a comparable group and reference. This configuration assumes that such a powerful video transmission system exists and assumes the performance of the single multicopter. The parameter of the advanced communication (COM) device is defined as $0.13\ kg$ and $4.5\ W$ (see Table 5.4). This number is a reasonable assumption based on the benchmark study (see Appendix J). However, the price is difficult to define, so the price of the communication system is not included in the calculation. The estimated cost is the pure components cost and is the same for all the other multicopters. Then, by comparing their price, at least one point becomes clear: the price difference between the 'Single' configuration and the 'Chain' and 'Mother and Children' configurations are from $\$120$ to $\$140$. Thus, in actual designs, if the price difference between the advanced COM and standard COM is larger than this range, then the 'Single' configuration is a more expensive solution.

Table 5.6   The Optimisation results comparison.

Multicopter	Number of Valid Designs	Lightest						Cheapest						Least Energy Consumption					
		Mass	Price	Energy	N_r	N_c	d_p	Mass	Price	Energy	N_r	N_c	d_p	Mass	Price	Energy	N_r	N_c	d_p
Chain (1)	154	270.45	181.96	8.39	4	7	4	372.82	112.96	12.54	4	1	4	270.45	181.96	8.39	same as lightest		
Chain (2)	157	277.18	185.88	9.65	4	7	4	387.51	114.96	14.48	4	1	4	277.18	185.88	9.65	same as lightest		
Chain (3)	139	779.06	216.25	30.24	4	10	6	923.61	158.09	35.44	4	3	7	811.21	210.02	29.91	4	6	7
"Chain" total		1326.686							386.01							47.95			
C1	29	245.87	94.79	8.26	4	2	3	250.26	77.61	8.45	4	1	3	266.55	126.57	5.71	4	2	5
C2	46	272.54	138.66	8.62	4	3	4	332.63	109.28	11.80	4	1	4	276.75	128.68	7.29	4	2	5
M	116	1217.23	175.76	57.23	4	3	7	1217.23	175.76	57.23	same as lightest			1273.80	222.29	52.11	4	3	9
"Mother & Children" total		1735.642							362.65							65.11			
R1	114	1314.54	245.54	54.03	4	3	11	1314.54	245.54	54.03	same as lightest			1314.54	245.54	54.03	same as lightest		
R2	83	625.86	254.55	16.12	4	6	9	727.64	164.19	18.51	4	4	9	625.86	254.55	16.12	same as lightest		
R3	83	460.30	151.82	11.99	4	5	5	490.88	130.04	13.05	4	4	5	460.30	151.82	11.99	same as lightest		
"Russian Doll" total		2400.705							539.78							82.14			
Single	135	1486.17	468.43	76.18	4	9	11	2133.15	247.57	90.29	4	4	9	2038.54	468.43	55.81	same as lightest		

143

- The 'Russian Doll' configuration has the worst performance for all three factors. From the previous analysis, this configuration wastes a large portion of its power on the first aircraft. Its main mission is to hover and repeat the signal; however, it is also required to carry the other multicopters. Hence, it must be large and heavy to have a powerful propulsion system. However, for this mission, this ability is required for only the first third of the journey. For the remaining time, the large propulsion system does not offer any benefit but increases the hovering power consumption. For the last aircraft, which carries the camera, it is supposed to save energy by being carried by the previous multicopters, but for this mission, it eventually needs to hover for $400\ s$ and thus cannot be too light. Overall, this configuration is not a strong choice for any of the three main targets.

- The 'Chain' configuration demonstrates good potential for the mass and energy aspects but is beaten by the 'Mother and Children' configuration in terms of price. It is noticed that the two children multicopters are, as expected, indeed lighter and consume less energy than the first two 'Chain' multicopters. However, to transport them, the mother aircraft wastes some power during the final part of the mission without the children. It has the same problem as the 'Russian Doll' method: One part of the mission requires the multicopter to have higher extreme performance, but it is not required during the other parts. However, if considering this from the other aspect, higher extreme performance suggests that the mother aircraft should have better manoeuvrability and can better deal with emergencies, while the 'Chain' multicopters are suitable for only the mission and would not perform well under sudden conditions. Overall, if the multiple-aircraft configuration is necessary (when the single com is not available in the mission), both the 'Chain' and 'Mother and Children' configurations can be good options based on the specific requirements.

Table 5.7   The comparison of the middle parameters of Chain (1) and Chain (2).

Mass Properties (g)	Motor Mass	ESC Mass	Propeller Mass	Arm Mass	Battery Mass	Body Mass
Chain (1)	14.18	2.19	3.63	1.69	55.02	8.68
Chain (2)	13.83	2.18	3.63	1.67	63.27	8.68
Price Properties ($)	Motor Price	ESC price	Propeller Price	Arm Price	Battery Price	Body Price
Chain (1)	33.19	8.98	0.58	0.95	5.91	1.26
Chain (2)	33.96	8.98	0.58	0.94	6.80	1.26
Middle Parameters	Max Motor Power (W)	Max Motor Thrust (N)	Motor Hovering Power (W)	Max Rotation Speed (rev/s)	Minimum KV	Max Current Through ESC (A)
Chain (1)	29.53	1.15	8.44	1602.85	791.34	2.06
Chain (2)	29.39	1.16	8.76	1590.21	785.09	2.05

- It is worth mentioning that Chain (1) and Chain (2) are quite similar in terms of mass and energy consumption. As the details are checked, the results are correct (see Table 5.7).
- The two multicopters have the same design parameters ($N_r = 4, N_c = 7, d_p = 4$), and for the mission specifications (see Table 5.3), the only difference is the forward flight time

(i.e. the endurance); this situation is discussed in Section 4.5.3. The suggested result is an increase in battery mass and slight reduction a in the maximum power and motor mass. Finally, $GTOM$ slightly increases and is exactly the same in Table 5.7.

5.4   Optimisation Session 2

5.4.1 Optimisation Settings

In Session 2, the 'Chain' and 'Mother and Children' configurations are compared as the total range of the mission changes. If the total range is divided into X segments, the range is defined as $S = X \cdot 500$, and the mission specifications of the two configurations can be expressed in Table 5.8. The mission of the mother multicopter is more complex, since the payload is changing from phase to phase.

Table 5.8   The flight time of the multicopters.

	Forward Flight Time	Hovering Time	Launching	Recovering	Take Off	Landing
Chain (1)	100	400			30	30
Chain (2)	200	400			30	30
Chain (X-1)	$(X-1)*100$	400			30	30
Chain Ender (X)	$X*100$	400			30	30
C1		500	5	5		
C2		610	5	5		
C(X)		$390 + 110*X$	5	5		

Table 5.9   The mission specifications of the mother multicopter.

Phase	1	2	3	4	5	...	$2*X$	$2*X+1$	...	$4*X+1$
Mission Segment		1		2			X			
Behaviour	TO	F	H launches C_{x-1}	F	H launches C_{x-2}		F	H	Symmetric	LD
Flight Time/s	30	50	5	50	5		50	400		30
Horizontal Displacement/m	0	500	0	500	0		500	0		0
Vertical Displacement/m	300	0	0	0	0		0	0		-300
Payload/kg	$m_{pl,tot}$	$m_{pl,tot}$	$m_{pl,tot} - m_{c,(x-1)}$	$m_{pl,tot} - m_{c,(x-1)}$	$m_{pl,tot} - m_{c,(x-1)} - m_{c,(x-2)}$		m_{cam}	m_{cam}		$m_{pl,tot}$

The coding of the multicopter sequence is as follows: Chain (1) refers to the last take-off multicopter in the 'Chain' configuration. No matter how many other multicopters are ahead, its only mission is to fly to point 'A', hover for the mission time, and return. Chain (2) is the second-to-last to take off, and its mission extends to point 'B'. This continues one multicopter after another. Chain $(X-1)$ is the second take-off multicopter, and the chain ender (X) is the first to take off. The only difference between an ender and the other nodes is that its payload includes the camera mass. The 'Mother and Children' configuration name the multicopters in the reversed manner.

145

The last multicopter to be launched from the mother is called C1, while the first one launched is called C_{x-1}. The mother itself is the X_{th} multicopter. For the children, once the range and sequence are decided, their flight time can be calculated (see Table 5.8). However, the mother cannot be calculated until all the children are determined. This is because the payload of the mother is changing once it launches or recovers a child. The load is significant in the calculation of the energy consumption in each phase.

5.4.2 Optimisation Results

The optimisation results are presented in Figure 5.5, Figure 5.6 and Figure 5.7. The $GTOM$, price and energy consumption all refer to the total number of all the multicopters in a configuration. For each given range, the mission specifications have a certain group of values. Each multicopter in the configurations is involved in a full optimisation loop and produces tens of valid designs. Among all the valid designs, the outstanding two or three are recorded. All the multicopters from a configuration cooperate with one another to complete the full mission, so they are treated as one.

Based on Figure 5.5, the following points can be concluded:

- In each configuration, the $GTOM$ of different multicopter shapes demonstrates the following sequence: Octocopter > Hexacopter > Quadcopter.
- In terms of the $GTOM$, the 'Chain' configuration is superior. As the range is longer, the difference is larger. When the range reaches $3\ km$ (requires six multicopters), the $GTOM$ of the quadcopter 'Mother and Children' is worse than the octocopter 'Chain'.

Figure 5.6 and Figure 5.7 reveal similar conclusions. In terms of price, the 'Chain' configuration is better for most of the ranges, but in short ranges (less than $1500\ m$), the 'Mother and Children' configuration does offer a competitive price.
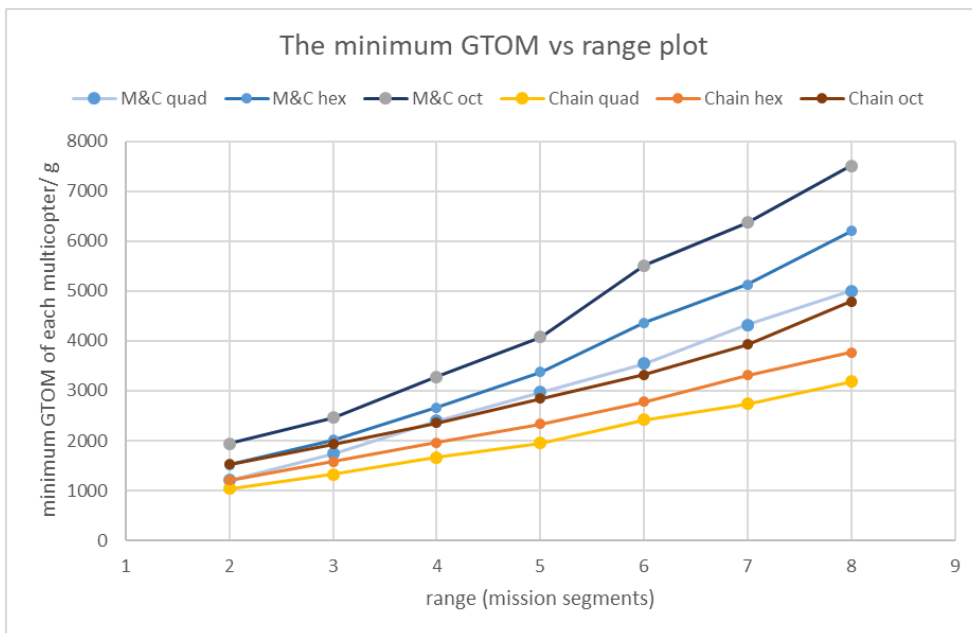
Figure 5.5 The minimum $GTOM$ of multicopters vs range.
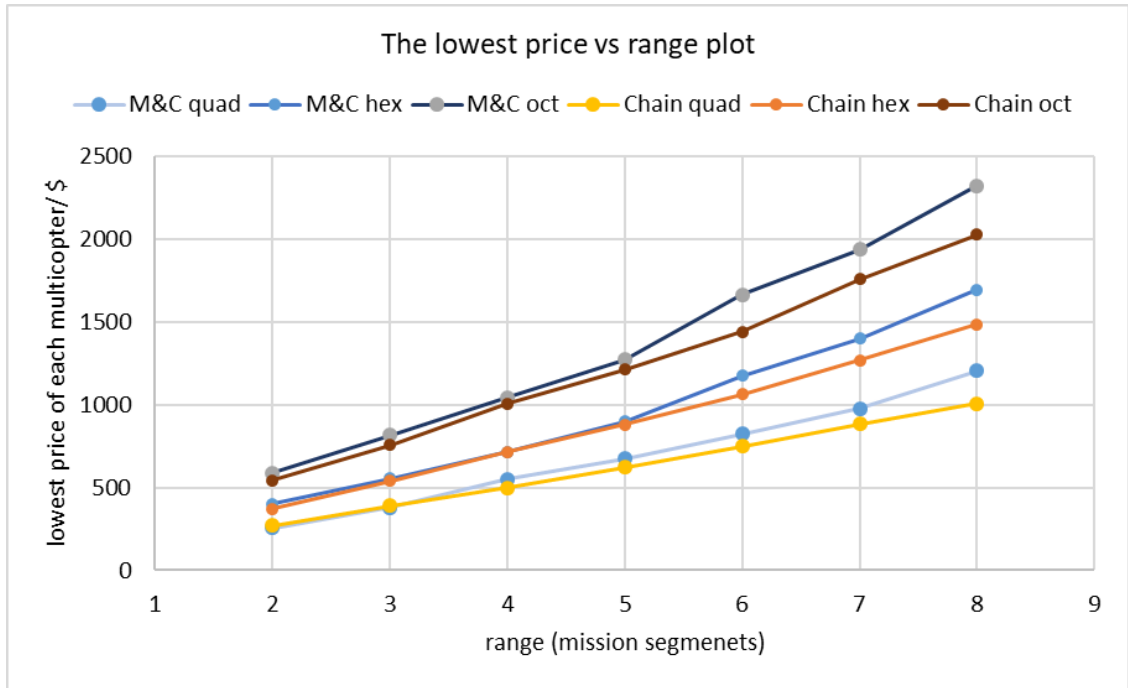
Figure 5.6 The lowest price of multicopters vs range.
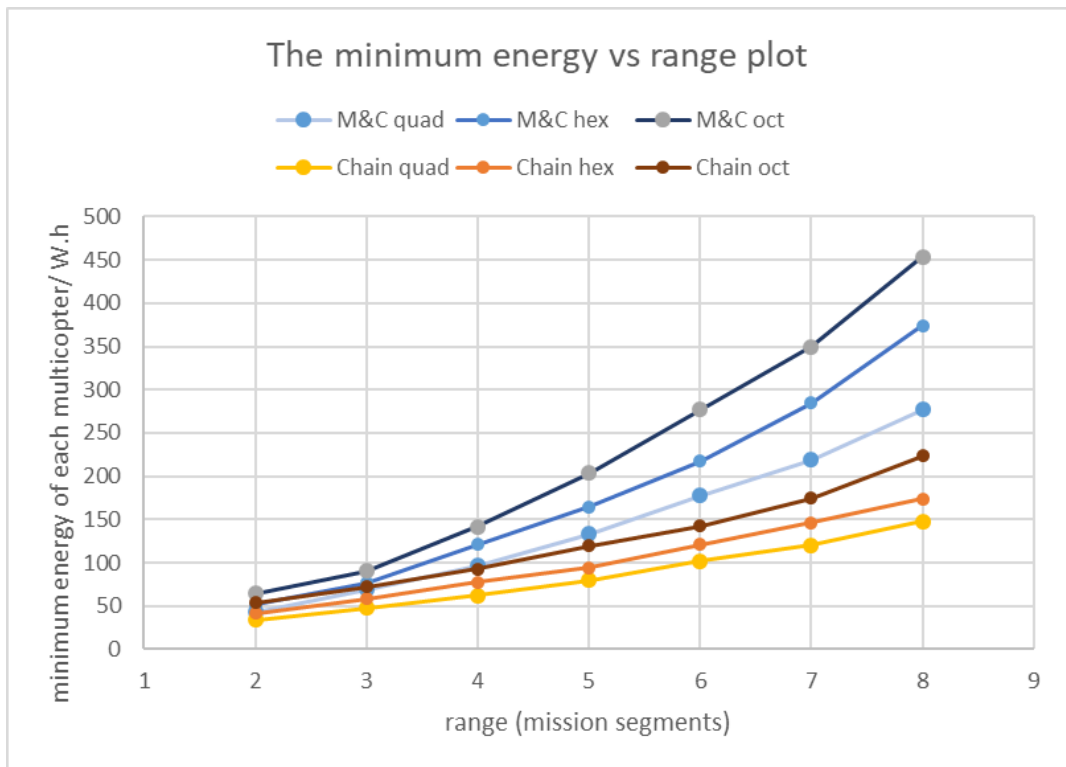
Figure 5.7 The minimum energy consumption of multicopters vs range.

147

Table 5.10 The detailed optimisation results of "Chain" quadcopters

design parameters range		chain 1	chain 2	chain 3	chain 4	chain 5	chain 6	chain 7
$N_{c,min}$		1	1	1	1	1	1	3
$N_{c,max}$		6	6	6	7	7	7	8
$d_{p,min}$		2	2	2	2	2	2	2
$d_{p,max}$		6	6	6	7	7	7	8
minimum $GTOM$	N_c	7	7	7	7	6	6	6
	d_p	4	4	4	4	4	4	4
	value	270.45	277.18	283.98	290.89	327.93	343.15	360.21
lowest price	N_c	1	1	1	1	1	1	1
	d_p	4	4	4	4	4	5	5
	value	112.96	114.96	112.40	119.69	122.54	120.15	118.17
minimum energy	N_c	7	7	7	7	6	6	6
	d_p	4	4	4	4	4	4	4
	value	8.39	9.65	10.92	12.22	15.01	16.95	19.13

design parameters range		Chain Enders	2	3	4	5	6	7	8
$N_{c,min}$			1	1	1	1	2	2	2
$N_{c,max}$			13	13	13	11	13	13	12
$d_{p,min}$			4	4	5	5	4	4	4
$d_{p,max}$			8	8	9	9	10	10	10
minimum $GTOM$	N_c		10	10	7	10	17	8	19
	d_p		7	6	7	6	7	7	7
	value		771.66	779.06	830.51	833.71	968.69	943.84	1031.77
lowest price	N_c		4	4	3	3	3	4	2
	d_p		6	6	7	7	7	7	8
	value		157.02	163.55	159.73	163.64	168.19	180.88	186.45
minimum energy	N_c		10	6	7	10	17	8	19
	d_p		7	7	7	6	7	7	7
	value		25.70	29.91	33.46	38.32	45.65	47.37	55.57

total aircraft numbers	2	3	4	5	6	7	8
total mass	1042.11	1326.69	1662.11	1956.20	2419.11	2737.41	3185.55
total price	269.98	391.47	500.05	623.65	750.74	883.57	1007.31
total energy	34.09	47.95	62.43	79.51	101.86	120.53	147.86

Table 5.11 The detailed optimisation results of "Mother and Children" quadcopters

design parameters range		C1	C2	C3	C4	C5	C6	C7
	$N_{c,min}$	1	1	1	1	1	1	2
	$N_{c,max}$	4	4	5	13	13	13	9
	$d_{p,min}$	2	2	2	3	3	3	4
	$d_{p,max}$	5	7	7	14	14	14	9
minimum $GTOM$	N_c	2	3	3	3	2	4	4
	d_p	3	4	5	5	7	5	5
	value	245.87	272.54	336.63	354.97	272.72	262.42	312.90
lowest price	N_c	2	1	1	1	2	1	2
	d_p	3	4	4	4	4	4	6
	value	94.79	109.28	112.11	115.01	114.97	108.20	128.33
minimum energy	N_c	2	2	5	9	2	2	2
	d_p	4	5	6	8	7	7	7
	value	7.02	7.29	11.23	12.22	8.10	9.92	12.27

design parameters range	mother	one child	two children	three children	four children	five children	six children	seven children
$N_{c,min}$		2	2	3	3	4	4	4
$N_{c,max}$		8	8	9	9	10	10	10
$d_{p,min}$		4	4	5	5	6	6	6
$d_{p,max}$		8	8	9	9	10	10	10

		mother	one child	two children	three children	four children	five children	six children	seven children
minimum $GTOM$	N_c		13	3	3	3	3	3	3
	d_p		7	7	10	10	10	10	13
	value		966.22	1217.23	1543.86	1760.79	2062.44	2578.99	2946.98
lowest price	N_c		3	3	3	3	3	3	3
	d_p		7	7	10	10	10	10	13
	value		161.82	176.42	236.33	242.04	279.89	324.98	422.52
minimum energy	N_c		13	3	3	3	3	3	3
	d_p		7	10	10	10	13	13	13
	value		35.96	55.11	71.49	95.51	131.72	163.01	208.98

total aircraft numbers	2	3	4	5	6	7	8
total mass	1212.09	1735.64	2398.90	2970.80	3545.18	4324.15	5005.04
total price	256.61	380.49	552.51	673.23	826.04	979.33	1205.20
total energy	42.98	69.41	97.03	133.27	177.58	218.79	277.03

5.5 Conclusion

This chapter discusses two practical problems in depth. Both can be solved using the proposed multicopter conceptual design algorithm. Based on the results of the second scenario, four solutions to the problem are evaluated, two of which are used in a further parameters study. The results and conclusions are useful in guiding multicopter design for similar problems.

Chapter 6 Summary and Conclusions

6.1 Summary of Research

This research is motivated by the situation that there do not exist many efficient conceptual design tools for multicopters. Although mature design procedures exist for fixed-wing aircraft and large-scale rotorcraft, they cannot be adopted directly to the design of multicopters. In the literature, people have attempted to propose new approaches for multicopter design and draw particular conclusions for the components of multicopters; however, most of the attempts are limited to a particular area or target.

Hence, a conceptual design algorithm is developed. Functionally, the algorithm can determine the optimal design parameters for a particular objective based on the given mission scenario and requirements. Compared with previous works, the proposed algorithm has more accurate estimation of each component by introducing the random forest technique; it is valid for a larger range of multicopters; it considers the entire aircraft rather than focussing on only a single separated system; and it can optimise not only the $MTOM$ but also the price, endurance, total energy consumed and maximum speed. Although the optimisation process is still single objective, the result is a pool of valid design configurations. It is possible to pursue further multi-objective optimisation analysis, and it considers all the flight conditions when determining the maximum required power.

To determine the performances of the multicopter under different flight conditions, the structural drag is considered, which is an improvement over previous study. The calculation results of some example cases reveal that when the multicopter transits from hover to forward flight, the required power is first reduced and then increased. This is because, as the forward speed increases, the induced power is becoming smaller, while the parasite power grows larger. After a certain speed, the impact of the drag is so large that the parasite power becomes the dominant item. This conclusion agrees with the theory of helicopter principles.

In the regression of some components, such as the motor mass, propeller price and ESC price, a problem arises. The problem is that, for some components, the mass or price is related to multiple parameters. For example, the motor mass is related to its maximum power, maximum torque and maximum operational voltage; the ESC mass is related to its maximum working current, whether it has a head sink, whether it is in a 4in1 configuration; and the propeller price is related to its size, material, and brand, among others. Traditional regression functions are weak for these situations. Hence, the random forest technique is introduced, which is good at huddling a high-dimension (multiple variables) data set, even if there are interactions between the features (variables). Compared with previous studies, the estimation of the motor mass using the random forest model is much more accurate through a large range of models (20 g–400 g).

All the calculations in the algorithm are justified in the literature. The values of certain coefficients are justified by analysing the database, and the regression of each component is validated by a comparison of group data. The entire algorithm is validated in two ways: First, five commercial multicopters are selected, and the performance and components are calculated using design parameters identical to the candidates. Second, one multicopter is selected, and the full optimisation process is operated based on its mission requirements. Finally, the initial design is compared with the 106 valid designs produced by the algorithm. On each optimisation target, there exists a best design that has superior performance to the initial design.

The sensitivity study is performed for some coefficients. Among the three examined parameters, it is found that parameters impact different areas in different ways. The FM of rotors primarily influences the battery mass, while it has little impact on the mass of the motors and the ESCs. Meanwhile, the minimum motor efficiency primarily impacts the mass and price of the ESCs but has little impact on the $MTOM$. With the sensitivity analysis of more parameters, the parameters that have high impact can be spotted, and the source of uncertainties in the algorithm becomes clearer.

In the end, the validated algorithm is used as a tool to analyse the solutions for a particular mission. In this mission, multiple aircraft are required to complete a long-range mission. When one main aircraft arrives at the mission region and does work, the other aircraft should act as signal repeaters at each waypoint. There are a variety of ways, called configurations, to transport the multicopters. Four configurations are proposed, and optimal designs are determined with the proposed algorithm and are compared based on all the performance aspects. The results reveal that, assuming three multicopters, the chain configuration without docking is the lightest and most energy-saving solution, while the mother-children configuration is the cheapest solution. The other two configurations perform poorly on these objectives. More general conclusions can be drawn:

- Theoretically, any type of 'carrier' configuration is more energy consuming than single aircraft flying one by one. This is because the 'carrier' configuration transports additional mass and hence consumes extra energy.
- Although the 'carrier' configuration consumes more energy, it is possible to have lighter or cheaper solutions than the single-aircraft configuration by having the proper design. To complete the mission, all the configurations would develop a pool of valid designs. The previous conclusions compare only the optimised ones.
- Generally speaking, for a given mission, the quad configuration is typically lighter than the octo configuration. In most cases, it is a synthetical decision that considers several requirements rather than only a single objective to optimise.

To conclude, the developed conceptual design algorithm is trustworthy and can be used for practical problem solving. It offers great potential both academically and commercially.

- A complete conceptual design process is proposed which combines the advantages from the literature and improves on some drawbacks. It considers up to five parameters as possible optimisation objectives. Although the optimisation process is still single objective, the result is a valid design configuration pool. It is possible for pursuing further multi-objective optimisation analysis, and it considers all flight conditions when determining the maximum required power.

- An abundant database of multicopter platforms and multicopter components is developed using a spider tool. The regression results from previous studies are validated by the database. A problem regarding the regression of motor mass was noticed, which no previous studies mentioned. This problem was solved by introducing the random forest technique for regression, which improved the accuracy of estimation and expanded the applicable range of the component models.

- The proposed algorithm is validated, and sensitivity study is performed.

- The proposed algorithm is used to analyse a novel signal-repeating scenario by evaluating four possible configurations. Three of the solutions take advantage of multiple-aircraft cooperating work, and two of them involve the aerial docking between multicopters.

- Instead of using FEA simulation, basic material mechanics theory is introduced for evaluating the strength of the arms and the optimisation of the arm geometries. The FEA method is time consuming and is more suitable for the preliminary design or detailed design phase. Meanwhile, the proposed theory is faster and suitable for the conceptual design phase. Material mechanics theory is not new, but it is novel to apply this theory to multicopter conceptual design.

6.2 Contribution to Knowledge

The contribution to knowledge is reflected in two ways:

1. The novel methods used as tools to compound the entire conceptual design process. These include the random forest technique for regression, material mechanics principles for structural strength analysis, consideration of general flight conditions and the optimisation objectives.

2. The application of the proposed algorithm for a very complicated mission.

6.3 Limitations and Future Works

Due to the limited time, all the main works are finished under rush conditions. Some detailed works must be completed in the long term to improve the quality of this algorithm:

- Collect information on the propeller average chord and propeller solidity. Improve the model of propellers
- Include calculation of coaxial rotor system
- Include consideration to the air density change caused by height

- Include calculation of a tandem rotor system and changeable adjacent rotor distance

- Deeper study on the central frame sizing and strength check

- Full optimisation for the study of parameters' sensitivity feature

- The sensitivity study to the regression—how does the regression function change influence the multicopter design results? The current regression reflects only the average standard, while in the future, the distribution of the regression could be accomplished. Then, by introducing the Monte-Carlo process and a large quantity of repetition, the quality of a design and its possibility could be estimated

- Introduce multiple-objective optimisation to the process, and make it possible to evaluate a design from a comprehensive perspective using a mathematical method

- For the study of the signal repeating scenario, in the process of modelling the problems, many assumptions are made to simplify unnecessary factors. In addition, the algorithm is based on several assumptions, and the results can reflect only an aspect of the design principles, especially for the second scenario. Except for what has been done, some questions still must be explored, such as how the mission set-up would influence the performance of multicopter cooperation configurations. Furthermore, if the time for hovering were shorter in the mission, it can be asked whether the result would be different. Another example is to combine the two scenarios; that is, if the multicopters can move forward and upward simultaneously, what design is the most efficient?

Another scenario should be studied in the initial plan: to survey and search for a target on the ocean within a certain range. When the cooperative multiple-aircraft configuration is introduced, which way is quicker at locating the target? The use of multiple aircraft might not be suitable for missions that pursue the minimum $GTOM$ or energy consumption, but it is a strong candidate for reducing the searching time.

References

Admin (2016) *How to Choose Motor and Propeller for Quadcopter*, *Top-10-Drones.com*. Available at: https://top-10-drones.com/blog/choose-motor-propeller-quadcopter/ (Accessed: 9 March 2019).

Aleksandrov, D. and Penkov, I. (2012) 'Optimal gap distance between rotors of mini quadrotor helicopter', in *Danube Adria Association for Automation & Manufacturing, 8th International DAAAM Baltic Conference 'Mechatronics and System Engineering'*, pp. 19–21. Available at: http://innomet.ttu.ee/daaam/proceedings/pdf/Aleksandrov.pdf.

Alphonso, R. *et al.* (2015) 'Design and Development of Quadcopter Prototype'. Available at: http://repository.untar.ac.id/83/2/2816-6076-1-PB.pdf (Accessed: 10 January 2019).

Amadori, K. *et al.* (2010) 'Validation of Models for Small Scale Electric Propulsion Systems', in *48th AIAA Aerospace Sciences Meeting Including the New Horizons Forum and Aerospace Exposition*. doi: 10.2514/6.2010-483.

Ampatis, C. and Papadopoulos, E. (2014) 'Parametric Design and Optimization of Multi-Rotor Aerial Vehicles', *Springer Optimization and Its Applications*, 30(3), pp. 1–25. doi: 10.1007/978-3-319-04720-1_1.

Bachmann, A. *et al.* (2009) 'Automation of Aircraft Pre-Design Using A Versatile Data Transfer and Storage Format in A Distributed Computing Environment', in *3rd International Conference on Advanced Engineering Computing and Applications in Sciences, ADVCOMP 2009*. doi: 10.1109/ADVCOMP.2009.22.

Ballin, M. G. (1987) 'Validation of a Real-Time Engineering Simulation of the UH-60A Helicopter', in *NASA Technical Memorandum 88360*.

Beltramo, M. N. (1980) 'Parametric Study of Helicopter Aircraft Systems Costs and Weights'.

Benoit, B. *et al.* (2000) 'HOST, a General Helicopter Simulation Tool for Germany and France', *American Helicopter Society 56th Annual Forum*.

Brandt, J. B. *et al.* (2015) *UIUC Propeller Database*, *University of Illinois at Urbana-Champaign*.

Brazinskas, M., Prior, S. and Scanlan, J. (2016) 'An Empirical Study of Overlapping Rotor Interference for a Small Unmanned Aircraft Propulsion System', *Aerospace*, 3(4), p. 32. doi: 10.3390/aerospace3040032.

Chen, X. (2017) *Enablers for Uncertainty Quantification and Management in Early Stage Computational Design an Aircraft Perspective*. Cranfield University.

Chesebro, J. (2011) *Aerospace Report of Flight Plan 2011: Unmanned Aircraft Systems (UAS)*.

International Trade Administration. Available at:
http://www.trade.gov/static/aero_rpt_flight_plan_2011_uas.pdf.

Christian, A. and Lawrence, J. (2016) 'Initial Development of a Quadcopter Simulation Environment for Auralization'. Available at: https://ntrs.nasa.gov/search.jsp?R=20160009104 (Accessed: 28 March 2019).

Devaprakash, D. and Raj, P. (2014) 'Design Of A Quadcopter Using PID Control Algorithm', *Recent Trends in Electronics & Communication Systems*, 1(1), pp. 13–20. Available at: http://stmjournals.com/tech/index.php?journal=RTECS&page=article&op=view&path%5B%5D= 122 (Accessed: 27 June 2019).

Dingeldein, R. C. (1954) *Wind-Tunnel Studies of the Performance of Multirotor Configurations*, *National Advisory Committee for Aeronautics, NACA-TN-3236*. Available at: https://ntrs.nasa.gov/search.jsp?R=19930083899.

Doyle, S. and Donaldson, P. (2008) *Handbook, Unmanned Vehicle*, *Handbook*. Edited by P. Donaldson. Burnham, UK: The Shephard Press Ltd. Available at: https://uvsr.org/docs/UV_Handbook-2008.pdf.

Gadda, J. S. (2015) 'Quadcopter (UAVS) for Border Security With GUI System', *International Journal of Research in Engineering and Technology*. doi: 10.15623/ijret.2013.0212106.

Gatti, M. (2017) 'Complete Preliminary Design Methodology for Electric Multirotor', *Journal of Aerospace Engineering*, 30(5), p. 04017046. doi: 10.1061/(ASCE)AS.1943-5525.0000752.

Gong, A. and Verstraete, D. (2017) 'Experimental Testing of Electronic Speed Controllers for UAVs', *53rd AIAA/SAE/ASEE Joint Propulsion Conference*. Reston, Virginia: American Institute of Aeronautics and Astronautics, (July). doi: 10.2514/6.2017-4955.

Green, C. R. and McDonald, R. A. (2015) 'Modeling and Test of the Efficiency of Electronic Speed Controllers for Brushless DC Motors', in. doi: 10.2514/6.2015-3191.

Hanafi, D. *et al.* (2013) 'Simple GUI Wireless Controller of Quadcopter', *International Journal of Communications, Network and System Sciences*. doi: 10.4236/ijcns.2013.61006.

Harrington, A. M. (2011) *Optimal Propulsion System Design for a Micro Quad Rotor*.

Harrington, A. M. and Kroninger, C. (2013) *Characterization of Small DC Brushed and Brushless Motors*, *ARL-TR-6389*.

Hassanalian, M. and Abdelkefi, A. (2017) 'Classifications, Applications, and Design Challenges of Drones: A Review', *Progress in Aerospace Sciences*, 91(May), pp. 99–131. doi: 10.1016/j.paerosci.2017.04.003.

Hassanzadeh, H. R. and Rouhani, M. (2010) 'A Multi-Objective Gravitational Search Algorithm',

in *Proceedings - 2nd International Conference on Computational Intelligence, Communication Systems and Networks, CICSyN 2010*. doi: 10.1109/CICSyN.2010.32.

Ho, T. K. (1995) 'Random Decision Forests', in *Proceedings of the International Conference on Document Analysis and Recognition, ICDAR*. doi: 10.1109/ICDAR.1995.598994.

Hystad, A. V. and Lehn, J. B. (2015) *Model, Design and Control of a Quadcopter*. Norwegian University of Science and Technology. Available at: https://brage.bibsys.no/xmlui/handle/11250/2352467.

Jha, A. R. (2016) *Next-Generation Batteries and Fuel Cells for Commercial, Military, And Space Applications*, *Next-Generation Batteries and Fuel Cells for Commercial, Military, and Space Applications*.

Jiang, L. (2018) 'The Development History of Multicopters', *yuchen360.com*.

Jiang, X. (2005) *The Handbook Of Aircraft Design, Volumn 19 Helicopter Design*. Aviation Industry Press.

Johnson, W. (1980) *Helicopter Theory*, *Aircraft Engineering and Aerospace Technology*. Dover publications. doi: 10.1108/eb030686.

Johnson, W. (1994) 'Helicopter Theory - TOC', in *Helicopter Theory*. Available at: file:///home/jzt473/Documents/PhD_work/PhD/Literature/Library/Johnson/Helicopter Theory/Johnson - 1980 - Helicopter Theory - TOC.pdf.

Johnson, W. (2010) *NDARC --- NASA Design and Analysis of Rotorcraft --- Validation and Demonstration*.

Layton, D. M. (1992) 'Introduction to Helicopter Design', *AIAA Professional Studies Series*.

Leishman, J. G. (2006) *Principles of Helicopter Aerodynamics*. 2nd edn. Cambridge University Press.

Liersch, C. M. and Hepperle, M. (2011) 'A Distributed Toolbox for Multidisciplinary Preliminary Aircraft Design', *CEAS Aeronautical Journal*. doi: 10.1007/s13272-011-0024-6.

Linden, D. and Reddy, T. B. (2002) *Handbook of Batteries, third edition*, *McGraw-Hill*. doi: 10.1016/0378-7753(86)80059-3.

Liu, F. *et al.* (2018) 'Design Optimization and Strength Analysis of a Heavyduty Quadrotor UAV', *ADVANCES in AERONAUTICAL SCIENCE and ENGINEERING*, 9(1).

Magnussen, Ø., Ottestad, M. and Hovland, G. (2015) 'Multicopter design optimization and validation', *Modeling, Identification and Control*, 36(2), pp. 67–79. doi: 10.4173/mic.2015.2.1.

Mascarello, L. N. (no date) 'Design and Development of a Multicopter For Medical Applications',

pp. 1–10.

Maskew, B. (1987) 'Program VSAERO Theory Document: A Computer Program for Calculating Nonlinear Aerodynamic Characteristics of Arbitrary Configurations', *Nasa Cr-4023*.

Mauro Gatti (2015) *Design and Prototyping High Endurance Multi-Rotor*, *Aerospace Sciences Sector*. University of Bologna. doi: dkn499 [pii]\r10.1093/jac/dkn499.

McCormick, B. W. (1979) 'Aerodynamics Aeronautics and Flight Mechanics John Wiley & Sons.', *Inc., New York*. doi: 10.2514/6.2005-1033.

Morris, S. J. (2002) 'Miniature Spy Planes: The Next Generation of Flying Robots', in *Frontiers of Engineering: Reports on Leading-Edge Engineering from the 2001 NAE Symposium on Frontiers of Engineering*. National Academies Press, p. 10.

Moyano Cano, J. (2013) *Quadrotor UAV for Wind Profile Characterization*. Available at: https://e-archivo.uc3m.es/handle/10016/18105 (Accessed: 28 March 2019).

Nicolai, L. M. and Carichner, G. E. (2010) *Fundamentals of Aircraft and Airship Design*, *Fundamentals of Aircraft and Airship Design*. doi: 10.2514/4.867538.

Nie, S. (2017) *The Development and Evaluation of the Design of Multicopters*. North China University Of Technology.

Palasis, D. (1992) 'Erstellung eines Vorentwurfsverfahrens für Hubschrauber mit einer Erweiterung für das Kipprotorflugzeug', *Fortschritt-Berichte VDI: Reihe 7*.

Powell, M. J. D. (2007) 'A View of Algorithms for Optimization', *Cambridge Na Reports Optimization Online Digest*, (5), pp. 170–174.

Prouty, R. W. (2002) *Helicopter, Performance, Stability and Control*.

Quan, Q. (2017) *Introduction to Multicopter Design and Control*, *Introduction to Multicopter Design and Control*. doi: 10.1007/978-981-10-3382-7.

Ramasamy, M. (2013) 'Measurements Comparing Hover Performance of Single, Coaxial, Tandem, and Tilt-Rotor Configurations', *Presented at the AHS 69th Annual Forum*.

Raymer, D. P. (2012) *Aircraft Design: A Conceptual Approach*. American Institute of Aeronautics and Astronautics. Available at: https://books.google.co.uk/books?id=9jBsLgEACAAJ.

Russell, C. R., Theodore, C. R. and Sekula, M. K. (2018) 'Incorporating Test Data for Small UAS at the Conceptual Design Level', *Proceedings of the AHS International Technical Meeting on Aeromechanics Design for Transformative Vertical Flight 2018*.

Seddon, J. and Newman, S. (2011) *Basic Helicopter Aerodynamics*, *Basic Helicopter Aerodynamics*. doi: 10.1002/9781119994114.

References

Song, W. and Luo, Z. (2019) 'The Design and Model Selection of a Heavy Lift Multicopter Platform', *Construction & Design For Project*. doi: 10.13616/j.cnki.gcjsysj.2019.09.256.

Stepniewski, W. Z. (1983) 'A Comparative Study of Soviet vs. Western Helicopters', *National Aeronautics and Space Administration, Scientific and Technical Information Branch*, Vol. 3579. Available at: https://scholar.google.co.uk/scholar?hl=en&as_sdt=0%2C5&q=A+Comparative+Study+of+Soviet+vs.+Western+Helicopters%3A+Part+2+-+Evaluation+of+Weight%2C+Maintainability%2C+and+Design+Aspects+of+Major+Components&btnG= (Accessed: 27 June 2019).

Sweet, G. E. and Langley (1960) *Hovering Measurements for Twin -Rotor Configurations with And Without Overlap*. doi: 10.1039/c3ja50039j.

Theodore, C. R. (2018) 'A Summary of the NASA Design Environment for Novel Vertical Lift Vehicles (DELIVER) Project', in *Proceedings of the AHS International Technical Meeting on Aeromechanics Design for Transformative Vertical Flight 2018*.

Theys, B. *et al.* (2016) 'Influence of Propeller Configuration on Propulsion System Efficiency of Multi-Rotor Unmanned Aerial Vehicles', *2016 International Conference on Unmanned Aircraft Systems, ICUAS 2016*, (2), pp. 195–201. doi: 10.1109/ICUAS.2016.7502520.

Thomas, M. *et al.* (2016) 'Design and Analysis of a Quadcopter Using Catia', *nternational Journal of Scientific & Engineering Research*, 7(3), pp. 140–156. Available at: http://www.ijser.org (Accessed: 10 January 2019).

Unknown (2002) *Composite Materials Handbook Volume 2. Polymer Matrix Composites Materials Properties*. USA DEPARTMENT OF DEFENSE.

Unknown (2014) 'RPAS ReferenceSection', in Blyenburgh, P. Van (ed.) *RPAS (Remotely Piloted Aircraft Systems) Yearbook 2014: The Global Perspective*. 12th edn. Paris, France: Blyenburgh & Co. Available at: http://uvs-info.com/index.php?option=com_flippingbook&view=book&id=19&page=1&Itemid=874.

Valavanis, K. P. and Vachtsevanos, G. J. (2015) *Handbook of Unmanned Aerial Vehicles*, *Handbook of Unmanned Aerial Vehicles*. Springer Publishing Company, Incorporated. doi: 10.1007/978-90-481-9707-1.

Verbeke, J. *et al.* (2014) 'The Design and Construction of a High Endurance Hexacopter Suited for Narrow Corridors', in *2014 International Conference on Unmanned Aircraft Systems, ICUAS 2014 - Conference Proceedings*, pp. 543–551. doi: 10.1109/ICUAS.2014.6842296.

Vu, N. A., Dang, D. K. and Dinh, T. Le (2019) 'Electric Propulsion System Sizing Methodology for an Agriculture Multicopter', *Aerospace Science and Technology*. Elsevier Masson SAS, 1, pp. 1–13. doi: 10.1016/j.ast.2019.04.044.

Wang, W. *et al.* (2014) 'Research on Standardized Design Method of Airframe for Multi-Rotor UAV', *Machinery Design & Manufacture*, 5.

Weiand, P. *et al.* (2020) 'A Multidisciplinary Process for Integrated Rotorcraft Design', *CEAS Aeronautical Journal*. Springer Vienna, 11(1), pp. 145–160. doi: 10.1007/s13272-019-00408-y.

Winslow, J., Hrishikeshavan, V. and Chopra, I. (2017a) 'Design Methodology for Small-Scale Unmanned Quadrotors', in *AIAA SciTech Forum*. Reston, Virginia: American Institute of Aeronautics and Astronautics, pp. 1–9. doi: 10.2514/1.c034483.

Winslow, J., Hrishikeshavan, V. and Chopra, I. (2017b) 'Design Methodology for Small Scale Unmanned Quadrotors', (January), pp. 1–15. doi: 10.2514/6.2017-0014.

Zhang, C. (2007) *The Overall Design of Helicopters*. National Defence Industry Press.

Zhang, Y., Xue, H. and Gong, X. (2005) 'Multiobjective Optimization Method for Aircraft Configuration Parameter Design', *Fire Control and Command Control*, (11), pp. 76–78.

Zhao, J., July, Y. Y. and Yangwei, Y. (2011) 'Brushless DC Motor Fundamentals Application Note', *MPS, The future of Analog IC Technology*, (July 2011), pp. 1–19.

Zhu, R., Zeng, D. and Kosorok, M. R. (2015) 'Reinforcement Learning Trees', *Journal of the American Statistical Association*. doi: 10.1080/01621459.2015.1036994.

Appendix A　The List of Constants

Constants	Default Value	Unit
Cell voltage	4.2	V
Air density	1.225	kg/m^3
Gravitational acceleration	9.81	m/s^2
Sound velocity	340.3	m/s
Propeller static thrust coefficient	0.11	
Propeller static induced power coefficient	1.15	
Propeller drag coefficient	0.01	
Propeller average chord/radius ratio	0.116	
J_0 at highest efficiency	0.58	
Max J over J_0 at highest efficiency	1.2	
Prop tip Mach number	0.7	
Motor highest efficiency	0.8	
Motor lowest efficiency	0.65	
ESC max efficiency	0.95	
ESC lowest efficiency	0.75	
Battery efficiency	0.95	
Battery DOD	0.9	
Propeller gap/diameter ratio	0.124	
Fuselage downwash fixing factor	1.07	
Body drag coefficient	0.9	
Top vs front drags area ratio	6.69	
Top area vs disc area ratio	0.915	
Motor unloaded KV vs full-loaded KV ratio	1.52	
Total motor mass vs $MTOM$ ratio	0.1756	
Maximum payload vs $MTOM$ ratio	0.31	
Arm frequency separation	0.25	
Arm max deflection coefficient	80	
Arm strength safety factor	2	
Number of central body layers	2	
Density of copper	8960	kg/m^3

The second part of the constants table: Materials

Material Library	Carbon Fibre-T300 15k/976	Glass Fibre--RTP PA66 30 GF BLK	ABS Plastic	Aluminium 2024 T3
Density (kg/m^3)	1630	1360	1040	2780
Young's Modulus (Pa)	1.35E+11	9.31E+09	2.14E+09	7.31E+10
Shear Modulus (Pa)	6.27E+09	8.96E+09	6.27E+09	6.27E+09
Tension Strength (Pa)	1.45E+09	1.48E+08	42058000	2.75E+08
Compression Strength (Pa)	1.3E+09	1.45E+08	52745000	2.75E+08
Shear Strength (Pa)	76531806	2.41E+08	76531806	76531806
thickness factor	0.0033	N/A	N/A	N/A
Price Table ($\$/m^3$)				
shape/material	carbon fibre-T300 15k/976	glass fibre--RTP PA66 30 GF BLK	ABS plastic	aluminium 2024 T3
plate	145	N/A	N/A	N/A
box	N/A	N/A	N/A	N/A
tube	113.48	N/A	N/A	N/A
T section	N/A	N/A	N/A	N/A
channel	N/A	N/A	N/A	N/A
L section	562.33	N/A	N/A	N/A
I section	N/A	N/A	N/A	N/A
H section	N/A	N/A	N/A	N/A

Appendix B   Raymer's Power Calculation

For vertical climb, descent and hover the required power is given by Equation (106). For forward flight with or without climbing, it is given by Equation (107) (Raymer, 2012). In the equation the parameters are all in SI units.

$$P_v = \frac{(f \cdot MTOM)^{\frac{3}{2}}}{\sqrt{2\rho A}} + \frac{v_{climb} \cdot MTOM}{2} \qquad (106)$$

- f Downwash of the Fuselage
- A The Total Rotor Disc Area.
- ρ The Density of the Air
- v_{climb} The Climb Speed
  (A positive value refers to climb, a negative value refers to descent, while zero refers to hover.)

$$P_f = v_f \cdot \left[q \cdot \left(\frac{D}{q}\right) + \frac{MTOM^2}{4eqS} + MTOM \cdot \sin(\gamma) \right] \qquad (107)$$

- γ Climb Path Angle
- q   Dynamic Pressure $q = \frac{1}{2}\rho v_f^2$
- v_f Forward Flight Speed
- $\left(\frac{D}{q}\right)$ Drag Area*Drag coefficient
- e Oswald's Efficiency Factor $e \cong 0.5\ to\ 0.8$

This page is left intentionally blank.

Appendix C   The Comparison Between Raymer's and Leishman's Power Calculation

MTOM	23.8	kg	FM	0.6
MTOW	233.24	N	rho-air	1.29
Max Thrust Weight Ratio	1.71		g	9.8
Max Forward Speed	15	m/s	f	1.03
Propeller size	21	inch	Cd	0.9
Propeller radius	0.2667	m		
A	1.78	m2		
Number of Rotors	8			

D max	323.53	N			
q max	145.12	Pa	v_h	7.11	m/s
equivalent A	2.47	m2	hovering power	1658.6	W
n	4		max thrust	398.84	N
A1 top view	2.58	m2	alpha	0.9462	rad
A2 side view	0.64	m2	alpha	54.211	degree

v_f	q	alpha (rad)	D (N)	T (N)	v_i (m/s)	P Leishman (W)	P Raymer (W)	error 1
15	145.13	0.946	323.53	398.84	4.58	6677.88	6062.77	-9.2%
14	126.42	0.860	271.17	357.68	4.41	5374.31	5092.60	-5.2%
13	109.01	0.757	220.48	320.96	4.28	4241.38	4262.16	0.5%
12	92.88	0.635	171.81	289.69	4.22	3283.44	3573.86	8.8%
11	78.05	0.497	126.65	265.41	4.25	2520.35	3042.83	20.7%
10	64.50	0.362	88.29	249.39	4.41	1981.79	2697.52	36.1%
9	52.25	0.250	59.58	240.73	4.69	1665.13	2552.45	53.3%
8	41.28	0.169	39.89	236.63	5.05	1514.55	2587.43	70.8%
7	31.61	0.114	26.63	234.76	5.45	1465.14	2778.72	89.7%
6	23.22	0.075	17.53	233.90	5.84	1471.50	3129.57	112.7%
5	16.13	0.048	11.17	233.51	6.21	1505.52	3685.12	144.8%
4	10.32	0.029	6.69	233.34	6.53	1549.65	4563.34	194.5%
3	5.81	0.015	3.59	233.27	6.78	1592.76	6059.51	280.4%
2	2.58	0.007	1.54	233.25	6.97	1627.86	9076.21	457.6%
1	0.65	0.002	0.38	233.24	7.08	1650.68	18146.64	999.3%

This page is left intentionally blank.

Appendix D   The   Validation   of   Propeller Mass Estimation Using Prediction Interval

Actual products percentage			100.00%	91.67%	87.50%	87.50%	85.42%	54.17%	4.17%
Brand	**Diameter/in**	**Mass/g**	99% PI	95% PI	90% PI	80% PI	67% PI	35% PI	10% PI
KingKong	4	1.5	1	1	1	1	1	0	0
HobbyKing	4	3	1	1	1	1	1	1	0
Dalprops	4	3.1	1	1	1	1	1	1	0
Diatone	5	3	1	1	1	1	1	1	0
Diatone	5	4	1	1	1	1	1	1	0
Lumenier	5	2.9	1	1	1	1	1	1	0
Diatone	5	3.8	1	1	1	1	1	1	0
Gemfan	5	5.3	1	1	1	1	1	1	0
HobbyKing	5	1.45	1	1	1	1	1	0	0
Gemfan	5	5.8	1	1	1	1	1	1	0
Gemfan	5	2.7	1	1	1	1	1	1	0
HobbyKing	6	2.2	1	1	1	1	1	0	0
HobbyKing	6	4.7	1	1	1	1	1	1	0
HobbyKing	6	4.4	1	1	1	1	1	1	0
HobbyKing	6	4.75	1	1	1	1	1	1	0
Quanum	6	4.5	1	1	1	1	1	1	0
Diatone	6	5.8	1	1	1	1	1	1	1
HobbyKing	7	6	1	1	1	1	1	1	0
HobbyKing	7	4.9	1	1	1	1	1	1	0
HobbyKing	8	4.5	1	1	1	1	1	0	0
HobbyKing	8	4.5	1	1	1	1	1	0	0
HobbyKing	9	7.4	1	1	1	1	1	1	0
Gemfan	9	12.5	1	1	1	1	1	0	0
HobbyKing	9.4	24.6	1	0	0	0	0	0	0
HobbyKing	10	9	1	1	1	1	1	1	0
HobbyKing	10	10	1	1	1	1	1	1	0
HobbyKing	10	15	1	1	1	1	1	0	0
HobbyKing	11	15	1	1	1	1	1	1	0
HobbyKing	11	16	1	1	1	1	1	0	0
Quanum	11	15	1	1	1	1	1	1	0
HobbyKing	12	17	1	1	1	1	1	1	0
T motor	13	14.2	1	1	1	1	1	1	0
HobbyKing	13	17.9	1	1	1	1	1	1	0
T motor	14	19.2	1	1	1	1	1	1	1
DJI	15	15	1	1	1	1	1	0	0
HobbyKing	15	20	1	1	1	1	1	1	0
T motor	15	26.5	1	1	1	1	1	0	0

Dynam	16	33.2	1	1	1	1	0	0	0
Dynam	17	39.8	1	1	0	0	0	0	0
T motor	17	34	1	1	1	1	1	0	0
Quanum	17	34	1	1	1	1	1	0	0
Dynam	18	49	1	0	0	0	0	0	0
Quanum	20	56	1	0	0	0	0	0	0
T motor	20	44	1	1	1	1	1	0	0
DJI	21	58	1	1	0	0	0	0	0
T motor	22	56	1	1	1	1	1	0	0
T motor	22	56	1	1	1	1	1	0	0
Quanum	24	78	1	0	0	0	0	0	0

Appendix E　Propeller　Parameters　from UIUC Database

ID	Brand	Series	d_p/in	Pitch/in	Min rpm	ct0 min	Max rpm	ct0 max	Average ct0	Min rpm	J1@η_max	Max rpm	J2@η_max	average J@η_max
1	APC	sport	4.2	2	2067	0.06	15000	0.09	0.08	6000	0.36	15000	0.42	0.39
2	APC	free flight	4.2	4	1490	0.13	9880	0.13	0.13	6000	0.68	10000	0.8	0.74
3	APC	sport	7	6	2981	0.09	7002	0.10	0.09	4000	0.56	7000	0.7	0.63
4	APC	sport	7	9	2533	0.09	6792	0.12	0.10	4000	0.7	6800	0.96	0.83
5	APC	carbon fibre	7.4	8.25	2492	0.13	6800	0.15	0.14	4000	0.6	6800	0.8	0.7
6	APC	carbon fibre	7.8	6	2484	0.09	6804	0.11	0.10	4000	0.56	6800	0.65	0.605
7	APC	carbon fibre	7.8	7	2502	0.10	6705	0.11	0.11	4000	0.62	6700	0.78	0.7
8	APC	slow flyer	8	3.8	3030	0.10	7015	0.11	0.10	4000	0.4	7000	0.48	0.44
9	APC	sport	8	4	2994	0.07	7082	0.09	0.08	4000	0.4	7000	0.52	0.46
10	APC	thin electric	8	4	3037	0.09	6989	0.10	0.09	4000	0.44	7000	0.52	0.48
11	APC	sport	8	5	3014	0.08	7016	0.10	0.09	4000	0.48	7000	0.56	0.52
12	APC	slow flyer	8	6	2485	0.14	6611	0.16	0.15	4000	0.64	6600	0.76	0.7
13	APC	sport	8	6	2993	0.09	6883	0.10	0.10	4000	0.48	6900	0.68	0.58
14	APC	thin electric	8	6	2534	0.11	6700	0.12	0.11	4000	0.56	6700	0.76	0.66
15	APC	sport	8	7	3021	0.09	6814	0.11	0.10	4000	0.56	6800	0.66	0.61
16	APC	sport	8	8	2516	0.10	6602	0.11	0.10	4000	0.65	6600	0.8	0.725
17	APC	thin electric	8	8	2519	0.12	6412	0.13	0.13	4000	0.72	6400	0.82	0.77
18	APC	sport	8	9	2486	0.09	6395	0.11	0.10	4000	0.76	6400	0.88	0.82
19	APC	sport	8	10	2022	0.11	6202	0.12	0.12	3000	0.8	6000	1	0.9
20	APC	slow flyer	9	3.8	2504	0.09	6713	0.11	0.10	4000	0.36	6800	0.4	0.38
21	APC	free flight	9	4	2504	0.08	6785	0.09	0.09	4000	0.38	6800	0.44	0.41
22	APC	thin electric	9	4.5	2499	0.09	6922	0.10	0.10	4000	0.4	6900	0.48	0.44
23	APC	slow flyer	9	4.7	2763	0.11	6768	0.12	0.12	4000	0.38	6800	0.44	0.41
24	APC	free flight	9	5	2726	0.09	6918	0.10	0.10	4000	0.4	6900	0.56	0.48
25	APC	slow flyer	9	6	2397	0.14	6540	0.16	0.15	4000	0.6	6500	0.7	0.65
26	APC	sport	9	6	2564	0.10	6521	0.12	0.11	4000	0.48	6500	0.62	0.55
27	APC	thin electric	9	6	2333	0.11	6717	0.12	0.11	4000	0.52	6700	0.62	0.57
28	APC	sport	9	7	2489	0.10	6704	0.11	0.11	4000	0.52	6700	0.64	0.58
29	APC	slow flyer	9	7.5	2020	0.15	5607	0.18	0.17	3000	0.7	5600	0.8	0.75
30	APC	thin electric	9	7.5	2018	0.11	6089	0.13	0.12	3000	0.58	6000	0.74	0.66
31	APC	sport	9	8	1990	0.10	6193	0.11	0.10	3000	0.56	6000	0.67	0.615
32	APC	sport	9	9	2011	0.10	5900	0.11	0.11	3000	0.66	5900	0.76	0.71
33	APC	thin electric	9	9	1986	0.12	5932	0.14	0.13	3000	0.64	5900	0.84	0.74
34	APC	sport	9	10	1987	0.10	6040	0.12	0.11	3000	0.72	6000	0.88	0.8
35	APC	sport	10	3	2468	0.06	6698	0.07	0.06	4000	0.28	6700	0.34	0.31
36	APC	sport	10	4	2463	0.08	6499	0.09	0.09	4000	0.36	6400	0.42	0.39

37	APC	slow flyer	10	4.7	2377	0.11	6528	0.13	0.12	4000	0.4	6500	0.48	0.44
38	APC	sport	10	5	2002	0.09	6309	0.11	0.10	4000	0.44	6300	0.5	0.47
39	APC	thin electric	10	5	2508	0.09	6708	0.10	0.10	4000	0.44	6700	0.52	0.48
40	APC	sport	10	6	2023	0.09	6489	0.12	0.11	4000	0.48	6500	0.6	0.54
41	APC	slow flyer	10	7	2283	0.14	5987	0.16	0.15	3000	0.56	6000	0.68	0.62
42	APC	sport	10	7	2077	0.10	6012	0.12	0.11	3000	0.5	6000	0.6	0.55
43	APC	thin electric	10	7	1975	0.10	6542	0.11	0.11	4000	0.52	6500	0.64	0.58
44	APC	sport	10	8	1759	0.10	6218	0.12	0.11	3000	0.58	6000	0.7	0.64
45	APC	sport	10	9	1374	0.11	5395	0.12	0.11	3000	0.58	5400	0.72	0.65
46	APC	sport	10	10	1511	0.10	5215	0.12	0.11	2000	0.66	5000	0.78	0.72
47	APC	sport	11	3	2529	0.05	6400	0.07	0.06	4000	0.26	6400	0.32	0.29
48	APC	slow flyer	11	3.8	2154	0.08	6523	0.10	0.09	3000	0.28	6000	0.36	0.32
49	APC	sport	11	4	1673	0.06	6549	0.09	0.08	3000	0.32	6000	0.38	0.35
50	APC	slow flyer	11	4.7	1666	0.10	6021	0.13	0.11	3000	0.36	6000	0.44	0.4
51	APC	sport	11	5	1745	0.08	6293	0.10	0.09	3000	0.4	6000	0.48	0.44
52	APC	thin electric	11	5.5	1868	0.08	6473	0.09	0.08	3000	0.4	6000	0.48	0.44
53	APC	sport	11	6	1752	0.09	6259	0.11	0.10	3000	0.48	6000	0.56	0.52
54	APC	slow flyer	11	7	1868	0.15	5745	0.16	0.16	3000	0.52	5500	0.65	0.585
55	APC	sport	11	7	1583	0.10	6170	0.12	0.11	3000	0.52	6000	0.64	0.58
56	APC	thin electric	11	7	1966	0.10	6320	0.11	0.10	3000	0.47	6000	0.6	0.535
57	APC	sport	11	8	1674	0.10	5994	0.12	0.11	3000	0.56	6000	0.7	0.63
58	APC	thin electric	11	8	1655	0.10	6213	0.11	0.10	3000	0.52	6000	0.64	0.58
59	APC	thin electric	11	8.5	1973	0.10	6122	0.11	0.10	3000	0.5	6000	0.64	0.57
60	APC	sport	11	9	1791	0.11	5793	0.12	0.11	3000	0.6	5800	0.8	0.7
61	APC	thin electric	11	10	1989	0.10	5711	0.11	0.10	3000	0.6	5500	0.8	0.7
62	APC	thin electric	14	12	1496	0.09	3506	0.09	0.09	2000	0.52	3500	0.64	0.58
63	APC	sport	14	13	1502	0.11	3501	0.12	0.11	2000	0.6	3500	0.82	0.71
64	APC	thin electric	17	12	1392	0.09	3290	0.09	0.09	2000	0.56	3400	0.64	0.6
65	APC	thin electric	19	12	1261	0.09	3007	0.10	0.09	1500	0.48	3000	0.6	0.54

Appendix F   The TrW Ratio of 30 Models

Brand and Model Name	Purpose	MTOM	Number of Rotors	Single Motor Max Thrust	Thrust/Weight ratio
DJI..MG-1	Carrier	22500 g	8	5100.0 g	1.813333
DJI..MG-1P	Carrier	23800 g	8	5100.0 g	1.714286
DJI..MG-1S	Carrier	23800 g	8	5100.0 g	1.714286
Mikrokopter..MK8-3500	Carrier	7850 g	8	2500.0 g	2.547771
GS..1000	Carrier	8000 g	4	3200.0 g	1.6
DJI..flame wheel f330	Hobby	1200 g	4	600.0 g	2
DJI..flame wheel f450	Hobby	1600 g	4	600.0 g	1.5
DJI..flame wheel f550	Hobby	2400 g	6	600.0 g	1.5
3DR..Iris	Hobby	1282 g	4	970.0 g	3.026521
KINGKONG..Hex300	Hobby	680 g	6	540.0 g	4.764706
USQA..F450	Hobby	1600 g	4	885.0 g	2.2125
LOTUS RC..T580G	Hobby	1530 g	4	1260.0 g	3.294118
DJI..Matrice 600	Photography	15500 g	6	5100.0 g	1.974194
Microdrones..MD4-1000	Photography	6000 g	4	3010.0 g	2.006667
DJI..Matrice 100	Professional	3600 g	4	2100.0 g	2.333333
Microdrones..MD4-200	Professional	1100 g	4	395.0 g	1.436364
Microdrones..MD4-3000	Professional	16000 g	4	7142.9 g	1.785714
Armattan..JAPALURA 4	Racing	300 g	4	785.0 g	10.46667
Diatone..GT M200	Racing	554 g	4	1661.0 g	11.99278
Eachine..Lizard 95	Racing	111 g	4	162.0 g	5.848375
Eachine..Wizard X220S	Racing	535 g	4	780.0 g	5.831776
Zing..110	Racing	90 g	4	130.0 g	5.777778
EMAX..NIGHTHAWK	Racing	698 g	4	440.0 g	2.52149
LHI..ROBOCAT	Racing	581 g	4	440.0 g	3.02926
Speedy..Gonzalas	Racing	570 g	4	1762.0 g	12.36491
VXR..190	Racing	479 g	4	1844.0 g	15.3859
Stigg..195	Racing	560 g	4	1355.0 g	9.678571
MorpheusX..195	Racing	558 g	4	1788.0 g	12.8287
Furibee..Darkmax 220	Racing	487 g	4	1020.0 g	8.377823
Lisam..210	Racing	416 g	4	950.0 g	9.134615

This page is left intentionally blank.

Appendix G   The Calculated Max Tilt Angle of 30 Commercial Drones

Model	Purpose	MTOM /kg	Number of Rotors	Max Speed /ms-1	motor thrust /kg	total thrust /kg	calculated max tilt angle/°
DJI..MG-1	Carrier	22.5	8	22	5.1	40.8	56.5
DJI..MG-1P	Carrier	23.8	8	15	5.1	40.8	54.3
DJI..MG-1S	Carrier	23.8	8	15	5.1	40.8	54.3
Mikrokopter..MK8-3500	Carrier	7.85	8		2.5	20	66.9
GS..1000	Carrier	8	4	8	3.2	12.8	51.3
DJI..flame wheel f330	Hobby	1.2	4		0.6	2.4	60.0
DJI..flame wheel f450	Hobby	1.6	4		0.6	2.4	48.2
DJI..flame wheel f550	Hobby	2.4	6		0.6	3.6	48.2
3DR..Iris	Hobby	1.28	4		0.97	3.88	70.7
KINGKONG..Hex300	Hobby	0.68	6		0.54	3.24	77.9
USQA..F450	Hobby	1.6	4		0.885	3.54	63.1
LOTUS RC..T580G	Hobby	1.53	4		1.26	5.04	72.3
DJI..Matrice 600	Photography	15.5	6	18	5.1	30.6	59.6
Microdrones..MD4-1000	Photography	6	4	12	3.01	12.04	60.1
DJI..Matrice 100	Professional	3.6	4	22	2.1	8.4	64.6
Microdrones..MD4-200	Professional	1.1	4	8	0.395	1.58	45.9
Microdrones..MD4-3000	Professional	16	4	20	7.14	28.57	55.9
Armattan..JAPALURA 4	Racing	0.3	4		0.785	3.14	84.5
Diatone..GT M200	Racing	0.55	4	44.26	1.66	6.64	85.2
Eachine..Lizard 95	Racing	0.11	4		0.16	0.65	80.2
Eachine..Wizard X220S	Racing	0.54	4	30.4	0.78	3.12	80.1
Zing..110	Racing	0.09	4		0.13	0.52	80.0
EMAX..NIGHTHAWK	Racing	0.70	4		0.44	1.76	66.6
LHI..ROBOCAT	Racing	0.58	4		0.44	1.76	70.7
Speedy..Gonzalas	Racing	0.57	4	64.82	1.76	7.05	85.4
VXR..190	Racing	0.48	4	74.2	1.84	7.38	86.3
Stigg..195	Racing	0.56	4	41.7	1.35	5.42	84.1
MorpheusX..195	Racing	0.56	4		1.79	7.15	85.5
Furibee..Darkmax 220	Racing	0.49	4	44.3	1.02	4.08	83.1
Lisam..210	Racing	0.42	4		0.95	3.8	83.7

This page is left intentionally blank.

Appendix H The Validation of the Components' Mass Estimation of the Algorithm

Model description	MTOM (including payload)	GTOM	Avionics mass	Landing gear	Diagonal size-Ld	Payload	Number of Rotors	Coaxial	Max power consumption	Hovering power consumption
GEPRC..Hummingbird[39]	120 g	120 g			110 mm		4	0	504 W	
calculated	162 g	162 g							395 W	19 W
Lisam..210[40]	550 g	550 g	29.3	4	210 mm		4	0	1632 W	
calculated	549 g	549 g	29.3	4					1437 W	78 W
3DR..Iris[41]	1682 g	1282 g	200	8	550 mm	400 g	4	0	757 W	
calculated	1764 g	1364 g	200	8		400 g			758 W	201 W
DJI..Matrice 100[42]	3355 g	2355 g	300	400	650 mm	1000 g	4	0	1135 W	
calculated	3554 g	2554 g	300	400		1000 g			3009 W	411 W
DJI..Spreading wings S1000[43]	9500 g	5945 g	270	450	1045 mm	3555 g	8	0	4000 W	1500 W
calculated	9959 g	6404 g	270	450		3555 g			3991 W	1060 W

Model description	Thrust Weight Ratio	Disk Loading	Min Endurance (with max payload)	Max endurance without payload	Cruise endurance	Max Forward Speed	Cruising Speed	Max ascent speed
GEPRC..Hummingbird	7.97	145.05	4 min			33.33333	25	
calculated	5.34	145.04		15 min	10 min	33.33333	25	0
Lisam..210	6.91	106.37	4 min			30	0	
calculated	4.93	106.37		13 min	7 min	30	0	0
3DR..Iris	2.31	56.22	8 min			11	5	
calculated	1.80	56.22		15 min	19 min	11	5	0
DJI..Matrice 100	2.50	67.38	13 min	22 min		22	8	5
calculated	2.84	67.38		22 min	37 min	22	8	5
DJI..Spreading wings S1000	0.00	63.88	15 min			16.6	5	
calculated	1.52	63.88		30 min	22 min	16.6	5	0

[39] https://hobbyking.com/en_us/geprc-hummingbird-racing-drone-2-inch-bnf-frsky.html
[40] https://fpvdronereviews.com/fpv-racing-drone-budget-parts-list/
[41] http://www.arducopter.co.uk/iris-quadcopter-uav.html
[42] https://www.dji.com/uk/matrice100/info#specs
[43] https://www.dji.com/uk/spreading-wings-s1000/spec

Model description	Central frame size-dc	Thickness	Volume / cm3	Calculated mass/ g	Pure central frame mass	Central frame mass (including landing gear and avionics)	Central frame material
GEPRC..Hummingbird						34 g	carbon fibre
calculated	61.61 mm	2.90 mm	8.656	14.11	14 g	14 g	
Lisam..210	85.80 mm	6.00 mm	34.691	56.55		90 g	carbon fibre
calculated	95.12 mm	5.54 mm	39.397	64.22	64 g	98 g	
3DR..Iris	169.00 mm	2.00 mm	44.864	122.03	202 g	410 g	Fibre Glass
calculated	181.63 mm	5.50 mm	142.503	232.28	194 g	402 g	
DJI..Matrice 100	191.50 mm	5.00 mm	144.012	234.74			carbon fibre
calculated	203.20 mm	4.29 mm	139.122	226.77	227 g	927 g	
DJI..Spreading wings S1000	337.50 mm	3.00 mm	268.385	874.94	610 g	1330 g	carbon fibre
calculated	279.55 mm	6.90 mm	423.306	689.99	690 g	1410 g	

Model description	Mechanics Arm length-la	Arm mass (including prop, motor and ESCs)	Pure arm mass	Calculated mass	Arm Cross Section	Arm height	Arm width	Arm thickness	Arm volume/ cm3
GEPRC..Hummingbird	55.00 mm	.0 g			rectangular plate				
calculated	55.00 mm	29.94	3.5 g	24.4 g		6.24 mm	6.24 mm	2.33 mm	14.94
Lisam..210	80.70 mm	.0 g		10.3 g	rectangular plate	3.00 mm	26.00 mm		6.29
calculated	105.00 mm	73.70	8.4 g	22.7 g		7.01 mm	7.01 mm	1.56 mm	13.95
3DR..Iris	198.87 mm	121 g	53 g	115.7 g	rectangular truss	13.80 mm	31.00 mm		85.08
calculated	275.00 mm	162.83	51.3 g	91.8 g		43.70 mm	43.70 mm	0.80 mm	56.34
DJI..Matrice 100	212.80 mm			32.4 g	hollow circle	21.30 mm	21.30 mm	1.50 mm	19.86
calculated	325.00 mm	266.61	30.4 g	48.9 g		23.66 mm	23.66 mm	0.80 mm	30.01
DJI..Spreading wings S1000	386.00 mm	325.0 g	119.0 g	112.7 g	hollow circle	22.00 mm	22.00 mm	3.00 mm	69.12
calculated	522.50 mm	360.64	100.4 g	100.4 g		47.73 mm	47.73 mm	0.80 mm	61.62

Model description	Landing gear type	Landing Gear mass	Landing gear height-h	Propeller size	Propeller pitch	Prop dia mm	Prop mass	Prop gap ratio
GEPRC..Hummingbird	four supports under motors			2.0 in	4.0 in	50.8 mm	1 g	0.531137
calculated			31.12 mm				2 g	
Lisam..210	four supports under motors			5.0 in	4.5 in	127.0 mm	4 g	0.169232
calculated			59.41 mm				5 g	
3DR..Iris	four supports under motors	g	96.97 mm	10.5 in	4.5 in	266.7 mm	6.3	0.458225
calculated			155.60 mm				13 g	
DJI..Matrice 100	four supports under motors		149.00 mm	13.0 in	4.5 in	330.2 mm	19 g	0.391942
calculated			183.89 mm				17 g	
DJI..Spreading wings S1000	two T skids	455.06	305.00 mm	15.0 in	5.2 in	381.0 mm	13 g	0.049617
calculated			295.63 mm				22 g	

Model description	ESC max Current	ESC mass without	ESC mass	Motor ID	Stator Size	KV	Motor Database. Weight	Maximum power	Thrust
GEPRC..Hummingbird	12 A	3 g		1061	11x06	6000	7.1 g	126.0 W	239.0 g
calculated	12 A	10.9	12.07 g			9615	12.6 g	98.8 W	
Lisam..210	40 A	36		657	22x05	2300	28.0 g	408.0 W	950
calculated	36 A	32.0	36.63 g			2520	24.1 g	359.3 W	
3DR..Iris	35 A	31		1100	28x30	850	62.0 g	189.3 W	970.0 g
calculated	30 A	26.5	36.62 g			754	62.3 g	189.5 W	
DJI..Matrice 100	20 A	30 g	43	1064	35x10	350	106.0 g	283.8 W	2100
calculated	41 A	36.8	51.24 g			467	168.3 g	752.4 W	
DJI..Spreading wings S1000	40 A	35 g		1074	41x14	400	158.0 g	500.0 W	
calculated	40 A	35.8	59.00 g			291	179.5 g	498.8 W	

Model description	No of Bats	Battery Database. Weight	Capacity	Energy	Cells	Discharge Rate Constant	Max current
GEPRC..Hummingbird	1	42.00	450 mAh	5.67	3 S	75 C	33.75
calculated		28.04	377 mAh	4.371869		135 C	
Lisam..210	1	155.00	1300 mAh	21.84	4 S	65 C	84.5
calculated		156.55	1579 mAh	21.2277		100 C	
3DR..Iris	1	262.00	3500 mAh	44.1	3 S	8	28
calculated		310.40	4175 mAh	47.34972		30 C	
DJI..Matrice 100		600.00	4500 mAh	113.4	6 S		0
calculated		560.83	3772 mAh	85.5507		45 C	
DJI..Spreading wings S1000	1	2015.00	16000 mAh	403.2	6 S	12 C	192
calculated		2109.24	14186 mAh	328.8977		25 C	

This page is left intentionally blank.

Appendix I   The Material Mechanics Basis

I.1   Cross-Section Area Moment of Inertia[44,45,46,47,48,49]

- Plate
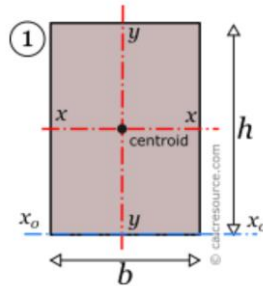
$$Ix = bh^3/12$$

- Hollow Rectangular & I section & Lie Down Channel

$$I_x = \frac{BH^3 - bh^3}{12}$$
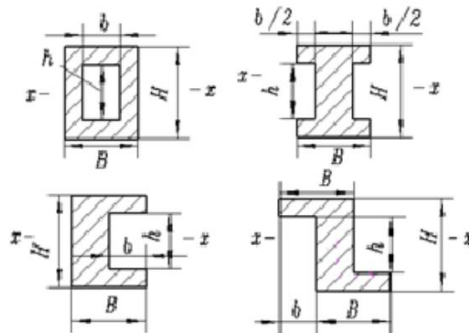
[44] https://calcresource.com/moment-of-inertia.html
[45] https://wenku.baidu.com/view/44f6b9f59e3143323968938e.html
[46] https://www.engineeringtoolbox.com/area-moment-inertia-d_1328.html
[47] https://en.wikipedia.org/wiki/List_of_second_moments_of_area
[48] http://structx.com/Shape_Formulas_035.html
[49] https://www.amesweb.info/SectionalPropertiesTabs/SectionalPropertiesTbeam.aspx

- Hollow Oval and Circle (a=b)
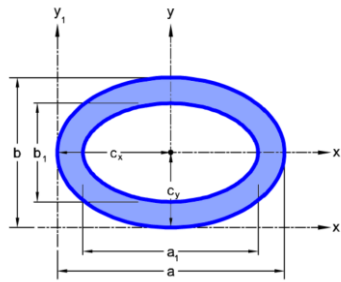
$$I_x = \frac{\pi}{64}\left(ab^3 - a_1 b_1^3\right)$$

- T Section & Channel Section
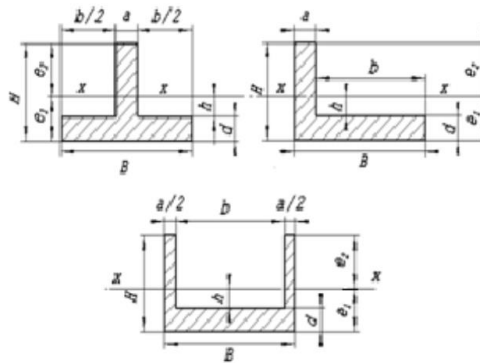
$$I_x = \frac{Be_1^3 - bh^3 + ae_2^3}{3}$$

$$e_1 = \frac{aH^2 + bd^2}{2(aH + bd)}$$

- Lie Down I (H) and Lie Down T
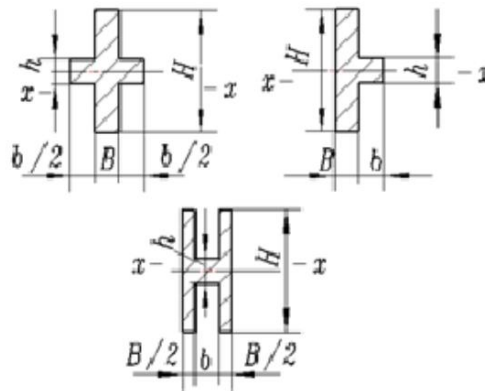
$$\mathbf{I_x} = \frac{BH^3 + bh^3}{12}$$

I.2   Natural Frequency of Cantilever Beam Calculation[50,51,52,53]
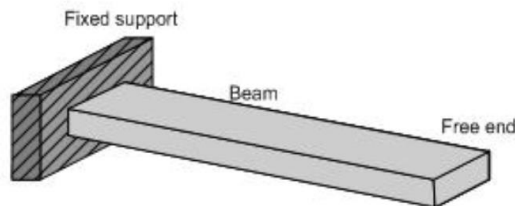

Fig. 4.1 (a): A cantilever beam

$$\boldsymbol{\omega}\mathbf{n} = k^2 \sqrt{\frac{EI}{\rho AL^4}}$$

K=1.875, 4.694, 7.855, 10.996 for 1st 2nd 3rd and 4th mode

$$\mathbf{f}_n = \frac{\boldsymbol{\omega}\mathbf{n}}{2\boldsymbol{\pi}}$$

When the rotor is rotating, there are both thrust change and torque change, the torque–caused bending about z axis, so two axes should all be considered (I is different).

I.3 Deflection Calculation

Cantilever beam

1. Given force load

$$d_{max} = \frac{FL^3}{3EI_x}$$

2. Given moment at the end, equivalent to a reverse cantilever beam have force load at the root F=M/L, I_y should be used here

There seems no standard to define the deflection limit for multicopter design, in this thesis, L/300 will be used as the limit.

I.4 Stress in a Beam

Load analysis: Thrust (-x,+x), torque (x).

Thrust caused normal stress over x axis, and shear stress at the root on -y direction

Torque caused normal stress over y axis

The calculation of the overall normal stress:

$$\sigma_{xx} = \frac{\left(M_y I_{zz} + M_z I_{yz}\right)z - \left(M_z I_{yy} + M_y I_{yz}\right)y}{\left(I_{yy} I_{zz} - I_{yz}^2\right)}$$

The xx here is the zz in my research, y is the x axis, z is the y axis

I.5   Shear Stress Calculation

The calculation of the shear stress over different cross-section

$$Tao_{max} = \frac{F}{A_{section}}$$

Table I.1   Shear stress calculation for different cross sections.

Cross-section	$A_{section}$
Rectangular	$\frac{2}{3}A$
Box	$2A_{web}$
Hollow Oval	
T/L	
Channel	
I	A_{web}

Stress constraints: $\sqrt{\sigma^2 + 3\tau^2} \leq 1.1f$

$$\sigma_{max} = \frac{M_{max}y_{max}}{I_x} \leq \frac{[\sigma]}{SF}$$

Optimisation target: 1. Frequency (Quan, 2017)—3.2, 2. Strength, 3. Deformation (Quan, 2017)

For frequency

(1) Generally, the lateral vibration strength is less than 0.3g, while the longitudinal vibration strength

is less than 0.5g. (Note: g represents the acceleration of gravity here).

(2) In practice, the vibration strength along all axes is better bounded less than 0.1g.

For deformation

(1) The structure of airframe is designed to support limited payloads without detrimental permanent deformation. At any payload up to limit payloads, the deformation may not interfere with safe operation. Moreover, the structure is able to support ultimate payloads 1 without failure.

(2) After other necessary requirements have been achieved, the total weight is as light as possible.

I.6   Material Property

(Unknown, 2002)

The material properties are checked from the material handbook.

Table I.2   Material Properties of Glass Fibre E-Glass 7781/EA 9396

density	ρ	Kg/m3	1630
Young's Modulus	E	Pa	1.3514E11
Tension Strength	σ1	Pa	1.4548E9
Compression Strength	σ2	Pa	1.2962E9

Appendix J   Benchmark Study of Video Transmitters for Small RPAS

Digital Link	Image	Mass (g)	Price ($)	Frequency Band (GHz)	Transmission Power (mW)	Max Video Quality	Max Range (m)	URL
Holybro Atlatl		1.6	21.99	5.8	25 -100	analogue AV	120	https://www.banggood.com/Holybro-Atlatl-5_8G-40CH-25mW-100mW-mini-FPV-Video-Transmitter-19x16mm-for-RC-FPV-Racing-Drone-p-1393737.html?cur_warehouse=CN
Eachine VTX02		2.8	16.99	5.8	200	analogue AV	200	https://www.banggood.com/Eachine-VTX02-Super-Mini-5_8G-40CH-200mW-FPV-Transmitter-p-1114204.html?akmClientCountry=GB&cur_warehouse=CN

Wireless Solutions		16 (Tx) 120 (Rx)	64	2.4	200	analogue AV	300	https://www.aliexpress.com/item/32407539351.html
Flysight		19	42	5.8	700	analogue AV	550	https://www.amazon.com/Transmitter-5-8GHz-Wireless-TX5807-RPSMA-Flysight/dp/B01GE5CU16
Flysight Black Mamba		52	61	5.8	2000	analogue AV	850[54]	https://www.amazon.com/Flysight-TX5820-Transmitter-Long-Distance-Transmission/dp/B01D4CISRC

---

[54] In the specification, the range can get to 8 km-9 km LOS, however, tests of a customer hit the maximum range of 850 m.

ImmersionRC Tramp		4	49.99	5.8	600	analogue AV	600	https://www.banggood.com/ImmersionRC-Tramp-HV-5_8GHz-Video-TX-FPV-Transmitter-VTX-EU-Version-for-FPV-RC-Racing-Drone-Airplane-p-1527353.html?gmcCountry=GB&createTmp=1&utm_source=googleshopping&utm_medium=cpc_bgs&utm_content=faye&utm_campaign=ssc-all-gb-0925&gclid=CjwKCAjw3c_tBRA4EiwAICs8CtaCkDkAYLA2kgQ5iWg-3C0Ag2nGcJx1-K2BaCm06hbTZBap8K9GzRoCctcQAvD_BwE&cur_warehouse=HK
BOXX ATOM		253	5081	5	200	SDI, HD-SDI and HDMI 1080p 60 fps	600	https://cvp.com/product/boxx_tv_at-01s_atom_transmitter
ACCSOON CINEEYE		175	280	5	50	full HD 1080p 30fps	100	https://cvp.com/product/accsoon-cine-eye-transmitter?gclid=CjwKCAjw3c_tBRA4EiwAICs8Ch4WtfC9NC8_y34_5yDekbNiygAQu0vW7bdT2dyTShSQFsGUAJfi_RoCn1sQAvD_BwE

UNIVERSITY OF Southampton

PARALINX TOMAHAWK2		208	5196	5	200	full HD 1080p 60fps	600	https://cvp.com/product/paralinx_tomahawk_par_th2sht_tx
Wireless Solutions		388 (Tx) 120 (Rx)	486	1.3	5000	analogue AV	5000	https://www.aliexpress.com/item/32594250600.html
FT951		7	25	5.8	25	analogue AV	200	https://www.buildyourowndrone.co.uk/ft951-5-8ghz-25mw-22ch-fpv-racing-drone-video-transmitter-uk-legal

J-4

SUNTOR J11		94		2.4	1000	H.264+H.265 HDMI 1080P 60fps	1200	https://www.cofdm-transmitter.com/sale-10062688-h-264-h-265-drone-wireless-video-transmitter-and-receiver-hdmi-wireless-video-system.html
SafeGuard		151	3125	2.4	1000	HDMI, RJ45 Ethernet 1080P	1000	https://szsfgt.en.alibaba.com/product/60673853862-807619096/UAV_data_link_2_4GHz_full_duplex_tactical_COFDM_drone_video_transmitter.html
SUNTOR C130		98		0.34	5000	HDMI 1080P 60fps	15000	http://m.redessup.com/video-transmitter/long-range-video-transmitter/video-transmitter-and-receiver-long-range.html
LinkAV		105		0.9	1000	HDMI 1080P 60fps	2000	http://www.videowirelesstransmitters.com/sale-8775440-300-900mhz-long-range-wireless-video-transmitter-h-264-cofdm-wireless-video-transmitter-for-uav-uas-.html

Tomahawk		200 (Tx) 540 (Rx)	9000	5	200	HDMI 1080P 60fps	600	https://www.flyonixstore.co.uk/product/paralinx-tomahawk-hdmi-system/
WirelessSolution		82 (Tx) 120 (Rx)	96	1.2	1500	analogue AV	2000	https://www.aliexpress.com/item/32407630340.html

*__EMMT__: Exportable Multiband Miniature Transceiver, __EDL__: Enhanced Data Link, __FHSS__: Frequency-Hopping Spread Spectrum, __BPSK__: Binary Phase-Shift Keying, __QPSK__: Quadrature Phase-Shift Keying, __O-QPSK__: offset-QPSK, __QAM__: Quadrature Amplitude Modulation.

Appendix K   The Source Code

K.1 Layer_1.m

```matlab
function Min_err_per=layer_1(MissionName)
% clear all
% clc
% close all
global Ph FT Dp v m_pl P_pl Cstr C MP cx Shape Mat DesignParameters DsPm
MPr ...
    Motor_forest DOE_forest Mdl_pr_forest DOE_pr_forest prop_pr_forest...
    prop_pr_DOE   err_flag output err_percent results t count FUNoutput RUN

% MissionName='DJI SW 1000';
%% read missions, constraints and constants
% read mission specifications from a given prescenario
MissionSpecs=xlsread('MissionSpecs.xlsx',MissionName);
Ph=MissionSpecs(1,:);   % the ID of Phases
FT=MissionSpecs(3,:);   % the flight time of each phase
for i=1:length(Ph)
    Dp(i,1)=MissionSpecs(4,i);    % the x (horizontal) displacement
    Dp(i,2)=MissionSpecs(5,i);     % the y (vertical) displacement
    v(i,1)=Dp(i,1)/FT(i);     % the x average velocity, i.e. the cruise
speed
    v(i,2)=Dp(i,2)/FT(i);     % the y average velocity
end
m_pl=MissionSpecs(6,:); % the payload mass in each phase
P_pl=MissionSpecs(7,:); % the payload power in each phase
% read constraints from a given scenario
Cstr=xlsread('Constraints.xlsx',MissionName);
Cstr=Cstr(:,1);

Constants=xlsread('Constants.xlsx',MissionName);
C=Constants(1:39,1);                    % constants
n_M=length(Constants(42,:));     % number of materials
MP=Constants(42:49, 1:n_M);    % material properties table
MPr=Constants(53:60,1:n_M);    % material bill table (price based on shape)
%% read design parameter options
DesignParameters=xlsread('DesignParameters.xlsx',MissionName);
%read the swithes of design parameters
t=1;
for i=1:6
    if DesignParameters(i,3)==1
        N_r(t)=DesignParameters(i,4);    %read the available number of rotors
        cx(t)=DesignParameters(i,5);     %read the coaxial switch
        N_arm(t)=N_r(t)/(cx(t)+1);       %work out number of arms
        t=t+1;
    end
end
%read number of Li-Po battery cells. The spreadsheet defined the middle
%recommended vale and a range, the below code convert these two numbers
%into an array.
N_c(1)=DesignParameters(8,2)-DesignParameters(9,2);
for i=1:(DesignParameters(9,2)*2)
    N_c(i+1)=N_c(i)+1;
end
```

```matlab
for i=1:(DesignParameters(9,2)*2+1)
    if N_c(i)<0
        N_c(i)=0;
    end
end
N_c=nonzeros(N_c)';
%read propeller diameters
t=1;
if DesignParameters(13,2)==0
    d_p=DesignParameters(11,2);
else
    for
i=DesignParameters(11,2):DesignParameters(13,2):DesignParameters(12,2)
        d_p(t)=i;
        t=t+1;
    end
end
%read number of propeller blades
t=1;
for i=1:8
    if DesignParameters(i+18,3)==1
        Shape(t)=DesignParameters(i+18,1);
        t=t+1;
    end
end
t=1;
for i=1:5
    if DesignParameters(i+27,3)==1
        Mat(t)=DesignParameters(i+27,1);
        t=t+1;
    end
end
%read body material selection
t=1;
for i=1:5
    if DesignParameters(i+33,3)==1
        Mat_body(t)=DesignParameters(i+33,1);
        t=t+1;
    end
end
%% load regression forest models for motor mass and prop price estimation
load("Motor_forest.mat");
load("DOE_forest.mat");
load("Mdl_pr_forest.mat");
load("DOE_pr_forest.mat");
load("prop_pr_forest.mat");
load("prop_pr_DOE.mat");
%% pre-check of the design parameters, call level 2 process function and
constraint check
% t=1;
% count=1;
% RUN=1;
fun_dl=@layer_2_range;    % set the optimisation function
% Disk Loading is the only variable to be changed
ub_dl=Cstr(17);    % set upper boundary
lb_dl=Cstr(16);    % set lower boundary
DL0=lb_dl+0.001;  % set the starting point
options=optimset('Display','iter','TolFun',1e-5,'TolX',1e-4);
    timeoa=tic;
```

```
for i=1:length(N_arm)            %loop all the number of rotors
    for j=1:length(N_c)        %loop all the number of battery cells
        %for k=1:length(N_bl)
        for l=1:length(Mat_body)
            for m=1:length(d_p)   %loop all the propeller sizez
                d_pm=d_p(m)*25.4/1000;        % convert propeller diameter
from inch to m
DsPm(1)=N_r(i);
DsPm(2)=N_c(j);
DsPm(3)=0;       %N_bl(k);number of blade not considered in this version
DsPm(4)=d_pm;
DsPm(5)=Mat_body(l);
DsPm(6)=N_arm(i);


[opt_result(count,:),Min_err_per(count),existflag]=fminsearchcon(fun_dl,DL0,
lb_dl,ub_dl,[],[],[], options);
results(count,:)=FUNoutput;
count=count+1;
            end
        end
    end
end
end
```

K.2   Layer_2.m

```
function err_percent=layer_2 (DL)
%timewo=tic;
global  FT v Cstr C m_pl P_pl MidPara DsPm Load err_flag missionerr RUN
FUNoutput
err_flag(1:10)=0;      % clear the cache
missionerr=[0,0,0];
err_percent=0;
FUNoutput(1:66)=1;

%% fore calculation
% for notion: DsPm refers to design parameters: (1)N_r,number of rotors,
% (2) N_c, number of battery cells, (3) N_bl, number of propeller blades,
% (4) d_p, propeller diameter, unit,m, (5) body material flag, (6) N_arm,
% number of arms, (7) TrW, thrust weight ratio
As=pi*(DsPm(4)/2)^2;             % disk area of a single rotor
A=As*DsPm(1);                    % total disk area
GTOW=A*DL;                       % initial GTOW, disk loading times
% total disk area, unit N. not including payload weight
GTOM0=GTOW/C(3);                 % convert weigt to mass, N to kg
MTOM=GTOM0+max(m_pl);   % maximum take off mass, including max payload mass
MTOW=MTOM*C(3);      % max take off weight, including max payload
U=C(1)*DsPm(2);      % total voltage equals cell voltage times number of
cells
m_av=Cstr(13);       % avionics mass and power
P_av=Cstr(12);
% central body and landing gear
L_a=DsPm(4)*(1+C(23))/(2*sin(pi/DsPm(6)));   % the arm length of given
propeller
% it is defined as from the centre of body to the centre of a motor. By
% defining the gap ratio between two adjacent propellers, given the
% propeller diameter, the arm length can be determined.
```

```matlab
L_d=2*L_a;          % diagonal distance is considered twice of the arm length
% define some middle parameters to be used by layer_3 functions
MidPara(:,1)=[As;0;GTOW;0;MTOM];
% MidParameters={As,'As-Disk Area of one rotor';A1,'A1-topview
area';GTOW,'GTOW-gross takeoff weight';...
%      v_h,'v_h-hovering induced velocity';MTOM,'max takeoff mass'};
%% propeller estimation
[m_p,pr_p]=layer_3_prop(DsPm(4));      %% call a level 3 funciton to
calculate the mass and price of a single propeller
%% central body estimation
[m_body,pr_body,A_c, d_body, th_body]=layer_3_body(L_d);  % mass, price, and
the central frame area
%% Landing Gear Constraints
H_lg_max=0.2829*L_d;                        % maximum allowed landing gear
height
m_lg=Cstr(21);                              % Landing gear mass
%% Drag calculation from max straight forward condition
% the calculated top area should be within a reseanable range, here
% consider 90% of the total disk area+central part area (10% overlap).
A1=(A+A_c)*0.9;
A2=A1/C(27,1);   % the front area, it is normally the body+payload+landing
gear
% projection area, it is much smaller than the top area, according to
% database conclusion, there is an average number
MidPara(2,1)=A1;
%% Hovering condition--with maximum payload
var_h=[0,0,MTOM];
[Ts_h,n_hp,Psp_hp]=layer_3_general(var_h);
Psp_mot=Psp_hp*Cstr(14);        % when considering maximum thrust mode,
% also need to multiply by the minimum thrust to weight ratio to cover
manueverbility
Ts_max(1)=Ts_h*Cstr(14);
Ps_max(1)=Psp_mot;
n_max(1)=n_hp;       % record candidate one for maximum motor output
%% max straight forward flight --with no payload
if Cstr(1)==0
    v_f_max=max(max(v(:,1)),Cstr(7));
else
    v_f_max=Cstr(1);     % get maximum forward speed ;
end
if Cstr(22)==1
    var_fmax=[v_f_max,0,MTOM];
else
    var_fmax=[v_f_max,0,GTOM0];
end
[Ts_max(2),n_f_max,Ps_f_max]=layer_3_general(var_fmax);
Psp_f_max=Ps_f_max*C(24)/ C(9) ;              % maximum output power
happens at extreme
% conditions, the prop efficiency is considered to be the allowed
% worst, 60%. Also considers the average fuselage downwash for multicopters
Ps_max(2)=Psp_f_max;
n_max(2)=n_f_max;       % record candidate two for maximum motor output
% power and rotation speed
%% maximum vertical  ascent condition---no payload
if Cstr(2)==0
    v_a_max=max(v(:,2));
else
    v_a_max=Cstr(2);
end
```

```matlab
if Cstr(22)==1
    var_amax=[0,v_a_max,MTOM];
else
    var_amax=[0,v_a_max,GTOM0];
end
[Ts_max(3),n_a_max,Ps_a_max]=layer_3_general(var_amax);
Psp_a_max=Ps_a_max*C(24)/ C(9);                  % maximum output power happens
at extreme
% conditions, the prop efficiency is considered to be the allowed
% worst, 60%. Also considers the average fuselage downwash for multicopters
Ps_max(3)=Psp_a_max;
n_max(3)=n_a_max;        % record candidate three for maximum motor output
% power and rotation speed
%% extreme condition analysis
% this condition is to work out the power and current requirement uncer the
% extreme performance, it will then estimate the mass and price of motors,
% ESCs and arms
[Ps_in_max, I]=max(Ps_max);    % find the max power and it's condition
n_max_req=n_max(I);    % rotation speed of the rotor, unit: rev/s
Ts_max_req=Ts_max(I); % maximum thrust, unit: N
if Ts_max_req<max(Ts_max)
    err_flag(3)=1;      % error: max power and max thrust are not the same
condition
    Ts_max_req=max(Ts_max);
end
TrW=Ts_max_req*DsPm(1)/MTOW;          % expected TrW
if (TrW<Cstr(14)) || (TrW>Cstr(15))
    err_flag(4)=1;            % TrW not in the appropriate range
end
%Mach0.7 tip velocity check
omega_max=n_max_req*2*pi;
v_tip=omega_max*DsPm(4)/2;
if v_tip/C(4)>C(11)
    err_flag(9)=1;  % the prop tip velocity Mach number is exceeded,
possible
    % noise and efficiency drop, should avoid.
    %      FUNoutput(19)=10;
    %      FUNoutput(18)=100000;
    return;
end

% kv_min=ceil(n_max_req*60*C(29)/(U*10))*10;
kv_min=n_max_req*60*C(29)/U;
% kv is rpm per volt, so the rotation speed needs
% a unit conversion. The kv calculated from the minimum rpm is the minimum
% requirement. The actual kv mush be larger than this number, normally,
there
% is a ratio between the noted (unloaded) kv vs the full-loaded kv: 1.52

% There are three parameters used to estimate the mass of the motor: 1.
minimum kv,
% 2. maximum output power, 3. maximum voltage
param_motor(1)=kv_min;
param_motor(2)=Ps_in_max;
param_motor(3)=U;
[m_mot,pr_mot]=layer_3_motor(param_motor);
%% ESC build up and mass estimation
P_mt_in_max=Ps_in_max/C(14);      % C(14) is the lowest efficiency of motor
```

```matlab
% in the extreme operation condition. !!!!need verify
P_esc_in_max=P_mt_in_max/C(18); % C(18) is the lowest ESC efficiency
I_dc_max=P_esc_in_max/U;              % max current through a single ESC

% There are two parameters used to estimate the mass and price of the
% ESC: 1. maximum input current, 2. the arm length
param_esc(1)=I_dc_max;
param_esc(2)=L_a;
[m_esc,pr_esc,m_esc_chip]=layer_3_esc(param_esc);
%% efficient condition
% normally it is hover or forward cruise, but it could also be forward
% and climbing at the same time in a low speed.But no matter what, the
% movemenets in the mission specification are all considered in the
% efficient mode.
for i=1:length(FT)
    GTOM_ph=GTOM0+m_pl(i);
    var=[v(i,1),v(i,2),GTOM_ph];     % variables for general function
    [~,~,Psp_g]=layer_3_general(var);
    Ps_g_mot=Psp_g*C(24)/C(7);     % the motor output power in other
conditions.
    % consider maximum prop efficiency here.also consider fuselage downwash
    Ps_g=Ps_g_mot/(C(12)*C(17));   % the ESC input power, consider in
efficient mode
    % all the components are working at the highest efficiency
    P_ph(i)=(Ps_g*DsPm(1)+P_pl(i)+P_av)/C(20); % total power equals to the
    % power consumed by all the motors, the payload and the avionics. unit:
W
    % consider the battery internal loss, apply the efficiency factor
    E_ph(i)=P_ph(i)*FT(i)/3600;     % energy consumed in this phase, unit:
W*h
end
E_tot=sum(E_ph);          % total energy
FT_tot=sum(FT);           % total flight time, unit: s
%% calculate the possible endurance
% .1. Hovering with average payload
GTOM_e=GTOM0+Cstr(6);     % here not consider a specific mission, but use an
% average payload mass. Below, uses average payload power.
var_he=[0,0,GTOM_e];
[~,n_he,Psp_he]=layer_3_general(var_he);
Ps_he_mot=Psp_he*C(24)/C(7);     % the motor output power in other
conditions.
% consider maximum prop efficiency here.also consider fuselage downwash
Ps_he=Ps_he_mot/(C(12)*C(17));   % the ESC input power, consider in
efficient mode
% all the components are working at the highest efficiency
P_he=(Ps_he*DsPm(1)+Cstr(5)+P_av)/C(20);
FT_he=floor(E_tot/P_he*3600);  % hovering endurance, unit: s
% .2. Hovering without payload
var_he2=[0,0,GTOM0];
[~,n_he2,Psp_he2]=layer_3_general(var_he2);
Ps_he_mot2=Psp_he2*C(24)/C(7);     % the motor output power in other
conditions.
% consider maximum prop efficiency here.also consider fuselage downwash
Ps_he2=Ps_he_mot2/(C(12)*C(17));   % the ESC input power, consider in
efficient mode
% all the components are working at the highest efficiency
P_he2=(Ps_he2*DsPm(1)+Cstr(5)+P_av)/C(20);
FT_he2=floor(E_tot/P_he2*3600);  % hovering endurance, unit: s
% .3. Cruising with average payload
```

```matlab
var_ce=[Cstr(7),0,GTOM_e];
[~,n_ce,Psp_ce]=layer_3_general(var_ce);
Ps_ce_mot=Psp_ce*C(24)/C(7);       % the motor output power in other
conditions.
% consider maximum prop efficiency here.also consider fuselage downwash
Ps_ce=Ps_ce_mot/(C(12)*C(17));     % the ESC input power, consider in
efficient mode
% all the components are working at the highest efficiency
P_ce=(Ps_ce*DsPm(1)+Cstr(5)+P_av)/C(20);
FT_ce=floor(E_tot/P_ce*3600);   % cruising endurance, unit: s
%% Battery calculation and mass estimation
%E_max=max([E_tot,Ea_h,Ea_c]);     % the battery should be enough to provide
% energy in all the conditions (meet the mission requirement as well
% the general endurance constraints)
E_b_req=E_tot/C(21); %  consider battery discharge depth
[m_b,pr_b]=layer_3_bat(E_b_req) ;     % estimate the battery mass and price
from the energy view

Cb=E_b_req/U*1000; %calculate the capacity of the battery, unit: mAh

I_b_max=(P_esc_in_max*DsPm(1)+P_av+max(P_pl))/(C(20)*U);    %work out the
maximum curernt in the system to calculate C rate of battery
C_rate=ceil(I_b_max*1000/Cb/5)*5;     %calculate the required C rate
(discharge speed)
%% arm optimisation and mass estimation
% La_min=(dt+Dp)/2/sind(Alpha);      % La is the minimum length of arm

Load(1)=Ts_max_req;                 % the maximum thrust of a single rotor,
unit N
Load(2)=max(n_max);         % the minimum required rotation speed at maximum
thrust, unit rev/s
Load(3)=max(Ps_max)/omega_max;      % the maximum torque, unit N.m=W/(rad/s)
Load(4)=m_mot;                  % the motormass unit kg
Load(5)=n_he;                   % hovering motor rotation speed
Load(6)=n_ce;                   % cruising motor rotation speed
if Cstr(18)==1
    [m_arm, pr_arm,opt_geo]=layer_3_arm_propt(L_a);
else
    [m_arm,pr_arm, opt_geo]=layer_3_arm_mopt(L_a);
end
%% final add up
 M_tot=DsPm(1)*(m_mot+m_esc+m_p)+DsPm(6)*m_arm+m_b+m_body+m_av+m_lg;
M_err=abs(M_tot-GTOM0);
err_percent=M_err/GTOM0;

Pr_tot=DsPm(1)*(pr_mot+pr_esc+pr_p)+DsPm(6)*pr_arm+pr_b+pr_body;
% price estimation not including avionics and payload. Since they are
% prepared in advance.

%% performance constraints check
if L_d>Cstr(9) && Cstr(9)~=0
    err_size=1; % diagonal distance exceed max size constraint
    err_flag(1)=err_size;
end
if H_lg_max<Cstr(20)
    errC_lg_h=1;     % if this flag is on, it means this solution (if MTOM
    % is valid)is not acceptable due to a "Constraint mismatch of
landinggear height"
```

```matlab
    % the selected landing gear is too tall for this solution's frame size
    err_flag(2)=errC_lg_h;
end
% if v_f_max<Cstr(1)
%     err_max_vf=1;    % the error flag of max forward speed not meet the
mission requirment
%     err_flag(3)=err_max_vf;
% end
% if v_a_max<Cstr(2)
%     err_max_va=1;    % error flag of max ascent speed not meet the mission
requirement
%     err_flag(4)=err_max_va;
% end
if FT_he<Cstr(3)
    err_FT_h=1;       % error flag of hovering endurance not meet the mission
requirement
    err_flag(5)=err_FT_h;
end
if FT_ce<Cstr(4)
    err_FT_c=1;       % error flag of cruising endurance not meet the mission
requirement
    err_flag(6)=err_FT_c;
end
if M_tot+max(m_pl)>Cstr(8)  && Cstr(8)~=0
    err_MTOM=1;
    err_flag(7)=err_MTOM;
end
% err_flag(8) is an mistake of vertical descent speed, aircraft will fall
% into vortex ring state.
% err_flag(9) is an mistake that the propeller rotate too fast and the tip
% velocity exceeds the critical Mach number (Mach0.7).
% err_flag(3) max power and max thrust are not the same condition
% err_flag(4) is the indicator of thrust weight ratio out of range
%% mission constraints check
if v_f_max<max(v(:,1))
    missionerr(2)=1;    % the error flag of max forward speed not meet the
mission requirment
end
if v_a_max<max(v(:,2))
    missionerr(3)=1;    % error flag of max ascent speed not meet the mission
requirement
end
%% record the performance and design parameters of this multicopter

FUNoutput=[Cstr(18),DsPm(1:3),DsPm(4)*1000,DsPm(5:6),TrW,DL,opt_geo(1),...

opt_geo(2:5).*1000,opt_geo(6),L_d*1000,d_body*1000,th_body*1000,GTOM0*1000,M
_tot*1000,...
    err_percent,
Pr_tot,E_tot,FT_tot/60,FT_he/60,FT_he2/60,FT_ce/60,v_f_max,...

v_a_max,m_mot*1000,m_esc*1000,m_esc_chip*1000,m_p*1000,m_arm*1000,m_b*1000,m
_body*1000,...
    m_av*1000,m_lg*1000,
pr_mot,pr_esc,pr_p,pr_arm,pr_b,pr_body,P_av,Ps_in_max,Ts_max_req...

Psp_mot,omega_max,kv_min,I_dc_max,Cb,C_rate,H_lg_max*1000,err_flag,missioner
r];
fprintf('this is run # %d\n', RUN);
```

```
RUN=RUN+1;
% if sum(missionerr(2:3))~=0
%     M_err=GTOM0*100;
% end


end
```

K.3 layer_3_prop.m

```
layer_3_bodyfunction [m_p,pr_p]=layer_3_prop(dpm)
global C prop_pr_forest prop_pr_DOE MidPara DsPm

%% mass estimation

    dpi=round(dpm/0.0254);       % convert diameter unit from metre to inch
    m_p=(0.0036907*dpi^3-0.021325*dpi^2+0.9344*dpi)/1000;


    % for large propeller, the price shows a linear relationship, while for
    % smaller propellers, it's more like a poly3 relationship. the two
    % regression cross at dpi=13.11, so 13 inch is the turning point
%% price estimation
% fprintf('Predicting Validation set\n');
No_Trees_pr=length(prop_pr_forest.Trees);
X=dpi;
for i=1:No_Trees_pr
%     fprintf('Tree #%d\n',i);
    % define the leaf ID
    [~,leaf_ID] = predict(prop_pr_forest.Trees{i},X);

    for j=1:prop_pr_DOE{i}.NO_LEAF
        if sum(prop_pr_DOE{i}.LEAF_IDS(j)==leaf_ID)>0
%             fprintf('\tLeaf #%d\n',j);
            % calcualte the prediction
            [Y_PRED,SD_PRED] =
predict(prop_pr_DOE{i}.LEAF{j}.MODEL,X(leaf_ID==prop_pr_DOE{i}.LEAF_IDS(j),:
));
            % store the predictions
            Y_p(leaf_ID==prop_pr_DOE{i}.LEAF_IDS(j),i) = Y_PRED;
            SD_p(leaf_ID==prop_pr_DOE{i}.LEAF_IDS(j),i) = SD_PRED;

        end
    end
    % clc
end

% fprintf('Predicting based on weighted combination method:\n');
for i=1:size(Y_p,1)
    % define the matrix C0
    C0 = inv(diag(SD_p(i,:)));
    W (i,:)=
(C0*ones(No_Trees_pr,1))./(ones(1,No_Trees_pr)*C0*ones(No_Trees_pr,1));
    Price_p(i,1) = sum(Y_p(i,:).*W(i,:));
end
pr_p=Price_p;  %!!!!!needs to be finished


end
```

K.4 Layer_3_body

```
function [m_body,pr_body,A_c, d_body, th_body]=layer_3_body(L_d)
global C DsPm MP MPr

% This function is used to calculate the mass and price of the central,
% which is modeled as three-layered round plate. two layer are used to
% fix all the arms, while the extra layer provide space for all the
% avionics and the battery.
% DsPm(5) is the current material in use: 1. Carbon Fiber, 2. Glass Fiber,
% 3. ABS Plastic, 4. Aluminium Alloy, 5. Wood
    d_body=0.2714*L_d^0.6718;
    th_body=MP(8,DsPm(5))*L_d*C(35);       % this parameter depends on
materials
    % stronger material tend to need thinner plate.
    A_c=pi*(d_body/2)^2 ;     % area of the central plate
    Vol=A_c*th_body;  % the total volumn of all the layers
    m_body=MP(1,DsPm(5))*Vol;  % call density from the material peroperty
table
    pr_body=MPr(1,DsPm(5))*m_body;  % call unit price for plate material
from bill table


end
```

K.5 layer_3_general

```
function [Ts_g,n_g,Ps_g]=layer_3_general(var)
global C MidPara DsPm missionerr err_flag Cstr
% This function reads the velocity on two axis, and current GTOM, then
% estimate the required motor power, rotation speed and thrust.
% If it's the hovering condition, it will return the output power of the
% motor. However, if it's not hovering, it will only return the propeller
% output power, since the propeller efficiency would be different in
% differnt scenarios.

% there are three input variables: 1. forward speed, 2. ascending speed,
% 3. GTOM,

if var(1)<0.01
    v_f=0;
else
    v_f=var(1);
end

if var(2)<0.01
    v_a=0;
else
    v_a=var(2);
end
v_inf=sqrt(v_f^2+v_a^2);      % velocity of comming wind
alpha=pi/2;
GTOW=var(3)*C(3);
% hovering condition
T_h=GTOW;        % equilibrium
Ts_h=T_h/DsPm(1);               % thrust of a single rotor
v_h=sqrt(Ts_h/(2*C(2,1)*MidPara(1,1)))  ;    % induced velocity in hover
```

```matlab
if v_f==0 && v_a==0
    Ps_h=v_h*Ts_h;                      % required hovering power of a single
rotor
    Psp_h=Ps_h*C(24)/C(6);              % prop input power in hover, fixed by
FM
    % to consider the profile power, and fuselage downwash factor to
    % consider the frame area under the propeller.
    q=0;
    n_h=sqrt(Ts_h/(C(5,1)*C(2,1)*DsPm(4)^4));   % rotation speed of the
rotor, unit: rev/s
else
    if v_f==0
        % vertical descent
        if v_a<0 && v_a/v_h>-2
            % fprintf("Warning: descent speed not appropriate,the multicopter
will be in the VTR state, suggest move down-forward instead");
            missionerr(1)=1;
            %VTR; vortex ring state, it is an unstable state, the
mulitcopter
            %can't get out from this state and will keep dropping
        end
        gama=atan(v_a/v_f);
        beta=0;          % tilt angle
        alpha=gama;      % prop angle of attack
        v_inf=v_a;       % velocity of comming wind
        q=C(2,1)*v_inf^2/2;      % dynamic pressure
    elseif v_a>=0
        gama=atan(v_a/v_f);      % forward flght, alpha==beta
        v_inf=sqrt(v_f^2+v_a^2);     % velocity of comming wind
        q=C(2,1)*v_inf^2/2;      % dynamic pressure
        alpha_ub=pi/2;       % max tilt angle
        alpha_lb=0;          % min tilt angle
        var1=[gama,v_inf,q,GTOW,alpha_ub,alpha_lb];
        alpha=layer_3_alpha(var1);
    elseif v_a<0
        gama=atan(v_a/v_f);      % forward flght, alpha==beta
        v_inf=sqrt(v_f^2+v_a^2);     % velocity of comming wind
        q=C(2,1)*v_inf^2/2;      % dynamic pressure
        alpha_ub=pi/2;       % max tilt angle
        alpha_lb=-pi/2;          % min tilt angle
        var1=[gama,v_inf,q,GTOW,alpha_ub,alpha_lb];
        alpha=layer_3_alpha(var1);
    end
    D=q*C(26)*MidPara(2)*abs(sin(alpha)+cos(alpha)/C(27));  % Drag
    if pi/2-alpha<0.3
        Ts_g=(D+GTOW*sin(gama))/sin(alpha)/DsPm(1);
    else
        Ts_g=GTOW*cos(gama)/cos(alpha)/DsPm(1);
    end
%   T_g=Ts_g*DsPm(1);
    var_vi=[alpha, v_inf, Ts_g];
    v_i_g=layer_3_vi(var_vi);           % induced velocity
    %P_prop=(D+GTOW*sin(gama))*v_inf; % =T_g*v_inf*sin(alpha), total power
for movement
    Ps_prop=Ts_g*(v_i_g+v_inf*sin(alpha));
    %Ps_prop=P_prop/DsPm(1);            % single rotor power for movement
    n_f=(v_inf*sin(alpha)+v_i_g)/(C(8)*C(10)*DsPm(4));   % rotation speed of
the rotor, unit: rev/s
```

```matlab
    if Ps_prop<0
        Ps_prop=0;          % when descending up to a certain speed, the rotor
gets
        % into wind mill brake state, the wind will work on the propeller to
        % deaccelerate the aircraft
    end

end

if v_f==0 && v_a==0
    P_mot=Psp_h;              % the motor output power in hovering
    n_g=n_h;
    Ts_g=Ts_h;
else
    P_mot=Ps_prop;        % the propelelr output power in all other conditions
    n_g=n_f;
end

%calculation and constraint check of mu--advance ratio%%%%%%%%
mu=v_inf*cos(alpha)/(pi*DsPm(2)*n_g);
if mu>Cstr(23)
    err_mu=1;       % error flag of cruising endurance not meet the mission
requirement
    err_flag(10)=err_mu;
end
%%%%%%%%%%%%%%%%%%%%%

Ps_g=P_mot;

end
```

K.6 layer_3_alpha

```matlab
function a=layer_3_alpha(var)
global C MidPara

% four inputs:1. gama, 2. v_inf, 3. q, 4. GTOW, 5. alpha_ub, 6, alpha_lb
if var(1)==pi/2 || var(1)==-pi/2
    alpha=var(1);
else
Cons=var(3)*C(26)*MidPara(2)/(var(4)*cos(var(1)));

alpha =var(5)*0.999 ;    % the start point of alpha
alpha_old = 100;      % the alpha value in the last iteration
iter = 0;    % initialise the iteration flag
while abs((alpha_old-alpha)/alpha) > 10^-9 && alpha ~= 0 || alpha>var(5) ||
alpha < var(6)
    alpha_old = alpha;
    f_A=(sin(alpha)+cos(alpha)/C(27));
    f_Ad=(cos(alpha)-sin(alpha)/C(27));
    if f_A>0
    alpha=alpha-(Cons*f_A-tan(alpha)+tan(var(1)))/(Cons*f_Ad-
1/cos(alpha)^2);
    else
        alpha=alpha-(-Cons*f_A-tan(alpha)+tan(var(1)))/(-Cons*f_Ad-
1/cos(alpha)^2);
    end
```

```matlab
    % above is the Newton-Raphson method, alpha_n+1=alpha_n-
(f(alpha)/f'(alpha))_n;
    % f(alpha)=Cons*(sin(alpha)+cos(alpha)/n)+tan(gama)-tan(alpha)==0.
    % f'(alpha)=Cons*(cos(alpha)-sin(alpha)/n)-1/cos(alpha)^2
    % C=Cd*A1/MTOW
    iter = iter + 1;
    alpha_d=alpha*180/pi;
%     fprintf('Iteration %d: alpha=%.20f degree, %.20f rad, err=%.20f\n',
iter, alpha_d,alpha, alpha_old-alpha);
    %pause;
    if alpha>pi/2
        alpha=0.001;
    elseif alpha<-pi/2
        alpha=-0.001;
    end
end
gama_d=var(1)*180/pi;
%     fprintf('gamma= %.20f, beta=%.20f', gama_d,alpha_d-gama_d );
end
a=alpha;

end
```

K.7 layer_3_vi

```matlab
function v_i=layer_3_vi(var_vi)
global C MidPara

% four inputs:1. alpha, 2. v_inf, 3. Ts,

vi0 =20 ;   % the start point of alpha
vi=vi0;
vi_old = 100;    % the alpha value in the last iteration
iter = 0;   % initialise the iteration flag
while abs((vi_old-vi)/vi) > 10^-9 && vi ~= 0
    vi_old = vi;
    vi=vi-(vi^4+2*var_vi(2)*vi^3*sin(var_vi(1))+var_vi(2)^2*vi^2-
(var_vi(3)/(2*C(2)*MidPara(1)))^2)/...
        (4*vi^3+6*var_vi(2)*sin(var_vi(1))*vi^2+2*var_vi(2)^2*vi);
%     fprintf('Iteration %d: vi=%.20f m/s, err=%.20f\n', iter, vi, vi_old-
vi);
    % above is the Newton-Raphson method, alpha_n+1=alpha_n-
(f(alpha)/f'(alpha))_n;
    % f(x)=x^4+2*v_inf(i)*x^3*sin(alpha(i))+v_inf(i)^2*x^2-(T(i)/C)^2==0.
    % f'(x)=4x^2+6v_inf*sin(alpha)*x^2+2v_inf^2*x
    % C=Cd*A1/MTOW
    iter = iter + 1;
%     if vi<0
%         vi=vi0*iter*2;
%     end
end
v_i=vi;

end
```

K.8 layer_3_motor

```matlab
function [m_motor,pr_motor]=layer_3_motor(param_motor)

global C Motor_forest DOE_forest Mdl_pr_forest DOE_pr_forest MidPara DsPm
% read the forest models, the forest including 13 trees, each leave on the
% tree is a Gaussian Regresison Process model.
% Given the motor parameters, this function works out an estimated motor
% mass for each tree, then select the one that has least error to the
% average motor/MTOM ratio.

X=param_motor(1:3);        % read motor performance parameters
No_Trees_m=length(Motor_forest.Trees);
No_Trees_pr=length(Mdl_pr_forest.Trees);
%Y_p = nan(length(MASS_T),No_Trees);


%% mass estimation
%fprintf('Predicting Validation set\n');
for i=1:No_Trees_m
    %fprintf('Tree #%d\n',i);
    % define the leaf ID
    [~,leaf_ID] = predict(Motor_forest.Trees{i},X);

    for j=1:DOE_forest{i}.NO_LEAF
        if sum(DOE_forest{i}.LEAF_IDS(j)==leaf_ID)>0
            %fprintf('\tLeaf #%d\n',j);
            % calcualte the prediction
            [Y_PRED,~] =
predict(DOE_forest{i}.LEAF{j}.MODEL,X(leaf_ID==DOE_forest{i}.LEAF_IDS(j),:))
;
            % store the predictions
            Y_p(leaf_ID==DOE_forest{i}.LEAF_IDS(j),i) = abs(Y_PRED/1000);
            %SD_p(leaf_ID==DOE_forest{i}.LEAF_IDS(j),i) = SD_PRED;

        end
    end
    % clc
end

%fprintf('Predicting based on minimum ratio error method:\n');
rMTOM=Y_p.*DsPm(1)./MidPara(5,1);        % work out the motor/MTOM
% ratio for each estimated motor mass. Here takes the MTOM rather than
% GTOM because the regression is between the motor mass and the MTOM,
% it reflects a rough ability of lifting load.
eMTOM=abs(rMTOM-C(30));        % work out the ratio error with an average value
[~, p_e]=min(eMTOM');        % locate the minimum error tree

m_motor=Y_p(p_e);        % select the mass estimation from this tree.


%% price estimation
% fprintf('Predicting Validation set\n');
for i=1:No_Trees_pr
%     fprintf('Tree #%d\n',i);
    % define the leaf ID
```

```matlab
        [~,leaf_ID] = predict(Mdl_pr_forest.Trees{i},X);


        for j=1:DOE_pr_forest{i}.NO_LEAF
            if sum(DOE_pr_forest{i}.LEAF_IDS(j)==leaf_ID)>0
%                fprintf('\tLeaf #%d\n',j);
                % calcualte the prediction
                [Y_PRED,SD_PRED] =
predict(DOE_pr_forest{i}.LEAF{j}.MODEL,X(leaf_ID==DOE_pr_forest{i}.LEAF_IDS(
j),:));
                % store the predictions
                Y_p(leaf_ID==DOE_pr_forest{i}.LEAF_IDS(j),i) = Y_PRED;
                SD_p(leaf_ID==DOE_pr_forest{i}.LEAF_IDS(j),i) = SD_PRED;


            end
        end
      % clc
end


% fprintf('Predicting based on weighted combination method:\n');
for i=1:size(Y_p,1)
    % define the matrix C0
    C0 = inv(diag(SD_p(i,:)));
    W (i,:)=
(C0*ones(No_Trees_pr,1))./(ones(1,No_Trees_pr)*C0*ones(No_Trees_pr,1));
    Price_p(i,1) = sum(Y_p(i,:).*W(i,:));
end
pr_motor=Price_p;   %!!!!!needs to be finished
end
```

K.9 layer_3_esc

```matlab
function [m_esc,pr_esc,m_esc_chip]=layer_3_esc(param_esc)
    global C

    % This function is used to calculate the mass and price of an ESC. The
chip+wire model is given up. Use simple regression
    % ESC is modelled as the chip plus signal wire, plus two input wire and
    % three output wire, plus any other radiator
     % There are two parameters used to estimate the mass and price of the
    % ESC: 1. maximum input current, 2. the arm length

    %% old
    %d_in=0.0606*param_esc(1)+0.2941;    % a correlated relation to work out
    % the input wire diameter from the ampacity (continious maximum current)
    % unit: mm

    %n_in=floor(-39*log(d_in/0.127)/log(92)+36);    % get the id of gauge
    % from the estimated diameter.

    % n_out=n_in+2;   % the out put wire is assumed to be one gauge smaller
than
    % the input wire, since it's a three-phase current, the RMS current in
    % each wire is smaller than the input current. And this is also what
    % all the ESC manufacturers do.

    %m_wire_out=layer_3_wiremass(n_out,C(39));
    %%
```

```matlab
    n_in=floor(-4.016*log(param_esc(1))+29.998);
    %In order to meet the current
    % requirement, the gauge should be floor to the smaller integer (larger
diameter)

    % Assume use copper core for all the wires, and ignore the difference
    % between solid core and strand core. The density of copper is 8960
kg/m3.
    rho_cp=C(37);
    m_wire_in=layer_3_wiremass(n_in, param_esc(2));
    m_esc_chip=0.9121*param_esc(1)/1000;  % work out the chip mass from
regression
    m_esc=2*m_wire_in+m_esc_chip;  % two input wire, three output wire
    % plus the chip

    pr_esc=1.9318*param_esc(1)^0.5878;

end
```

K.10 layer_3_bat

```matlab
function [m_b,pr_b]=layer_3_bat(E_b_req)


    % This function is used to calculate the mass and price of a battery.

    m_b=0.0059*E_b_req;
    pr_b=0.6337*E_b_req;

end
```

K.11 layer_3_arm_mopt

```matlab
function [m_arm,pr_arm, opt_geo]=layer_3_arm_mopt(L_a)

global  Shape Mat input MPr C

%%%% the strategy here is a conbined optimisation that uses GA to locate the
local valley, and
% then use fmincon to go down the gradient. By doing so, it can find the
accurate minimum and
% saves a lot of time (from 20 s to 0.3 s for a single run).

%%% constraints for ga optimisation

%%% constraints for fmincon optimisation
% Linear constraints, thickness does not exceed 1/2 of the overall size
% therefore, 2*property(4)-property(2)<=0, 2*property(4)-property(3)<=0


%%%% optimisation process %%%%
%1. GA for rough optimisation
optionsga=optimoptions('ga','PopulationSize',100,'MaxGenerations',300,...
    'MaxStallGenerations', 20,'FunctionTolerance',1e-5,'Display','off');
intcon=[1,6];                        % Integer variables
nonlconga=@layer_3_armcons;
```

```matlab
lbga=[min(Shape),0.002,0.002,0.0008,L_a,min(Mat)];   % lower boundary of
variables
ubga=[max(Shape),L_a/C(36),L_a/C(36),L_a/(C(36)+1),L_a,max(Mat)];

[geo_optga(1:6),ma_optga,exitflag] =...

ga(@layer_3_armcalc_mid,6,[],[],[],[],lbga,ubga,nonlconga,intcon,optionsga);
if exitflag~=1

optionsga=optimoptions('ga','PopulationSize',100,'MaxGenerations',500,...
        'MaxStallGenerations', 100,'FunctionTolerance',1e-
5,'Display','off');
    [geo_optga(1:6),ma_optga] =...

ga(@layer_3_armcalc_mid,6,[],[],[],[],lbga,ubga,nonlconga,intcon,optionsga);

end
%2. fmincon for accurate optimisation
A=[-1,0,2,0; 0,-1,2,0];
b=[0; 0];
lb=[0.002,0.002,0.0008,L_a];                         % lower boundary of variables
ub=[L_a/5,L_a/5,L_a/12,L_a];          % ??? upper boundary of variables,
relate the size to La_min
%x0=ub;
nonlcon=@layer_3_armcons_fmin;                   % nonlinear constraints
optionslocal=optimoptions('fmincon','Algorithm','sqp-
legacy'  ,'CheckGradients', true,'OptimalityTolerance',...
    1e-8,'StepTolerance', 1e-8,'ConstraintTolerance',1e-
7,'MaxFunctionEvaluations',...
    3000, 'MaxIterations',1000,'Display','off');      %'Diagnostics',
'on',,'Display','iter-detailed'
x0=geo_optga(2:5);    % use the result as starting point for fmincon
input(1)=geo_optga(1);
input(6)=geo_optga(6);
[geo_opt,ma_opt] =
fmincon(@layer_3_armcalc_fmin,x0,A,b,[],[],lb,ub,nonlcon,optionslocal);
opt_geo=[input(1),geo_opt,input(6)];
m_arm=ma_opt;        % output mass
unit_price=MPr(opt_geo(1),opt_geo(6));
pr_arm=m_arm*unit_price;    % output price

end
```

K.12 layer_3_armcons

```matlab
%%% This function is a wrap of the LaWorkout function, it outputs the
%%% constrainsts.

function [cons,ceq]=layer_3_armcons(property)

Arm_output=layer_3_armcalc(property);
cons(1)=Arm_output.frequency_error_x;      % Consider the first order
frequency on both x and y axis
cons(2)=Arm_output.frequency_error_y;      % the motor frequency should be
smaller than these frequencies
cons(3)=Arm_output.deflection_error;        % deflection constraint
cons(4)=Arm_output.shear_stress;
```

```
cons(5)=Arm_output.normal_compression_stress;
cons(6)=Arm_output.normal_tension_stress;

ceq=[];

end
```

K.13 layer_3_armcalc_mid

```
%%% This function is a wrap of the LaWorkout function, it only output the
%%% mass of the arm, and this function is used for the mass optimisation.

function m_a=layer_3_armcalc_mid(property)


Arm_output=layer_3_armcalc(property);

if Arm_output.frequency_error_x<0 && Arm_output.frequency_error_y<0 &&...
        Arm_output.deflection_error<1.2e-6 && Arm_output.shear_stress<0
&&...
        Arm_output.normal_compression_stress<0 &&
Arm_output.normal_tension_stress<0

    m_a=Arm_output.mass;
else
    m_a=Arm_output.mass*100;
end


end
```

K.14 layer_3_armcons_fmin

```
%%% This function is a wrap of the LaWorkout function, it outputs the
%%% constrainsts.

function [cons,ceq]=layer_3_armcons_fmin(property)
global input
for i=2:5
    input(i)=property(i-1);
end

Arm_output=layer_3_armcalc(input);
cons(1)=Arm_output.frequency_error_x;       % Consider the first order
frequency on both x and y axis
cons(2)=Arm_output.frequency_error_y;       % the motor frequency should be
smaller than these frequencies
cons(3)=Arm_output.deflection_error;        % deflection constraint
cons(4)=Arm_output.shear_stress;
cons(5)=Arm_output.normal_compression_stress;
cons(6)=Arm_output.normal_tension_stress;

ceq=[];

end
```

K.15 layer_3_armcalc_fmin

```
%%% This function is a wrap of the LaWorkout function, it only output the
%%% mass of the arm, and this function is used for the mass optimisation.

function m_a=layer_3_armcalc_fmin(property)

global input

for i=2:5
    input(i)=property(i-1);   %test
end


Arm_output=layer_3_armcalc(input);

if Arm_output.frequency_error_x<0 && Arm_output.frequency_error_y<0 &&...
        Arm_output.deflection_error<1.2e-6 && Arm_output.shear_stress<0
&&...
        Arm_output.normal_compression_stress<0 &&
Arm_output.normal_tension_stress<0

    m_a=Arm_output.mass;
else
    m_a=Arm_output.mass*1000;
end


end
```

K.16 layer_3_arm_propt

```
function [m_arm, pr_arm, opt_geo]=layer_3_arm_propt(L_a)

global  Shape Mat input MPr C

%%%% the strategy here is a conbined optimisation that uses GA to locate the
local valley, and
% then use fmincon to go down the gradient. By doing so, it can find the
accurate minimum and
% saves a lot of time (from 20 s to 0.3 s for a single run).

%%% constraints for ga optimisation

%%% constraints for fmincon optimisation
% Linear constraints, thickness does not exceed 1/2 of the overall size
% therefore, 2*property(4)-property(2)<=0, 2*property(4)-property(3)<=0


%%%%  optimisation process %%%%
%1. GA for rough optimisation
optionsga=optimoptions('ga','PopulationSize',100,'MaxGenerations',30,'Displa
y','off');
intcon=[1,6];                    % Integer variables
nonlconga=@layer_3_armcons;
```

```matlab
lbga=[min(Shape),0.002,0.002,0.0008,L_a,min(Mat)];   % lower boundary of
variables
ubga=[max(Shape),L_a/C(36),L_a/C(36),L_a/(C(36)+1),L_a,max(Mat)];

[geo_optga(1:6),pra_optga,exitflag] =...

ga(@layer_3_armcalc_prmid,6,[],[],[],[],lbga,ubga,nonlconga,intcon,optionsga
);

%2. fmincon for accurate optimisation
A=[-1,0,2,0; 0,-1,2,0];
b=[0; 0];
lb=[0.002,0.002,0.0008,L_a];                         % lower boundary of variables
ub=[L_a/5,L_a/5,L_a/12,L_a];         % ??? upper boundary of variables,
relate the size to La_min
%x0=ub;
nonlcon=@layer_3_armcons_fmin;                       % nonlinear constraints
optionslocal=optimoptions('fmincon','Algorithm','sqp-
legacy'  ,'CheckGradients', true,'OptimalityTolerance',...
    1e-8,'StepTolerance', 1e-8,'ConstraintTolerance',1e-
7,'MaxFunctionEvaluations',...
    3000, 'MaxIterations',1000,'Display','off');      %'Diagnostics',
'on',,'Display','iter-detailed'
x0=geo_optga(2:5);     % use the result as starting point for fmincon
input(1)=geo_optga(1);
input(6)=geo_optga(6);
[geo_opt,pra_opt] =
fmincon(@layer_3_armcalc_fmin,x0,A,b,[],[],lb,ub,nonlcon,optionslocal);
opt_geo=[input(1),geo_opt,input(6)];

pr_arm=pra_opt; % the output price
unit_price=MPr(opt_geo(1),opt_geo(6));
m_arm=pr_arm/unit_price;     % the output mass


end
```

K.17 layer_3_armcalc_prmid

```matlab
%%% This function is a wrap of the LaWorkout function, it only output the
%%% mass of the arm, and this function is used for the mass optimisation.

function pr_arm=layer_3_armcalc_prmid(property)
global MPr

Arm_output=layer_3_armcalc(property);

if Arm_output.frequency_error_x<0 && Arm_output.frequency_error_y<0 &&...
        Arm_output.deflection_error<1.2e-6 && Arm_output.shear_stress<0
&&...
        Arm_output.normal_compression_stress<0 &&
Arm_output.normal_tension_stress<0

    m_a=Arm_output.mass;
else
    m_a=Arm_output.mass*1000;
end
```

```matlab
pr_unit=MPr(property(1),property(6));        % check the unit price from the
material price table
pr_arm=m_a*pr_unit;


end
```

K.18 layer_3_armcalc


```matlab
function Arm=layer_3_armcalc(property)

global C MP Load err_flag
Arm = struct('mass', 1,'price', 1,'frequency_error_x',
1,'frequency_error_y', 1,'deflection_error', 1,...
    'shear_stress', 1,'normal_compression_stress',
1,'normal_tension_stress', 1);


%read fixed parameters from a given scenario
%FixedParameters=xlsread('FixedParameters.xlsx',MissionName);
% read fixed parameters from a given scenario

%%%% read geometry parameters

SFL=property(1);          % Shape flag 1:rectangular plate, 2: hollow
rectangular, 3: hollow oval, 4: T section, 5: Channel section, 6: I section
w=property(2);               % width,unit m
h=property(3);                % height,unit m
t=property(4);             % thickness,unit m
L=property(5);             % Length of the amr, unit m
MFL=property(6);           % Material Flag 1: Carbon Fibre, 2: Glass Fibre, 3:
ABS plastic, 4: Aluminium

%read material parameters

rho=MP(1,MFL);              % material density, kg/m3
E=MP(2,MFL);               % Young's modulus, Pa
G=MP(3,MFL);               % shear modulus, Pa
xigma_tn=MP(4,MFL);        % Tension yield/ultimate strength, Pa
xigma_cp= MP(5,MFL);       % Compression yield/ultimate strength, Pa
tao=MP(6,MFL);             % Shear yield/ultimate strength, Pa
Pr_uni=MP(7,MFL);          %??? unit price of the material

if t>w/2 || t>h/2
    m_arm=5;
    Pr_arm=1000;
    fex=1;
    fey=1;
    de=1;
    tao_err=1e8;
    xigma_err=[1e8,1e8];
else
    %% %%%% calculation of the load %%%%%%%
    T_max=Load(1);          % unit N
    n_max=Load(2);          % unit rev/s=Hz, workout the rotation speed
    Q_max=Load(3);          %unit N.m, workout the torque of the motor
```

```matlab
    Fx=T_max-Load(4)*C(3);
    Mx=Fx*L;
    My=Q_max;


    %% %%%%calculation of geometry properties, including cross section area
(A) and area moment of inertia (Ix) %%%%
    % syms w h t   for test
    switch SFL
        case 1  % rectangular
            Ix=w*h^3/12;          % x axis area moment of inertia
            Iy=h*w^3/12;          % y axis area moment of inertia
            Ixy=0;
            A=w*h;                % cross section area
            Sx=w*h/2*h/4;         % the area moment to the dangerous area (for
shear stress calculation)
            we=w;
            Ae=Ix*we/Sx;           % equivalent area for shear stress, The
explanation is below
            h_mc=h/2;
            h_mt=-h/2;
            w_mc=w/2;
            w_mt=-w/2;
        case 2  % hollow rectangular (box)
            Ix=(w*h^3-(w-2*t)*(h-2*t)^3)/12;
            Iy=(h*w^3-(h-2*t)*(w-2*t)^3)/12;
            Ixy=0;
            A=w*h-(w-2*t)*(h-2*t);
            Ae=2/3*(w*h^3-(w-2*t)*(h-2*t)^3)/(h^2+2*(w-2*t)*(h-t));
            h_mc=h/2;
            h_mt=-h/2;
            w_mc=w/2;
            w_mt=-w/2;
        case 3  % hollow oval (oval cilindar)
            Ix=pi*(w*h^3-(w-2*t)*(h-2*t)^3)/64;
            Iy=pi*(h*w^3-(h-2*t)*(w-2*t)^3)/64;
            Ixy=0;
            A=pi*(w*h-(w-2*t)*(h-2*t))/4;
            Ae=3*pi/4*((w/2)*(h/2)^3-(w/2-t)*(h/2-t)^3)*t/((w/2)*(h/2)^2-
(w/2-t)*(h/2-t)^2);
            k=-(My*Ix+Mx*Ixy)/(Mx*Iy+My*Ixy);
            %               syms w_m h_m;
            %               eq1=k==-h^2*w_m/(w^2*h_m);
            %               eq2=w_m^2/(w/2)^2+h_m^2/(h/2)^2==1;
            % %             eq1=k+h^2*w_mc/(w^2*h_mc);
            % %             eq2=w_mc^2/(w/2)^2+h_mc^2/(h/2)^2==1;
            %               [h_m,w_m]=solve(eq1,eq2);        % solve a two
parameter power two
            %               % equations to find the coordinate of the tangent
point on the oval
            %               % There are two point where max tension stress and
compression
            %               % stress happens
            w_mt=w^2*k/(2*sqrt(w^2*k^2+h^2));
            h_mt=-h^2/(2*sqrt(w^2*k^2+h^2));
            w_mc=-w^2*k/(2*sqrt(w^2*k^2+h^2));
            h_mc=h^2/(2*sqrt(w^2*k^2+h^2));
        case 4  % "T" section
```

```
        e1=(w*t+h^2-t^2)/(h-t+w)/2;
        Ix=(w*e1^3-(w-t)*(e1-t)^3+t*(h-e1)^3)/3;
        Iy=(t*w^3+(h-t)*t^3)/12;
        Ixy=0;
        A=w*t+(h-t)*t;
        Ae=2/3*(w*e1^3-(w-t)*(e1-t)^3+t*(h-e1)^3)/(h-e1)^2;
        w_mt=-t/2;
        h_mt=e1-h;
        w_mc=t/2;
        h_mc=e1;
    case 5  % Channel section
        e1=(w*t+2*(h^2-t^2))/(2*h+w-2*t)/2;
        Ix=(w*e1^3-(w-2*t)*(e1-t)^3+2*t*(h-e1)^3)/3;
        Iy=(h*w^3-(h-t)*(w-2*t)^3)/12;
        Ixy=0;
        A=w*t+(h-t)*2*t;
        Ae=2/3*(w*e1^3-(w-2*t)*(e1-t)^3+2*t*(h-e1)^3)/(h-e1)^2;
        w_mt=-w/2;
        h_mt=e1-h;
        w_mc=w/2;
        h_mc=e1;
    case 6 % "L" section
        ey=(w*t+h^2-t^2)/(h-t+w)/2;
        ex=(h*t+w^2-t^2)/(h-t+w)/2;
        Ix=(w*ey^3-(w-t)*(ey-t)^3+t*(h-ey)^3)/3;
        Iy=(h*ex^3-(h-t)*(ex-t)^3+t*(w-ex)^3)/3;
        Ixy=w*h*t*(w-t)*(h-t)/4;
        A=w*t+(h-t)*t;
        Ae=2/3*(w*ey^3-(w-t)*(ey-t)^3+t*(h-ey)^3)/(h-ey)^2;

        w_mt=ex-t;      % assume torque is to the right ->, and thrust
is to the up,then
        % the combined torque is to the upright. the optimal shape of
        % the beam cross section is like "7" or "L", not the reverse.
        h_mt=ey-h;
        w_mc=ex;
        h_mc=ey;
        %           w_mt=-ex;     % This is when place the
crosssection like "J"
        %           or "F".assume the same load direction
        %           h_mt=ey-h;
        %           w_mc=w-ex;
        %           h_mc=ey;

    case 7   % "I" section
        Ix=(w*h^3-(w-t)*(h-2*t)^3)/12;
        Iy=(2*t*w^3+(h-2*t)*t^3)/12;
        Ixy=0;
        A=w*h-(w-t)*(h-2*t);
        Ae=2/3*(w*h^3-(w-t)*(h-2*t)^3)/((h-2*t)^2+4*w*(h-t));
        h_mc=h/2;
        h_mt=-h/2;
        w_mc=w/2;
        w_mt=-w/2;

    otherwise % "H" section
        Iy=(h*w^3-(h-t)*(w-2*t)^3)/12;
        Ix=(2*t*h^3+(w-2*t)*t^3)/12;
```

```matlab
            Ixy=0;
            A=w*h-(h-t)*(w-2*t);
            Ae(1)=2/3*w*(2*h^3+w*t^2-2*t^3)/(2*h^2+w*t-2*t^2);        % middle
plane
            Ae(2)=2/3*t*(2*h^3+w*t^2-2*t^3)/(h-t)^2;                  % edge
of middle plane
            h_mc=h/2;
            h_mt=-h/2;
            w_mc=w/2;
            w_mt=-w/2;
    end


    %% %%%% calculation of the beam performance (constraints) %%%%%%
    fnx=sqrt((3*E*Ix/L^3)/(rho*A*L*33/140+Load(4)))/(2*pi);          %???? the
equation should be corrected for a cantilever beam with tipped mass at the
free end
    fny =sqrt((3*E*Iy/L^3)/(rho*A*L*33/140+Load(4)))/(2*pi);
    FEX(1)=C(32)-abs(fnx-n_max)/fnx; % ????the frequency error from the
natural frequency should be larger than 0.3
    FEX(2)=C(32)-(fnx-Load(5))/fnx;
    FEX(3)=C(32)-(fnx-Load(6))/fnx;
    FEY(1)=C(32)-abs(fny-n_max)/fny;
    FEY(2)=C(32)-(fny-Load(5))/fny;
    FEY(3)=C(32)-(fny-Load(6))/fny;

    fex=max(FEX);
    fey=max(FEY);
    if fnx<n_max || fny<n_max
        err_flag(8)=1;  % the natural frequency of the beam is smaller than
        % the maximum rotation speed,
    end

    dmax_x=Fx*L^3/(3*E*Ix);        % the maximum x deflection of the beam
    dmax_y=My*L^2/(2*E*Iy);         % the maximum y deflection of the beam
    dmax=sqrt(dmax_x^2+dmax_y^2);
    d_limit=L/C(33);                % ???? work out the deflection limit
    de=dmax-d_limit;                % the maximum deflection error

    for i=1:length(Ae)
        tao_dan(i)=Fx/Ae(i);    % calculate shear stress on all the
dangerous planes
    end
    tao_max=max(tao_dan);                      % the maximum flexural shear
stress caused by thrust
    tao_err=tao_max-tao/C(34);        % error between allowed maximum shear
stress vs the max shear stress on the cross section
    % tao=Fx*Sx/(Ix*we), [Fx] is the shear force, [Sx] is the area moment to
    % the dangerous plane, [Ix] is the area moment of inertia, and [we] is
the
    % equivalent width. This canbe written as tao=Fx/Ae, so for each shape,
    % the equivalent stress area Ae=Ix*we/Sx.

    xigma_max_com=abs(((Mx*Iy+My*Ixy)*h_mc-(My*Ix+Mx*Ixy)*w_mc)/(Ix*Iy-
Ixy^2));
    xigma_max_ten=abs(((Mx*Iy+My*Ixy)*h_mt-(My*Ix+Mx*Ixy)*w_mt)/(Ix*Iy-
Ixy^2));
    %xigma_max=Mx*h_m/Ix-My*w_m/Iy;    % the maximum stress in the beam, it
is
```

```matlab
    % the overall stress under both thrust and torque applied on the beam.
    % In this euqation, [h_m] and [w_m] are the distances from the
    % dangerous point (max stress point) to the centroid point.

    % xigma_maxq=Q_max*(w/2)/Iy;   %??? the maximum stress caused by torque
    xigma_err(1)=xigma_max_ten-xigma_tn/C(34); % ????the error between the
allowed normal stress vs the actual maximum normal stress
    xigma_err(2)=xigma_max_com-xigma_cp/C(34);


    m_arm=rho*A*L;            % final mass of the arm
    Pr_arm=Pr_uni*m_arm;      % final price of the arm
end

%% %%%%final output of the function %%%%

Arm = struct('mass', m_arm,'price', Pr_arm,'frequency_error_x',
fex,'frequency_error_y', fey,'deflection_error', de,...
    'shear_stress', tao_err,'normal_compression_stress',
xigma_err(2),'normal_tension_stress', xigma_err(1));
end
```